

BIOPHYSICAL STUDIES OF LIGAND BINDING TO HUMAN HDAC8

A Dissertation
Submitted to the Graduate Faculty
of the
North Dakota State University
of Agriculture and Applied Science

By

Raushan Kumar Singh

In Partial Fulfillment
for the Degree of
DOCTOR OF PHILOSOPHY

Major Department:
Chemistry and Biochemistry

May 2014

Fargo, North Dakota

NORTH DAKOTA STATE UNIVERSITY
Graduate School

Title

Biophysical Studies of Ligand Binding to Human Histone Deacetylase-8

By

Raushan Kumar Singh

The Supervisory Committee certifies that this **disquisition** complies with North Dakota State University's regulations and meets the accepted standards for the degree of

DOCTOR OF PHILOSOPHY

SUPERVISORY COMMITTEE:

Prof. D. K. Srivastava
Chair

Prof. Derek Killilea

Prof. Robert Sparks

Prof. Larry Reynolds

Approved:

02/06/14
Date

Prof. Gregory R. Cook
Department Chair

ABSTRACT

Due to an involvement in various patho-physiological conditions, human histone deacetylases (HDACs) are high priority drug targets for the treatment of several diseases, such as cancer, heart failure, neurodegeneration, etc. An effector (inhibitor/activator) of these enzymes has a great potential to alleviate the above disease conditions. In this regard, HDAC inhibitors – Zolinza[®] and Istodax[®] - have already been approved by the FDA for the treatment of T-cell lymphoma, aside from several other inhibitors which are in the advanced level of clinical trials.

HDAC8 serves as a prototype to study structural-functional and catalytic features of human HDACs. In order to pursue the biophysical studies of the ligand-binding, HDAC8 was cloned, expressed, and purified from *E. coli*. A high-throughput screening (HTS) of an in-house library of small molecules was performed utilizing a trypsin-coupled *in vitro* HDAC8 assay to discover novel effectors of HDAC8, and the N-acetylthiourea and the thiopyridine derivatives were discovered as the isozyme-selective inhibitors and activators of HDAC8, respectively.

In vitro HDAC8 assay utilizing a fluorogenic peptide as a substrate often produces artifactual results. Therefore, a substrate-independent HDAC8 assay was developed utilizing a fluorescent analog of a pan-HDAC-inhibitor. In view of the fact that the downstream cellular response of a drug is often dictated by the transient kinetic and thermodynamic parameters of its interaction with the target, the transient kinetics and thermodynamics of interaction of the selected HDAC8 inhibitor with the enzyme were thoroughly investigated. It was observed that the dissociation off-rate (k_{off}) and/or the enthalpy of binding (ΔH^0) of an HDAC8 inhibitor to the enzyme could play a crucial role in determining its *in vivo* efficacy. A rationale has been

presented that the above parameters of the ligand-protein interaction could be utilized for optimizing a drug candidate (HDAC8 inhibitor) in order to enhance its *in vivo* potency.

ACKNOWLEDGEMENTS

I am deeply indebted to my adviser, Prof. D.K. Srivastava, for his superb mentorship which has made me confident to pursue my future research career in Protein Science. He has been my father figure since I arrived in Fargo. I am also grateful to my thesis advisory committee members, Prof. Robert Sparks, Prof. Derek Killilea, and Prof. Larry Renoyds, for their guidance and generous support without which it would have been impossible to complete my graduate studies.

I wish to thank the current (Nitesh, Travis, Junru, Joe, Katie, and Dustin) and past (Kunle, Alex, Sumathra, Shakila, Bratati, Joel, and Dan) members of Srivastava's group for their support during my stay in the lab. I also wish to thank my collaborators, Prof. Greg Cook and Prof. Sanku Mallik, for their support during my research career at NDSU.

I would like to acknowledge Prof. Debi P. Sarkar of Delhi University (India) for inspiring me to pursue my graduate studies in the USA. Words are inadequate to express my deep gratitude to Emily Grenz, Center for Writers (NDSU), for editing my thesis. Finally, special thanks go to my parents and the Almighty, who always inspire to help others, and to achieve the best in life.

TABLE OF CONTENTS

ABSTRACT.....	iii
ACKNOWLEDGMENTS.....	v
LIST OF TABLES.....	vii
LIST OF FIGURES.....	ix
LIST OF SCHEMES.....	xiv
LIST OF ABBREVIATIONS.....	xv
CHAPTER 1. INTRODUCTION.....	1
CHAPTER 2. STATEMENT OF PROBLEM.....	61
CHAPTER 3. MATERIALS.....	63
CHAPTER 4. METHODS.....	65
CHAPTER 5. RESULTS.....	85
CHAPTER 6. DISCUSSION.....	216
REFERENCES.....	243

LIST OF TABLES

<u>Table</u>	<u>Page</u>
1.1. Different types of post-translational modifications (PTMs) of Histone.....	2
1.2. Characteristics of human HDAC class I.....	5
1.3. Characteristics of human HDAC class IIa.....	6
1.4. Characteristics of human HDAC class IIb.....	7
1.5. List of HDAC inhibitors in clinical trial.....	60
4.1. Composition of Buffer used in different experiments.....	84
5.1. Summary of the HDAC8 purification by Affinity Chromatography.....	90
5.2. Summary of the high-throughput screening of thiol-based compounds for the HDAC8 inhibitors/activators	107
5.3. Summary of the high-throughput screening of hydroxybenzoic acid and hydroxypicolinic /nicotinic acid based compounds for the HDAC8 inhibitors.....	113
5.4. Summary of the high-throughput screening of the thiourea derivatives for the HDAC8 activators/inhibitors.....	119
5.5. Summary of the high-throughput screening of hydrazone derivative for the HDAC8 inhibitors/activators.....	124
5.6. Summary of the high-throughput screening result of hydrazide derivatives for the HDAC8 inhibitor/activator.....	126
5.7. Summary of the high-throughput screening of the miscellaneous compounds for the HDAC8 inhibitors/activators.....	128
5.8. Inhibition potency of fluorescent analogs of SAHA as well as other the hydroxamate inhibitors of HDAC8.....	133
5.9. Summary of the high-throughput screening result of the hydroxamate derivative of the cinnamic acid for the HDAC8 inhibitors/activator.....	136
5.10. Inhibitory potency of hydroxamate inhibitors containing the pyrene moiety as a cap.....	139
5.11. Summary of the inhibition data of the urea derivatives of 2-amino-5-mercapto, 1, 3, 4, - thiodiazole.....	141

5.12. Summary of the high-throughput screening result of the cinnamic acid derivatives of o-phenylenediamine for an HDAC8 inhibitor/activator.....	142
5.13. Summary of the high-throughput screening result of the <i>cyclen</i> -based compounds for an HDAC8 inhibitor/activator.....	145
5.14. Summary of the high-throughput screening of the miscellaneous compounds for the HDAC8 inhibitor/activator.....	148
5.15. Activation/inhibition of HDAC isozymes at 100 μM of compound.....	151
5.16. Steady state enzyme kinetic parameters of the HDAC8 catalyzed reaction in the absence and presence of the activator at 50 μM	153
5.17. The apparent activation constant and the Hill-coefficient for the binding of TM-2-51 to HDAC8 determined at various concentration of SAHA.....	155
5.18. The inhibition constant (K_i) of the HDAC8-SAHA complex measured at various concentrations of TM-2-51.....	156
5.19. Comparison between K_i and K_d values of HDAC8 inhibitors.....	160
5.20. Comparison of K_d calculated from transient kinetic method with spectrofluorometric titration.....	172
5.21. Summary of the thermodynamic parameters for the binding of TSA, SAHA, and VYU-2-24 at 25 $^{\circ}\text{C}$	182
5.22. Intrinsic enthalpy for the binding of inhibitors to HDAC8.....	186
5.23. Effect of buffers on the binding of TSA to HDAC8 at 25 $^{\circ}\text{C}$	187
5.24. Effect of buffers on the binding of SAHA to HDAC8 25 $^{\circ}\text{C}$	188
5.25. Effect of buffers on the binding of VYU-2-24 to HDAC8 25 $^{\circ}\text{C}$	189
5.26. Temperature dependence of ITC parameters for the binding of TSA to HDAC8.....	192
5.27. Temperature dependence of thermodynamic parameters for the binding of SAHA to HDAC8.....	193
5.28. Temperature dependence of thermodynamic parameters for the binding of VYU-2-24 to HDAC8.....	194
5.29. Activation parameters for the bimolecular step of the binding of TSA and SAHA to HDAC8.....	204
6.1. Transient kinetic parameters for the interaction of TSA and SAHA with HDAC8.....	234

LIST OF FIGURES

<u>Figure</u>	<u>Page</u>
1.1. The classification of human HDACs.....	4
1.2. The stereo view of the HDAC8-SAHA complex is shown in stick model.....	16
1.3. Ribbon structure of human HDAC8 bound with a p-53-derived deacetylated substrate.....	17
1.4. Enlarged view of the two potassium ion binding sites depicted as K1 and K2.....	18
1.5. The proposed mechanism of the HDAC8 catalyzed reaction.....	20
1.6. (A)The space filling model of the HDLP active site pocket (11Å) bound with Trichostatin A (TSA). (B) The superimposed surface representation of HDLP (blue) and HDAC8 (yellow) internal cavities.....	21
1.7. The surface representation of human HDAC2 bound to a benzamide inhibitor.....	23
1.8. The ribbon structure of HDAC3 bound to a SMRT-DAD and inositol tetrphosphate (IOP).....	25
1.9. Superposition of the ribbon structure of HDAC8 (yellow) and HDAC3 (green).....	25
1.10. The ribbon structure of the catalytic domain of HDAC4 (cdHDAC4) bound to a trifluoromethylketone (TFMK) inhibitor.....	27
1.11. The stereo view of HDAC4 active site bound to a hydroxamic inhibitor.....	29
1.12. The superposition of the ribbon structure of HDAC8 (red) and cdHDAC4 (grey).....	30
1.13. (A) The stereo view of the superimposed active site residues of the GOF HDAC4-TFMK [pdb 2VQO] and the HDAC8-SAHA [pdb 1T69] complexes. (B) The stereo view of the superimposed active site residues of the GOF HDAC4-HA [pdb 2VQV] and HDAC8-SAHA [pdb 1T69] complexes.....	31
1.14. The ligation scheme of structural the zinc ion of HDAC4.....	32
1.15. The stereo view of the metal binding sites of HDAC7.....	34
5.1. The vector map of the pCMV-SPORT.....	86
5.2. The vector map of the pLIC-His vector used for cloning the human HDAC8 gene.....	87
5.3. The ligation independent cloning strategy for the sub-cloning of the human HDAC8 gene.....	88

5.4. The agarose gel electrophoresis showing the PCR amplified HDAC8 gene using the pLIC compatible forward and reverse primers.....	89
5.5. The elution profile of the HDAC8-His6 from the Ni ²⁺ IDA HisTrap™ HP column.....	91
5.6. The SDS-PAGE showing the purity of the HDAC8-His6 at different stages of purification.....	91
5.7. Schematic representation of the trypsin-coupled assay to measure the initial rate of the HDAC8 catalyzed reaction.....	94
5.8. The excitation and the emission spectra of the fluorogenic substrate (Fluoro-de-Lys™) and the final product of the trypsin-coupled assay.....	95
5.9. Measurement of the initial velocity of the HDAC8 catalyzed reaction employing the trypsin-coupled assay.....	95
5.10. Steady state kinetic traces for determining the initial rate of the HDAC8 catalyzed reaction measured as function of the coupling enzyme (trypsin) concentration in the trypsin-coupled assay.....	96
5.11. The initial velocities of the HDAC8 catalyzed reaction as a function of substrate concentration.....	98
5.12. Standard curve prepared from the fluorescence end point reading of the known concentration of the fluorophore.....	99
5.13. UV-visible spectrum of the recombinant form of human HDAC8.....	100
5.14. Circular Dichroism spectrum in the far-UV region of 8 μM HDAC8.....	101
5.15. Analysis of Circular Dichroism spectrum of HDAC8 using DichroWeb.....	102
5.16. Steady state fluorescence emission spectra of 1.5 μM HDAC8.....	104
5.17. Quenching of steady state fluorescence of HDAC8 upon binding to TM-2-51.....	104
5.18. Steady state kinetics for the inhibition of HDAC8 enzyme activity by VYU-2-24, VYU-2-221, VYU-2-270 and VYU-3-54.....	111
5.19. Steady state kinetics for the inhibition of HDAC8 enzyme activity by VYU-3-56, VYU-2-136, VYU-2-219, and VYU-2-134.....	112
5.20. Steady state kinetics for the inhibition of HDAC8 enzyme activity by SAHA, TM-2-3 (c-SAHA), TSA, SBHA and M-334.....	134
5.21. Steady state kinetics for the inhibition of HDAC8 enzyme activity by MH-9/34B, MH-9/35B, MH-9/36B, MH-9/37B, MH-9/38B, and MH-9/39B.....	137

5.22. Steady state kinetics for the inhibition of HDAC8 enzyme activity by MH-9/40B, MH-9/41B, MH-9/42B, and MH-9/44B.....	138
5.23. Steady state kinetics for the inhibition of HDAC8 enzyme activity by MH-12/4, MH-12/5, MH-12/6, MH-12/7, MH-12/9, and MH-12/11.....	140
5.24. Initial velocities of the HDAC8 catalyzed reaction as a function of substrate concentration in the presence of 50 μ M TM-2-51.....	152
5.25. The cooperative binding of TM-2-51 to HDAC8.....	155
5.26. Excitation and fluorescence emission ($\lambda_{\text{ex}} = 325$ nm) spectra of c-SAHA.....	158
5.27. Binding isotherm for the interaction c-SAHA with HDAC8.....	159
5.28. Time-resolved fluorescence decay ($\lambda_{\text{ex}} = 340$ nm, $\lambda_{\text{em}} = 400$ nm) curves for the free (left panel) and the enzyme-bound form (right panel) of c-SAHA.....	159
5.29. Determination of binding affinity of the representative HDAC8 inhibitors using the c-SAHA as a fluorescent probe.....	160
5.30. Binding isotherms for the interaction of TSA, SAHA, and VYU-2-24 with HDAC8.....	162
5.31. Binding isotherm for the interaction of TM-2-51 with HDAC8.....	163
5.32. Transient kinetics of the interaction of TSA with HDAC8.....	168
5.33. Transient kinetics of the interaction of SAHA with HDAC8.....	169
5.34. Transient kinetics of the interaction of VYU-2-24 with HDAC8.....	170
5.35. Representative stopped-flow traces for the dissociation of the enzyme-bound HDAC8 inhibitor	173
5.36. Transient kinetics of the interaction of c-SAHA with HDAC8.....	177
5.37. Representative stopped-flow trace for the dissociation of the bound coumarin-SAHA from HDAC8.....	177
5.38. Representative ITC profile for the binding of TSA to HDAC8.....	182
5.39. Representative ITC profile for the binding of SAHA to HDAC8.....	183
5.40. Representative ITC profile for the binding of VYU-2-24 to HDAC8.....	184
5.41. Dependence of the ΔH^0_{obs} for the binding of TSA to HDAC8 on the ΔH^0_{ion} of different buffers.....	187
5.42. Dependence of the ΔH^0_{obs} for the binding of SAHA to HDAC8 on the ΔH^0_{ion} of different buffers.....	188

5.43. Dependence of the ΔH^0_{obs} for the binding VYU-2-24 to HDAC8 on the ΔH^0_{ion} of different buffers.....	189
5.44. Enthalpy-entropy compensation plot for the binding of TSA to HDAC8.....	192
5.45. Enthalpy-entropy compensation plot for the binding of SAHA to HDAC8.....	193
5.46. Enthalpy-entropy compensation plot for the binding of VYU-2-24 to HDAC8.....	194
5.47. Effect of temperature on the enthalpy of binding (ΔH^0) of TSA to HDAC8.....	195
5.48. Effect of temperature on the enthalpy of binding (ΔH^0) of SAHA to HDAC8.....	195
5.49. Effect of temperature on the enthalpy of binding (ΔH^0) of VYU-2-24 to HDAC8.....	196
5.50. Titration of the free and SAHA-bound form of HDAC8 by TM-2-51.....	200
5.51. Titration of the TM-2-51-bound form of HDAC8 by SAHA.....	201
5.52. Temperature dependence of the relaxation rate constants for the bimolecular and the isomerization step of the HDAC8 interaction with TSA and SAHA.....	204
5.53. Arrhenius plots for the forward (k_{+1}) and reverse (k_{-1}) rate constants for association step for the interaction of TSA to HDAC8.....	205
5.54. Arrhenius plots for the forward (k_{+1}) and reverse (k_{-1}) rate constants for association step for the interaction of SAHA to HDAC8.....	205
5.55. Arrhenius plots for the observed dissociation off-rate of TSA and SAHA measured using c-SAHA.....	207
5.56. The steady state emission spectra of 2 μM of the native (black trace) and the GdmCl-denatured form (red trace) of HDAC8.....	210
5.57. Guanidinium chloride induced unfolding of the free (Panel A) and SAHA-bound form (Panel B) of HDAC8 as monitored by the change in the ratio of the fluorescence emission intensities at 354 nm and 341 nm ($\lambda_{\text{ex}} = 295 \text{ nm}$).....	210
5.58. Temperature dependence of the ellipticity at 222 nm of 8 μM of the free and the SAHA-bound form of HDAC8.....	212
5.59. The Ligand induced alteration in the secondary structure of HDAC8.....	213
5.60. Effect of the binding of VYU-2-24 on the Tryptophan fluorescence life time of HDAC8.....	215
6.1. The interaction of CRA-A with HDAC8.....	219
6.2. Molecular docking of TM-2-51 to HDAC8.....	225

6.3. Closer view of the HDAC8-substrate-TM-2-51 complex.....	225
6.4. Interaction between dimethyl aniline moiety of TSA and Y100 in HDAC8-TSA complex.....	228
6.5. The hydrogen-bonding interaction between HDAC8 and SAHA.....	233
6.6. Free energy profile for the binding of TSA and SAHA.....	234
6.7. Enthalpic profile for the bimolecular complexes of HDAC8 with TSA and SAHA.....	235

LIST OF SCHEMES

<u>Scheme</u>	<u>Page</u>
4.1. Trypsin-coupled assay.....	70
4.2. Measurement of dissociation off-rate of HDAC8 inhibitor.....	79
4.3. Two step unfolding of protein.....	82
5.1. Two step binding mechanism of HDAC8 inhibitors.....	167
5.2. Dissociation kinetics of HDAC8 inhibitors from the enzyme's site.....	171
5.3. Two step binding mechanism for the association c-SAHA to HDAC8.....	175
5.4. Dissociation kinetics of c-SAHA from the enzyme's site	176

LIST OF ABBREVIATIONS

HDAC.....	Histone Deacetylase
Pfu.....	<i>Pyrococcus furiosus</i>
Sac II.....	Benzotriazole-1-yl-oxy-tris-dimethylamino)-phosphonium
PMSF.....	Phenylmethylsulfonyl fluoride
SAHA.....	Suberoylanilide hydroxamic acid
TSA.....	Trichostatin A
c-SAHA.....	Coumarin-SAHA
SBHA.....	Suberoyl bis-hydroxamic acid
M-344.....	4-Dimethylamino-N-(6-hydroxycarbonylhexyl)-benzamide
LIC.....	Ligation independent cloning
DMSO.....	Dimethylsulfoxide
HDAC8.....	Histone Deacetylase 8
IDA.....	Iminodiacetic acid
ITC.....	Isothermal titration microcalorimetry
min.....	Minute
PAGE.....	Polyacrylamide gel electrophoresis
PCR.....	Polymerase chain reaction
s.....	Second
SDS.....	Sodium dodecyl sulfate
TCEP.....	tris-2 carboxy ethyl phosphine

CHAPTER 1. INTRODUCTION

1.1. A Literature Review on Human Histone Deacetylase

1.1.1. Epigenetics and Histone Code

In a eukaryotic cell a chromatin structure is comprised of DNA and histones. A nucleosome, the basic unit of chromatin, consists of an octamer (two copies each of H2A, H2B, H3 and H4) wrapped with 147 bp of DNA. The chromatin is essentially a very compact structure mainly due to the electrostatic interaction between DNA and histone [1]. In order to carry out the basic chromatin functions, such as transcription, replication, and repair, the chromatin has to be decondensed and made accessible to enzyme/transcription factors. The decondensation is mainly mediated via the acetylation of lysine residue of histone tail thereby neutralizing its positive charge. Aside from the acetylation, the histone tail undergoes several other types of posttranslational modifications (PTMs), such as methylation, phosphorylation, ubiquitination, etc. These PTMs modulate the chromatin structure by altering the interactions between DNA and histone in addition to recruiting several proteins which serve as chromatin remodelers. More importantly, it provides a unique signature to the specific region of chromatin referred to as “histone code” which leads to a unique downstream cellular function [2].

More than 60 different residues of a histone tail undergo different types of PTMs as summarized in Table 1.1 [3]. In addition, several lysine residues of the globular (core) region of histones are the target of the post-translational modification system. The PTM system of histone essentially has three components, namely, writer, eraser and interpreter [4]. For example, Histone Acetyltransferase (HAT) catalyzing the acetylation of lysine residue serves as the writer. The removal of the acetyl group is mediated via Histone deacetylase (HDAC) working as eraser. The DNA-binding proteins containing the specific domain such as bromo and chromo domain

function as an interpreter. Notably, the above processes are dynamic in nature and the status of a PTM is contingent on the nature of the external stimuli that cells encounter [5].

Table 1.1. Different types of post-translational modifications (PTMs) of Histone [4]

PTM type	Target Residue	Enzymes (Writer/eraser)	Interpreter of PTM
Unmodified lysine	K	-----	PHD
Acetylation	K	HAT/HDAC	Bromodomain
Methylation	K/R	Methylase/Demethylase	HEAT, MBT, PHD, Tudor
Phosphorylation	S/T	Kinase/Phosphatase	14-3-3, BIR, BRCT
Ubiquitination	K	Enzymes of ubiquitin system	?
Sumoylation	K	Enzymes of SUMO conjugation/cleavage	?
ADP-ribosylation	K	ADP-ribosyltransferase	?
Butyrylation	K	?	?
Propionylation	K	Propionyltransferase/ Depropionylase (Sirt1)	?

It has been widely known that the PTMs of histone work in a combinatorial fashion forming a “histone code” where the multiple PTMs collectively lead to a unique downstream function in gene regulatory pathway [2]. As a result of that, cells possessing even the same sequence of DNA attain a different morphology and undergo tissue specification via the process of cell differentiation. A differentiated cell thereafter transfers its unique signature acquired in the form histone code to the daughter cells during the cell division. This phenomenon forms the basis of “epigenetics”, which is the study of inheritable characters mediated via the factors other than the DNA sequence [5, 6]. In order to understand the meaning of the histone code in terms of the cellular function extensive studies have been carried out in various laboratories. However, there is still a debate among scientists whether a strict code in the form of histone PTMs truly exists.

1.1.2. Classification and Functions of Human HDACs

HDACs or their homologs are found in all major forms of life i.e., archaeobacteria, prokaryotes and eukaryotes [7, 10]. Based on a sequence homology, HDACs have been classified into four classes. Class I, II and IV are NAD⁺ independent enzymes whereas class III enzymes are unrelated and require NAD⁺ as a co-substrate. The class III enzymes are also named as Sirtuins in humans because they share a homology with a protein “Sir” found in yeast [11]. The primary aim of the proposed research work for this dissertation was to investigate the physiochemical properties of human HDAC8; hence a thorough literature review on this enzyme is presented here.

Figure 1.1 shows the classification of human HDACs based on their sequence homology and the structure of the catalytic domain (~350 amino acids) [12]. The 18 HDACs identified in humans so far, are classified into four major classes. Class I HDACs (HDAC1, 2, 3 and 8) share a high degree of similarity with Rpd3, a transcriptional regulator of yeast. Class II HDACs, which are homologs of the Hda1 of *Saccharomyces cerevisiae*, are further classified into IIa (HDAC4, 5, 7 and 9) and IIb (HDAC6 and 10) based on the sequence homology and structural features of the catalytic domain. Class III HDACs (Sirtuins) are unrelated to all other HDACs, and require NAD⁺ as a cofactor for catalyzing the deacetylation reaction. Unlike Class I and II HDACs, the reactions catalyzed by Sirtuins are metal independent. Due to a poor gene sequence homology of HDAC 11 with other HDACs, it has been categorized under a separate Class IV [13]. The cloning and characterization of human HDAC isozymes have been reviewed by Gray *et al.* [14]. The characteristic features of different isozymes of human HDAC have been summarized in Table 1.2-1.4. Due to the involvement of various HDAC isozymes in several human diseases, there have been growing interests in discovering small molecule

inhibitors/activators of these enzymes which could potentially be used to alleviate the disease conditions as described in the subsequent section.

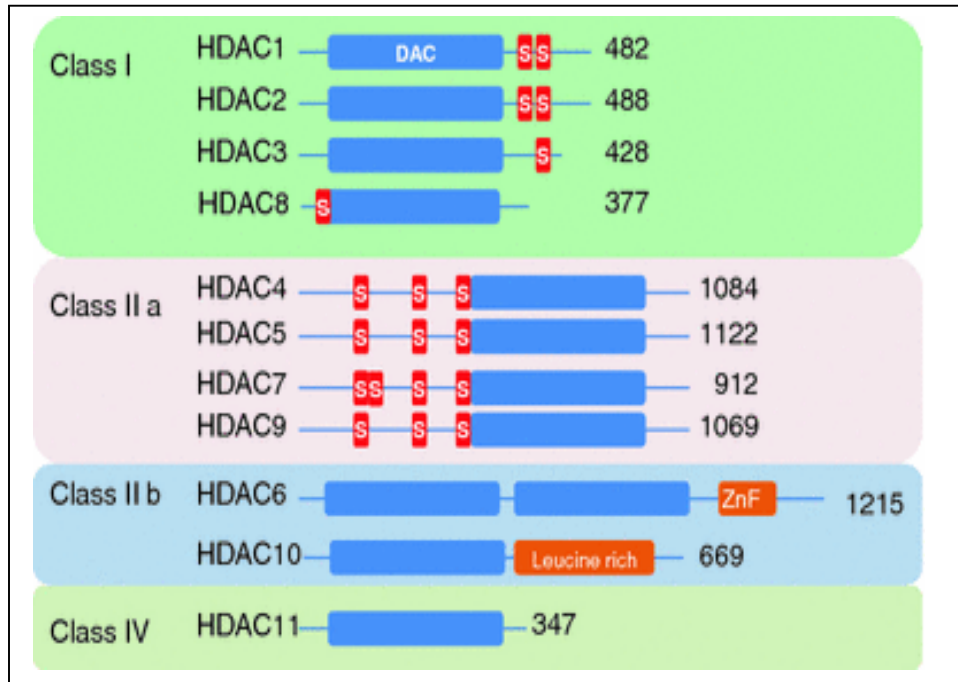


Figure 1.1. The classification of human HDACs. The blue color represents the catalytic domain. The serine residues which undergo phosphorylation are shown by red color. The number at right represents the size of the full length protein. Adapted from ref. [12]

Table 1.2. Characteristics of human HDAC class I [10, 12, 14]

	Class I HDACs			
	HDAC1	HDAC2	HDAC3	HDAC8
Cellular Localization	Nucleus	Nucleus	Nucleus	Nucleus
Chromosomal localization	1p34.1	6q21	5q31	Xq13
Molecular Size (AAs)	482	488	428	377
Tissue distribution	Ubiquitous	Ubiquitous	Ubiquitous	Ubiquitous
Non-histone substrate	Androgen receptor, SHP, p 53, MyoD, EF2, Stat3	Glucocorticoid receptor, YY-1, Bcl-6, Stat3	SHP, YY-1, GATA-1, RelA, Stat3, MEF-2D,	SMC3
Interacting partners	Sin3, SAP30, HDAC2	P66,Mi2,LSD1,RbAp6, HDAC1	CDK9, SP1, PP4c, KDM4A,N-CoR/SMRT	EST1B
Knockout phenotype in mice (Global deletion)	Lethal (developmental defects)	Lethal (developmental defects)	Lethal (gastrulation defects)	Perinatal lethal (skull instability)

Table 1.3. Characteristics of human HDAC class IIa [10, 14]

	Class IIa HDACs			
	HDAC4	HDAC5	HDAC7	HDAC9
Cellular Localization	Cytosol/nucleus	Cytosol/nucleus	Cytosol/nucleus	Cytosol/nucleus
Chromosomal localization	2q37.2	17q21	12q13	7p21-p15
Molecular Size (AAs)	1084	1122	855	1011
Tissue distribution	Heart, smooth muscle, bone	Heart, smooth muscle, bone	Smooth muscle, heart, placenta, pancreas	smooth muscle, bone
Non-histone substrate	ANKRA, RFXANK	CAMPTA, REA, estrogen receptor	FOX3P, HF-1 α , Bcl-6, endothelin receptor	FOX3P
Interacting partners	RUNX2,GATA	GATA, GCMA,	α -actinin, dndogen receptor, Tip60	
Knockout phenotype in mice (Global deletion)	Defect in chondrocyte differentiation	Cardiac defect	Reduction in vascular integrity	Cardiac defect

Table 1.4. Characteristics of human HDAC class IIb [10, 14]

	Class IIb HDACs		
	HDAC6	HDAC10	HDAC11
Cellular Localization	Mostly Cytosol	Mostly Cytosol	Cytosol/nucleus
Chromosomal localization	Xp11.22-23	22q13.31-q13.33	3p25.2
Molecular Size (AAs)	1215	669	347
Tissue distribution	Heart, lung, kidney, pancreas	Heart, smooth muscle, kidney	Smooth muscle, heart, bone, kidney
Deacetylase activity	Weak	Weak	Weak
Non-histone substrate	A-tubulin, HSp90, SHp, Smad7		
Interacting partners	RUNX2,GATA	RUNX2	
Knockout phenotype in mice (Global deletion)	Cardiac defect		

1.1.2.1. Functions of Class I HDACs

1.1.2.1.1. HDAC1 and HDAC2. HDAC1 was the first among all HDACs identified in humans followed by others which have been named according to the chronological order of their discovery [10]. HDAC1 and HDAC2 share approximately 82 % sequence homology and contain a single catalytic domain. They have several binding partners in common, such as Sin3, NuRD and Co-REST [15, 16]. The catalytic domain is located in the N-terminal region of the protein. The deacetylase activity of these enzymes is modulated in the presence of the co-repressors. HDAC1 and 2 are exclusively localized in the nucleus due to lack of a nuclear export signal (NES) [10]. Despite a high degree of similarity, these two enzymes are not redundant in their function. For example, the homozygous disruption of HDAC1 is lethal due to abnormal embryonic development which cannot be mitigated by the presence of HDAC2 [17]. Both HDAC1 and HDAC2 undergo a post-translational modification mainly via phosphorylation at multiple serine residues (421, 424 in HDAC1 and 422, 424 in HDAC2) [18]. They contain a tandem casein-kinase phosphorylation sites in the C-terminal region. The catalytic activity, as well as the ability to associate with other interacting partners, is regulated via phosphorylation. The hyper-phosphorylation of HDAC1 and 2 increases the enzyme activity but it reduces their interactions with other binding partners such as, RbAp48, MTA-2, Sin3A, and CoREST [16].

HDAC1 and 2 have been involved in variety of physiological processes and have been extensively review by Nina Reichert *et al.* [12]. The progression of the cell cycle in the cells of B-cell lineage is regulated by a concerted activity of HDAC1 and 2. The global deletion of HDAC1 and 2 in mice leads to death in the early developmental stage. Witting *et al.* has described the roles of HDAC1 and 2 in hematopoiesis [19]. Dover *et al* reported that HDAC1 cannot substitute the role of HDAC2 in embryonic stem cell differentiation [12]. In HDAC1

deficient mice, the cell cycle inhibitors, such as p21 and p27 are up-regulated leading to an inhibition in cell proliferation [20]. This finding rationalizes the utility of an HDAC inhibitor for preventing the growth of cancer cells. Deficiency of HDAC1 and 2 in the central nervous system of mice causes an aberration in cortical, hippocampal and cerebellar region of the brain leading to postnatal death [21]. Additionally, a Schwann cell deficient in HDAC1 and 2 are devoid of a myelin sheath [22].

HDAC1 and 2 do not interact to DNA directly. They usually associate with transcription factors, such as SP1, p53, pRb, Tbx2, NF- κ B, MyoD, etc., in order to regulate the transcription of myriad variety of genes. Recently, HDAC1 and 2 have been reported to play crucial role in non-homologous end joining in response to DNA damage [23].

1.1.2.1.2. HDAC3. HDAC3 contains a single catalytic domain (Figure 1.1). It differs from both HDAC1 and HDAC2 in terms of sequence homology as well as its binding partners [10]. However, it is evolutionarily closer to HDAC8 with a sequence homology of 34 %. Notably, a non-conserved C-terminal region is also essential for the catalytic activity as well as its ability to recruit various proteins, such as SMRT/N-CoR and other nuclear hormone receptors [24]. HDAC3 contains both a nuclear localization signal as well as a nuclear export signal, and its sub-cellular localization is dependent on the cell type and environmental conditions. It interacts with almost every isozyme of class II HDACs, namely, HDAC4, 5, 7 and 10. It contains a single casein-kinase phosphorylation site unlike HDAC1 and 2. The HDAC3 enzyme activity as well as its interaction with SMRT/N-CoR is regulated via phosphorylation at Ser 424 [25]. Recently, Peter J. Watson *et al.* has described the significance of inositol tetrakisphosphate in the activation of HDAC3 [26]. A global deletion of HDAC3 in mice impairs embryonic development leading to death during gastrulation [27].

1.1.2.1.3. HDAC8. HDAC8 was first cloned and characterized by three independent research groups [28-30]. It has several unique features differentiating it from other HDAC isozymes. HDAC8 contains a nuclear localization signal (NLS) at the center of the catalytic domain, and it has been reported to be localized in nucleus. However, David Waltregny *et al.* reported the cytosolic localization of HDAC8 in muscle cell [31]. Two transcript variants of different length namely 2.0 kb and 2.4 kb have been identified, which are produced due to an alternative splicing of the RNA primary transcript. HDAC8 does not associate with any co-repressors; presumably, due to the lack of an extra C-terminal region [32]. Unlike HDAC1 and 2, the catalytic activity of HDAC8 is reduced upon phosphorylation at Ser 39 residue localized in the catalytic domain [33]. Haberland *et al.* reported that the global deletion of HDAC8 in mice leads to prenatal death due to instability of skull [34]. The HDAC8 expression level has been correlated with neuroblastoma tumorigenesis where an HDAC8 selective inhibitor has potential to alleviate the disease condition [35]. In Cornelia de Lange syndrome, the cohesin acetylation cycle has been reported to be impaired due to mutations in the HDAC8 gene [36]. The enzyme activity of Class I HDACs including HDAC8 has been found to be reduced in Chronic Obstructive Pulmonary Disease (COPD) [37]. HDAC8 forms a complex with protein phosphatase 1 (PP1), which leads to the inactivation of CREB mediated transcription. Both HDAC1 and HDAC8 are involved in dephosphorylation of Ser 133 of CREB in association with PP1 [38]. Durst *et al.* have reported that the inv (16) produces an oncogenic fusion protein (CBF β -SMMHC) in acute myeloid leukemia, which reportedly associates with HDAC8 [39]. Their interaction is disrupted in the presence of an HDAC8 inhibitor, suggesting the therapeutic utility of an HDAC8 selective inhibitor in acute myeloid leukemia.

1.1.2.2. Functions of Class II HDACs

1.1.2.2.1. HDAC 4, HDAC5, HDAC7 and HDAC9 (HDAC class IIa). Class IIa HDACs contain a catalytic domain located in the C-terminal region of the protein. The N-terminal region serves as an adaptor domain, and it helps in the recruitment of co-repressors/transcription factors which modulate the function of HDACs [40]. The phosphorylation of multiple serine residues of the adaptor region has a profound influence in the interaction of Class IIa HDACs with other binding partners. The catalytic activity of HDAC class IIa is regulated primarily via tissue specific gene regulatory factors, recruitment of distinct interacting partners and nucleocytoplasmic shuttling. The physiological functions of HDAC IIa has been extensively review by Martin *et al.* [41]. Class IIa HDACs have several interacting partners in common, such as, HDAC3, nuclear receptors, N-CoR, B-CoR and SMRT complexes and muscle specific transcription factor (MEF2) [40, 41]. HDAC4 binds with MEF 2 (Myocyte Enhancer Factor 2), and their association is essential for muscle differentiation as well as for the inhibition of cardiomyocyte hypertrophy [42, 43]. HDAC5 and HDAC9 inhibit the cardiac hypertrophy which is stimulated due to a stress signal [44]. Dequiedt *et al.* described the role of HDAC7 TCR-mediated apoptosis [45]. Notably, the above class IIa HDAC mediated cellular processes are independent of their deacetylase activity. In fact, class IIa HDACs show a very weak deacetylase activity on a standard acetylated substrate [46, 47]. HDAC9 has been cloned and characterized by Zhou *et al.* [48]. It has three known splice variants (HDAC9a, HDAC9b and HDAC9c), and its catalytic domain in located in the N-terminal region. HDAC9 plays important role in muscle differentiation, and one of its variants has recently been linked with large vessel ischemic stroke [48].

1.1.2.2.2. HDAC6 and HDAC10 (HDAC class IIb). HDAC6 and HDAC10 share 37 % sequence homology in their genes [10]. HDAC6 contains two catalytic domains in tandem. HDAC10 contains one full catalytic domain and an additional vestigial domain. It is not yet clear whether HDAC6 requires both the catalytic domains to catalyze the deacetylation reaction. HDAC6 is primarily localized in the cytosol and it catalyzes the deacetylation of tubulin, which is a key protein involved in cell motility and cell-cell interaction [49, 50]. HDAC6 has been linked to Autophagy and Ubiquitin-proteasome system (UPS), which clears out the misfolded proteins in neurons [51]. It is co-localized with cylindromatosis (deubiquitinating enzyme) and is involved in the regulation of cell proliferation. HDAC6 is susceptible to degradation via a ubiquitination pathway because of the HUB domain located in C-terminal region [52]. Additionally, HDAC6 is involved in several cellular processes such as, apoptosis, inflammation, platelet activation, and metabolic responses which have been extensively reviewed by Li *et al.* [51]. It does not interact with any other HDACs except HDAC 11 present inside nucleus. HDAC10 is predominantly found in the nucleus and is known to interact with HDAC3 and SMRT. HDAC10 has been cloned and characterized by Fischer *et al.* [53]. It is localized both in the nucleus as well as in the cytoplasm. It contains a single N-terminal catalytic domain. A pseudo-repeat of catalytic domain, which harbors at C-terminal region, shares a homology with the catalytic domain. The transcription repression mediated via HDAC10 is dependent on the deacetylase activity of the catalytic domain.

1.1.2.3. Functions of Class IV HDAC

HDAC11 has been cloned and characterized by Gao *et al.* [54]. HDAC11 has a poor gene sequence homology with other human HDACs. Thus, a separate class of HDAC (class IV) has been made in the HDAC phylogenetic tree. HDAC11 contains a catalytic domain in the N-

terminal region, shows catalytic activity with the standard acetylated substrate and is inhibited trapoxin [54]. So far, no binding partners of HDAC11 have been identified. Moreover, its physiological significance is yet to be thoroughly investigated.

1.2. Crystallographic Studies of Human HDACs

The catalytic domain of human HDACs, namely, HDAC2, HDAC3, HDAC4, HDAC7 and HDAC8 have been cloned, expressed and purified from heterologous host, and their crystal structures have been solved in different laboratories [55]. They contain an α/β -deacetylase domain comprising a catalytic machinery for the deacetylation reaction. The active site contains a penta-coordinated catalytic Zn^{2+} ion showing a square pyramidal geometry. The HDAC residues co-coordinating with the Zn^{2+} are well conserved among different isozymes. The crystal structure of HDPL (from *Aquifex aeolicus*), a bacterial homolog of human class I HDAC HDLP which shares 35.2 % sequence homology with human HDAC1, has been solved by Finnin *et al.* [56]. HDLP shows an enzyme activity with acetylated histone substrate and is inhibited by canonical HDAC inhibitors, such as TSA and SAHA. However, the functional significance of this protein in bacteria has not been identified yet. Among all HDAC isozymes, HDAC8 serves as prototype for studying the structure-activity relationship for an HDAC catalyzed reaction, presumably, because of the ease in its purification from a heterologous host, as well as its structure determination by X-ray crystallography.

1.2.1. Crystal Structure of Human HDAC8

The crystal structures of human HDAC8 have been primarily solved by two independent research groups [57, 58]. HDAC8 was the first among the HDAC isozymes whose crystal structure became available. Figure 1.2 shows the ribbon structure of HDAC8 bound with a canonical hydroxamate inhibitor, SAHA (Suberoylanilide Hydroxamic Acid) [pdb 1T69].

HDAC8 contains a single α/β -deacetylase domain consisting of 13 α -helices and an eight-stranded parallel β -sheet. Multiple loops, which emanate from the protein core, play a significant role in maintaining the appropriate geometry of the catalytic pocket. The α/β -fold of the above kind was first observed in a metalloenzyme, Arginase. The active site of HDAC8 contains a tubular cavity leading to catalytic machinery at the end. The catalytic machinery is comprised of a Zn^{2+} ion penta-coordinated with a square pyramidal geometry. The residues His 180, Asp 267 and Asp 176 occupy the three co-ordination sites, whereas the hydroxamate moiety of SAHA occupies the remaining two sites. In addition, the carbonyl oxygen of the hydroxamate moiety forms a hydrogen bond with Tyr 306. In the absence of any ligand (substrate/inhibitors), two water molecules are bound to the Zn^{2+} ion. The linker domain of the inhibitor interacts with the residues, namely, Phe 152, Phe 208, His 180, Gly 151, and Met 274, which forms a hydrophobic tunnel. Notably, the above residues involved in the inhibitor/substrate binding, as well as the catalysis, have been found to be conserved during the course of evolution among class I HDACs.

The crystal structure of a mutant (Y306A) and catalytically inactive form of HDAC8 bound with a p53-derived deacetylated peptide substrate (pdb 2V5W) has been solved by Vannini *et al.* (Figure 1.3) [59]. The structure is very similar to the HDAC8-inhibitor complex reported previously except for the mode of binding of the ligand. The carbonyl moiety of the acetyl-lysine binds to the catalytic Zn^{2+} in a monodentate fashion by removing one of the zinc-bound water molecules. However, the hydroxamate moiety of a competitive HDAC inhibitor binds to the Zn^{2+} ion in a bidentate fashion, removing both of the Zinc-bound water molecules. Notably, a single Zinc-bound water molecule present in the HDAC8-substrate complex serves as a nucleophile in the deacetylation reaction. In addition, it makes hydrogen bonding with the N ϵ 2 atom of imidazole of His 142 and His 143, which reportedly form a charge-relay system,

respectively, with Asp 176 and Asp 183. The charge-relay system enhances the basicity of the N ϵ 2 of the imidazole and has been reported previously in serine proteases [57]. Notably, the carbonyl oxygen of the acetyl-lysine substrate forms a hydrogen bond with the hydroxyl moiety of Y306.

Aside from the catalytic Zn²⁺ ion, the enzyme activity of HDAC8 is dependent on the presence of the monovalent ion, K⁺/Na⁺ [60]. The crystal structure of HDAC8 shows the presence of two binding sites for K⁺ (Figure 1.4) [58]. The first K⁺ binding site (K1) is located in the vicinity of the enzyme catalytic machinery, and it is hexacoordinated (octahedral geometry) with His 180 (carbonyl oxygen of the main chain), Asp 176 (oxygen atom of the main chain and side chain), Leu 200 (carbonyl oxygen of the main chain), and Ser 199 (O γ). Notably, His 180 and Asp 176 are the common residues coordinated with both the catalytic Zn²⁺ as well as the K⁺ ion. The second binding site for K⁺ ion (K2) is located 15Å away from the catalytic Zn²⁺ ion. It is hexacoordinated (octahedral geometry) with F189, T192, V195, Y225 as well as two water molecule (Figure 1.4). Gantt *et al.* reported that the binding of a K⁺ ion to K1 and K2, respectively, leads to the inhibition and activation in HDAC8 deacetylase activity [60]. Additionally, the presence of K⁺ ion at K1 site neutralizes the positive charge of tetrahedral oxyanion intermediate produced during the deacetylation reaction. It is important to note that the HDAC8 residues binding to the K⁺ ions are strictly conserved among class I HDACs [58].

The crystal structure of HDAC8-substrate complex (pdb 2V5W) elucidates the role of an aspartate residue (D101) in the substrate binding [59]. Asp 101 resides on the L2 loop and its carboxylate moiety makes two consecutive hydrogen bonds with the backbone of the p53-derived deacetylated peptide substrate as shown in Figure 1.3. Mutation of Asp 101 to Ala abolishes the HDAC8 catalytic activity, signifying its role in substrate binding. More

importantly, the Asp residue has been found to be strictly conserved among different HDAC isozymes, further emphasizing its importance in the substrate binding.

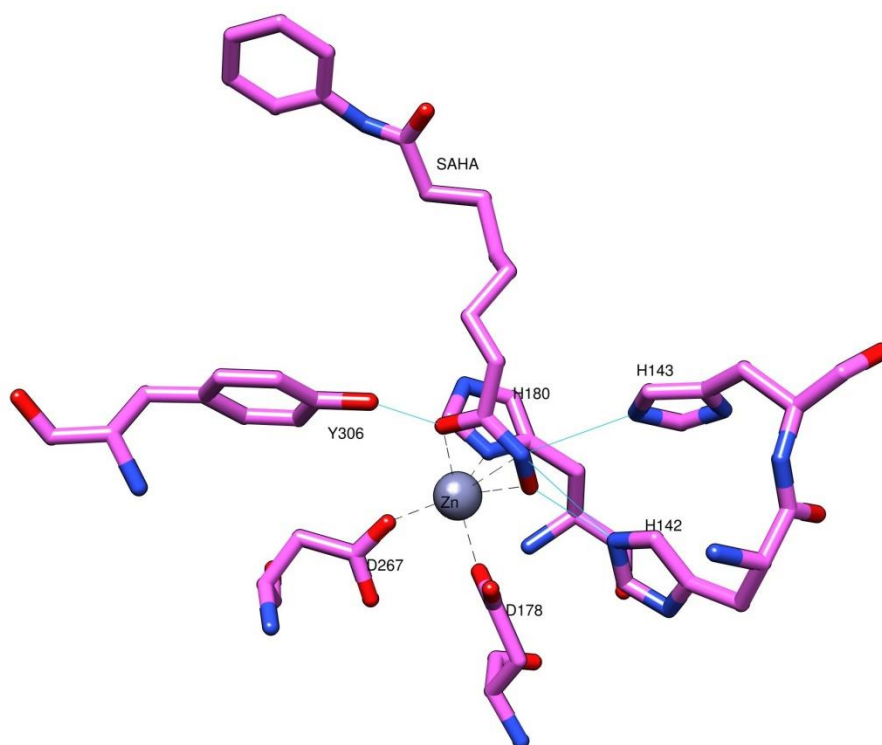


Figure 1.2. The stereo view of the HDAC8-SAHA complex is shown in stick model. The zinc ion is the centerpiece of the catalytic machinery, and it is penta-coordinated with square pyramid geometry. The potential hydrogen bonds are represented by dashed /blue lines. The figure was generated using the software package UCSF Chimera (pdb 1T69) [<http://www.cgl.ucsf.edu/chimera>].

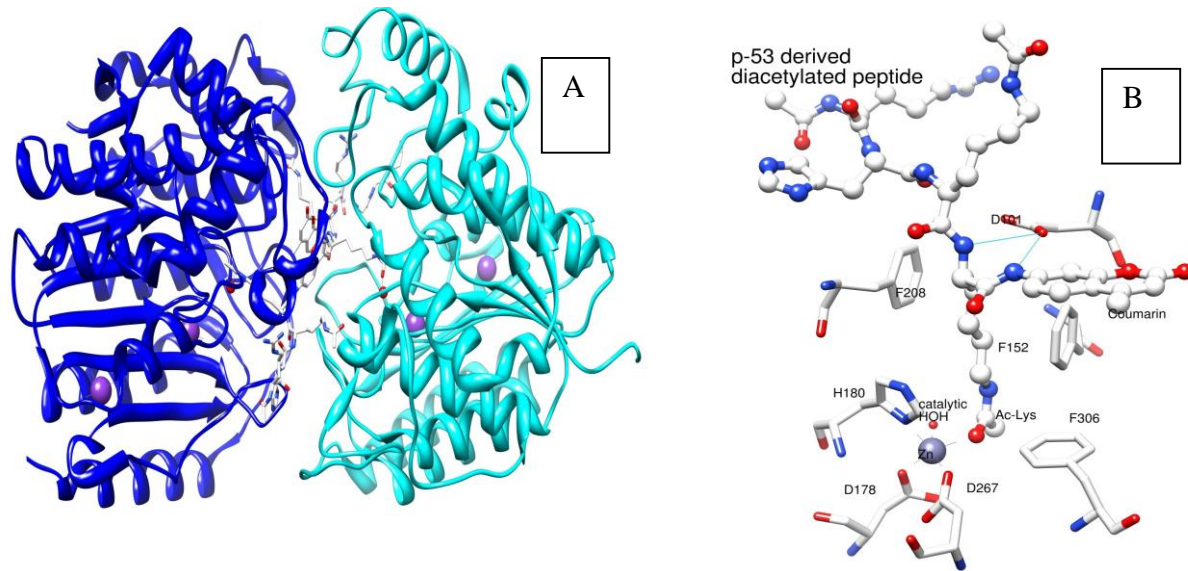


Figure 1.3. (A) Ribbon structure of human HDAC8 bound with a p-53-derived deacetylated substrate. The structure of the HDAC8-substrate complex described here exists as a dimer, presumably due to the favorable interactions mediated via the coumarin moiety of the substrate. (B) The stereo view of the HDAC8 active site showing the interactions between HDAC8 and the substrate. The substrate has been crystallized with a mutant and catalytically inactive form of HDAC8 which contains a Phenylalanine residue in place of Tyr 306. The catalytic water molecule serving as a nucleophile is shown as a red sphere. The alkyl group of the substrate is stabilized by interactions with Phe 208 and Phe 152. The Asp 101 is located at the rim of the active site pocket. It makes two hydrogen bonds (depicted as blue lines) with the substrate backbone and is very crucial for the substrate binding. The figure was generated using the software package UCSF Chimera (pdb 2V5W).

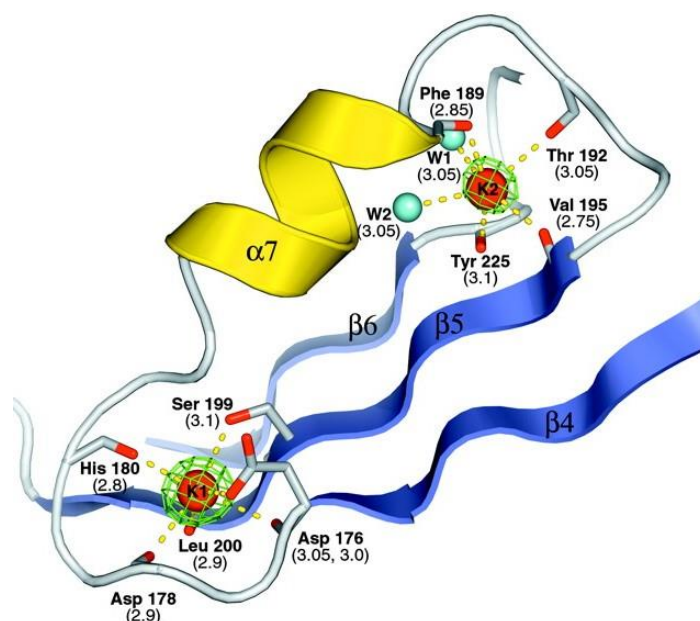


Figure 1.4. Enlarged view of the two potassium ion binding sites depicted as K1 and K2. K1 is located near the active site and, whereas K2 is located 15Å away from the catalytic zinc ion. The coordination bonds are depicted by yellow lines. The protein's residues coordinating with the K⁺ ions are shown by stick representation. Binding of a K⁺ ion to K1 and K2, respectively, leads to an inhibition and activation in HDAC8 deacetylase activity [58].

Based on the crystallographic studies, a mechanism of the HDAC8 catalyzed reaction has been proposed (Figure 1.5) [55]. The zinc ion plays a pivotal role in the entire catalytic process. It reduces the entropy by bringing the water and the acetyl-lysine substrate together to initiate the deacetylation reaction. Binding of the substrate to Zn^{2+} polarizes its carbonyl group thereby increasing its electrophilicity. In addition, the pK_a of the Zn^{2+} bound water molecule is lowered, making it a stronger nucleophile. The deacetylation reaction starts with a nucleophilic attack of the catalytic water on the carbonyl carbon of the acetyl-lysine, producing a tetrahedral oxyanion intermediate that is stabilized via an electrostatic interaction with the Zn^{2+} ion as well as a hydrogen bonding with the hydroxyl group of Tyr 306. The collapse of the tetrahedral intermediate is mediated via the transfer of a proton from His 142, leading to the production of an acetate ion and a deacetylated lysine.

The release of the acetate ion generated during the HDAC8 catalysis is mediated via an acetate release channel (exit tunnel), which is located adjacent to the active site pocket. A similar channel has been observed in HDLP as shown in Figure 1.6 [58]. Hieder *et al.* have described the importance of a strictly conserved residue Arg 37 involved in the release of acetate ion through the exit pocket [61]. Mutation of Arg 37 to Ala reduces HDAC8 activity, suggesting that the product (acetate) release could be the rate limiting step in the HDAC8 catalyzed reaction. Additionally, Vannini *et al.* have proposed the involvement of Tyr 18, Tyr 20, and His 42 in the exchange of acetate with the bulk water [58]. These residues are located on the external surface of the HDAC8 exit tunnel. Recently, it has been demonstrated by Ruchi Khanna *et al.* that replacement of the above residues by mutagenesis with an Ala significantly reduces the k_{cat} value of the HDAC8 catalyzed reaction with Fluoro-de-LysTM substrate [unpublished data]. Although the residues proposed to be involved in the acetate release are strictly conserved among HDAC

class I and II, no acetate release channel has been observed in the crystal structure of HDAC3, HDAC4, and HDAC7.

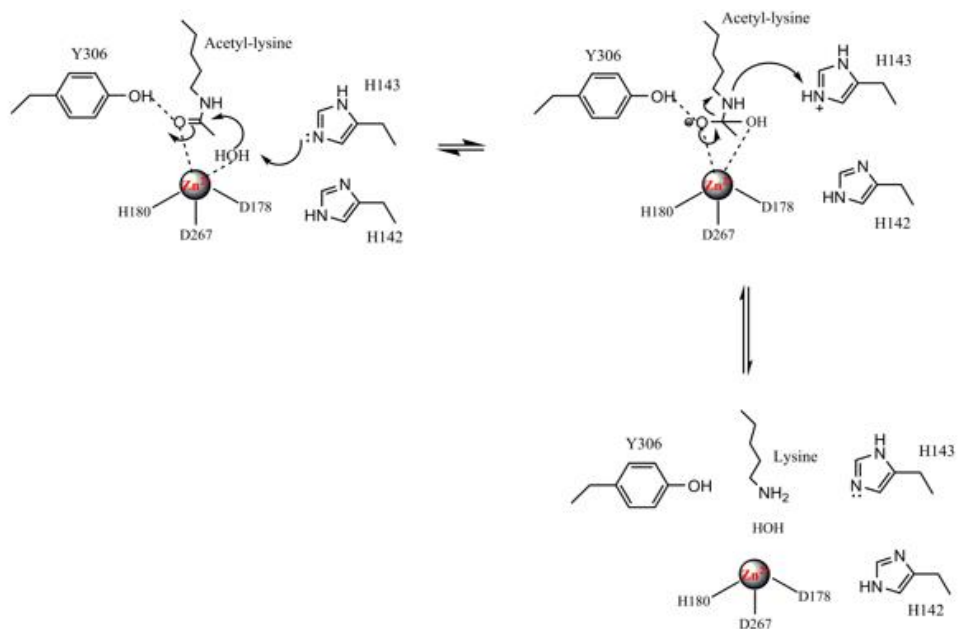


Figure 1.5. The proposed mechanism of the HDAC8 catalyzed reaction. The carbonyl carbon of the acetyl group of the substrate is attacked by the zinc bound water molecule (nucleophile), leading to the formation of an oxyanion tetrahedral intermediate, which is stabilized by hydrogen bonding with Tyr 306. The collapse of the intermediate is mediated via a proton transfer from His 142, yielding a lysine and an acetate ion [55].

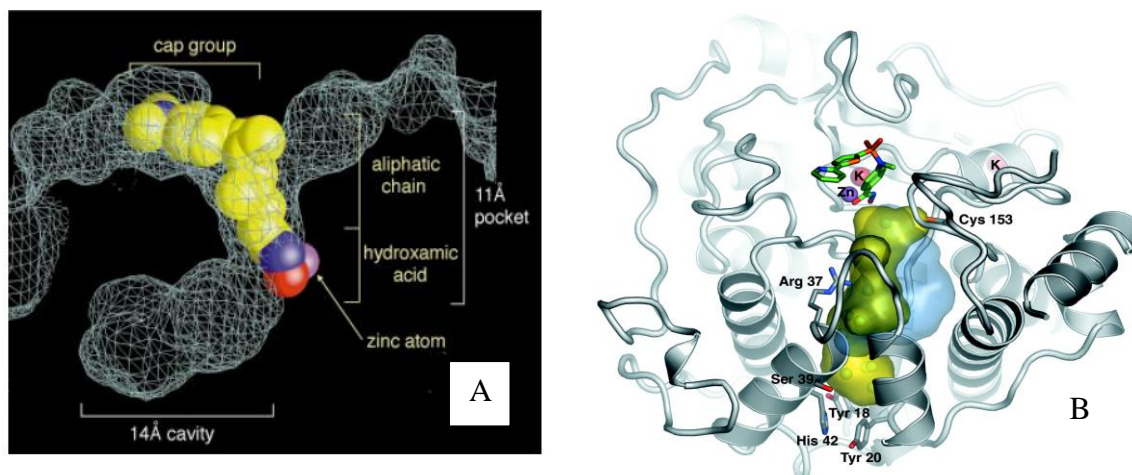


Figure 1.6. (A) The space filling model of the HDLP active site pocket (11Å) bound with Trichostatin A (TSA). A 14Å internal cavity located adjacent to the pocket serves as the acetate release channel. (B) The superimposed surface representation of HDLP and HDAC8 internal cavities are shown. The ribbon structure of HDAC8 is shown in gray, and the residues (Arg 37, Tyr 18, Tyr 20, and His 42) facilitating the release of the acetate ion are represented by a stick model [58].

HDAC8 has several intriguing features which distinguish it from other HDAC isozymes. It lacks the 50-111 AAs segment extending beyond the C-terminal of the catalytic domain which is utilized to recruit other co-repressor/transcription factors [57]. It is likely that HDAC8 could have evolved to function in isolation. The crystallographic studies of HDAC8 with the structurally diverse hydroxamate inhibitors, namely, TSA, SAHA, M-334 and CRA-A, reveal an inherent malleability of its active site pocket, which is primarily due to the presence of the L1 loop (S30-K38) [57]. Moreover, the phosphorylation of Ser 39 by PKA has been reported to reduce the rate of the HDAC8 enzyme catalyzed reaction, presumably by slowing down the release of acetate through the release channel mediated via an electrostatic repulsion [58].

Recently, Cole *et al.* solved the crystal structure of HDAC8 bound with a depsipeptide inhibitor, Largazole (pdb 3RQD) [62]. The inhibitor is a pro-drug which produces a thiol moiety upon hydrolysis of the thioester linkage. The structure observed here was similar to the HDAC8-

SAHA complex with the following salient differences. The thiolate ion serves as a monodentate ligand for the Zn^{2+} ion as opposed to SAHA, which is bidentate. The zinc ion coordination geometry is tetrahedral in case of HDAC8-largazole thiol complex, which is unique among all the crystal structures of HDAC isozymes known so far. Additionally, HDAC8 was required to undergo relatively larger conformational changes in the L1 and L2 loop region to accommodate the bulky and rigid inhibitor, largazole.

The crystal structures of HDAC8 containing different metal ions such as Co^{2+} , Fe^{+2} , and Zn^{2+} in the active site, have also been determined [63]. However, no significant difference in the HDAC8 structures was observed upon the substitution of the catalytic metal ion.

Daniel P. Dowling *et al.* reported the crystal structure of HDAC8 in a monoclinic form (pdb 3F07), which was different from the form previously described in literature as orthorhombic [64]. Additionally, it was possible to obtain the crystal of the apo form of HDAC8, which was free from any ligand. A comparison of the ligand-bound (holoenzyme) vs. ligand-free (apoenzyme) forms of HDAC8 showed that the L2 loop becomes ordered upon binding to the ligand, APHA, 3-(1-methyl-4-phenylacetyl-1H-2-pyrrolyl)-N-hydroxy-2-propenamide [64].

1.2.2. Crystal Structure of Human HDAC2

The crystal structure of human HDAC2 bound with an N-(2-aminophenyl) benzamide inhibitor (pdb 3MAX) has been solved by Bressi *et al.* [65]. The structure is comprised of an α/β deacetylase domain. The active site is made up of a lipophilic tube, the catalytic machinery, and a foot pocket. The foot pocket lies in the vicinity of the catalytic machinery, and it is reminiscent of the acetate release channel observed in HDAC8 and HDLP. The catalytic Zn^{2+} is pentacoordinated showing a square pyramidal geometry. The HDAC2 residues, namely, D181, D269, and H183 occupy the three coordination sites, while the inhibitor binds to Zn^{2+} in a

bidentate fashion as shown in Figure 1.7. The other structural and catalytic features are very similar to HDAC8.

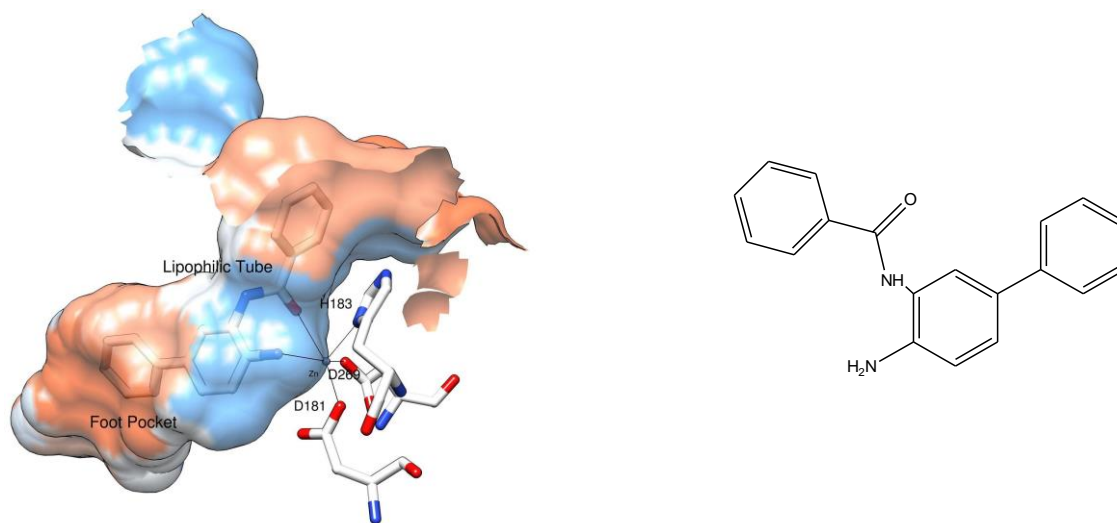


Figure 1.7. The surface representation of human HDAC2 bound to a benzamide inhibitor. The phenyl moiety of the inhibitor binds to an internal cavity (foot pocket) located adjacent to the substrate binding pocket (lipophilic tube). The foot pocket in HDAC2 is reminiscent of the acetate release channel of HDLP/HDAC8. The inhibitor coordinates the zinc ion in a bidentate fashion. The HDAC2 residues binding to the zinc ion are represented by the stick model [65]. The figure was generated using the software package UCSF Chimera (pdb 3MAX).

1.2.3. Crystal Structure of Human HDAC3

The crystal structure of human HDAC3 with a deacetylase domain (DAD) of the nuclear receptor co-repressor 2 (NCOR2), also named as SMRT (Silencing Mediator for Retinoid or Thyroid hormone), has been determined by Watson *et al.* [66]. The structure reveals the structural basis of the activation of HDAC3 catalytic activity mediated via the association of SMRT-DAD.

HDAC3 contains an α/β -deacetylase domain which is conserved among class I HDACs [pdb 4A69]. The catalytic machinery of the enzyme resides at the end of a tubular cavity

containing the zinc ion pentacoordinated with D259, D170, H172 and the carboxylate moiety of acetate (Figure 1.8). The acetate is the end product of the deacetylation reaction observed in the crystal structure. Similar to HDAC8 two potassium ions have been observed in addition to the catalytic zinc ion. The SMRT-DAD interacts with the N-terminal region (4-49) of HDAC3. In fact, the association of HDAC3 to SMRT-DAD is mediated via a D-myo-inositol-(1, 4, 5, 6)-tetrasphosphate (Ins (1, 4, 5, 6) P4), which serves as an intermolecular glue. Ins (1, 4, 5, 6) P4 contains a negatively charged phosphate moiety which neutralizes the positive charges being present on the interface of the HDAC3-SMRT-DAD complex. Notably, the residues interacting with Ins (1, 4, 5, 6) P4 and the SMRT-DAD are strictly conserved among class I HDAC except for HDAC8, which further emphasize the fact that HDAC8 does not require the association of any co-repressor to function [66].

The binding of the SMRT-DAD to HDAC3 has been proposed to facilitate the binding of the substrate by modulating the conformation as well as the dynamics of the enzyme, thereby enhancing the enzyme activity. The interaction between the two proteins is primarily mediated via a pseudo-helix (H1) and L6 loop. HDAC8 has a regular helix and the L1 loop in the analogous region. The L1 loop is shorter in length by two amino acids and contains a proline residue, which helps to keep the loop away from substrate binding site. As a result of that, the active site pocket of HDAC8 is easily accessible for the substrate binding and does not require any assistance of any co-repressor. As shown in Figure 1.9 the ribbon structure of HDAC8 and HDAC3 superimpose on each other except for the pseudo-helix (H1) region. In fact, H1 serves as a regulatory switch which attains a regular secondary structure upon association with the SMRT-DAD.

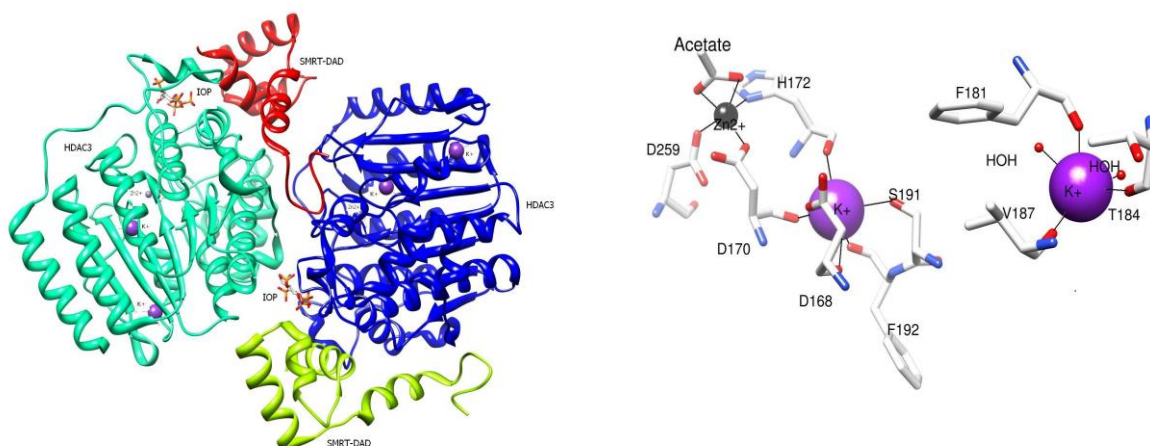


Figure 1.8. (A) The ribbon structure of HDAC3 bound to a SMRT-DAD and inositol tetraphosphate (IOP). The complex has been reported to form a dimer. The IOP is represented as sticks. (B) The enlarged view of the HDAC3 active site pocket and the potassium binding sites. The catalytic zinc and the potassium ions are shown as black and purple spheres. The catalytic Zn^{2+} is bound to an acetate ion, the end product of the deacetylation reaction. The coordination bonds are shown by thin black lines. The figure was generated using the software package UCSF Chimera (pdb 4A69).

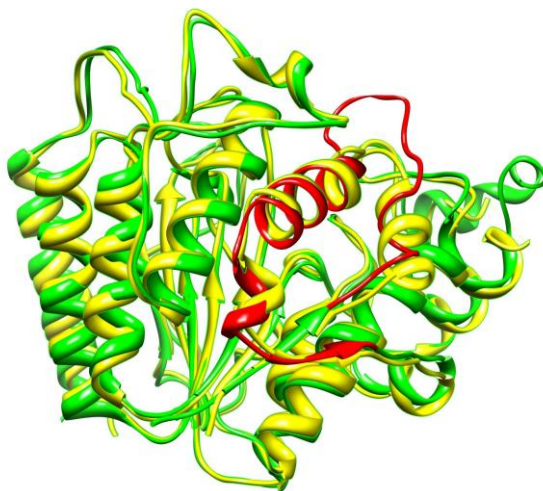


Figure 1.9. Superposition of the ribbon structure of HDAC8 (yellow) and HDAC3 (green). The deacetylase domains superimpose well on each other except the pseudo-helix of HDAC3 shown in red color. The H1 attains a regular helical structure upon binding to SMRT-DAD and Inositol tetraphosphate. The figure was generated using the software package UCSF Chimera.

1.2.4. Crystal Structure of Human HDAC4

The crystal structure of the HDAC4 catalytic domain (648-1057) has been solved by Bottomley *et al.* [67]. The full length HDAC4 has been known to interact with the HDAC3-NCOR2 complex. The deacetylase activity of the ternary complex measured with an acetylated histone substrate is solely contributed by HDAC3 [47], because HDAC4 cannot utilize the canonical HDAC substrate efficiently. Moreover, the natural substrates of HDAC4 are yet to be identified. The crystallographic studies of HDAC4 provide the structural basis for the intrinsically low enzyme activity the class IIa HDACs [67].

Figure 1.10 shows the crystal structure of the catalytic domain of the wild type HDAC4 bound with a trifluoromethylketone (TFMK) inhibitor (pdb 2VQJ). HDAC4 contains a single α/β deacetylase domain consisted of 21 α -helices and 10 β -strands. The catalytic machinery is very similar to class I HDACs except for the Y976 being replaced by His 976. Interestingly, the gain of function mutant form of HDAC4 (H976Y) exhibits an enhanced enzyme activity, which is comparable to class I HDACs. The catalytic Zn^{2+} in HDAC4 is pentacoordinated showing a square pyramidal geometry. Asp 840, His 842, and Asp 934 occupy three coordination sites, and the hydrated form of the trifluoro moiety of TFMK chelates Zn^{2+} as a bidentate ligand. As shown in Figure 1.10, the side chain of His 976 is moved away from the active site creating a vacant space occupied by a water molecule (W2) which forms hydrogen bonds with carbonyl group of TFMK and the backbone nitrogen atom of Gly 975. The hydrogen bond is the reminiscent of the interaction between Tyr 306 and the carbonyl oxygen of SAHA in the HDAC8-SAHA complex (pdb 1T69).

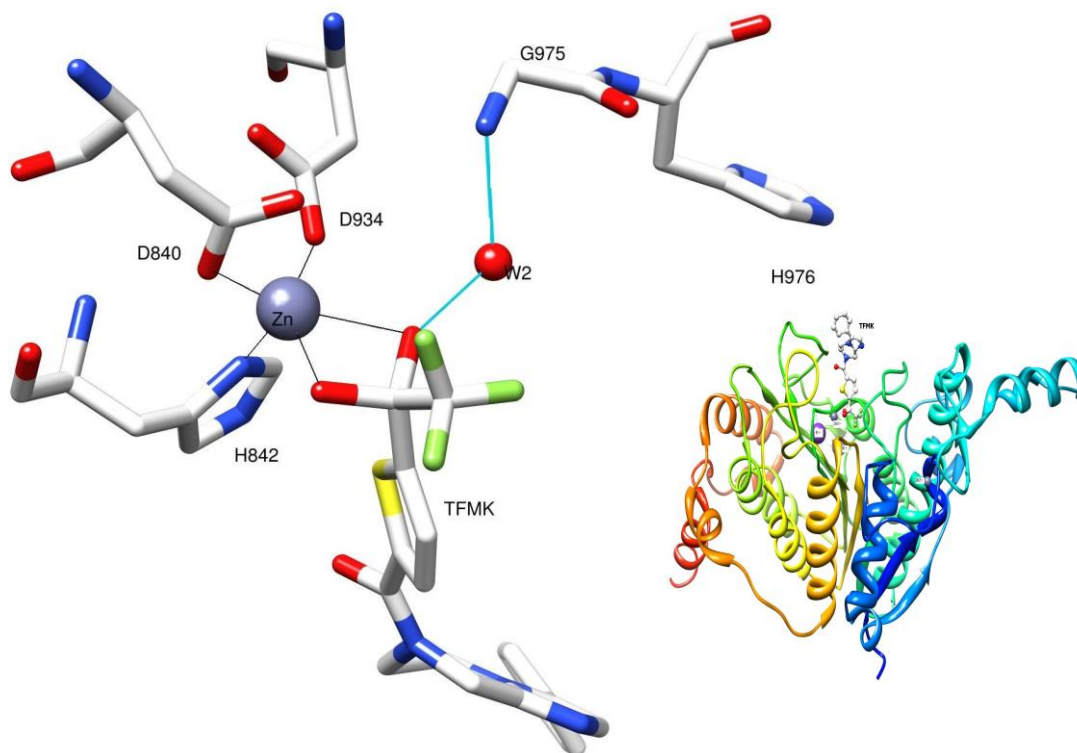


Figure 1.10. The ribbon structure of the catalytic domain of HDAC4 (cdHDAC4) bound to a trifluoromethylketone (TFMK) inhibitor. HDAC4 has a single α/β -deacetylase domain. The stereo view of the active site pocket of cdHDAC4 shows the interactions between the protein and the inhibitor. The hydrated form of TFMK binds to the catalytic zinc ion occupying the two coordination sites. The His 976, which occupies an analogous position of Tyr 306 of HDAC8, is moved away from the active site creating the room for a water molecule (W2). The W2 establishes two hydrogen bonds in cdHDAC4-TFMK complex shown by blue lines and has been proposed to stabilize the oxyanion tetrahedral intermediate generated during the catalytic process. The above figure was generated using the software package UCSF Chimera.

The crystal structure of HDAC4 with hydroxamic acid (pdb 2VQV) provides the molecular basis of the intrinsically low enzyme activity of class IIa HDAC on canonical acetamide substrate. Evidently, the hydroxamate moiety binds to the catalytic Zn^{2+} in a monodentate fashion (Figure 1.11), and a water molecule (W1) substitute for one of coordination sites observed in cdHDAC4-TFMK complex. It has been proposed that during the catalytic cycle, W2 stabilizes the tetrahedral oxyanion intermediate, albeit less efficiently than the tyrosine

residue of class I HDACs. As a result, HDAC4 is less efficient in utilizing the canonical acetamide substrate. However, it shows a remarkably high activity with a trifluoroacetamide substrate. This is because the fluorine atom increases the electrophilicity of carbonyl carbon of the acetyl group of the substrate that could easily be attacked by the zinc-bound water molecule (nucleophile) during the catalytic process.

The crystal structure of gain of function (GOF) mutant of cdHDAC4 with TFMK as well hydroxamic acid has also been determined. The GOF mutant has been produced by replacing His 976 by a Try residue via a site directed mutagenesis. The cdHDAC4 GOF shows a very poor activity with trifluoroacetamide substrate, as oppose to the canonical acetamide one. This could be explained from the fact that the Y976 is moved away from the active site due to the steric hindrance posed by the bulky fluorine atom in the cdHDAC4 (GOF) - trifluoroacetamide complex, which is very similar to the cdHDAC4 (GOF)-TFMK complex (Figure 1.13). Notably, with the exception of HDAC8, other members of class I HDAC such as, HDAC1, HDAC2, HDAC3, show very poor enzyme activity with trifluoroacetamide substrate. HDAC8 active site has been reported to be malleable and because of which it is well equipped to accommodate even the bulky ligand such as, trifluoroacetamide substrate without displacing away the tyrosine residue involved in catalysis.

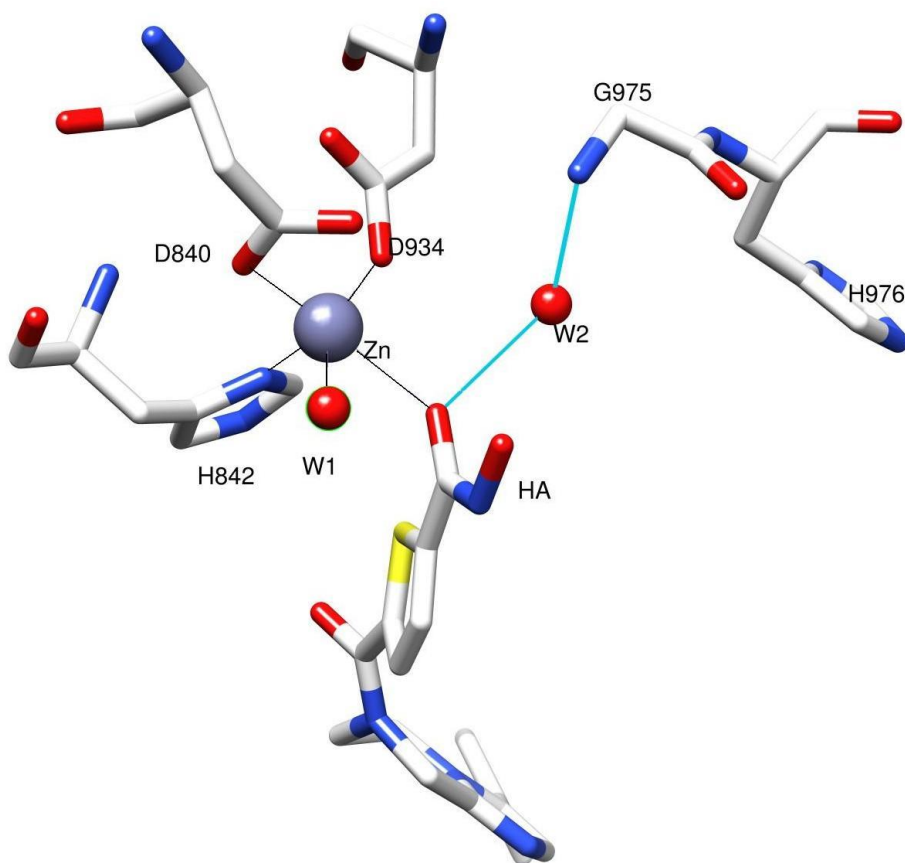


Figure 1.11. The stereo view of HDAC4 active site bound to a hydroxamic inhibitor. The inhibitor binds to the catalytic zinc ion through the carbonyl oxygen of the hydroxamate (monodentate chelation). A water molecule (W1) occupying the second coordination site observed in HDAC4-TFMK complex serves as a nucleophile in the HDAC4 catalyzed reaction. The figure was generated using the software package UCSF Chimera [pdb 2VQV].

Aside from catalytic zinc ion, the cdHDAC4 contains a structural one which holds together the two segments of the protein originating from the core. In apo-HDAC4, the Zn^{2+} ion is tetrahedrally coordinated with His 665, His 678, Cys 667, and Cys 751 (Figure 15). Upon binding of the inhibitor (TFMK), His 665 and Cys 678 are replaced by His 675 and Cys 669. Interestingly, mutation in the above residues such as, C669A/H675A abrogates the association of HDAC4 with the HDAC3-NOCR2 complex, suggesting the role of structural zinc ion as a

regulatory switch in protein-protein interaction. Moreover, the binding of HDAC4 to an inhibitor (TFMK) also diminishes its potential to interact with HDAC3-NOCR2 complex [67]. Notably, the amino acids residues coordinating with the structural Zn^{2+} are conserved among the members of class IIa HDACs. It has been argued that the class IIa HDACs utilize their inherent conformational flexibility mediated via the structural zinc ion to regulate the substrate specificity as well the binding partners. In order to compare the structures of the catalytic domain of class I and IIa HDACs, the ribbon structure of HDAC8 and cdHDAC4 have been superimposed on each other as shown in Figure 1.12. Evidently, their deacetylase domains are structurally similar except for HDAC4 containing the structural zinc binding motif at the C-terminal region.

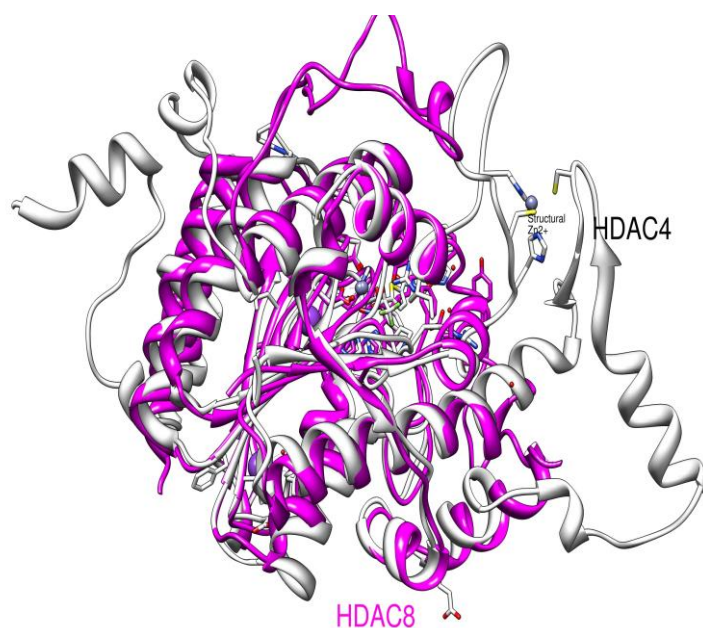


Figure 1.12. The superposition of the ribbon structure of HDAC8 (red) and cdHDAC4 (gray). The α/β -deacetylase domain of the two enzymes superimpose well on each other except for the C-terminal region of HDAC4 containing a structural zinc ion. The zinc ion, which is tetrahedrally coordinated with four residues of HDAC4, holds the two segments of the protein originating from the protein core. The figure was generated using the software package UCSF Chimera.

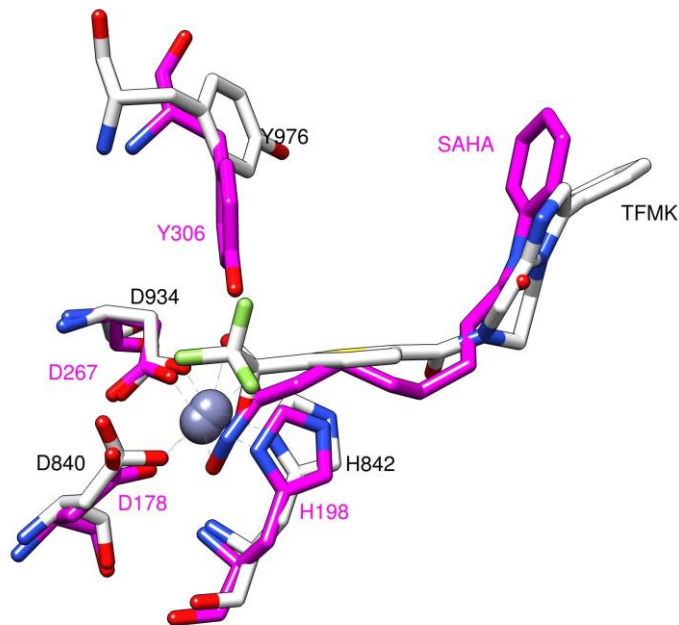


Figure 1.13. (A) The stereo view of the superimposed active site residues of the GOF HDAC4-TFMK [pdb 2VQO] and the HDAC8-SAHA [pdb 1T69] complexes. Evidently, the catalytic machinery of the two proteins is very similar except for Tyr 976 being moved away from the active site in HDAC4. The figure was generated using the software package UCSF Chimera.

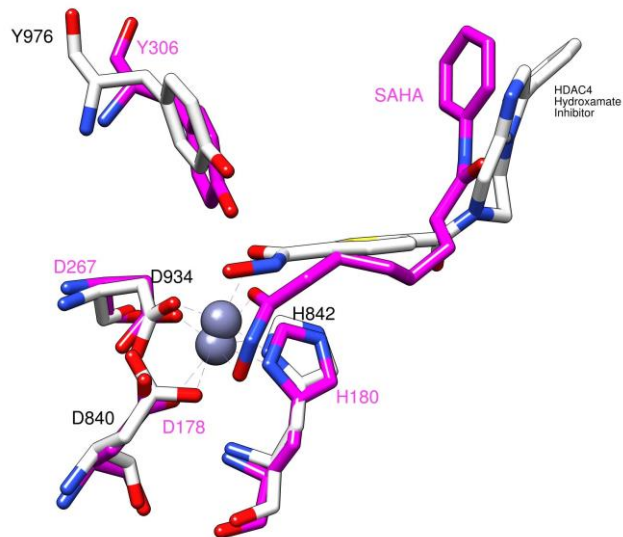


Figure 1.13. (B) The stereo view of the superimposed active site residues of the GOF HDAC4-HA [pdb 2VQV] and HDAC8-SAHA [pdb 1T69] complexes superimposed on each other. Evidently, the catalytic machinery of the two proteins is very much similar. The figure was generated using the software package UCSF Chimera.

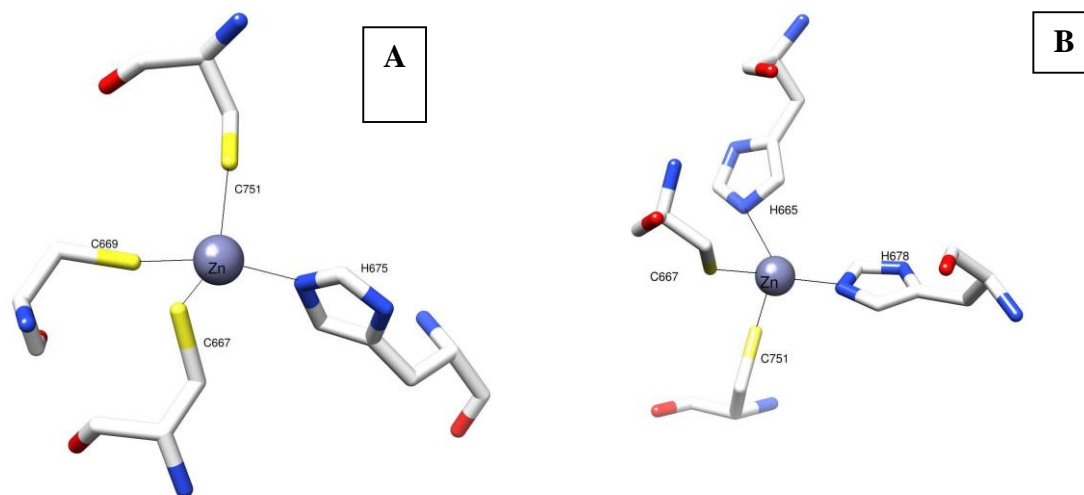


Figure 1.14. The ligation scheme of structural the zinc ion of HDAC4. It is switched from A to B upon binding to an inhibitor in the active site of the enzyme [67]. The zinc coordinating residue Cys 669 and His 675 in the apo form of the enzyme is replaced by His 665 and His 678 in the inhibitor bound one. The figure was generated using the software package UCSF Chimera

1.2.5. Crystal Structure of Human HDAC7

The crystal structure of the catalytic domain of human HDAC7 (cdHDAC7) has been solved by Schutz *et al.* [68]. The protein contains a single deacetylase domain comprised of 21 α -helices and 10 β -strands (Figure 1.15). A structural comparison with HDAC4 reveals that the active site pocket is well conserved among class IIa HDACs. The enzyme contains the binding sites for two Zn^{2+} ions, one being involved in catalysis while the other plays a structural role in maintaining the protein structure. The apo-cdHDAC7 contains a catalytic zinc ion tetrahedrally coordinated with Asp707, Asp 801, Asp709, and a water molecule. The cdHDAC7 shows a poor activity with a canonical substrate, which has been attributed to the lack of tyrosine residue (replaced by His 843) required to stabilize the oxyanion tetrahedral intermediate during the deacetylation reaction. The gain of function (GOF) mutation (H843Y) of cdHDAC7 restores the enzyme activity comparable to the class I HDACs measured with Fluoro-de-LysTM substrate. Figure 1.15 shows the crystal structure of wild type cdHDAC7 bound with SAHA. The hydroxamate moiety occupies a single coordination site as has been reported previously in the case of HDAC4. His 843 attains an outward conformation creating a room for a water molecule which has been proposed to stabilize the oxyanion tetrahedral intermediate.

The structural zinc-binding motif (CCHC) of cdHDAC7 is comprised of Cys 533, Cys 535, His 541, and Cys 618 coordinated with a Zn^{2+} ion. Although the CCHC motif does not seem change its ligation scheme upon binding to a ligand unlike HDAC4, it has a potential to serve as a modulator of the protein conformation, which could play substantial a role in regulating the specificity of the substrate and binding partner.

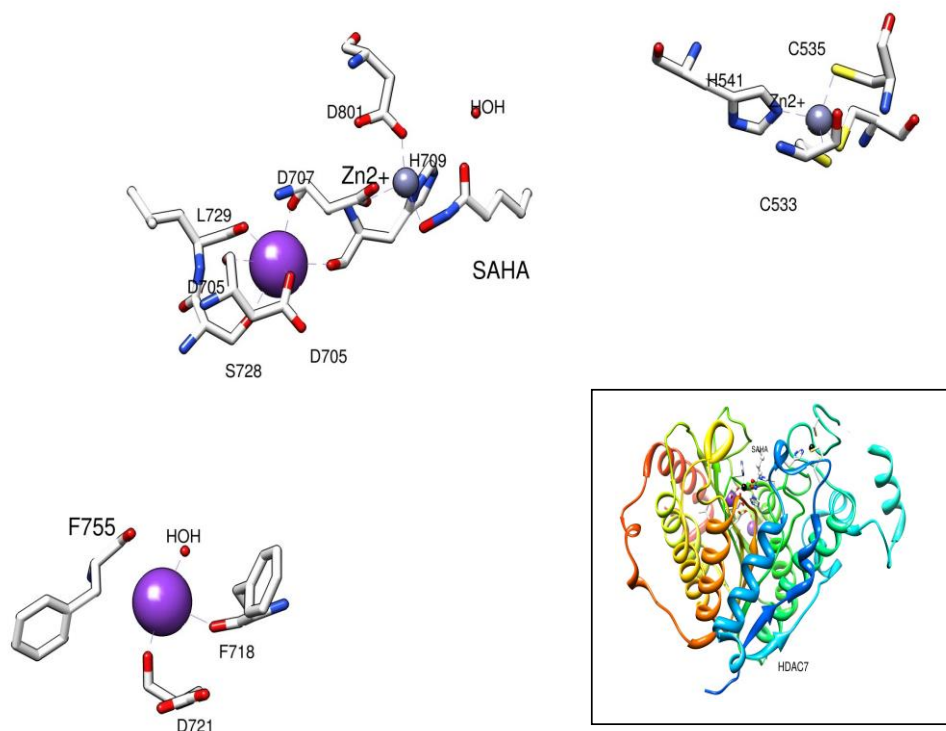


Figure 1.15. The stereo view of the metal binding sites of HDAC7. The inset shows the ribbon structure of the catalytic domain of human HDAC7 bound with SAHA [pdb 3COZ]. SAHA is shown with a ball and stick representation. The potassium and the zinc ions are shown by large purple and small blue spheres, respectively. The potential hydrogen bonds are depicted by dashed lines. The figure was generated using the software package UCSF Chimera.

1.3. *In vivo* Substrates/Targets of Human HDACs

Post-translational modification of a protein via the acetylation/deacetylation at specific lysine residues regulates its structural-functional features. The above activity plays a pivotal role in the regulation of myriad of physiological processes. Histone was identified as the first target for human HDACs, and by now, over 3700 distinct acetylation sites have been identified in human proteome, emphasizing the fact that the acetylation may rival phosphorylation [9, 69]. The above acetylation sites could serve as targets for various HDAC isozymes *in vivo*.

Various attempts have been made to identify specific *in vivo* and *in vitro* targets/substrates of human HDACs and to elucidate their specificity and selectivity. The biochemical techniques, such as pull-down assay, chromatin immunoprecipitation, si-RNA mediated gene knock-out, etc., widely utilized for the identification of HDAC targets, often suffer from the following limitations [70]. First, they fail to identify the targets where a transient interaction is adequate to produce a cellular response. Second, the experimental conditions used in the above biochemical techniques would alter the enzyme activity, in addition to its interactions with other targets. Nonetheless, several *in vivo* substrate/ targets of HDACs have been identified, which are helpful in discerning the physiological functions of specific HDAC isozymes.

In an attempt to elucidate the physiological function of HDAC8, several researchers have focused their study towards the identification of *in vivo* targets/substrates of HDAC8. Initially, based on the nuclear localization of HDAC8, as well as its ability to utilize histone as *in vitro* substrate, it was proposed that HDAC8 utilizes histone as its target *in vivo* [10]. In a subsequent study performed by Keris *et al.*, it was found that an HDAC8 selective

inhibition *in vivo* do not alter the acetylation level of histone; suggesting the fact that HDAC8 does not utilize histone as a substrate *in vivo* [71]. Nevertheless, a full length histone or its acetylated peptide fragment has been widely used as *in vitro* substrate for measuring the rate of HDAC8 catalyzed reaction.

David Waltregny *et al.* studied the role of HDAC8 in smooth muscle differentiation. HDAC8 was found to be associated with a smooth muscle α -actin and regulate the muscle contraction [31]. The fact that HDAC8 utilizes a cytosolic protein (α -actin) in muscle cell as a non-histone target, strongly suggests that HDAC8 is localized in cytosol, at least in muscle cell. Additionally, the above finding spurred the identification of several non-histone targets of human HDAC8. HDAC8 has been found to be associated with inv (16) in acute myeloid leukemia (AML) [39]. The inv (16) is produced due to a chromosomal translocation leading to a fusion of the first 165 amino acids of the core-binding factor β (CBF β) to the coiled-coil region of a smooth muscle myosin heavy chain (SMMHC). The fusion protein CBF β -SMMHC simultaneously binds with HDAC8 as well as AML1 (a transcription factor), and thereby represses the transcription of AML1-related genes which leads acute myeloid leukemia. Notably, the inv (16) mediated repression of AML1 regulated genes are sensitive to an HDAC8 inhibitor, rationalizing the therapeutic potential of an HDAC8 selective inhibitor for the treatment of AML [72]. However, it remains to be confirmed as to whether HDAC8 utilizes inv (16) as a substrate for deacetylation reaction.

In a recent study performed by Yan *et al.*, HDAC8 was found to regulate the transcription of p53 gene [73]. However, the above process was reported to be dependent on the presence of a transcription factor, HoxA. HDAC1 and Sirt1 have already been

known to deacetylate p53 *in vivo*. It is still not clear whether HDAC8 utilizes HoxA and/or p53 as substrate/s for deacetylation. However, an acetylated peptide comprised of the C-terminal domain of p53 serves as a substrate for HDAC8 in *in vitro* enzyme assay.

Deardroff *et al.* investigated the link between mutation in HDAC8 gene and Cornelia de Lange Syndrome (CdLS), a developmental disorder which affects growth and intellectual development in children [36]. The disease is primarily caused due to an unequal distribution of sister chromatids in daughter cells during cell division. The sister chromatids are held together prior to their segregation in anaphase stage of cell division via a core cohesin complex. Structural Maintenance of Chromosome 3 (SMC3) serves as essential subunit of the core cohesion complex, and it has been reported to be *in vivo* target of HDAC8. An HDAC8 mediated deacetylation of SMC3 relieves sister chromatids from the core cohesion complex prior to cytokinesis. Furthermore, the SMC3 mediated segregation of sister-chromatids is severely impaired due to a mutation in HDAC8 gene.

Four missense mutations, namely, T311M, G320R, H334R, and H180R have been reported in CdLS, in addition to a nonsense mutation (R164X) [36]. These mutations have a significant impact on the enzyme activity of HDAC8 measured on Fluoro de LysTM substrate. The H180R mutation is likely to influence the binding of the catalytic zinc ion to HDAC8. The T311M mutation seems to influence the orientation of Y306, which plays a pivotal role in HDAC8 catalysis. The other mutations, presumably, affect the overall protein structure which is likely to perturb the geometry of active site pocket of the enzyme.

Estrogen-Related Receptor α (ERR- α) reportedly serve as *in vivo* target of HDAC8 [74]. ERR- α is an orphan nuclear receptor which associates with co-activator/co-repressor

and regulates the transcriptions of various genes involved in energy metabolism. HDAC8 deacetylates a specific lysine residue of ERR- α located at the DNA-binding domain and thereby reduces its affinity for DNA. Notably, an HDAC8 selective effector (inhibitor/activator) could be used as a therapeutic agent to modulate the function of ERR- α , which has been found to be intimately linked with several human diseases, such as cancer, diabetes, and metabolic syndromes.

Lee *et al.* has reported the interaction of HDAC8 with human ever-shorter telomere 1B (hEST1B), a telomerase associated protein, and the interaction was found to be dependent on the PKA-mediated phosphorylation of HDAC8 [75]. Notably, the above interaction protects hEST1B from an ubiquitin-mediated degradation, increasing the half-life of hEST1B. Furthermore, hEST1B has been known to influence the telomerase activity *in vivo*. It is important to note that the cancer cells modulate their telomerase activity in order to escape from the cell cycle check points. Therefore, an HDAC8 selective effector (inhibitor/activator) could be used as a modulator to alter the telomerase activity by modulating the HDAC8-hEST1B interaction, which could produce an anticancer effect.

1.4. *In vitro* Assay to Determine HDAC Enzyme Activity

HDACs are high priority drug target for the treatment of various human diseases including cancer. In this regard, serious attempts have been made to discover their small molecule effectors which could potentially alleviate the disease conditions. A high-throughput screening (HTS) approach utilizing *in vitro* HDAC assay has been widely used to identify novel HDAC effectors. A typical *in vitro* HDAC assay usually requires a synthetic/artificial substrate, recombinant form of HDAC, and an analytical tool to monitor time-dependent conversion of substrate into product generated during an enzyme catalyzed

reaction. Notably, in order to make HTS fast, simple, and cost effective, attempts have made to develop a convenient *in vitro* HDAC assay [76].

The first *in vitro* HDAC assay was developed utilizing a full length histone or a fragment of histone tail as substrate [76]. The above assay has the following drawbacks. In order to monitor the HDAC mediated deacetylation, the target lysine residues of the substrate are isotopically labeled, which has safety issues associated with the handling of hazardous radioactive material. Moreover, the HDAC used in the above assay requires a cumbersome purification from animal cell/tissue. Notably, the assay is non-homogenous which requires the separation of the product from the reaction mixture, and it is not suitable to be adopted in high throughput format.

A significant attempt was made by Nare *et al.* to develop a homogenous HDAC assay, which is well suited for HTS [77]. The above assay is based on the principle of a scintillation proximity assay which utilizes a biotinylated [³H] acetyl-peptide and a streptavidin coated SPA beads. The HDAC activity is measured by a time-dependent reduction in the scintillation signal due to deacetylation of biotinylated [³H] acetyl-peptide substrate. Notably, the above assay is homogenous, but it requires the handling of hazardous radioactive material.

Manfred Jung and coworkers developed the first non-isotopic *in vitro* HDAC assay utilizing a fluorescence-labeled acetyl-lysine as a substrate [78]. The substrate, as well as the deacetylated product generated in the above assay, is fluorescent, but they have a different molecular weight and/or chemical property. A reverse phase HPLC system equipped with a fluorescence detector is used for quantitative measurement of the reaction

product. Evidently, the assay is non-isotopic which does not require handling of a radioactive material. However, it is non-homogenous and not suitable for HTS.

The first non-isotopic and homogenous HDAC assay was developed by Schwienhorst and coworkers [79]. The above assay utilizes a fluorogenic substrate where the acetyl-lysine moiety is covalently attached to a fluorophore, amino methyl coumarin (AMC) via an amide linkage. The assay is essentially a trypsin-coupled assay in which the product of HDAC catalyzed reaction is paired with trypsin, generating a free AMC as a highly fluorescent product. The background fluorescence signal due to the presence of the substrate is considerably low. The time-dependent increase in fluorescence of the AMC is directly correlated with the HDAC activity. Evidently, the above trypsin-coupled HDAC assay is simple and convenient to be adopted in high-throughput format. However, it requires optimization to be used in continuous format, which is a preferred method for studying steady state enzyme kinetics.

Brian E. Schultz and co-worker developed a non-isotopic and homogeneous HDAC assay utilizing an acetyl-Gly-Ala (N^ε-acetyl-Lys)-AMC as a fluorogenic substrate which can be conveniently used in continuous assay format [80]. In principle, the above assay is similar to the trypsin-coupled HDAC assay developed by Schwienhorst *et al.* However, it offers several advantages over the end-point HDAC assay. First, it closely represents an HDAC catalyzed reaction monitored on real-time basis and provides a very reliable result. Second, it can easily detect any non-linearity in reaction progress curve, which often arises due to substrate depletion and/or enzyme inactivation during the course of the assay. Additionally, a deviation in the lag phase of reaction progress curve provides a way to distinguish an effector of the coupling enzyme, which is often mistakenly identified as

HDAC effector. Furthermore, the assay is well suited to study the steady state kinetics of HDAC catalyzed reaction.

Brian E. Schultz *et al.* performed a comparative study on the steady state enzyme kinetics of class I and II HDAC catalyzed reaction utilizing the above trypsin-coupled assay [80]. HDAC8 was found have the lowest catalytic efficiency ($k_{\text{cat}}/K_m = 60 \text{ M}^{-1} \text{ s}^{-1}$) among all HDAC isozymes, implying its slow reactivity at least on an acetyl-Gly-Ala (N^{ϵ} -acetyl-Lys)-AMC substrate. In order to ensure that the bulky coumarin-moiety has no influence on the kinetic parameters of HDAC catalyzed reaction, the above researcher utilized an alternative substrate, where the bulky group is not attached just immediate to acetyl-lysine moiety. Notably, the kinetic parameters for HDAC catalyzed reactions essentially remained the same for both the substrates, negating the influence of bulky AMC moiety on the reactivity of HDAC isozymes.

Hildmann *et al.* made an attempt to develop an *in vitro* HDAC assay based on the quantitative measurement of the product (acetate) generated during the deacetylation reaction [81]. The above assay utilizes a peptide containing an acetylated-lysine as substrate. Evidently, the product of the HDAC catalyze reaction, acetate, does not provide any direct detectable signal for its quantitative measurement. The consecutive activity of three enzymes, which is paired with HDAC catalyzed reaction, is utilized to produce NADH from acetate as described below. The amount of NADH is easily quantified by measuring an absorbance at 340 nm. The first coupling enzyme, acetyl CoA-synthetase, converts acetate into acetyl-coA utilizing an ATP. The acetyl CoA produced in the above reaction is taken up by the second coupling enzyme, citrate synthase, which produces a citrate molecule by condensation reaction utilizing an ATP and oxaloacetate. In order to

provide a continuous supply of an oxaloacetate in the above reaction, malate dehydrogenase is used which utilizes malate and NAD^+ to produce an oxaloacetate and NADH. Notably, the above HDAC assay is cumbersome which requires multiple coupling enzymes. Moreover, its utility has only been validated for measuring the activity of a bacterial homolog (HDAH) from *Bordetella Alcaligenes*.

Weiping Zheng and colleagues developed a simple spectrophotometric assay to measure the rate of HDAC8 catalyzed reaction [82]. As opposed to the previously developed pan HDAC assay, it can only be used to measure HDAC8 enzyme reactivity. The assay utilizes a thioacetyl-lysine containing p53 peptide as substrate. The HDAC8 mediated dethioacetylation of the substrate produces a thioacetate, which is easily quantified spectrophotometrically at 412 nm using an Ellman reagent. The assay is not suitable to be adopted in the continuous format presumably because Ellman reagent has a potential to denature HDAC8 while reaction is in progress during the course of the continuous assay.

Sheraz Gul and co-workers developed a bioluminescence based HDAC assay utilizing a substrate which contains an acetylated-lysine peptide conjugated with aminoluciferin [83]. The HDAC mediated deacetylation of the above substrate, followed by the treatment with developer (trypsin) produces an aminoluciferin, which is detected using a widely used luciferase assay system.

Recently, Kazuya Kikuchi and coworkers developed a one step HDAC assay utilizing a fluorogenic probe as substrate [84]. The probe, $\text{K}_4(\text{Ac})\text{-CCB}$, is comprised of a H3 peptide containing an acetyl-lysine and a coumarin moiety attached to a carbonate ester. The HDAC mediated deacetylation of the acetyl-lysine moiety of the probe produces an

intermediate, which undergoes a spontaneous transesterification reaction to produce a highly fluorescent product. The fluorescent product provides the detectable signal to monitor the reaction progress of the HDAC catalyzed reaction at 466 nm. Notably, the above HDAC assay is simple and convenient, and it does not require any coupling enzyme.

1.5. Substrate Specificity of Human HDAC8

Substrate specificity of HDAC8 catalyzed reaction has been widely studied utilizing artificial substrates. This is presumably because a limited number of *in vivo* substrates of HDAC8 are currently known. Dineal Riester *et al.* made the first attempt to elucidate the substrate specificity of various HDAC isozymes and investigated the effect of the following parameters on HDAC8 catalyzed reaction: the length of ϵ -acyl moiety, enantioselectivity of acetyl-lysine side chain, and nature of the acyl leaving-group [85]. The important findings of the above study are summarized as follows: (1) HDAC8 does not catalyze the deacylation of lysine other than acetyl group, implying that a bulky acyl group has a steric-effect in the binding of the substrate. (2) HDAC8 targets only an L-isomer of lysine residue. An acetyl-ornithine, which has a shorter side chain than acetyl-lysine, does not serve as substrate for HDAC8, irrespective of the D and L isomers. (3) The rate of HDAC8 mediated deacetylation measured on a trifluoroacetyl-lysine is remarkably higher because of the trifluoroacetyl moiety being a strong leaving group.

In a separate study Danial Riester and colleagues investigated the influence of the local sequence of the ϵ -acetyl-lysine moiety of substrate on HDAC8 catalyzed reaction [86]. In the above study a synthetic library of the fluorogenic substrate of the following format was generated: Ac- P₂- P₁-Lys (ϵ -Ac)-MCA, where P₂ and P₁ can be any amino acid residue except cysteine. It was observed that HDAC8 prefers an aromatic or large

aliphatic amino acid at P₋₁ position. Furthermore, it prefers polar amino acids, such as Arg, Lys, Met, Pro, Ser, and Gln, at P₋₂ position. Evidently, the HDAC8 reactivity is dependent on the local sequence of the synthetic peptide substrate.

There were two significant issues which were overlooked in study performed by Danial Riester *et al.* (1) The fluorogenic substrate utilized in the above study would have a marked influence on the HDAC substrate specificity due to the presence of a bulky fluorogenic moiety. (2) The local sequence can be varied only at the N-terminus of the acetyl-lysine moiety of the substrate. This is because the fluorophore (AMC) is directly attached to the acetyl-lysine residue of the substrate via an amide linkage. The above issues were addressed by Gurard-Levin *et al.*, who investigated the effect of the local as well as the distal sequence of acetyl-lysine moiety the HDAC8 catalyzed reaction [87]. The substrate used by Mrksich *et al.* is a derivative of the N-terminal tail (residues 8-19 with 12 being acetylated) of the H4 and is devoid of any bulky fluorogenic group. The researchers argued that the above substrate is a true mimic of the natural substrate. As opposed to a fluorescence-based detection, mass spectrometry was utilized to monitor the deacetylation of acetyl-lysine moiety of the above substrate. It was observed that the deletion of a distal sequence, KRHR residues (16-19), from the substrate diminished the HDAC8 reactivity. It was proposed that the KRHR binds to an exosite of enzyme and influences the HDAC8 catalysis. Notably, the mutation of Gly to Arg at position 11 restored the HDAC8 activity on a peptide substrate lacking the KRHR sequence. Taken together, the HDAC8 substrate specificity is dependent on the nature of the local and distal sequence of its target acetyl-lysine residue. Furthermore, the HDAC8 mediated deacetylation reaction follows a strict order for a substrate containing multiple acetyl-lysine residues. In addition, the methylation

of substrate at Lys 20 reportedly has a direct influence on acetylated-lysine moiety at position 12.

In a subsequent study, Milan Mrksich and colleagues investigated the influence of a local sequence of the ϵ -acetyl-lysine moiety of substrate on HDAC8 catalyzed reaction utilizing a substrate of the following sequence: Ac-GXK^{Ac}ZC-NH₂, where X and Z represent all amino acid except cysteine [88]. HDAC8 showed the highest specificity for the substrate containing the RK^{Ac}F sequence. It is argued that the coumarin moiety present in the fluorogenic tripeptide substrate previously reported by Andreas Schwienhorst *et al.* serves as an analog of the aromatic amino acid, phenylalanine (F). Furthermore, HDAC8 did not show any reactivity with a substrate of the following sequence: Ac-RHKK^{Ac}-NH₂, which lacks a phenylalanine (F) or coumarin adjacent to acetyl-lysine moiety at C-terminus. In view of the above facts, it was cautioned that a fluorogenic peptide substrate, widely used for *in vitro* HDAC8 assay, would produce erroneous results. Furthermore, the crystal structure of HDAC8 with a fluorogenic peptide substrate clearly showed that the methyl-coumarin moiety (fluorophore) plays a significant role in the binding of the ligand to the enzyme, which strengthens the above argument.

1.6. Substrate Independent HDAC8 Assay for HTS of HDAC8 Effectors

In vitro HDAC enzyme assay, developed utilizing a fluorogenic peptide substrate, has been widely used for high throughput screening for novel HDAC effectors. However, it suffers from the following limitations. The fluorogenic moiety of the substrate is likely to interact with an effector molecule which would provide a false positive/negative result. For example, resveratrol was reported to serve as an activator of Sirt1 based on the enzyme assay which utilizes a fluorogenic peptide substrate [89]. Later, it was observed that

resveratrol does not serve as a direct activator of Sirt 1 *in vivo*. Furthermore, *in vitro* coupled-enzyme assay, an effector of the coupling enzyme (trypsin) could be mistakenly identified as an HDAC effector.

Even though the *in vitro* HDAC8 assay developed by Milan Mrksich and co-workers utilizes a non-fluorogenic substrate, it has the following limitations. The assay requires an immobilization of peptide substrate on an inert solid surface, which has a potential to modulate the enzyme structure/activity. Additionally, it uses mass spectrometry as an analytical tool, which is expensive and requires skilled personnel to perform the assay.

In order to overcome the above limitations, serious attempts have been made to develop an alternative *in vitro* assay which is based on the direct binding of the effector (inhibitor/activator) to HDAC. Daniel Riester *et al.* developed a competitive binding assay to determine the binding affinity of a non-fluorogenic ligand to histone deacetylase like aminohydrolase (HDAH) [90]. The above assay utilizes a fluorogenic hydroxamate-based inhibitor, FAHA (2-Furylacryllohydroxamate). The binding of FAHA to HDAH quenches its tryptophan fluorescence via a fluorescence resonance energy transfer (FRET). In a competitive binding situation, the potency of a non-fluorogenic HDAH inhibitor is determined based on its ability to displace FAHA from enzyme's site leading to an enhancement in the tryptophan fluorescence. The K_d values of few selected HDAH inhibitors derived from the above competitive assay showed a close agreement with the IC_{50} obtained via enzyme activity assay. Furthermore, the assay is quite simple, convenient, and well suited for HTS. However, the authenticity/utility of the assay has not been reported beyond HDAH. In addition, FAHA being a tight binding inhibitor, its displacement from

enzyme's site requires an excessive concentration of a test inhibitor, which would potentially produce an inner filter effect.

In order to avoid the inner-filter effect often encountered in fluorescence intensity measurement, Jan Clardy and co-workers developed a fluorescence polarization-based assay to determine the binding affinity of an HDAC ligand [91]. The above assay utilizes an FITC-conjugated pan HDAC inhibitor as a probe whose polarization is increased upon binding to the enzyme due to its restrained mobility. In a competitive binding situation, the potency a non-fluorogenic HDAC inhibitor is determined based on its ability to displace the probe from enzyme's site, leading to a reduction in the polarization of the probe. Notably, the above assay is reasonably simple and well suited to be adopted in high throughput format. However, its utility/validity has not been tested except for HDAC3/NCoR and HDAC6.

Franz-Josef Meyer-Almes and co-workers developed a dual parameter based HDAC assay utilizing a fluorescent hydroxamate-based inhibitor, Atto 700-HA to determine the binding affinity of the enzyme ligand [92]. The binding of the Atto 700-HA to HDAC increases its fluorescence polarization as well as life-time. In a competitive binding situation, the potency a non-fluorogenic HDAC inhibitor is determined based on its ability to displace Atto 700-HA from the enzyme's site leading to a reduction in the polarization as well as the life-time of the probe. Notably, the above assay is more reliable because of the fact that it utilizes two parameters (polarization and life-time) to determine the binding affinity of the ligand. Additionally, it is well suited to be adopted in high throughput settings.

Recently, Steve Riddle and co-workers developed an HDAC assay based on a time-resolved FRET (TR-FRET) [93]. The assay utilizes an HDAC inhibitor conjugated with Alexa Fluor[®] 647 as a tracer, a GST-tagged HDAC, and a europium labeled anti-GST antibody. Upon a simultaneous binding a Eu-GST antibody and the tracer to HDAC leads to a fluorescence resonance energy transfer (FRET) from europium (donor) to Alexa Fluor[®] 647. In a competitive binding situation, the displacement of tracer by a non-fluorescent HDAC abolishes the above FRET, which is evaluated by measuring the ratio of the fluorescence intensities of donor and acceptor. The above assay has been reported to be suitable for both the class I and II HDACs.

1.7. Metal Dependence on HDAC8 Catalyzed Reaction

HDAC8 is a metalloenzyme which requires a divalent metal ion for catalysis. The identity of the catalytic metal ion reportedly affects the ligand-binding as well as the catalytic features of the enzyme. Carol Fierke and co-workers investigated the metal-dependence on the rate of the HDAC8 catalyzed reaction [94]. The catalytic efficiency of HDAC8 measured on a fluorogenic peptide substrate was found to be dependent on identity the catalytic metal ion, and its value showed the following order: $\text{Ni}^{2+} < \text{Zn}^{2+} < \text{Fe}^{2+} < \text{Co}^{2+}$. Surprisingly, the HDAC8 structure is not dependent on the identity of divalent ion present in the active site pocket, suggesting that the protein dynamics is likely to play pivotal role in the ligand- binding and the catalysis of HDAC8.

HDAC8 has been identified as a Zn^{2+} dependent metalloenzyme. However, the identity of the *in vivo* metal ion is being questioned in recent years, partly because the HDAC8 can utilize other bivalent ion *in vitro* for catalysis in addition to Zn^{2+} . The Co^{2+} ion being a rare metal *in vivo* is unlikely to be incorporated in HDAC8 during protein

expression. The concentration of Fe^{2+} inside cell is considerably higher than Zn^{2+} , suggesting that Fe^{2+} could serve as *in vivo* metal for HDAC8. But, the binding of Zn^{2+} ion to HDAC8 is thermodynamically more favored over the Fe^{2+} ion. Recently, based on an exchangeable concentration of Zn^{2+} and Fe^{2+} in a physiological environment, it has been proposed that both the Zn^{2+} and Fe^{2+} ions could equally serve as *in vivo* metal for HDAC8. In addition, metallochaperones have been reported to play a significant role in regulating the distribution of metal ions to various metalloenzymes [94]. The recombinant form of HDAC8 isolated/purified from *E. coli* or other sources has been found to contain Zn^{2+} as a catalytic metal ion. It is likely that Fe^{2+} ion present in HDAC8 is easily oxidized to into Fe^{3+} in an aerobic condition widely used in protein purification. The HDAC8- Fe^{3+} is catalytically inefficient, and its metal ion is readily exchanged with Zn^{2+} because of a favorable thermodynamics.

Aside from the divalent catalytic metal ion, HDAC8 activity is influenced by presence of a monovalent ion, such as K^+ and Na^+ . The crystal structures of HDAC8 solved by two independent research groups showed the presence of two distinct sites for the binding of monovalent ions to HDAC8. Carol Fierke and co-workers performed an extensive study to elucidate the role of monovalent metal ions in the HDAC8 catalysis [60]. It was observed that binding of K^+/Na^+ to site 1(K1), which is close vicinity of the catalytic metal ion, inhibits HDAC8 activity. Furthermore, the binding of the monovalent ion to site 2 (K2), which is $> 20 \text{ \AA}$ away from the site 1, activates HDAC8 via an allosteric modulation in the protein structure. The binding to K^+/Na^+ to K1 is proposed to reduce the pK_a of His 143, which is an integral component of in charge-relay system involved in HDAC8 catalysis. Notably, K^+ ion has the higher affinity for K1 ($K_{d1} = 3.4 \text{ mM}$) than K2

($K_{d2} = 26 \text{ mM}$). Moreover, the catalytic activity of the other forms of HDAC8, such as HDAC8- Co^{2+} and HDAC8- Fe^{2+} are also modulated via the presence of monovalent ions [94].

1.8. HDACs as Therapeutic Target for Human Diseases

HDACs are high priority drug target for the treatment of several human diseases including cancer [95]. Towards this end, serious attempts have been made to discover their small molecule effectors, which could potentially alleviate the disease condition. HDACs have been found to overexpressed in various forms of human cancer [95]. HDAC1 is primarily overexpressed in gastric, prostate, colon, and breast cancer [95, 96]. The expression of HDAC2 is elevated in breast, colon, colorectal and cervical cancer [97]. An overexpression of HDAC3 has been linked with breast and colon cancer [98]. Notably, among all HDAC isozymes, an exclusive overexpression of HDAC8 has been reported in neuroblastoma cell [99].

Serious attempts have been made by several research groups to elucidate the link between HDAC and cancer. A global loss of H4 acetylation at Lys 16 has been reported in various forms of cancer, suggesting that histone modification is closely link to cancer [100]. Class I HDAC isozymes are reportedly involved in expression p21, a cyclin-dependent kinase inhibitor [101]. The p21 primarily inhibits an uncontrolled cell proliferation, and thereby helps to prevent/eliminate the malignant condition in human cell/tissue.

Several non-histone targets of HDACs, such as p53, $\text{NF}\kappa\text{B}$, etc., are intimately linked with cancer initiation and progression pathways [102]. A mutation in p53 gene has been widely reported in cancer patients [103]. HDAC1 and 2 have been found to reduce the

expression of cadherin-E, which plays a crucial role cancer metastasis. HDACs are recruited to several fusion proteins, such as RAR-PML, RAR-PLZF, which are intimately linked with various forms of hematological malignancies [104]. Recently, HDAC8 has been shown to regulate the expression of both the wild type and the mutant form of p53 in a HoxA dependent manner [103].

An inhibition of HDAC has been known to induce an anticancer affect both *in vitro* as well as in xenograft animal model [105]. However, a pan-HDAC inhibitor usually shows a considerable side affect in a clinical setting, primarily because of an indiscriminate inhibition of the multiple HDAC isozymes involved in several vital cellular processes. In view of the above fact, serious attempts are being made to understand the roles of each HDAC isozyme in a specific form of cancer, so that it can be selectively targeted by an isozyme selective HDAC inhibitor. Notably, isozyme selective inhibitors are likely to have a lower side effect as compared to a pan-inhibitor.

In addition to malignancy, HDACs have been found to regulate learning, memory and cognition in human [106]. Several HDAC isozymes are widely expressed in brain tissues. HDAC2 expression level is reduced in *nucleus accumbens* region of human brain afflicted with a chronic depression [107]. Li-Hui Tsai and co-workers reported the role of HDAC2 in regulation of memory and synaptic plasticity [108]. Valproic acid, an HDAC inhibitor, has been widely used for the treatment of psychiatric disorders [109]. Mutation in HDAC8 is linked with Cornelia de Lange syndrome, where the cognitive behavior of children is severely affected [36]. Furthermore, HDAC inhibitors have shown promising results in ameliorating the neurodegenerative conditions associated with Alzheimer and Hutchinson diseases [109].

Recently, HDACs have emerged as therapeutic target for the treatment of heart diseases [110]. Joseph A. Hill and co-workers discovered the role of HDAC1 and 2 in autophagy mediated cardiac hypertrophy [111]. HDAC4, 5 and 9 are reportedly involved in cardiac hypertrophy in an MEF-2-dependent manner. Timothy has reviewed the therapeutic potential of HDAC inhibitors for the treatment of symptoms associated with heart failure [110]. In addition to cancer and heart disease, HDACs are linked with several inflammatory diseases, such as chronic obstructive pulmonary disease (COPD) and rheumatoid arthritis [112]. In COPD, HDAC enzyme activity is reportedly low [113].

1.9. Therapeutic Potential of HDAC Effectors

HDACs inhibitors have been widely known to have an anticancer effect. They induce growth inhibition, dedifferentiation, and even cell death in cancer cell both *in vitro* as well as in a xenograft animal model [72]. Attempts have been made to elucidate the molecular mechanism of anticancer effect mediated via an HDAC inhibitor. It is important to note that, an HDAC inhibitor such as SAHA influences the expression of only 2-10 % of the total genes in cancer cell [114]. Surprisingly, normal cells essentially remain unaffected upon the treatment with same dosage of inhibitor. An HDAC inhibitor modulates the expression of various genes which are primarily involved in cell cycle, differentiation and caspase-mediated cell death [115]. Several HDAC inhibitors have been reported to down-regulate the expression of an angiogenic factor (VEGF) primarily involved in cancer metastasis, rationalizing the utility of an HDAC inhibitor for the treatment of metastatic cancer [116]. Additionally, the anticancer effect of an HDAC inhibitor has also been found to be mediated via an immunomodulation. Thomas B. Tomasi and co-workers reported that an immunomodulatory effect of an HDAC inhibitor in cancer cell, which is primarily due

to the elevated expression of major histocompatibility complex (MHC I and MHC II) and CD40 [117]. The molecular mechanisms by which an HDAC inhibitor influences the expression of few selected genes are not yet understood [118]. However, it is widely known that a pan-HDAC inhibitor significantly affects the acetylation status of its histone as well as several non-histone proteins, such as HSP90, p53, tubulin, etc. Notably, the anticancer effect of an HDAC inhibitor is also dependent inhibitor-type and the nature of cancer cell, suggesting that underlying molecular mechanism of anticancer effect is different in various forms of cancer [119,120].

HDAC inhibitors have been shown to be very effective for the treatment various hematological malignancy [72]. However, their therapeutic efficacy is reportedly low, and they are ineffective against solid tumors [121]. A combination therapy utilizing an HDAC inhibitor along with other anticancer drugs has been proposed, which is likely to enhance the efficiency of cancer therapy in various forms of cancer including solid tumors. Ravi Bhatia and co-workers have reported an enhanced efficacy of an HDAC inhibitor in reducing the number leukemic stem cells, when it is used in combination with an another anticancer drug, Imatinib Mesylate [122]. Notably, cancer stem cells essentially remain unaffected by an HDAC inhibitor alone, often leading to a relapse/remission of malignancy after chemo and/or radiotherapy.

In recent years, it has been realized that targeting a specific form of cancer by isozyme selective inhibitor of HDAC would boost up the efficiency of cancer therapy, especially because of their limited side effects [123]. However, the above approach has the following limitations. Firstly, HDAC isozymes in human share a high degree of similarity in the geometry of their catalytic pocket, which limits the development of an isozymes

selective inhibitor. Secondly, the link between a specific HDAC isozyme with a particular form of cancer is not well defined.

Therapeutic efficacy of HDAC inhibitor *in vivo* is difficult to predict a priori. It has been widely known that even the structurally similar HDAC inhibitors show a differential effect on the same cancer cell/tissue. P. G. Parson and co-workers investigated the antitumor activity of selected hydroxamate-based inhibitors, namely Alelaic bishydroxamate (ABHA) and Trichostatin A (TSA), *in vitro* and in a xenograft animal model. Both the above inhibitors showed a similar anticancer effect *in vitro*, while the TSA failed to exhibit any effect *in vivo* [119]. Furthermore, in a study performed by J. Chang *et al.* TSA and Romidepsin, which contain an unrelated Zn-binding group, were found to induce a different cellular response even within the same cancer cell line [120]. In view of the above facts, it is now widely realized that it is difficult to assess the therapeutic efficiency of an HDAC inhibitor based on its *in vitro* inhibitory potency.

Therapeutic potential of HDAC activators have not been well understood so far. However, there are several human diseases where an HDAC activator could be of great therapeutic benefits. In COPD and CLdS where the HDAC enzyme activity has been reported to be reduced, HDAC activators have a potential to ameliorate the disease conditions [113, 36]. Based on a recent study performed by X. Chen and co-worker, therapeutic potential of an HDAC8 selective activator for the treatment of various forms of cancers has recently emerged. In the above case the expression of the tumor suppressor protein (p53) is reportedly suppressed by HDAC8 [103].

1.10. Approaches for Designing Novel HDAC Inhibitors

In view of a considerable side effect (especially cardiotoxicity) of the currently known HDAC inhibitors, there has been an urgent need to search for their alternative [124]. In that pursuit, various attempts have been made to develop novel HDAC inhibitors utilizing different approaches as described below. As opposed to HDAC inhibitors, there has been a limited interest in development of novel HDAC activators, primarily because of the lack of the knowledge about their therapeutic benefits. Moreover, a structure-based design of an allosteric activator of an enzyme is always challenging because of the fact that it is difficult to assign an allosteric binding site in an enzyme. Additionally, a random conformational modulation in enzyme/protein structure, induced upon the binding of an allosteric ligand, is rarely translated into an enhanced catalytic efficiency of the enzyme. Crystallographic studies of various human HDACs provide a valuable insight into a structure-based design of HDAC inhibitors. In absence of a crystal structure, homology modeling, molecular docking, and computer simulation techniques play indispensable role in designing the novel inhibitors as well as understanding their structure-activity relationship [125]. A canonical HDAC inhibitor, which is primarily competitive in nature, is comprised of the following domains/groups: metal chelator, linker, and a cap. The chelator serves as a metal ion binding group. The linker, serving as a mimic of the methylene group of substrate's lysine, is accommodated in the hydrophobic tunnel of the active site. The cap group interacts with the enzyme's surface at the entrance of the catalytic pocket. In order to design novel HDAC inhibitors various synthetic approaches have been utilized in different research groups [126]. In addition, natural inhibitors of HDAC, such as TSA, romidepsin, and largazole have also been discovered [127-128, 62].

More recently, a special interest has emerged among researchers towards the development of an isozyme selective inhibitor of HDAC via an exploration of the acetate release channel [129], which is exclusively present in class I HDACs.

A hydroxamate group has been widely used as metal chelator for designing inhibitors for various metalloenzymes [130]. However, significant progress has been made to find out the alternative (non-hydroxamate), primarily because of an associated side effect of the hydroxamate-based drugs [124]. Several non-hydroxamate-based inhibitors of HDAC, which contain an alternative metal chelator group, such as the derivatives of sulfur, ketone, boron, and phosphorous, have been reported [126]. Romidepsin and largazole are well known non-hydroxamate, natural inhibitors of HDAC, which produce a thiol moiety as a metal binding group in a reducing environment. Nicolai Cramer and co-workers synthesized several derivatives of largazole and evaluated their potency on various cancer cell lines [131]. Several ketone derivatives have been synthesized by Olaf Kinzel *et al.*, which serve as isozyme selective inhibitors of class I HDAC [132]. Furthermore, other metal chelating groups, such as boronic acid, phosphorous derivative, trifluomethylketone, etc., which serve as a mimic for an oxyanion intermediate produced during HDAC catalysis, have been utilized to develop novel HDAC inhibitors [134-135, 67]. Notably, the crystal structures of HDAC8 and HDAC4, respectively, with largazole [62] and TFMK [67] have shown that the thiol and ketone moieties indeed serve as a metal chelator. The crystal structures of various HDAC isozymes have shown a significant difference in the accessibility of the hydrophobic tunnel for different ligands, which provides an important avenue for development of isozymes selective HDAC inhibitor. The crystal structure of HDAC8 bound with an aromatic linker containing hydroxamate-based inhibitor

(compound 2) suggests that a bulky linker group is less likely to be accommodated in HDAC8 due to a steric hindrance posed by Trp141 at the bottom of the hydrophobic tunnel [58]. The Trp141 is replaced by an analogous residue, Leu, in HDAC1 and 3. A bezamide-based inhibitor, MS27-275, which contains a bulky linker group, does not serve as a potent inhibitor of HDAC8, as oppose to HDAC1 and 3, strengthening the above argument. P. Bertnand and co-workers synthesized various analogs of TSA, SAHA and MS27-275, which differ in terms of rigidity and hydrophobicity of their linker group and evaluated their efficacy on various cancer cell lines [135, 136]. Scoff M. Ulrich and co-workers designed several linkerless and isozyme selective inhibitor of HDAC by exploring the sub-pocket, which has been observed in the crystal structure of HDAC8 bound with CRA-A [71, 57].

Various HDAC isozymes have evolved to catalyze deacetylation of acetylated lysine moiety which resides in variety of natural substrates/targets. It is likely that the substrate specificity of an HDAC would at least partially be dictated via the surface interactions in the vicinity of catalytic pocket. In view of the above fact, it has been proposed that the isozyme selective inhibitors of HDAC could be developed by varying the nature of the cap group of a canonical inhibitor, which is likely to interact differently with various enzymes' surface. In fact, cyclic tetrapeptides, which contains a distinct bulky cap group, have been reported to be selective for class I HDACs [137]. Olaf Wiest and co-workers used various computational methods, such as homology modeling, molecular docking, and molecular dynamic simulation to investigate of structural basis of interactions between an inhibitor with individual HDAC isozymes, such as HDAC1, 2, 3, and 8 [138]. In the above study, it was found that the cap group of an inhibitor dictates the isozymes

selectivity. M. Reza Ghadiri *et al.* synthesized several analogs of cyclic tetrapeptide inhibitors of HDAC and evaluated their potency [137]. Isozyme selectivity was again found to be dependent on the interaction between protein surface and the cap group of the inhibitor. Interestingly, several linkerless inhibitors of HDAC8 have been reported, where the selectivity is not mediated via the cap group [71].

In recent years, an interest has emerged among various investigators to design a class specific HDAC inhibitor via the exploration of acetate release channel [129], which is exclusively found in class I HDACs. Thomas A. Miller and co-workers synthesized several biaryl benzamide, which have been proposed to bind to acetate release channel [139]. Furthermore, Lewis Whitehead *et al.* synthesized several amino acid derivatives in pursuit of designing isozyme selective inhibitors of HDAC [140]. The crystallographic studies of HDAC8 with the above inhibitors, indeed, showed that isozymes selectivity in above case is primarily mediated via binding to the acetate release channel [140].

1.11. Therapeutic Efficacy of HDAC Inhibitors in Clinical Settings

Therapeutic efficacy of several HDAC inhibitors has been widely evaluated in clinical settings [141]. Table 1.5 shows the list of HDAC inhibitors which are at different stages of clinical trials for the treatment of various forms of cancer. Notably, SAHA (Zoliza[®]) and Romidepsin (Istodax[®]) have already been approved by FDA for the treatment of cutaneous T-cell lymphoma [141]. The HDAC inhibitors listed in the above table are usually classified into the following four classes: hydroxamate, short chain fatty acid, benzamide, and cyclic peptide. The hydroxamate based inhibitors usually have high potency (nanomolar range). However, they usually show a considerable toxicity *in vivo*. Romedepsin is a cyclic peptide inhibitor and reportedly shows an IC₅₀ in a nanomolar

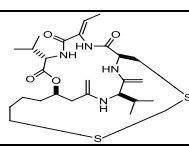
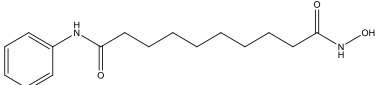
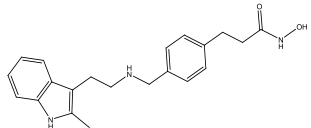
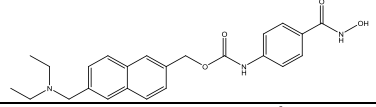
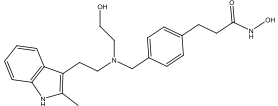
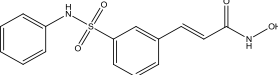
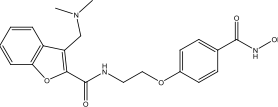
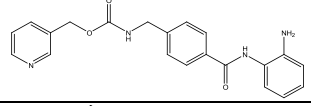
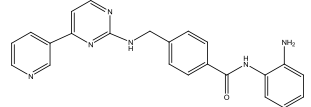
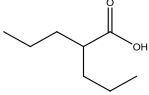
range. Benzamide inhibitors, such as Entinostat (SNDX-275), Mocetinostat (MS27-275), have been found to be relatively selective toward class I HDAC inhibition. Short chain fatty inhibitors, such as valproic acid, phenylbutyrate have a low inhibitory potency.

Therapeutic efficacy of an HDAC inhibitor in clinical settings reportedly depends on its biophysical properties, interaction with receptor/target, bioavailability, pharmacokinetics and pharmacodynamics, as well as on the genotype of a cancer cell, where it is tested [141]. The above properties of an inhibitor are primarily dependent on its chemical structure/nature. Additionally, the side effect an HDAC inhibitor is often dependent on its class. For example, hydroxamate-based drugs usually show higher side effects than the others [124]. Even within a class, a therapeutic efficacy has been found to be very different [119]. In view of the above fact, there has been an ongoing effort to develop novel HDAC inhibitors which would show a better therapeutic efficacy in clinic than the currently known inhibitors.

Veronica Novoty-Diermayr and co-workers evaluated the efficacy of the two structurally similar hydroxamate inhibitors, namely, SAHA and SB939, and reported the following major differences [142]. The bioavailability and half-life of SB939 was significantly higher (3-4 fold) than SAHA, which is likely to be translated into a higher efficacy of the former *in vivo* as well as in a xenograft animal model. Thomas Becker *et al.* reported the class specific differences in the pharmacological properties of HDAC inhibitors, such as hydroxamate vs. benzamide [143]. Clarie Bonfils *et al.* developed an *in vivo* enzyme assay utilizing a fluorogenic substrate and validated its utility for studying the pharmacodynamics of MGCD0103 [144]. Interestingly, a change in the expression level of an HDAC has been found to influence the *in vivo* efficacy of HDAC inhibitors. Debdutta *et*

al. reported that an overexpression of HDAC1 in cancer cells produces a drug resistance against sodium butyrate [145]. Furthermore, truncation mutation in HDAC2 is linked with the drug resistance in cancer cells against several HDAC inhibitors. More recently the presence of a biomarker, HR32B, which is involved in shuttling a cargo to proteasome, has been reported to influence the therapeutic efficacy of an HDAC inhibitor in cancer cells [141].

Table 1.5. List of HDAC inhibitors in clinical trial

Name	Structure	Class	Potency Range
Romidepsin (Istodax®)		Cyclic peptide	Nanomolar
SAHA (Zoliza®)		Hydroxamate	Micromolar /nanomolar
Panobinostat (LBH589)		Hydroxamate	nanomolar
Givinostat (ITF2357)		Hydroxamate	nanomolar
Dacinostat (LAQ824)		Hydroxamate	nanomolar
Belinostat (PXD101)		Hydroxamate	nanomolar
PCI-24781		Hydroxamate	nanomolar
Entinostat (SNDX-275)		Benzamide	micromolar
Mocetinostat (MGCD0103)		Benzamide	micromolar
Valproic acid		Short chain fatty acid	millimolar

CHAPTER 2. STATEMENT OF PROBLEM

Histone deacetylase 8 (HDAC8) is a high priority drug target for the treatment of various human diseases including cancer. Zolinza[®] and Istodax[®] are the HDAC8 inhibitors which have already been approved by the FDA for the treatment of T-cell lymphoma. Additionally, several other inhibitors are in advanced stages of clinical trials for treatment of other human malignancies. In view of the fact that the currently known inhibitors of HDAC8 contain severe side effects, there is an urgent need to search for alternative. Aside from the inhibitors, therapeutic potential of an HDAC8 activator has recently been discovered.

The high-throughput screening (HTS) approach to discover a novel effector of an enzyme is often inconvenient, expensive, and time-consuming. In order to circumvent the problems associated with HTS, a structure-based approach is widely utilized in order to enhance the *in vitro* potency of a lead compound. However, even a highly potent lead compound/drug candidate often fails to produce an *in vivo* efficacy. Notably, kinetics and thermodynamics of the binding of an effector to its target play a very crucial role in dictating its *in vivo* efficacy.

In view of the above background information, a research project entitled “Biophysical studies of ligand binding to HDAC8” was undertaken with the following specific aims:

- (1) To discover novel effectors of HDAC8 via a high-throughput screening of an in-house library of small molecules, and to test their isozyme-selectivity against various HDAC isozymes.

- (2) To develop a substrate-independent enzyme assay for high-throughput screening of HDAC inhibitors.
- (3) To investigate the kinetics and the thermodynamics of ligand binding to the recombinant form of human HDAC8.
- (4) To elucidate the effect of the ligand binding on the conformational stability of HDAC8.

The above study was primarily aimed to discover novel effectors of HDAC8, and to provide valuable insight for the optimization of lead compounds based on the transient kinetic and thermodynamic investigation of ligand-binding to the enzyme.

CHAPTER 3. MATERIALS

The plasmid containing the coding sequence of human HDAC8 (pCMV-SPORT6) was obtained from Open Biosystems Huntsville, AL. The ligation independent cloning (LIC) compatible *E. coli* expression vector pLIC-His was a kind gift from Prof. Stephen P. Bottomley (Monash University, Australia). Cloned *Pfu* DNA polymerase, BL21 CodonPlus[®] DE3 (RIL) and DH5 α *E. coli* cells were purchased from Stratagene (La Jolla, CA). The primers used for subcloning HDAC8 were synthesized by Integrated DNA Technologies (Coralville, IA). *SacII* restriction endonuclease and T4 DNA polymerase were obtained from New England Biolabs (Ipswich, MA). Miniprep plasmid DNA isolation kit and Qiaquick[®] gel purification kit were purchased from Qiagen (Valencia, CA). Yeast extract and tryptone were purchased from Becton Dickinson (Sparks, MD). Ampicillin, chloramphenicol, and PMSF (phenylmethylsulfonyl fluoride) were obtained from CalBiochem. Nonidet P-40 substitute was purchased from USB Corporation, Cleveland. HisTrap 5 ml columns were purchased from GE healthcare life sciences. Dialysis tubing was purchased from Spectrum[®] laboratories. Zeba spin desalting columns, BSA (bovine serum albumin) standard and TCEP (tris-2 carboxy ethyl phosphine) were purchased from Thermo Fisher Scientific (Rockford IL). Protein molecular weight marker was purchased from Amersham Biosciences. 40 % polyacrylamide solution, Bradford reagent was purchased from BioRad (Hercules, CA). SAHA (suberoylanilide hydroxamic acid) was custom synthesized by Biomol Laboratories (Plymouth Meeting, PA). Fluor-de-Lys[™] substrate, Fluor-de-Lys[™] deacetylated standard and the recombinant forms of human HDAC isozymes, namely, HDAC1, HDAC2, HDAC3, HDAC6, HDAC10, HDAC11, SBHA (Suberoyl bis-hydroxamic acid), M344 (4-Dimethylamino-N-(6-

hydroxycarbamoylhexyl)-benzamide) and TSA (Trichostatin A) were purchased from Enzo Life Sciences. Tris, Hepes, Bicine Triethanolamine, trypsin from bovine pancreas, ammonium per sulfate, 2-mecaptoethenol, imidazole, magnesium chloride, and lactose were purchased from Sigma. Glycine, sodium chloride and glycerol were purchased from VWR international (West Chester, PA). DMSO (dimethyl sulfoxide) and potassium chloride was obtained from Fisher Scientific (Pittsburgh, PA). All the compounds of TM and VYU series were synthesized by Dr. Tanmay Mandal and Dr. Vesela Ugrinova, respectively, in the laboratory of Prof. Greg Cook (NDSU). Compounds of MH series were synthesized by Dr. Manas Haldar in the laboratory of Dr. Sanku Mallik (NDSU). The other chemicals used in the research were of analytical grade.

CHAPTER 4. METHODS

4.1. Cloning, Expression and Purification of Recombinant Human HDAC8

4.1.1. Sub-cloning of Human HDAC8 Gene

In order to clone the human HDAC8 gene into an *E. coli*-based expression vector, the cDNA clone of HDAC8 gene was purchased from Open Biosystem (clone ID 5761745). The cDNA was available as an insert in mammalian expression vector pCMV-SPOR6. The colonies of recombinant *E. coli* cell (strain DH10B) were isolated after streaking the inoculum on LB agar plate containing 100 µg/ml ampicillin. A single colony was picked up, grown overnight at 37 °C in 5 ml LB medium containing 100 µg/ml ampicillin. The cells were harvested, and the plasmid was isolated using QIAprep® miniprep DNA isolation kit. The isolated plasmid was used as the template for PCR to amplify the HDAC8 gene for sub-cloning. The HDAC8 gene was cloned into a pET-based *E. coli* expression vector, pLIC-His. The pLIC-His vector was obtained as a gift from Prof. Stephen P. Bottomley, Monash University, Australia. The vector has been designed for Ligation Independent Cloning (LIC) which does not require DNA ligase [147]. In LIC cloning strategy, the gene of interest is amplified by Polymerase Chain Reaction (PCR) with an extra 12-15 bp end sequence. The PCR product is treated with T4 DNA polymerase in the presence of dNTP. The exonuclease activity of T4 produces an overhang which facilitates its insertion into a complementary vector with simple annealing at room temperature.

The LIC-His vector was linearized using *SacII* restriction enzyme. For 100 µL of *SacII* restriction digestion reaction of the pLIC-His vector, the reagents used were as followed: 25 µL of pLIC-His (200 ng/µL), 10 µl of 10X NEBuffer 4, 10 µl of 10X BSA,

and 5 μL of 20 U/ μL *SacII*. The linearized vector was purified from agarose gel using QIAquick gel extraction kit and the concentration was determined using UV-spectrophotometer.

The gel purified vector was subjected to T4 DNA polymerase treatment. For 200 μL reaction mixture the following reagents were used: 100 μL gel purified DNA (4 ng/ μL), 20 μL of 10X NEBuffer 2, 20 μL of 10X BSA, 2 μL of dTTP (100 mM in water), and 0.5 μL of T4 DNA polymerase (3 U/ μL). The reaction mixture was incubated at 16 $^{\circ}\text{C}$ for 1 hour followed by heat inactivation at 75 $^{\circ}\text{C}$ for 20 minutes.

For PCR amplification of HDAC8 gene using the pCMV-SPORT plasmid as the template, the following sense and antisense primers were used

5'-CCAGGGAGCAGCCTCGATGGAGGAGGAGCCGGAGGAACCG-3' sense primer

5'-GCAAAGCACCCGGCCTCGTTAGACCACATGCTTCAGATTCCC-3' antisense primer

The PCR was performed on the MiniCycler™ (MJ research) for 25 cycles under the following experimental conditions: initial denaturation at 94 $^{\circ}\text{C}$ for 50 sec, denaturation at 94 $^{\circ}\text{C}$ for 45 sec, annealing at 62 $^{\circ}\text{C}$ for 50 sec, extension at 72 $^{\circ}\text{C}$ for 90 sec. The reagents used for 50 μL of PCR reaction were as follows: 5 μL of 10X cloned *Pfu* DNA polymerase buffer, 1.25 μL of dNTPs mixture (containing 10 mM of each dNTP), 1.0 μL of template (50-100 ng/ μL), 2 μL of the primer mix (containing 250 ng/ μL of each primer), and 1.5 μL of cloned *Pfu* DNA polymerase and 5 μL glycerol. The PCR amplified DNA was gel purified using QIAquick gel extraction kit.

To create the overhang, the gel purified PCR product was subjected to T4 DNA polymerase treatment. The reagents used for the 50 μL reaction mixture for T4 DNA

polymerase treatment were: 1.5 μL of gel purified PCR amplified DNA (50 $\text{ng}/\mu\text{L}$), 5 μL of 10X BSA, 0.5 μL of T4 DNA polymerase (3 $\text{U}/\mu\text{L}$), and 1.5 μL of dATP (100 mM in water). The reaction mixture was incubated at 16 $^{\circ}\text{C}$ for one hour followed by heat inactivation at 75 $^{\circ}\text{C}$ for 20 minutes.

The pLIC-His vector and the PCR product could easily anneal with each other because of the overhangs being generated by T4 DNA polymerase treatment. For annealing reaction 2 μL of the vector was mixed with 4 μL of the PCR product. The reaction mixture was incubated for one hour at 22 $^{\circ}\text{C}$. The reaction was stopped by the addition of 1 μL of 25 mM EDTA solution in water, pH 8.0 (adjusted with NaOH). The DNA present in the reaction mixture was transformed using standard molecular biology protocol into high efficiency chemically competent DH5 α cells (Invitogen). A single colony of the recombinant *E. coli* cells was inoculated in 5 mL LB (Luria Bertani) medium supplemented with 50 $\mu\text{g}/\text{ml}$ ampicillin and grown overnight at 37 $^{\circ}\text{C}$. The cells were harvested by centrifugation at 1200 rpm using a table top centrifuge (Eppendorf model 5415C). The recombinant plasmid (pLIC-His6-HDAC8) was isolated using QIAprep[®] miniprep DNA isolation kit. The cloning of the coding regions of the HDAC8 gene in the pLIC-His vector was confirmed by sequencing of the plasmid at University of Chicago Cancer Research Center (Chicago, IL).

4.1.2. Expression and Purification of Recombinant Human HDAC8

For the overexpression of the HDAC8 gene, the pLIC-His-HDAC8 plasmid was transformed into *E. coli* BL21 codon plus DE3 (RIL) chemically competent cells (Stratagene) using standard molecular biology protocol. The transformed cells were grown in LB (Luria Bertani) medium (BD Franklin Lakes, NJ USA) supplemented with 100

$\mu\text{g/mL}$ ampicillin and $30 \mu\text{g/mL}$ chloramphenicol at 37°C (shaker speed = 220 rpm) until the optical density of 0.6-0.8 was reached at 600 nm. The protein expression was induced by the addition of 0.05% (w/v) lactose. At this point, the LB medium was supplemented with $100 \mu\text{M}$ ZnCl_2 . The cells were further grown at 18°C (shaker speed = 220 rpm) overnight and were harvested by centrifugation at 5000 g using Sorvall[®] RC-5B with SLA-3000 rotor for 15 minutes at 4°C . The pellet was suspended in a lysis buffer (50 mM Tris-HCl, pH 8, containing 150 mM KCl, 3 mM MgCl_2 , 1 mM 2-mercaptoethanol, 1 mM PMSF (Phenylmethylsulfonyl fluoride) and 0.25 % Triton X-100. The cells were lysed by sonication in Branson Sonifier 450. The crude extract was centrifuged at 15000 g for 30 min at 4°C to remove the cellular debris. The resulting supernatant was filtered with $0.2 \mu\text{m}$ syringe filter and the filtrate was loaded onto a 5 ml HisTrap column pre-equilibrated with the lysis buffer with 5 mM imidazole minus PMSF and the detergent. The HDAC8 purification was performed using AKTA[™] purifier UPC 10 (GE healthcare Life Sciences). The column was washed with 20 column volume of 20 mM imidazole in the purification buffer (50 mM Tris-HCl, pH 8, containing 150 mM KCl, 3 mM MgCl_2 , 1 mM 2-mercaptoethanol) to remove the weakly bound contaminating protein to the column. A linear gradient of 50 column volumes of imidazole in purification buffer ranging from 20-130 mM was used to elute HDAC8 from the column. The elution of the protein was monitored at on real time basis using the light absorption device (280 nm) built in the AKTA purifier.

4.1.3. SDS-PAGE Analysis of HDAC8 Purification

The purity of HDAC8 eluted from HisTrap columns in different fractions were evaluated using SDS-PAGE. The electrophoresis was performed in 4 % stacking gel and

10 % resolving gel using a Laemmli buffer (Bio-Rad laboratories). The resolving gel contained 10 % acrylamide + 0.1 % SDS and the stacking gel contained 4 % acrylamide + 0.1 % SDS prepared in 1.5 M Tris, pH 8.8 and 0.5 M Tris, pH 6.8. The protein samples were diluted (1:1) in 2X loading dye containing (10 % SDS, 25 % glycerol, 5 mM β -mercaptoethanol, 0.015 % bromophenol blue and 30 mM Tris, pH 6.8) The samples were mixed and heat denatured by boiling for 5 minutes in a water-bath at 90 °C. The denatured protein samples were then loaded in the gel. The electrophoresis was performed with 200 volt direct current using Bio-Rad gel electrophoresis apparatus. The running buffer used in the electrophoresis was tris-glycine containing 0.1 % SDS, 25 mM Tris, 190 mM glycine, pH 8.3. To visualize the protein bands on the gel, it was stained with 0.1 % Coomassie Blue in 10 % acetic acid and 10 % methanol for 15 min and destained by 10 % acetic acid and 40 % methanol. The fractions containing HDAC8 with more than 95 % purity were pooled and dialyzed overnight at 4 °C against the HDAC8 storage buffer (10 mM Tris, pH 7.5, containing 100 mM NaCl, 3 mM MgCl₂, 10 % glycerol and 1 mM TCEP). The protein was kept at -70 °C for long term storage.

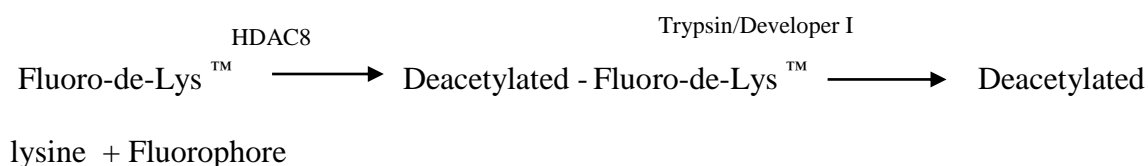
4.1.4. Estimation of Protein Concentration

The concentration of HDAC8 was estimated by Bradford assay using BSA as a standard protein. The assay was performed in absorption micro plate reader (Spectra Max PLUS³⁸⁴, Molecular Devices). A mixture of 1:1 diluted HDAC8 in storage buffer was mixed with 1:4 diluted Bradford reagent [148]. The mixture was incubated for 5 minutes at room temperature and the absorbance was measured at 595 nm. The molar concentration was calculated taking the molecular weight of HDAC8 as 42 kDa.

4.2. Steady State Enzyme Kinetic Methods

4.2.1. Coupled Assay for the HDAC8 Catalyzed Reaction

To measure the rate of the HDAC8 catalyzed reaction, a continuous trypsin-coupled assay was developed using Fluoro-de-LysTM substrate. In the above coupled assay, the reaction catalyzed by HDAC8 was coupled with trypsin generating a fluorogenic product as shown in the Scheme 4.1.



Scheme 4.1. Trypsin-coupled assay

The substrate contains the acetylated lysine residue which is attached to an amino methyl coumarin moiety (AMC) via an amide linkage. Removal of the acetyl group from the Fluoro-de-LysTM by the HDAC8 catalyzed reaction produces a deacetylated product, which is hydrolyzed by trypsin liberating AMC. The free AMC being highly fluorogenic ($\lambda_{\text{ex}} = 365 \text{ nm}$ and $\lambda_{\text{em}} = 500 \text{ nm}$) could be easily detected using spectrofluorometer. The enzyme assay was performed at 25 °C in HDAC8 assay buffer (50 mM Tris-HCl buffer, pH 7.5, containing 137 mM NaCl, 2.7 mM KCl, 1 mM MgCl₂, 1 mg/ml BSA) using 150 μM Fluor de LysTM as the fluorogenic substrate, 250 nM Trypsin and 250 nM HDAC8. The initial velocity of the enzyme catalyzed reaction was determined by monitoring the time dependent increase in the fluorescence intensity at 500 nm ($\lambda_{\text{ex}} = 365 \text{ nm}$) using a fluorescence microplate reader (SpectraMax Gemini, Molecular Devices). The concentration of trypsin in the enzyme assay was optimized such that the HDAC8 catalyzed reaction limits the overall rate of catalysis in the steady state condition.

Additionally, the trypsin concentration was kept lower (100-250 nM) to minimize the proteolytic cleavage of HDAC8. The presence of BSA (bovine serum albumin) in the assay buffer further protects HDAC8 from proteolytic degradation.

4.2.2. Steady State Kinetics of the HDAC8 Catalyzed Reaction

The trypsin-coupled assay in continuous mode was used to determine the steady state kinetic parameters of the HDAC8 catalyzed reaction using Fluor-de -LysTM as a substrate. To determine the K_m (Michaelis constant) of the substrate, initial velocity of the HDAC8 catalyzed reaction was measured as a function of increasing concentration of the substrate. The data were analyzed using the Michaelis-Menten equation 4.1:

$$v = V_{\max} / (1 + K_m / [S]) \quad \text{Eq. 4.1}$$

where v is the initial rate, K_m is the apparent dissociation constant of the substrate with the enzyme (given in μM) and V_{\max} (Relative Fluorescence Unit/sec) is the maximal steady state rate of HDAC8 catalyzed reaction. To determine the k_{cat} (turnover number) of the HDAC8 catalyzed reaction, the V_{\max} (RFU/sec) was converted into $\mu\text{M}/\text{sec}$ utilizing a standard curve prepared with the known concentration of deacetylated product generated after trypsin cleavage. The k_{cat} was estimated by dividing the V_{\max} ($\mu\text{M}/\text{sec}$) by the concentration of enzyme used the HDAC8 assay.

4.2.3. Screening of the HDAC Effectors

In pursuit of discovering novel inhibitors/activators (effectors) of HDAC8, several small molecules were synthesized in the laboratories of Prof. Greg Cook and Prof. Sanku Mallik in the departments of Chemistry and Biochemistry and Pharmaceutical Sciences at NDSU, respectively. To evaluate their effectiveness on the HDAC8 catalyzed reaction, the initial screening was performed by measuring the change in HDAC8 activity in the

presence of 10 μM of the potential effectors. The small molecules inhibiting the HDAC8 activity > 50% were selected for determining their inhibition constant (K_i). The compounds enhancing the HDAC8 activity at 10 μM by >3-5 fold were used for further studies. Isozyme selectivity of selected potent HDAC inhibitors/activators was tested with other commercially available recombinant forms of the HDAC isozymes (HDAC1, 2, 3, 4, 6 and 9) aside from HDAC8.

To determine the inhibition constant (K_i) of the HDAC8-inhibitor complex, initial velocities of the HDAC8 catalyzed reaction were measured as a function of increasing inhibitor concentration. The data were analyzed using the quadratic equation describing the competitive steady state model for the inhibitors (Eq. 4.2):

$$v = \frac{v_0 \cdot K_i}{K_i + \left([I]_t - 0.5 \left\{ ([I]_t + [E]_t + K_i) - \sqrt{([I]_t + [E]_t + K_i)^2 - 4 \cdot [I]_t \cdot [E]_t} \right\} \right)} \quad \text{Eq. 4.2}$$

where v_0 is the initial velocity of HDAC8 catalyzed reaction without any inhibitor, $[I]_t$ is total concentrations of the inhibitor, $[E]_t$ is the total concentration of HDAC8 used in the assay.

To determine the apparent activation constant (K_a) of the HDAC8 activators, the initial velocities of enzyme catalyzed reaction were measured in the presence of increasing concentration of the activator. The data were analyzed using Origin[®] software package for the hyperbolic/sigmoidal dependence of HDAC8 activity as a function of the activator concentration using Eq.4.3:

$$v = V_{\max} [A]^n / (K_a + [A]^n) + \text{offset} \quad \text{Eq. 4.3.}$$

where V_{\max} (RFU/sec) is the initial velocity of the HDAC8 catalyzed reaction at saturating concentration of the activator, $[A]$ is the total concentration of the activator, offset is the

rate of enzymatic reaction in the absence of the activator, n is the Hill coefficient and K_a is the apparent activation constant of the activator .

To study the influence of the activator on the steady-state kinetic parameters of the HDAC8 catalyzed reaction, K_m and k_{cat} of Fluoro-de-LysTM for HDAC8 were determined in the presence of 50 μ M activator.

4.3. Equilibrium Binding Studies for HDAC8-Ligand Interactions

4.3.1. Binding Isotherms for HDAC8-ligand Interactions via Change in Fluorescence Signal

All the steady-state spectrofluorometric studies were performed in HDAC8 storage buffer on a Perkin-Elmer lambda 50-B spectrofluorometer, equipped with a magnetic stirrer and thermostated water bath using a 4 x 4 mm² square quartz cuvette. The change in intrinsic fluorescence signal of the enzyme upon of ligand was used for titration of fixed concentration of HDAC8 with increasing concentration of the ligand to obtain the overall binding isotherms. The binding isotherm for the interaction of c-SAHA with HDAC8-complex was determined by titration of a fixed concentration of c-SAHA (0.1 μ M) with increasing concentrations of HDAC8 in the storage buffer described above. The fluorescence emission spectrum of c-SAHA was monitored in the range of 400–500 nm ($\lambda_{ex} = 325$ nm). The binding isotherm for the interaction of effectors (inhibitors/activators) with HDAC8 were determined by titration of the fixed concentration of HDAC8 (1.5 μ M) with increasing concentrations of the respective ligand in the storage buffer. The fluorescence emission spectrum of HDAC8 was monitored in the range of 330–500 nm after excitation at 280 nm. The excitation and the emission slit width in these experiments were 10 and 8 respectively with PMT (photo multiplier tube) voltage of 800. The resulting

binding isotherms for the HDAC8-ligand complex were analyzed via the complete solution of the quadratic equation (Eq.4.4):

$$F = (C * (L_{tot} + K_d + n * E_{tot}) - \sqrt{(E_{tot} * n + L_{tot} + K_d)^2 - 4E_{tot} * n * L_{tot}}) / 2 \quad \text{Eq. 4.4}$$

where F is fluorescence signal of protein/ligand after the addition of other interacting partner, E_{tot} , and L_{tot} refer to the total enzyme and total ligand concentration, K_d is the dissociation constant of the enzyme-ligand complex, n is stoichiometry of the enzyme-ligand complex and C is the change in amplitude of the signal.

4.3.2. Use of Coumarin-SAHA as a Probe for Determining the Dissociation Constants of Non-fluorescent HDAC8 Inhibitors

The fluorescence emission intensity of c-SAHA at 400 nm is quenched ($\lambda_{ex} = 325$ nm) upon binding to HDAC8. In the presence of a non-fluorescent ligand whose binding is mutually exclusive with c-SAHA, the fluorescence intensity is dependent on the fractional occupancy of the competing (fluorescent and non-fluorescent) ligands at the enzyme site. To determine the equilibrium dissociation constant of non-fluorescent ligands (SAHA, TSA, M344 and SBHA) from their respective binding isotherms, a mixture containing 500 nM c-SAHA and 0.2 μ M of the respective ligand was titrated with increasing concentration of HDAC8 in 10 mM Tris buffer, pH 7.5, containing 100 mM NaCl, 1 mM TCEP. For the binding of two competing ligands with high binding affinities for an enzyme, the algebraic expression required to obtain the overall binding isotherm (by combining all partial equilibria and mass balances) becomes “cubic” in nature with multiple possible roots. Finding solutions for these equations is computationally challenging. Hence, recourse was made by employing the recursive/iterative approach as elaborated by Kuzmic *et al.* using DynaFit software package [149] yielding the K_d values of the respective non-fluorescent inhibitor.

4.3.3. Isothermal Titration Calorimetric Studies

All calorimetric experiments were conducted on a VP-ITC (Microcal Inc., Northampton, MA). The calorimeter was calibrated by known heat pulses as described in the VP-ITC manual. During titration, the reference cell was filled with a 0.03 % azide solution in water. Prior to the titration experiment, both enzyme and inhibitor were thoroughly degassed under vacuum. The sample cell was filled with 1.8 mL (effective volume = 1.4 mL) with 10 μ M HDAC8 in 50 mM Tris, pH 7.5 containing 100 mM NaCl, 3 mM MgCl₂, 10 % glycerol and 1 mM TCEP. The content of the sample cell was titrated with 45 aliquots (4 μ l each) of TSA, SAHA or VYU-2-24 prepared in the buffer used for dialyzing HDAC8. During the titration, the reaction mixture was continuously stirred at 250 rpm. The enzyme concentration was adjusted by 2 % (as recommended by manufacturer) to include a dilution effect of the enzyme solution, which occurs following a buffer rinse. Raw experimental data were collected as the amount of heat produced per second following each injection of a ligand into the sample cell. The amount of heat produced per injection was calculated by integration of area under individual peaks by origin software, provided with the instrument. The observed heat in each injection is a function of the heat associated with binding as well as background signal that is mainly due to the heat of dilution. As the heats of dilution determined in control experiments were of essentially the same magnitude as the heats obtained at the end of the titration (at saturation), the average signal of last few injections was used as the background. Final data were presented as the amount of heat produced per injection versus the molar ratio of inhibitor to HDAC8. The data were analyzed by the origin software as has been described previously by Wiseman *et al.* [150]. All the parameters (*viz.*, n , K_a , and ΔH^0) were allowed

to vary during the curve fitting. The standard errors were derived from the best fit of the experimental data. The data analysis produced three parameters, viz. stoichiometry (n), association constant (K_a), and the standard enthalpy change (ΔH^0) for the binding of inhibitor to HDAC8. The standard free energy of (ΔG^0) for the binding was calculated according to the relationship $\Delta G^0 = -RT \ln K_a$. Given the magnitudes of ΔG^0 and ΔH^0 , the standard entropy changes (ΔS^0) for the binding process were calculated according to the standard thermodynamic equation, $\Delta G^0 = \Delta H^0 - T\Delta S^0$. To determine the heat-capacity change (ΔC_p^0) associated with the formation of the HDAC8-inhibitor complex, the above titrations were performed at various temperatures (5 – 25 °C). The temperature-dependent experiments were conducted in 50 mM Tris, pH 7.5 containing 100 mM NaCl, 3 mM MgCl₂, 10 % glycerol and 1 mM TCEP. As ΔC_p^0 is defined as the temperature dependence of ΔH^0 , a plot of ΔH^0 versus temperature was generated with the slope being equal to ΔC_p^0 .

For determining the proton inventory, the ITC studies were performed in the following buffers containing 100 mM NaCl, 3mM MgCl₂, 10% glycerol and 1mM TCEP: 50 mM HEPES ($\Delta H^0_{\text{ion}} = 5.02$ kcal/mol), 50 mM Bicine ($\Delta H^0_{\text{ion}} = 6.46$ kcal/mol), 50 mM Triethenolamine ($\Delta H^0_{\text{ion}} = 8.03$ kcal/mol) 50 mM Tris ($\Delta H^0_{\text{ion}} = 11.34$ kcal/mol). The ionization enthalpies of the above buffer were taken from Moren and Freire [151].

In order to understand the effect on the thermodynamic parameters of binding of activator and the inhibitors being influenced due to presence of each other, ITC experiments were performed under the following experimental conditions. The thermodynamic parameters of binding of TM-2-51 to HDAC8 in the absence and the presence of SAHA were obtained from ITC experiments performed in 50 mM Tris, pH 7.5 containing 100 mM NaCl , 3 mM MgCl₂, 10 % glycerol and 1 mM TCEP at 25 °C. 10 μ M

of HDAC8 (with and without 100 μM SAHA) in the sample cell was titrated with 45 aliquots (4 μl each) of 500 μM TM-2-51. For investigating whether the thermodynamic parameter of binding of SAHA is being influenced due to the presence of TM-2-51, the following ITC experiment was performed. A mixture 10 μM HDAC8 + 500 μM TM-2-5 in 50 mM Tris pH 7.5 containing 100 mM NaCl, 3 mM MgCl_2 , 10 % glycerol and 1 mM TCEP at 25 $^\circ\text{C}$ was titrated with 45 aliquots (4 μl each) of 200 μM SAHA. The data were analyzed with appropriate binding model using Origin® software package.

4.4. Fluorescence Life-time Measurements

4.4.1. Time Resolved Fluorescence Measurements

All the time resolved fluorescence measurements were performed on a QuantaMaster 30™ (Photon Technology International). The Light Emitting diodes (LEDs) were used as excitation sources for measuring the time resolved fluorescence decay. LED with maximum output at 280 nm and 340 nm were utilized to excite the protein and c-SAHA, respectively. The emitted light was detected by means of a stroboscopic emission monochromator configured, respectively, for protein and c-SAHA fluorescence emission at 340 nm and 400 nm. The instrument response function (IRF) was obtained using the dilute starch solution under the same experimental settings. The experimental settings for data collection were as follows: start delay = 70 ns, end delay = 110 ns, channels = 200, integration time = 1 sec. At least 20 data were averaged to enhance the signal to noise ratio.

The analysis of the fluorescence decay curves was performed using Felix32™ software (Photon Technology International) providing the life time. The data were analyzed using the single or double exponential rate equations of the following format.

$$I(t) = \sum_{i=1}^n \alpha_i \exp(-t / \tau_i) \quad \text{Eq. 4.5}$$

where α_i and τ_i represent the amplitude and fluorescence lifetime, respectively, for the i^{th} component. To evaluate the goodness of the fit of the exponential data the statistical parameters such as reduced chi-square (χ^2), the Durbin Watson, and Z values were used as described in the PTI manual.

4.5. Transient Kinetic Methods

4.5.1. Transient Kinetics of HDAC8-ligand Interaction

To determine the rate constants of binding as well as dissociation of HDAC8 ligand from the enzyme site, transient kinetic experiments were performed using an Applied Photophysics SX-18MV stopped-flow system. The stopped-flow system (dead time = 1.3 ms) was operated in the fluorescence mode with an emission path length of 2 mm. The time-dependent change in the tryptophan fluorescence was monitored by exciting the reaction at 280 nm. The change in protein fluorescence signal was detected using a cut-off filter of 320 nm. For studying the transient kinetics of c-SAHA binding and dissociation, the time-dependent changes in the c-SAHA fluorescence was monitored by exciting the reaction mixture at 325 nm, and the emission intensity was detected after passing the light through a 390 nm high-pass cut-off filter. All the transient kinetic experiments were performed at least ten times in 10 mM Tris buffer, pH 7.5, containing 100 mM NaCl, 1 mM TCEP and the resultant kinetic traces were averaged and analyzed by the data analysis package provided by Applied Photophysics. For association kinetics all the experiments were performed in pseudo first order condition. The kinetic traces were analyzed using single or double exponential rate equations as follows. For the single exponential time dependent change in the fluorescence signal, Eq. 4.6 was used:

$$\text{Flu}_t = \text{Amp} * \exp^{-t/\tau} + \text{offset} \quad \text{Eq. 4.6}$$

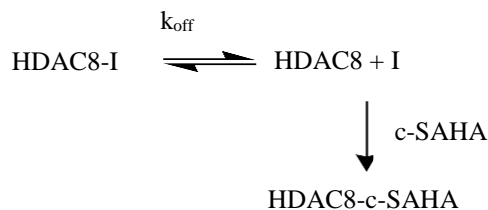
where Flu_t is the fluorescence at a given time. Amp and $1/\tau$ are the total amplitude and relaxation rate constant respectively. The double exponential rate equation (Eq. 4.7) was used to analyze the kinetic traces

$$Flu_t = Amp1 * \exp^{-t/\tau_1} + Amp2 * \exp^{-t/\tau_2} + offset \quad \text{Eq. 4.7}$$

where Flu_t is the fluorescence at a given time. Amp1 and Amp 2 are the respective amplitudes associated with relaxation rate constants ($1/\tau_1$ and $1/\tau_2$). Relaxation rate constants were measured as a function of the ligand concentration and data were analyzed using appropriate kinetic models as described in the results section.

4.5.2. Determination of the Dissociation Off-rates of HDAC8-inhibitor Complexes

A competitive binding of c-SAHA to HDAC8 (concomitant with displacement of the enzyme bound inhibitors) results in a decrease in the fluorescence signal at 400 nm ($\lambda_{ex} = 325$ nm). This time dependent change in the fluorescence signal was used to measure dissociation off-rates of the enzyme-inhibitor. The scheme 4.2 outlines the principle involved in determining the dissociation off-rate of the HDAC8-inhibitor complex.



Scheme 4.2. Measurement of dissociation off-rate of HDAC8 inhibitor

When an enzyme-inhibitor complex is mixed with a high and excessive concentration of c-SAHA, the mass action would drive the overall equilibrium to enzyme-c-SAHA complex, and under such conditions the rate of formation of the enzyme-c-SAHA complex would be given by the dissociation off-rate of the inhibitor. In these experiments

the dissociation off-rate of the inhibitor was measured by mixing the following species: [HDAC8] = 1 μ M and [I] = 10/20 μ M (syringe I) with 40 μ M c-SAHA (syringe II) via the stopped flow system, and the time dependent decrease in fluorescence signal ($\lambda_{\text{ex}} = 325$ nm, “cutoff” filter = 395 nm) due to formation of HDAC8-c-SAHA complex was recorded. The time course of the fluorescence changes were analyzed using single exponential rate equation by data analysis software package provided by Applied Photophysics.

4.5.3. Determination of the Dissociation Off-rates of HDAC8-c-SAHA complex

To determine the dissociation off-rate of c-SAHA from the HDAC8-c-SAHA complex a mixture containing HDAC8 and c-SAHA ([HDAC8] = 1 μ M and [c-SAHA] = 10 μ M) was mixed with a high and excessive concentration of SAHA (200 μ M). The time dependent increase in the fluorescence of c-SAHA ($\lambda_{\text{ex}} = 325$ nm, “cutoff” filter = 395 nm) was used to measure the dissociation off-rate of coumarin-SAHA. The data were analyzed using data analysis software package provided by Applied Photophysics.

4.5.4. Temperature Dependence of Transient Kinetic Measurements

The temperature dependence of the relaxation (observed) rate constants for the binding of the ligands to the enzyme as well as the rate constants was determined by performing the stopped flow transient kinetic experiment. The rate constants were derived from the kinetic models for protein ligand interaction described in the result section. The experimental temperature was maintained by circulating water bath. The temperature dependence of the binding as well as the dissociation were analyzed by Arrhenius equation (Eq. 4.8) of the following format.

$$1/\tau \text{ or } 1/k = A e^{-E_a/RT} \quad \text{Eq. 4.8}$$

where $1/\tau$ and k , respectively, are the relaxation rate constant and the rate constant obtained from the transient kinetic experiment, A is the frequency factor, E_a is the Arrhenius activation energy and T is the temperature in degree Kelvin. To convert E_a into the transition state enthalpy (ΔH^\ddagger), the following relationship was used (Eq. 4.9):

$$\Delta H^\ddagger = E_a - RT \quad \text{Eq. 4.9}$$

The activation energy (ΔG^\ddagger) was calculated using the Eyring equation (Eq. 4.10):

$$\Delta G^\ddagger = -RT * \ln (k * h / k_B * T) \quad \text{Eq. 4.10}$$

where R is the gas constant ($1.986 \text{ cal K}^{-1} \text{ mol}^{-1}$), T is the absolute temperature, h is Plank's constant ($1.58 \times 10^{-34} \text{ cal s}$), and k_B is Boltzmann's constant ($3.3 \times 10^{-24} \text{ cal K}^{-1}$).

4.6. Thermal and Conformational Stability Studies

4.6.1. Guanidinium Chloride Induced Unfolding of HDAC8

Guanidinium chloride induced unfolding of HDAC8 was studied following a change in protein fluorescence ($\lambda_{\text{ex}} = 280 \text{ nm}$) upon unfolding. All the fluorescence measurements were performed in 10 mM Tris pH 7.5 containing 100 mM NaCl, 3 mM MgCl_2 , 10% glycerol and 1 mM TCEP at $25 \text{ }^\circ\text{C}$ on a Perkin-Elmer lambda 50-B spectrofluorometer, equipped with a magnetic stirrer and thermostated water bath using a $4 \times 4 \text{ mm}^2$ square quartz cuvette. Samples containing $2 \text{ }\mu\text{M}$ HDAC8 with varying concentration of guanidinium chloride was incubated for two hours at room temperature. Fluorescence spectra of HDAC8 ($\lambda_{\text{ex}} = 280 \text{ nm}$) for each sample were collected under the same experimental setting. The ratio of the fluorescence intensities at 354 nm and 340 nm was used as a normalized signal. Similar experiments were performed with $2 \text{ }\mu\text{M}$ HDAC8 being saturated with $12 \text{ }\mu\text{M}$ SAHA to evaluate the conformational stability of the SAHA-bound form of HDAC8 against guanidinium chloride denaturation.

The scheme 4.3 describes the protein unfolding with the assumption that no stable intermediates are present that predominate between the native and the denatured states at equilibrium. Both the conformational states yield a distinct experimental signal.



Scheme 4.3. Two step unfolding of protein

The two-state transition can be described by the following equation defined by Santoro and Bolen (Eq. 4.11) [152]:

$$\text{Signal} = \frac{(S_u + m_u * [D]) + (S_n + m_n * [D]) * e^{-(\Delta G^\circ_{n-u} + m_g * [D]) / RT}}{1 + e^{-(\Delta G^\circ_{n-u} + m_g * [D]) / RT}} \quad \text{Eq. 4.11}$$

where m_u and S_u , respectively, are the slope and the intercept of the linear portion of the plot at high concentrations of denaturant. The m_n and S_n , respectively, are the slope and intercept of the linear portion at lower concentrations of denaturant. ΔG°_{n-u} is the difference in free energy between the native and unfolded states in the absence of denaturant, and m_g is the slope of the line that describes the dependence of the observed ΔG on the denaturant concentration. The initial estimates of the baselines associated with the native and unfolded states were calculated by the linear regression of the respective regions, and the cumulative dataset was analyzed by the above equation.

4.6.2. Thermal Stability of Recombinant HDAC8

The Circular Dichroism (CD) spectrum of 8 μ M HDAC8 in the far-UV region was taken on Jasco-715 spectropolarimeters (Tokyo, Japan) in 1 mm path length quartz cuvette 5 mm Tris-Cl, pH 8.0 containing 0.5 % glycerol, 1 mM TCEP and 15 mM KCl. The

experimental settings used were as follows: data pitch = 1 nm, scanning mode = continuous, scan speed = 20 nm/minute, response = 8 sec, band width = 2.0 nm. Accumulation = 5. To measure the change in secondary structure of HDAC8 upon ligand binding, the CD spectra were collected in the presence of saturating concentration of the ligand using the same experimental settings.

To study the thermal stability of HDAC8, the CD spectra were taken under the experimental settings described above after heating the protein at 90 °C for 10 minutes and cooled to room temperature. The thermodynamic analysis of the unfolding of recombinant HDAC8 were performed by following the CD signal (mDeg) at 222 nm (θ_{222}) as a function of temperature. The instrumental settings used in these experiments were as follows: data pitch = 0.5, delay time = 30 s, temperature slope = 1 °C/minute, sensitivity = standard 100 mDeg, response = 8 sec, band width = 5.0 nm. The data were analyzed for two step thermal unfolding mechanism using Eq. 4.12 to calculate the T_m (transition temperature) and Vant's Hoff enthalpy of unfolding.

$$\text{Signal} = \frac{(Y_u + m_u * [T] + (Y_n + m_n * [T])) * e^{-(\Delta H/R * (1/T_m - 1/T [T]))}}{1 + e^{-(\Delta H/R * (1/T_m - 1/T [T]))}} \quad \text{Eq. 4.12}$$

where Y_u and m_u , respectively, are the intercept and the slope of the linear portion of the plot at the higher temperature. The Y_n and m_n , respectively, are the intercept and the slope and of the linear portion at lower temperature, and ΔH is the Vant's Hoff enthanpy at melting temperature (T_m), R is universal gas constant.

Table 4.1. Composition of buffers used in different experiments

Buffer	Composition
HDAC8 Lysis Buffer	50 mM Tris-HCl, pH 8, containing 150 mM KCl, 3 mM MgCl ₂ , 1 mM 2-mercaptoethanol, 1 mM PMSF (Phenylmethylsulfonyl fluoride) and 0.25% Nonidet P-40.
HDAC8 Purification buffer	50 mM Tris-HCl, pH 8, containing 150 mM KCl, 3 mM MgCl ₂ , 1 mM 2-mercaptoethanol
HDAC8 Storage Buffer	10 mM Tris, pH 7.5, containing 100 mM NaCl, 3 mM MgCl ₂ , 10% glycerol and 1 mM TCEP
HDAC8 Assay Buffer	50 mM Tris-HCl buffer, pH 7.5, containing 137 mM NaCl, 2.7 mM KCl, 1 mM MgCl ₂ , 1 mg/ml BSA
HDAC8 CD (Circular Dichorism) Buffer	50 mM Tris-Cl pH 8.0 containing 0.5% glycerol, 1 mM TCEP and 15 mM KCl

CHAPTER 5. RESULTS

5.1. Cloning Expression and Purification of Recombinant Human HDAC8

5.1.1. Sub-cloning of Human HDAC8 in pLIC-vector

The cDNA of the human HDAC8 gene was purchased from the Open Biosystems, which was available as an insert in a mammalian expression vector, pCMV-SPORT (Figure 5.1). As described in the product data sheet, the cDNA clone of the human HDAC8 gene (clone ID 5761745) has been constructed using the two restriction enzymes, namely, *Not I* and *EcoRv*. The sub-cloning of the human HDAC8 gene was performed in the pLIC-His vector as described in the Method section. The LIC vector has been designed to overexpress the recombinant protein under the control of the T7 promoter system [47]. The vector map of the pLIC-His vector is shown in Figure 5.2. The vector encodes for a hexa-histidine peptide followed by a TEV (Tobacco Etch Virus) protease recognition sequence and an LIC site. The HDAC8 gene was cloned within the LIC site, located downstream of the TEV recognition site. The hexa-histidine peptide (His-tag) serves as a purification tag for Immobilized Metal Affinity Chromatography. The digestion of the fusion protein with the TEV protease provides the native protein.

The steps involved in the sub-cloning of the HDAC8 gene in the LIC-His vector are shown in Figure 5.3. In the first step, the primers compatible with LIC vector were custom synthesized by Integrated DNA Technology (IDT). The PCR was performed using above primers to amplify the HDAC8 gene as described in the Methods section. In order to test the amplification of the HDAC8 gene, the PCR product was loaded on an agarose gel and the DNA was separated based on size by electrophoresis (Figure 5.4). The size of the PCR product was approximately 1.2 kb, expected for 1131 base pairs for the coding sequence of

HDAC8 with an additional 36 base pairs derived from the primers. As described in the Method section, the T4 polymerase treatment of the PCR product and the *Sac II* digested vector generated the compatible overhangs (step 2, Figure 5.3). In the fusion step (step 3), the T4 DNA polymerase treated LIC vector and the PCR product were mixed to anneal with each other, and the mixture was transformed into DH5 α cells to obtain the pLIC-His-HDAC8 (recombinant plasmid). In order to produce the recombinant protein, the above plasmid was transformed into the *E. coli* cells (host cells). The recombinant fusion protein was expressed and purified from the host cell utilizing an affinity chromatography. In the final step (step 4, Figure 5.3), the purification tag can be removed from the fusion protein using TEV protease to obtain the native protein

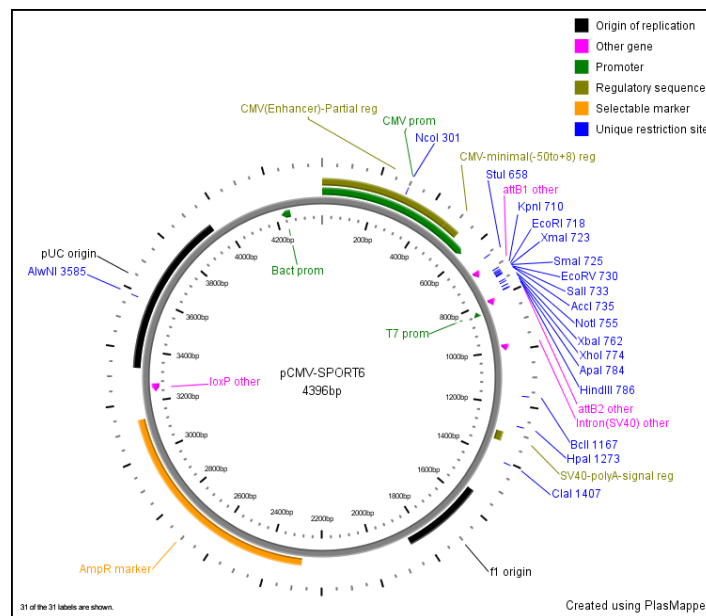


Figure 5.1. The vector map of the pCMV-SPORT. The restriction enzymes *NotI* and *EcoRV* were used to construct the human HDAC8 cDNA clone (commercially available from Open Biosystems).

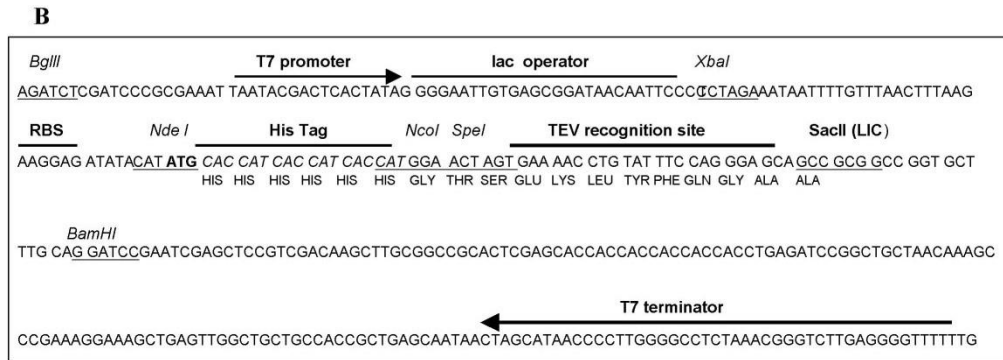
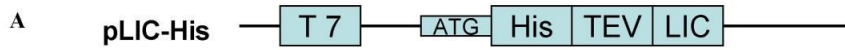


Figure 5.2. The vector map of the pLIC-His vector used for cloning the human HDAC8 gene. The pLIC-His has a T7 promoter based system (Panel B) and has been derived from the pET921b (+). The HDAC8 gene was cloned within the LIC site [147].

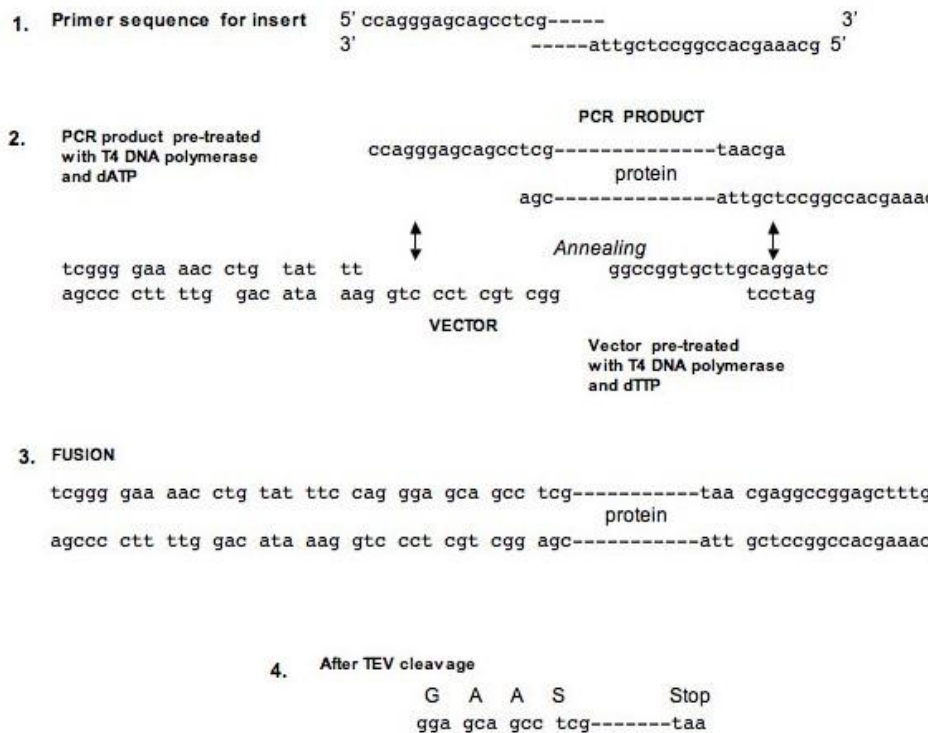


Figure 5.3. The ligation independent cloning strategy for the sub-cloning of the human HDAC8 gene. The LIC compatible primers were used to amplify the HDAC8 gene. The PCR product was treated with the T4 DNA polymerase in the presence of dATP. The pLIC–His vector was digested with the *SacII* restriction enzyme prior to the T4 DNA polymerase treatment in the presence of dTTP. The T4 treatment of the PCR product, as well as the digested vector, in the presence of the respective dNTP generated the cohesive ends which could anneal with each other on mixing. The annealed mixture was transformed into DH5 α *E.coli* cells. The nicks left in the recombinant plasmids were sealed by bacterial DNA ligase. In order to remove the His-tag from the fusion protein, TEV protease could be used leaving the four extra amino acids (GAAS) at the N-terminal of the recombinant protein [147].

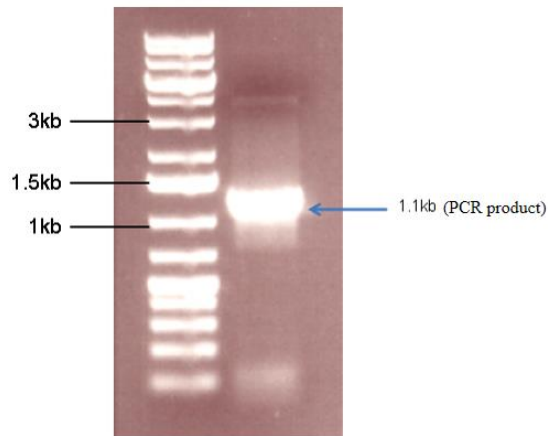


Figure 5.4. The agarose gel electrophoresis showing the PCR amplified HDAC8 gene using the pLIC compatible forward and reverse primers. The left lane shows the O'GeneRule™ 1 kb Plus DNA ladder.

5.1.2. Expression and Purification of Recombinant Human HDAC8

The pLIC-His plasmid was transformed in the *E. coli* BL-21 Star (DE3) cells. The expression of HDAC8 was induced with 0.05 % (w/v) lactose, which serves as an inducer of the T7 promoter-lac operator system. After induction cells were further grown at 18 °C with constant shaking overnight resulting in the expression of HDAC8 in the soluble (native) form. The cells were lysed by sonication, and HDAC8 was purified from the soluble fraction of the crude lysate via the Immobilized Metal Affinity Chromatography (IMAC) using a HisTrap column as described in the Method section. The HisTrap column was made up of the highly cross-linked agarose containing IDA (Iminodiacetic Acid) as an immobilized chelating group. Due to the presence of the imidazole ring of the histidine, the His-tagged protein specifically bound to the metal chelating sites, facilitating the specific binding of the recombinant protein. The non-specific and weak binding of the contaminating proteins was prevented by the addition of 10 mM imidazole in the HDAC8 cell lysis buffer. The addition of 1 mM of 2-mercaptoethanol maintained the stability of

HDAC8 during the course of purification, aside from preventing its co-purification with the contaminating proteins mainly due to the formation of the disulfide linkages. The addition of 0.25 % non-ionic detergent, Triton-X-100, reduced the non-specific hydrophobic interaction between the gel matrix and the protein. Washing the column with 20 mM Imidazole removed the weakly-bound contaminating proteins from the HisTrap column. A linear gradient of 20-130 mM imidazole in purification buffer was used to elute HDAC8 from the HisTrap column. Figure 5.5 shows the elution-profile of the HDAC8-His6 protein from the HisTrap column. The elution of the HDAC8 from the column started at 50 mM imidazole concentration until the completion at 120 mM, as represented by the elution peaks monitored at 280 nm. In order to assess the purity of HDAC8 eluted from the HisTrap column, the peak fractions were loaded on an SDS-PAGE (Figure 5.6). The SDS-PAGE result showed that the purity of the HDAC8 purified using the affinity chromatography was ≥ 95 %. All the fractions containing the absorbance greater than 50 mAU were pooled together and dialyzed against HDAC8 storage buffer. The yield of the purified HDAC8 obtained from the one liter of the bacterial culture was 0.9 mg. The summary of the one-step purification of HDAC8 with the specific activity measured using the trypsin-coupled assay is shown in the Table 5.1.

Table 5.1. Summary of the HDAC8 purification by Affinity Chromatography

Step	Volume (mL)	total protein (mg)	total units of HDAC8	Specific Activity	Fold Purification	% recovery
Crude extract	10	320	50	0.14	---	100
Affinity Chromatography	10	50	43	0.86	6.1	16

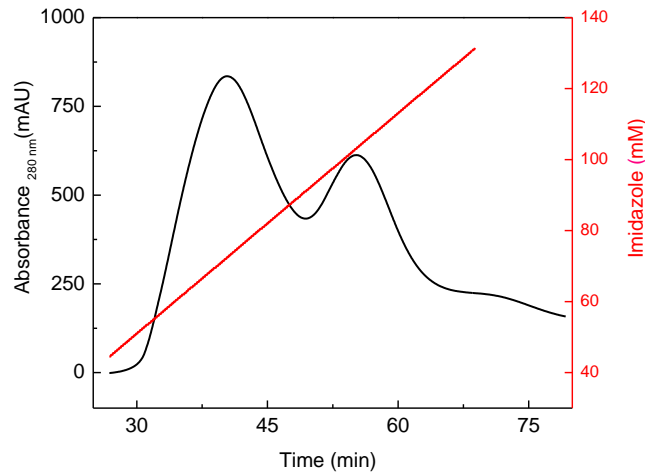


Figure 5.5. The elution profile of the HDAC8-His6 from the Ni²⁺ IDA HisTrap™ HP column. The crude extract supernatant containing the 10 mM imidazole in the purification buffer (50 mM Tris-Cl pH 8.0, 3 mM MgCl₂, 150 mM KCl, 5 % glycerol and 1 mM 2-mercaptoethanol) was loaded on to the HisTrap™ HP column. An AKTA purifier UPC10 (GE Healthcare Life Sciences) was used for the purification process. The column was washed with 20 column volume (CV) of 20 mM imidazole in the purification buffer. The linear gradient of 50 CV from 20-130 mM imidazole was used to elute the protein from the column. The elution of HDAC8 started from 50 mM until the completion at 120 mM concentration of imidazole.

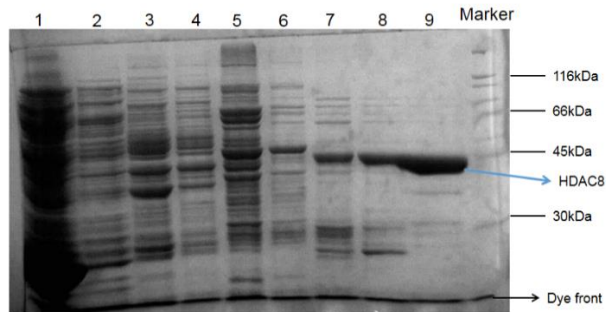


Figure 5.6. The SDS-PAGE showing the purity of the HDAC8-His6 at different stages of purification. The gel electrophoresis was performed using the Laemmli buffer system with 4 % stacking gel and 10 % resolving gel. To visualize the protein on the gel, it was subjected to staining with coomassie blue dye. Lane 1: crude extract supernatant, lane 2: flow through, lane 3, 4: 20 mM wash, lane 5, 6, 7, 8, 9: elution peak fractions, lane 10: protein molecular weight markers (Amersham Biosciences). A single band of 45 kDa in lane 9 shows the recombinant form of HDAC8.

5.2. Physicochemical Properties of Recombinant Human HDAC8

5.2.1. HDAC8 Activity Measurements by Trypsin-coupled Assay

Several *in vitro* enzyme assays have been developed by different research groups to measure the rate of the HDAC-catalyzed reaction (Introduction section 1.4). A trypsin-coupled assay utilizing a fluorogenic HDAC substrate, acetyl-Gly-Ala (N^ε- acetyl-Lys)-AMC, has been developed by Schultz *et al.* (Figure 5.7) [80]. The above assay is very convenient, cost effective, and amenable to be adopted in a high-throughput format. Additionally, it is well suited to be used in a continuous mode. Similar to the above assay, a trypsin-coupled assay was developed utilizing a commercially available HDAC substrate, Fluoro-de-LysTM. The substrate is the proprietary of the Enzo Life Science (Farmingdale, NY). However, based on the information available from data sheet of the substrate (Fluoro-de-LysTM), as well as its fluorescence properties, it appears that it contains the AMC (Aminomethyl coumarin) group presumably attached to the acetylated lysine moiety. The HDAC8 catalyzed deacetylation of the substrate generates the product, which is cleaved by trypsin (named as Developer I by Enzo Life Sciences). The assay conditions were optimized by performing experiments under various experimental settings on the microplate reader (SpectraMax Gemini, Molecular Devices). The settings used for the standard assay condition were as follows: $\lambda_{\text{ex}} = 365 \text{ nm}$, $\lambda_{\text{em}} = 500 \text{ nm}$, PMT = medium. In the above experimental conditions, the background signal, associated with the slow hydrolysis of the substrate by trypsin was negligible as compared to actual signal in the standard HDAC8 assay.

In order to optimize the signal to noise ratio of the overall reaction traces of the trypsin coupled-HDAC8 catalysis, the excitation and emission wavelengths were fine

tuned. In that pursuit, the excitation and emission spectra of the substrate and the final product of the trypsin-coupled enzyme assay were obtained. As shown in Figure 5.8, these spectra have a significant overlapping region. In order to minimize the inner filter effect produced by high concentration of Fluoro-de-LysTM (150 μ M) used in HDAC8 activity measurement, it became imperative to select 365 nm and 500 nm, respectively, as the excitation and emission wavelengths in the trypsin-coupled assay. The excitation and the emission spectra of Fluoro-de-LysTM and the final product of the trypsin-coupled assay have the least overlap at the above wavelengths (Figure 5.8), reducing the inner filter effect in fluorescence based enzyme kinetic assay.

Figure 5.9 shows the kinetic traces for measuring the steady state rate of the HDAC8 catalyzed reaction using the trypsin-coupled assay in the continuous mode. A lag phase, representative of the coupled assay, was observed prior to attainment of the steady state phase. The lag phase (30 minutes) was the time required to reach the steady state concentration of the deacetylated Fluoro-de-LysTM produced due to the HDAC8 catalyzed reaction. The cleavage of the deacetylated Fluoro-de-LysTM by trypsin, liberated a highly fluorogenic product which was monitored as a function of time.

To avoid kinetic complexity in measuring the steady state rate of the HDAC8 catalyzed reaction, it was essential to minimize the lag phase by increasing the concentration of the coupling enzyme without allowing it to cause significant proteolytic degradation of HDAC8. Additionally, it was crucial to ensure that the trypsin-catalyzed reaction was not the rate-limiting step in the HDAC8 activity measurement. In that pursuit, the steady state rate of the HDAC8 catalyzed reaction was measured as a function of an increasing concentration of trypsin, while maintaining the concentration of HDAC8 (250

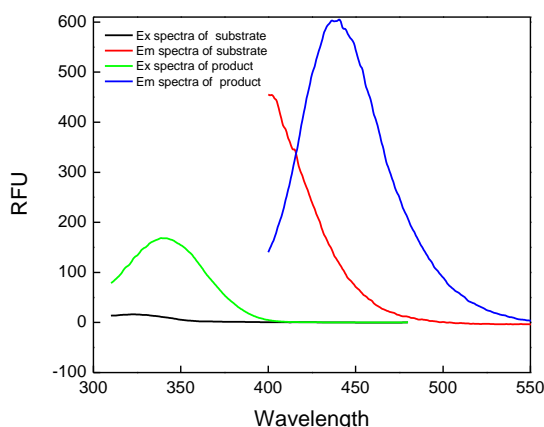


Figure 5.8. The excitation and the emission spectra of the fluorogenic substrate (Fluoro-de-LysTM) and the final product of the trypsin-coupled assay. The excitation spectra were obtained at the emission wavelength of 500 nm. To obtain the emission spectra, the fluorophores were excited at 365 nm. Due to significant overlap in the excitation and the emission spectra of the substrate and the product, the specific wavelengths i.e., $\lambda_{ex} = 365$ nm, $\lambda_{em} = 500$ nm, were chosen where the interference from the substrate was minimal, significantly reducing the inner filter effect.

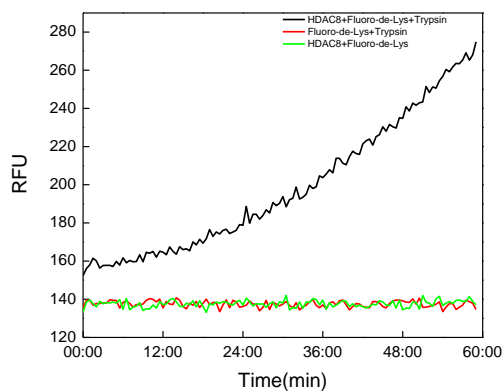


Figure 5.9. Measurement of the initial velocity of the HDAC8 catalyzed reaction employing the trypsin-coupled assay. The assay was performed at 25 °C in assay buffer (50 mM Tris-Cl pH 8.0, 137 mM NaCl, 2.7 mM KCl, 1 mM MgCl₂ and 1 mg/ml Bovine Serum Albumin) with 250 nM HDAC8, 250 nM trypsin, 150 μ M Fluoro-de-LysTM. The fluorogenic product released in the reaction was detected using Gemini fluorescence microplate reader (Molecular Devices). A lag phase, a characteristic of a coupled assay, of nearly 30 minutes was observed prior to the attainment of steady state. The control traces lacking HDAC8 or the coupling enzyme (trypsin), respectively, are shown in red and green color.

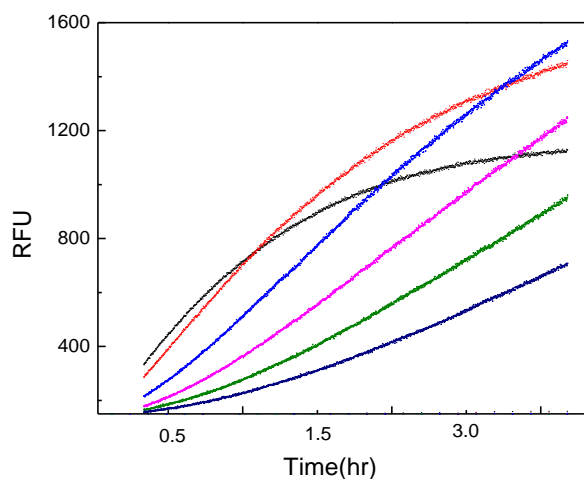


Figure 5.10. Steady state kinetic traces for determining the initial rate of the HDAC8 catalyzed reaction measured as function of the coupling enzyme (trypsin) concentration in the trypsin-coupled assay. The traces shown in dark-blue, green, red, blue, orange and light-green color, respectively, represent the steady state rate for the HDAC8 activity assay performed with 50 nM, 100 nM, 200 nM, 250 nM, 500 nM and 1 μ M concentration of trypsin. The lag phase gradually became shorter with an increase in the concentration of the coupling enzyme. The steady state rate, measured from the slope of the kinetic trace as the HDAC8 catalyzed reaction, was dependent on the trypsin concentration. Additionally, it attains an asymptote value at 250 nM (blue color trace) concentration of trypsin. The concentration of trypsin higher than 250 nM (with 250 nM HDAC8 and 150 μ M Fluro-de-Lys TM) used in the HDAC assay has no effect on the steady state rate (orange and light-green traces) except for reducing the duration of the steady state phase due to the trypsin-mediated cleavage of HDAC8.

5.2.2. Steady State Kinetic Parameters for the HDAC8 Catalyzed Reactions

The characterization of steady state kinetic parameters for an enzyme catalyzed reaction provides vital information about its structural-functional and catalytic features. Notably, the above parameters are often dependent on the type/nature of the substrate utilized in the assay. There has been very limited information about the *in vivo* substrate/s utilized by HDAC8 (Introduction section 1.3). However, *in vitro* HDAC8 assay widely

used to measure the rate HDAC catalyzed reaction utilizes *in vitro* substrate, which is often consists of a peptide fragment derived from a histone tail or C-terminal domain of p53.

In view of the above facts, steady state kinetic parameters of the HDAC8 catalyzed reaction were determined utilizing a commercially available *in vitro* HDAC8 substrate, Fluro-de-LysTM, in a trypsin-coupled assay. To measure the K_m value, initial velocities of the enzyme catalyzed reactions were measured as a function of the substrate concentration. As expected, the initial velocity was hyperbolically dependent on the substrate concentration. The data were analyzed using the Michealis-Menten equation and the solid line in Figure 5.11 represents the best fit of the experimental data, yielding the K_m and V_{max} values, respectively, as $543 \pm 60 \mu\text{M}$ and $0.70 \pm 0.03 \text{ RFU/s}$.

The value of k_{cat} of HDAC8 with Fluro-de-LysTM substrate was determined as follows. The value of V_{max} obtained as RFU/s from the trypsin-coupled assay was converted into $\mu\text{M/s}$ using a standard plot (Figure 5.12). The standard plot was generated by measuring the increase in fluorescence of the reaction product of the HDAC8 assay as function of fluorophore concentration. The fluorophore was prepared upon the treatment of the deacetylated standard (available from the Enzo Life Sciences) with $100 \mu\text{M}$ of trypsin for 10 minutes. The value of k_{cat} was calculated by dividing the V_{max} ($\mu\text{M/s}$) value with the concentration of HDAC8 used in the assay. The value of k_{cat} obtained was 0.07 s^{-1} . Furthermore, the catalytic efficiency of HDAC8 with the Fluro-de-LysTM substrate was calculated by taking the ratio of the k_{cat} and K_m being equal to $12 \text{ M}^{-1} \text{ s}^{-1}$. Schutlz and co-workers have reported the k_{cat}/K_m value of HDAC8 with the acetyl-Gly-Ala-(N^ε- acetyl-Lys)-AMC substrate as being equal to $60 \text{ M}^{-1} \text{ s}^{-1}$ [80]. The higher value of k_{cat}/K_m of HDAC8 with acetyl-Gly-Ala-(N^ε- acetyl-Lys)-AMC substrate compared to Fluro-de-Lys

TM suggests that the former substrate is utilized more efficiently by the enzyme as opposed to the latter. This could presumably be due to the inherent bulkiness of acetyl-Gly-Ala-(N^ε-acetyl-Lys)-AMC substrate aside from its peptide-sequence serving as a better mimic of the natural substrate. The significantly low value of k_{cat}/K_m suggested that HDAC8 is a very slow enzyme at least with Fluro-de-Lys TM substrate. The highest possible value of k_{cat}/K_m for the catalytically efficient enzyme is 10^8 - 10^9 M⁻¹ s⁻¹, where the rate of enzyme catalyzed reaction is limited by the rate of diffusion.

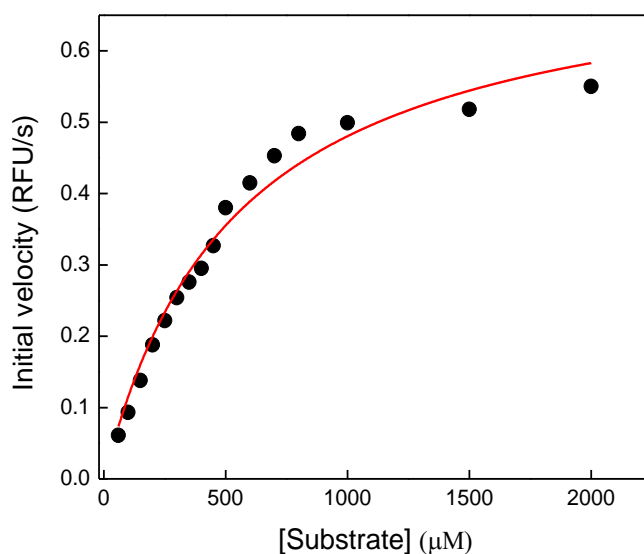


Figure 5.11. The initial velocities of the HDAC8 catalyzed reaction as a function of substrate concentration. The solid line is the best fit of the data using the Michaelis-Menten equation with K_m and V_{max} values as 543 ± 60 μM and 0.70 ± 0.03 RFU/sec. To determine the value of k_{cat} , V_{max} was converted into $\mu\text{M}/\text{s}$ using the standard curve shown in Figure 5.12. The value of k_{cat} was calculated as 0.007 s⁻¹.

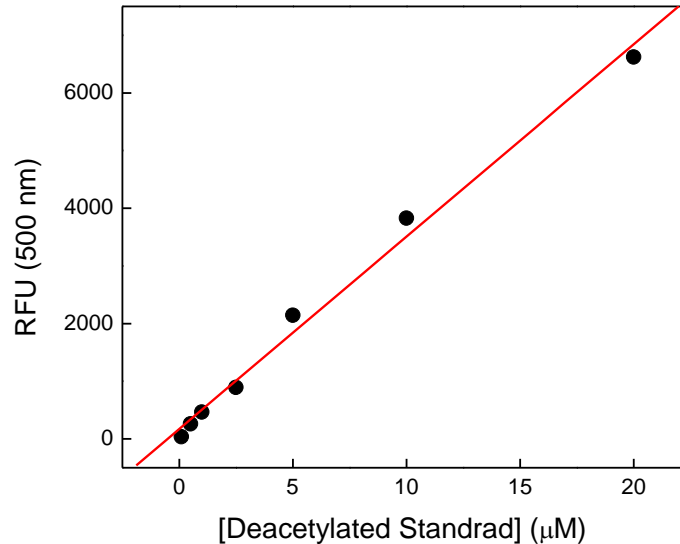


Figure 5.12. Standard curve prepared from the fluorescence end point reading of the known concentration of the fluorophore. The plot was generated upon the treatment of deacetylated standard with the 100 μM of trypsin. The experimental and the instrumental settings were the same as used in the trypsin-coupled assay.

5.2.3. UV-Visible Spectrum of Recombinant Human HDAC8

A protein absorbs light primarily because of the presence of peptide groups as well as the aromatic amino acids (Phe, Try, Trp). The molar extinction coefficient (ϵ) of a protein expressed as $M^{-1}cm^{-1}$ is dependent on the number of the above chromophores in addition to their molecular microenvironment in the protein structure. The molar concentration of a protein solution is often determined from its absorbance and its molar extinction coefficient utilizing Lambert-Beer law.

Figure 5.13 shows the UV-visible spectrum of the recombinant form of the human HDAC8 in 10 mM Tris-Cl, pH 7.5 containing 100 mM NaCl, 3 mM $MgCl_2$, 10 % glycerol and 1 mM TCEP. HDAC8 contain 13 phenylalanine, 21 tyrosine and 4 tryptophan residues which serve as the chromophores. As shown in the absorption spectrum, the absorbance of

18 μM HDAC8 at 280 nm measured in a 1 mm path length quartz cuvette was 0.562.

Notably, the concentration of the above protein sample was determined by the Bradford assay using bovine serum albumin (BSA) as standard [148]. From the absorbance value the molar extinction coefficient of HDAC8 was calculated as $54540 \text{ M}^{-1} \text{ cm}^{-1}$ using the Lambert Beer's law. This value was in close agreement with value $53915 \text{ M}^{-1} \text{ cm}^{-1}$ obtained from ExPASy-ProtParam tool, a Bioinformatics Resource Portal (www.expasy.org).

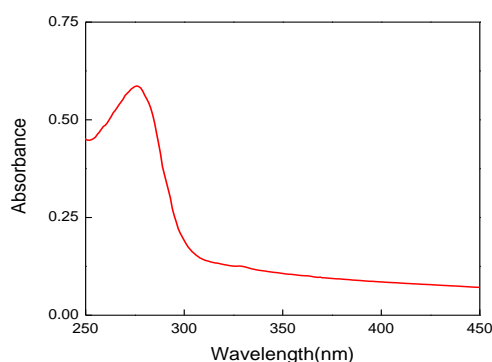


Figure 5.13. UV-visible spectrum of the recombinant form of human HDAC8. The spectrum was obtained using 18 μM HDAC8 in the storage buffer (10 mM Tris-Cl, pH 7.5, 100 mM NaCl, 3 mM MgCl_2 , 10 % glycerol and 1 mM TCEP).

5.2.4. Circular Dichroism Spectrum of Recombinant Human HDAC8

In order to ascertain that the recombinant form of the human HDAC8 (expressed and purified in the experimental conditions described in the Method section) retained the native protein conformation, it was imperative to take the Circular Dichroism spectrum of HDAC8 in the far-UV region. The CD spectrum of HDAC8, taken in 5 mm Tris-Cl pH 8.0 containing

0.5 % glycerol, 5 mM TCEP and 15 mM KCl, is shown in Figure 5.14. The shape of spectrum in the lower wavelength region (190-200 nm) as well as a double-dip observed in the 200-225 nm region, are the characteristic signatures for an α -helix. The spectrum is very similar to the one reported by Vannini *et al.* [58]. In order to estimate the secondary structural composition of the recombinant form of human HDAC8, the spectrum was analyzed using the K2D program available from DichroWeb, an online software available for the analysis the CD spectra [153]. It is important to note that analysis program K2D does not require any reference data set for analyzing the spectrum. The analysis of the data provided the values representing the percent contribution of the α -helix, β -strand and the random coil, respectively, as 33 %, 17 %, and 50 %. The experimental and the reconstituted spectra (obtained from the analysis of data) are represented by the green and blue lines, respectively, in Figure 5.15. The estimated values of the secondary structure content of HDAC8 estimated using DicroWeb were in close agreement with the values obtained from crystallographic studies (37 % α -helix and 11 % β -strand) [58].

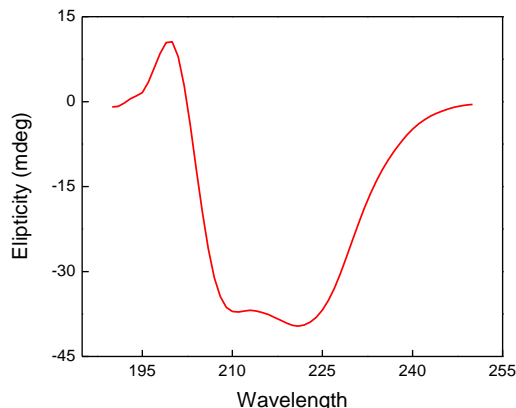


Figure 5.14. Circular Dichroism spectrum in the far-UV region of 8 μ M HDAC8. The spectrum was taken in 1 mm path length quartz cuvette in 5 mM Tris-Cl pH 8.0 containing 0.5 % glycerol, 5 mM TCEP and 15 mM KCl.

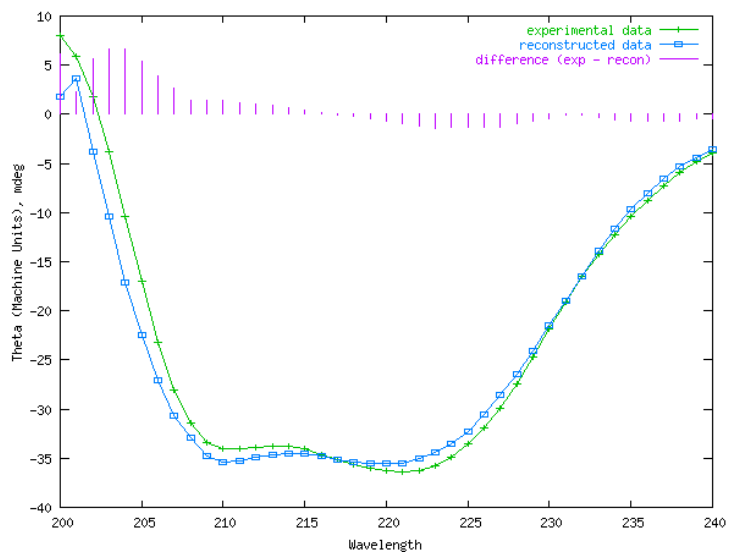


Figure 5.15. Analysis of Circular Dichroism spectrum of HDAC8 using DichroWeb. The data were analyzed using the analysis program, K2D, providing an estimate of the secondary structural components of HDAC8 as 33 %, 17 %, and 50 % for α -helix, β -strand and random coil, respectively. The experimental and the reconstituted (fitted) spectra are shown as the green and blue colored line, respectively [153].

5.2.5. Steady State Fluorescence Spectra of Recombinant Human HDAC8

The intrinsic fluorescence of a protein, which is primarily contributed by phenylalanine, tyrosine and tryptophan, is very sensitive to the change in the local environment. A quantitative measurement of the conformational change in protein fluorescence upon binding of a ligand has been widely used to study ligand-protein interaction [154]. Towards this end the steady state fluorescence spectra of HDAC8 was recorded both in the absence and presence of its ligand.

Figures 5.16 and 5.17 show the steady state fluorescence emission spectra of HDAC8 ($\lambda_{\text{ex}} = 280 \text{ nm}$) in the absence and the presence of its effector. The fluorescence spectrum has the emission maximum at 340 nm. Upon binding of an effector (inhibitor/activator) the intrinsic protein fluorescence was quenched for all the ligand under study. However, no shift in the fluorescence emission peak was observed. It is important to note here that the fluorescence quenching was more pronounced for the binding of TSA to HDAC8 as opposed to other inhibitors, namely, SAHA and VYU-2-24. This could be presumably due to the difference in extent of ligand-induced conformational change mediated via even structurally similar ligands such as TSA and SAHA. The above observation is further supported by the X-ray crystallographic studies of the HDAC8 bound with TSA and SAHA. The crystal structure of HDAC8 suggests that the active site of the enzyme is malleable, and the protein attains a distinct conformation in order to accommodate different ligands e.g., TSA and SAHA [57].

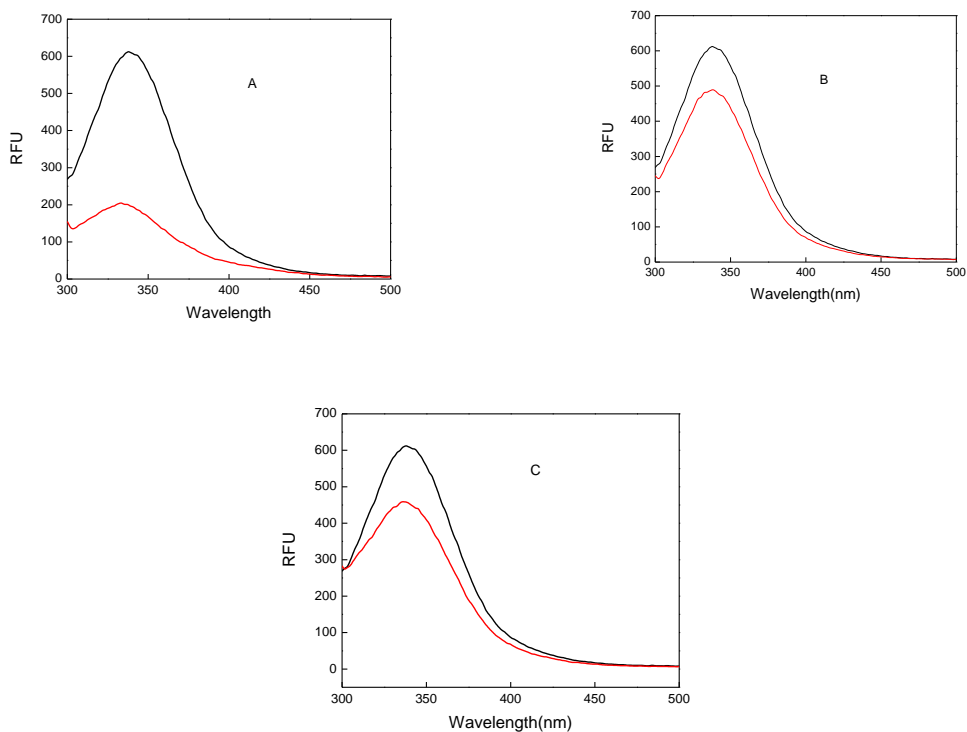


Figure 5.16. The steady state fluorescence emission spectra of HDAC8. The spectrum of 1.5 μM HDAC8 was taken in 10 mM Tris-Cl, pH 7.5, 100 mM NaCl, 3 mM MgCl_2 , 10 % glycerol and 1 mM TCEP) upon excitation at 280 nm. The protein fluorescence was quenched (red color traces) upon binding to the inhibitors, namely TSA, SAHA, and VYU-2-24, as shown in Panels A, B and C, respectively. The concentration of the respective inhibitor in these experiments was 2 μM .

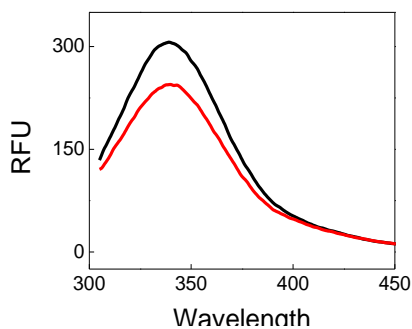


Figure 5.17. Quenching of steady state fluorescence of HDAC8 upon binding to TM-2-51. The spectra were obtained in 10 mM Tris-Cl, pH 7.5, 100 mM NaCl, 3 mM MgCl_2 , 10 % glycerol and 1 mM TCEP) upon excitation at 280 nm. The black and red traces, respectively, show the free and the ligand-bound form of 1 μM HDAC8. The concentration of TM-51 used in the measurement was 2 μM .

5.3. Potential Effectors of HDAC8

5.3.1. Screening of HDAC8 Effectors (Inhibitors/Activators)

HDACs have been high priority drug targets for the treatment of several human diseases including cancer [105, 110]. Hence, serious attempts have been made by several researchers to discover/design the novel effectors (inhibitors/activators) of HDAC8. The HDAC inhibitors have been found to prevent the growth of cancer cells both *in vitro* and in an animal model. Moreover, the HDAC inhibitors namely, SAHA and Romidepsin have already been approved by FDA for the treatment of T-cell lymphoma, and several other inhibitors are in the advanced level of the clinical trial [141]. Aside from the inhibitors, there has been an increasing interest in discovering the activators of HDAC. The activity of HDAC8 and HDAC2 has been found to be reduced in case of Chronic Obstructive Pulmonary Disease (COPD) [113]. More recently, mutant forms of HDAC8 with a reduced enzyme activity has been linked with Cornelia de Lange syndrome [36]. An HDAC activator has a potential to alleviate the above disease conditions associated with a reduced HDAC activity.

In pursuit of discovering novel HDAC effectors, several small molecules were synthesized in collaboration with the Department of Chemistry and Biochemistry and the Pharmaceutical Sciences at NDSU. The high-throughput screening of the compounds was performed in a 96-well format via the trypsin-coupled assay using a microplate reader (SpectraMax Gemini, Molecular Devices). The effectiveness of the compounds on the HDAC8 catalyzed reaction was tested in the presence of 10 μ M concentration of the effector. The compounds, inhibiting the HDAC8 catalyzed reaction >50 % at 10 μ M concentration, were selected for determining their inhibition constants as described in

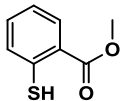
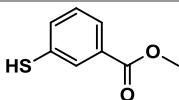
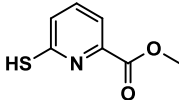
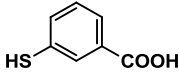
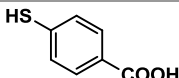
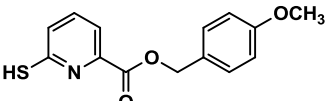
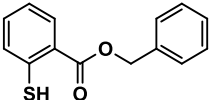
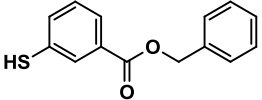
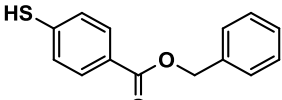
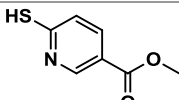
Methods section. Likewise, the compounds activating the HDAC8 catalyzed reaction in \geq 3-5 fold as compared to control were selected for the further kinetic study.

5.3.1.1. Screening of Thio-based Compounds for the Inhibitory Features against HDAC8

The thiol-based compounds containing a sulfahydril moiety as a metal-binding group, serve as the inhibitors of several metalloenzymes, such as Matrix Metalloprotease (MMP), Angiotensin Converting Enzyme (ACE), etc. [155]. Thiol-based analogs of SAHA have been reported as potent inhibitors of HDAC [156]. Romidepsin, a cyclic peptide inhibitor of HDAC, produces a thiol moiety upon reduction, which binds to the active site metal ion of the enzyme. Recently, the crystal structure of the HDAC8-largazole thiol complex has been reported which suggests that thiol-moiety of the inhibitor coordinate with the active site Zn^{2+} [62]. In view of the above information, attempts were made to synthesize various thiol-based inhibitors in the laboratory of Prof. Greg Cook, Department of Chemistry and Biochemistry at NDSU. Their effectiveness on the HDAC8 catalyzed reaction was tested via the trypsin-coupled assay. The summary of the high-throughput screening of the thiol-based inhibitors is presented in Table 5.2. It is important to note that these thiol-based inhibitors exist as dimer due to the formation as disulfide bond which was reduced in our experimental condition (the HDAC8 storage buffer contains TCEP as a reducing agent). Evidently, several novel thiol-based compounds namely, VYU-2-24, VYU-2-221, VYU-2-270, VYU-3-54, VYU-3-56, VYU-2-136, VYU-2-219, and VYU-2-134 were identified as potent HDAC8 inhibitors which have the inhibition potency in the micromolar range. The inhibition constants (K_i) of the above inhibitors were determined by measuring the initial rate of the HDAC8-catalyzed reaction as a function of inhibitor

concentration. The data were analyzed using the competitive K_i equation (Methods section). The solid lines of the Figures 5.18 and 5.19 represent the best of the experimental data using the above equation yielding for the K_i values mentioned in the figure legend.

Table 5.2. Summary of the high-throughput screening of thiol-based compounds for the HDAC8 inhibitors/activators

Entry	ID	Structure	% Inhibition
1	VYU-2-14		72 %
2	VYU-2-16		31.6 %
3	JES-1-21		15.7 %
4	VYU-2-17		26 %
5	VYU-2-19		23 %
6	VYU-2-24		79 %
7	VYU-2-26		NA/NI
8	VYU-2-28		NA/NI
9	VYU-2-30		NA/NI
10	VYU-2-56		NA/NI

(continues)

Table 5.2. Summary of the high-throughput screening of thiol-based compounds for the HDAC8 inhibitors/activators (continued)

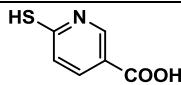
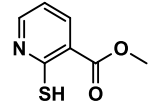
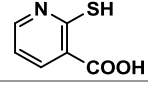
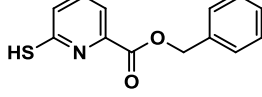
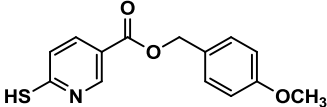
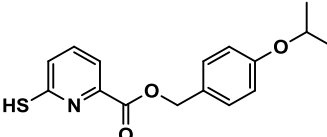
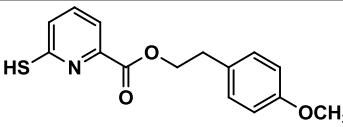
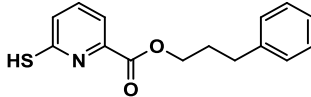
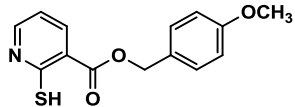
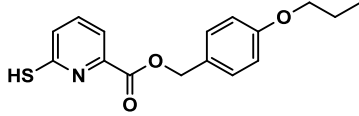
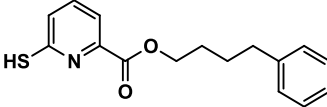
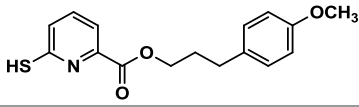
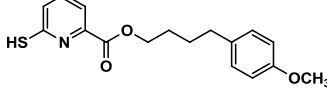
Entry	ID	Structure	% Inhibition
11	VYU-2-57		21 %
12	VYU-2-58		NA/NI
13	VYU-2-59		NA/NI
14	VYU-2-64		NA/NI
15	VYU-2-72		57 %
16	BNG-2-148		NA/NI
17	VYU-2-134		72 %
18	VYU-2-136		67 %
19	VYU-2-142		NA/NI
20	BNG-2-167		36.6 %
21	VYU-2-152		61 %
22	VYU-2-154		63 %
23	VYU-2-156		64 %

Table 5.2. Summary of the high-throughput screening of thiol-based compounds for the HDAC8 inhibitors/activators (continued)

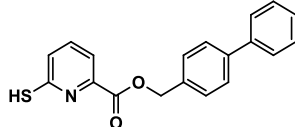
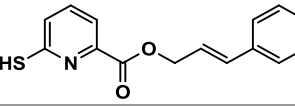
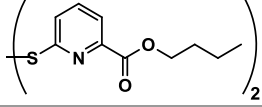
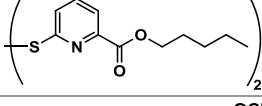
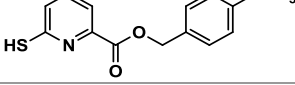
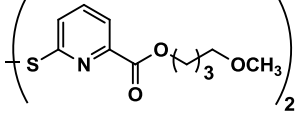
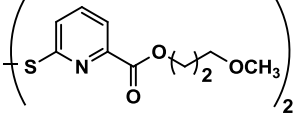
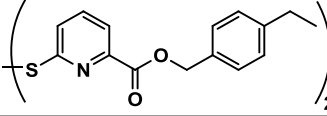
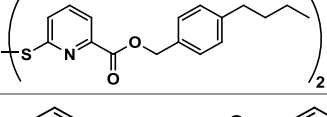
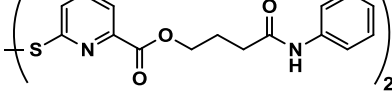
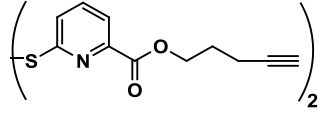
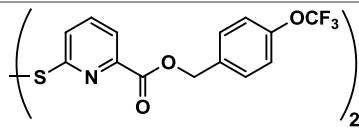
Entry	ID	Structure	% Inhibition
24	VYU-2-166		NA/NI
25	VYU-2-204		76 %
26	VYU-2-219		72 %
27	VYU-2-221		75 %
28	VYU-2-246		77 %
29	VYU-2-264		73 %
30	VYU-2-266		51 %
31	VYU-2-270		73 %
32	VYU-2-272		13 %
33	VYU-2-296		65 %
34	BNG-3-36		55.7 %
35	VYU-3-42		59 %

Table 5.2. Summary of the high-throughput screening of thiol-based compounds for the HDAC8 inhibitors/activators (continued)

Entry	ID	Structure	% Inhibition
36	VYU-3-54		76 %
38	MT-104		NA/NI
39	MT-105		30 %
40	MT-106		33 %
41	MT-109		10 %
42	MT-111		35.7 %
43	MT-114		17 %
44	MT-116		NA/NI
45	TM-1-246		12 %
46	DP-178		NA/NI
47	DP-180		NA/NI

Note: NA and NI respectively represent No Activation and No Inhibition

% = represents the % inhibition of HDAC8 enzyme activity at a concentration of 10 μ M inhibitor (dimer).

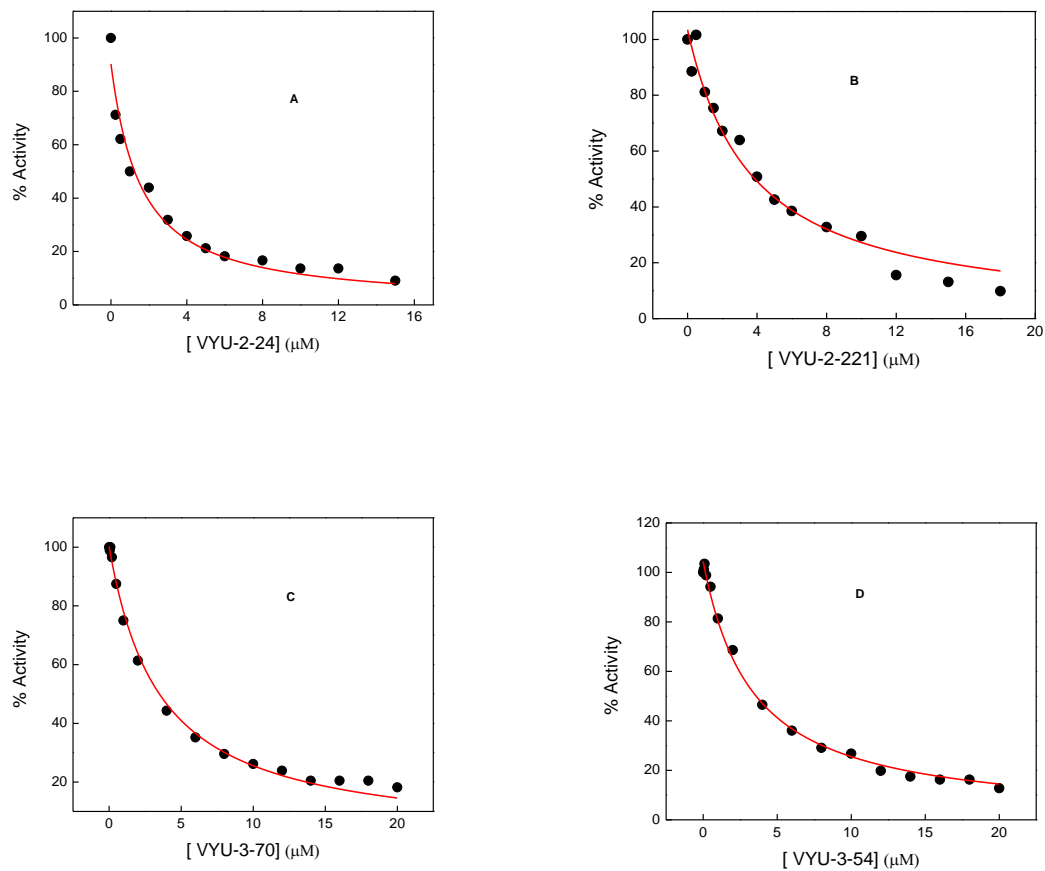


Figure 5.18. Steady state kinetics for the inhibition of HDAC8 enzyme activity by VYU-2-24, VYU-2-221, VYU-2-270 and VYU-3-54. They are shown in panels A, B, C, and D, respectively. The initial rates of the HDAC8 catalyzed reaction were plotted as a function of the inhibitor concentration (dimeric form). The solid lines are the best fit of the data using the competitive K_i equation yielding the K_i values of $1.5 \pm 0.2 \mu\text{M}$, $3.5 \pm 0.3 \mu\text{M}$, $3.3 \pm 0.1 \mu\text{M}$, and $3.2 \pm 0.1 \mu\text{M}$, respectively, for VYU-2-24, VYU-2-221, VYU-2-270, and VYU-3-54.

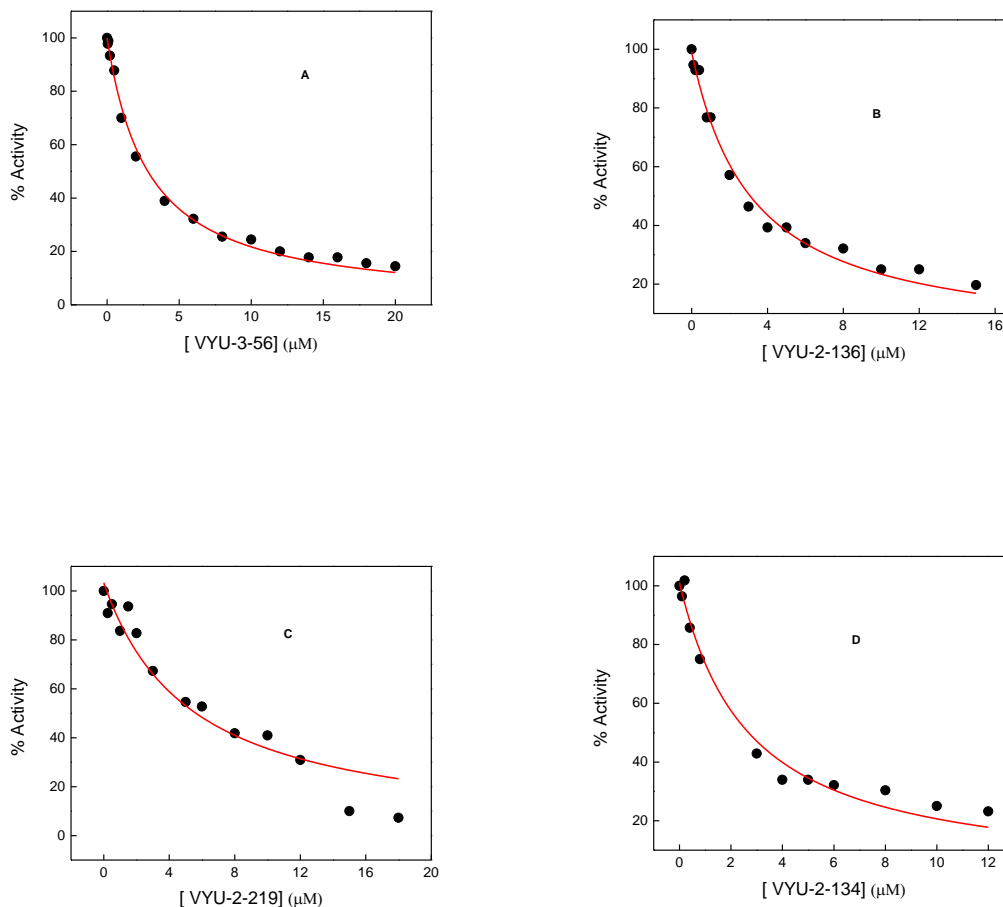


Figure 5.19. Steady state kinetics for the inhibition of HDAC8 enzyme activity by VYU-3-56, VYU-2-136, VYU-2-219, and VYU-2-134. They are, respectively, shown in panels A, B, C, and D. The initial rates of the HDAC8 catalyzed reaction were plotted as a function of the inhibitor concentration (dimeric form). The solid lines are the best fit of the data using the competitive K_i equation yielding the K_i values of $2.7 \pm 0.1 \mu\text{M}$, $3.3 \pm 0.2 \mu\text{M}$, $4.7 \pm 0.9 \mu\text{M}$, and $2.7 \pm 0.3 \mu\text{M}$, respectively, for VYU-3-56, VYU-2-136, VYU-2-219, and VYU-2-134.

5.3.1.2. Screening of Hydroxybenzoic, Hydroxypicolinic and Nicotinic Group Containing Compounds for the Inhibitory Features against HDAC8

Short chain fatty acids such as valproic acid and butyric acid are the well known inhibitors of HDAC [57]. The molecular docking and the simulation studies with VPA suggest that its carboxylate moiety coordinate with the active site metal ion [158]. In view of the above informations attempts were made to synthesize several compounds containing the hydroxybenzoic, hydroxypicolinic and nicotinic group, which have the potential to coordinate with the metal ion analogous to the carboxylate moiety of VPA, leading to HDAC8 inhibition. Their effectiveness on the HDAC8 catalyzed reaction was evaluated at 10 μ M concentration. The summary of the high-throughput screening of the above compounds is presented in Table 5.3. Unfortunately, none of the compounds tested for their inhibition potency was promising.

Table 5.3. Summary of the high-throughput screening of hydroxybenzoic acid and hydroxypicolinic /nicotinic acid based compounds for the HDAC8 inhibitors

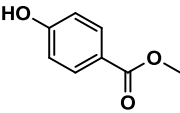
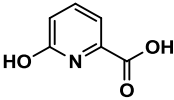
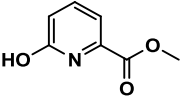
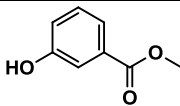
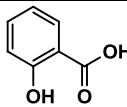
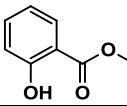
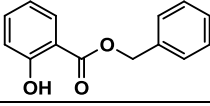
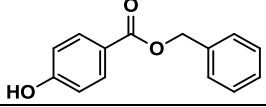
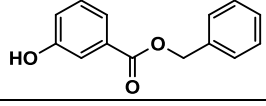
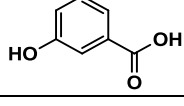
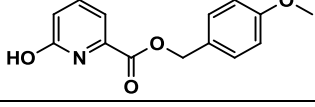
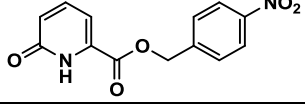
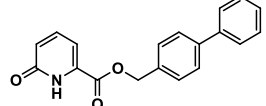
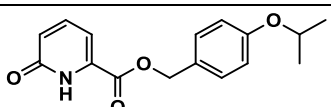
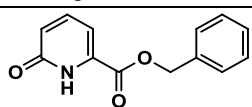
Entry	ID	Structure	% Inhibition or fold activation
1	VYU-2-10		NA/NI
2	VYU-2-13		NA/NI
3	VYU-2-22		NA/NI

Table 5.3. Summary of the high-throughput screening of hydroxybenzoic acid and hydroxypicolinic /nicotinic acid based compounds for the HDAC8 inhibitors (continued)

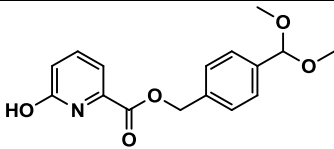
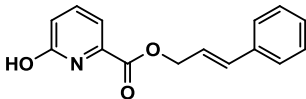
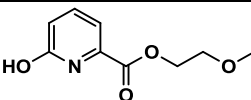
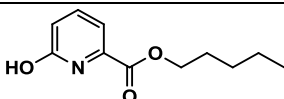
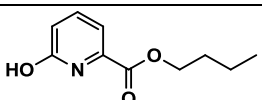
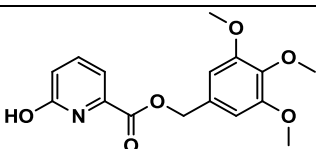
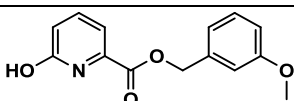
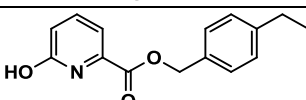
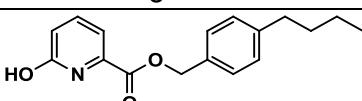
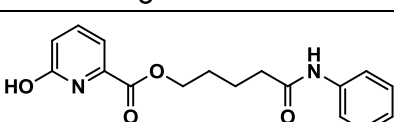
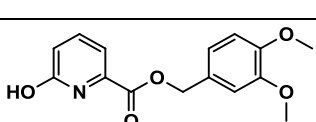
Entry	ID	Structure	% Inhibition or fold activation
4	VYU-2-20		NA/NI
5	VYU-2-62-1		NA/NI
6	VYU-2-62-2		NA/NI
7	VYU-2-44		NA/NI
8	VYU-2-48		NA/NI
9	VYU-2-46		NA/NI
10	VYU-2-23		7.4 %
11	VYU-2-94		NA/NI
12	TV-1-33		NA/NI
13	BNG-2-117		NA/NI
14	BNG-2-147		NA/NI
15	BNG-2-39		NA/NI

(continues)

Table 5.3. Summary of the high-throughput screening of hydroxybenzoic acid and hydroxypicolinic /nicotinic acid based compounds for the HDAC8 inhibitors (continued)

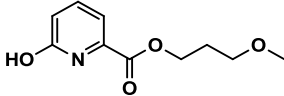
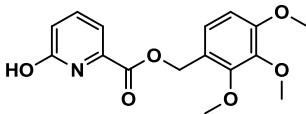
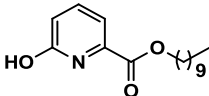
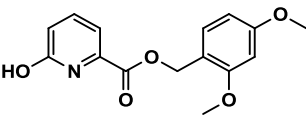
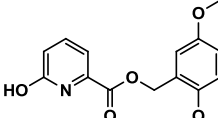
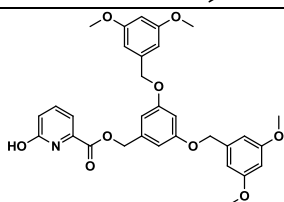
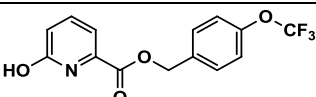
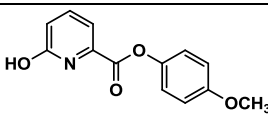
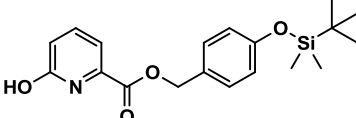
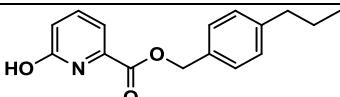
Entry	ID	Structure	% Inhibition or Activation
16	VYU-2-114		NA/NI
17	VYU-2-122		NA/NI
18	VYU-2-124		NA/NI
19	VYU-2-126		NA/NI
20	BNG-2-151		NA/NI
21	BNG-2-152		NA/NI
22	TM-1-291		NA/NI
23	VYU-2-110		NA/NI
24	VYU-2-98		NA/NI
25	BNG-2-175		NA/NI
26	BNG-2-182		NA/NI

Table 5.3. Summary of the high-throughput screening of hydroxybenzoic acid and hydroxypicolinic /nicotinic acid based compounds for the HDAC8 inhibitors (continued)

Entry	ID	Structure	% Inhibition or Activation
27	VYU-2-169		NA/NI
28	VYU-2-181		NA/NI
29	VYU-2-193		NA/NI
30	VYU-2-191		NA/NI
31	VYU-2-189		NA/NI
32	VYU-2-195		NA/NI
33	VYU-2-197		NA/NI
34	VYU-2-208		NA/NI
35	VYU-2-210		NA/NI
36	JES-1-45		NA/NI
37	VYU-2-234		NA/NI

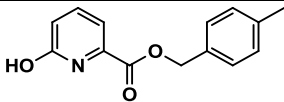
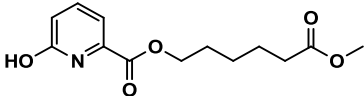
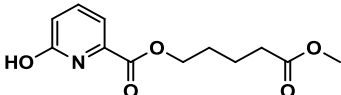
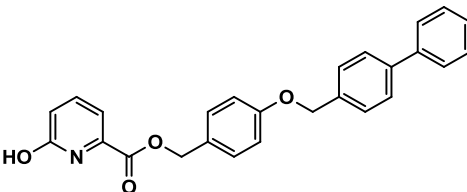
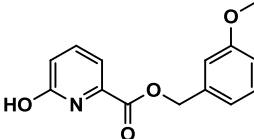
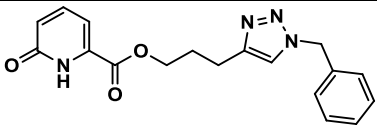
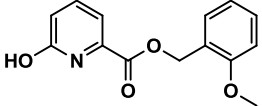
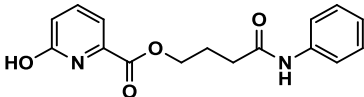
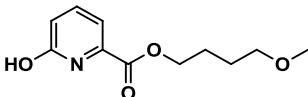
(continues)

Table 5.3. Summary of the high-throughput screening of hydroxybenzoic acid and hydroxypicolinic /nicotinic acid based compounds for the HDAC8 inhibitors (continued)

Entry	ID	Structure	% Inhibition or Activation
38	VYU-2-226		NA/NI
39	VYU-2-212		NA/NI
40	MJD-169		NA/NI
41	VYU-2-274		NA/NI
42	VYU-2-276		NA/NI
43	VYU-2-280		NA/NI
44	APB-177		NA/NI
45	APB-178		NA/NI
46	APB-181		NA/NI
47	OK-1-15		NA/NI

(continues)

Table 5.3 Summary of the high-throughput screening of hydroxybenzoic acid and hydroxypicolinic /nicotinic acid based compounds for the HDAC8 inhibitors (continued)

Entry	ID	Structure	% Inhibition or Activation
48	OK-1-16		NA/NI
50	VYU-3-38		NA/NI
51	VYU-3-40		NA/NI
52	VYU-3-45		NA/NI
53	VYU-2-278		NA/NI
54	BNG-3-33		NA/NI
55	VYU-2-224		NA/NI
56	JES-1-16		NA/NI
57	VYU-2-228		NA/NI

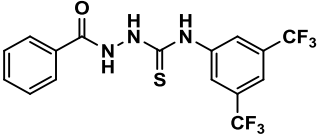
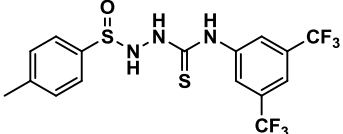
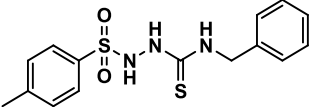
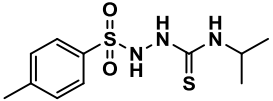
NI = No Inhibition, NA = No Activation

% = represents the % inhibition of HDAC8 enzyme activity at a concentration of 10 μ M inhibitor.

5.3.1.3. Screening of the Thiourea Derivatives against the HDAC8 Enzyme Activity

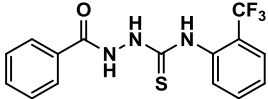
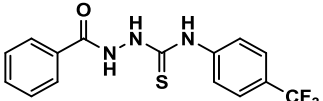
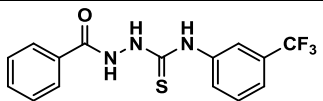
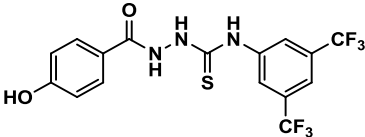
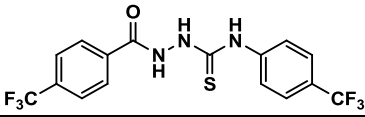
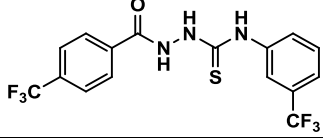
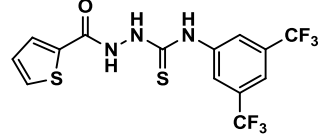
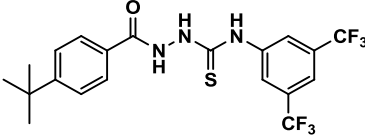
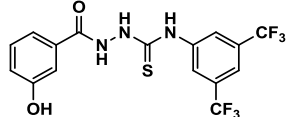
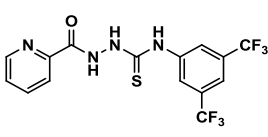
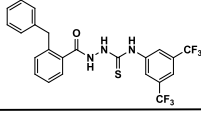
The thiourea derivatives have been reported to serve the inhibitors of the different classes of HDAC [159]. In pursuit of discovering novel HDAC inhibitor, several thiourea derivatives were synthesized. Their effectiveness on the HDAC8 catalyzed reaction was tested using the trypsin-coupled assay. Instead of serving as an inhibitor, surprisingly, several of the N-acetylthiourea derivatives tested at 10 μ M enhanced the rate of HDAC8 catalyzed. The results describing the fold activation of the HDAC8 activity in the presence of the 10 μ M concentration of the thiourea derivative are summarized in Table 5.4. The compounds serving as the activator of HDAC8 with the fold activation $\geq 3-5$ as compared the control, were selected for pursuing further the enzyme kinetic studies.

Table 5.4. Summary of the high-throughput screening of the thiourea derivatives for the HDAC8 activators/inhibitors

Entry	ID	Structure	% Inhibition or fold activation
1	TM-1-149		NA/NI
2	TM-1-155		NA/NI
3	TM-1-183		NA/NI
4	TM-1-185		NA/NI

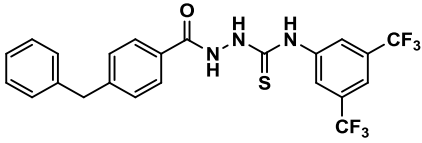
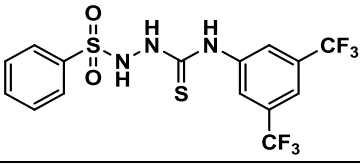
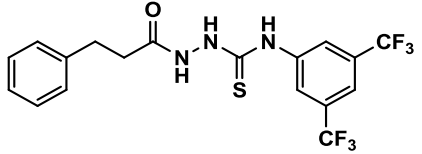
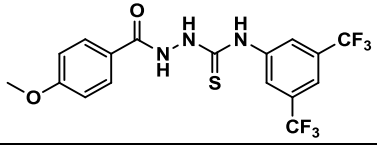
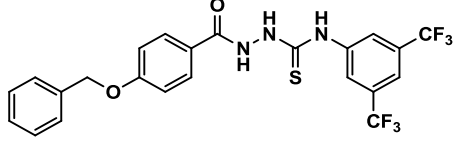
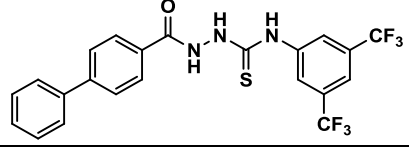
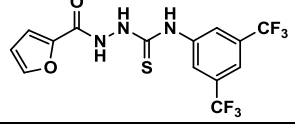
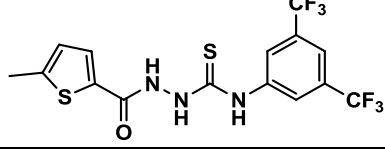
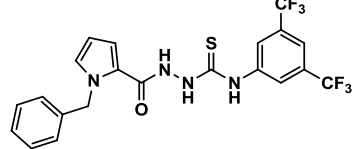
(continues)

Table 5.4. Summary of the high-throughput screening of the thiourea derivatives for the HDAC8 activators/inhibitors (continued)

Entry	ID	Structure	% Inhibition or Fold activation
5	TM-1-197		NA/NI
6	TM-1-202		NA/NI
7	TM-1-204		NA/NI
8	TM-1-227		9.5 %
9	TM-1-235		NA/NI
10	TM-1-236		NA/NI
11	TM-1-261		NA/NI
12	TM-1-267		NA/NI
13	TM-1-274		NA/NI
14	TM-1-278		NA/NI
15	TM-1-288		NA/NI

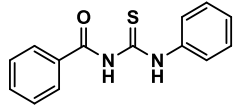
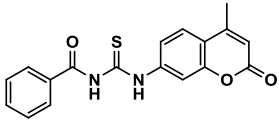
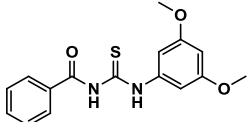
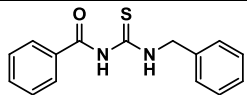
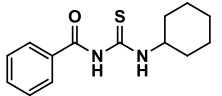
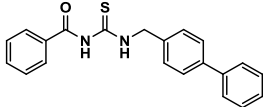
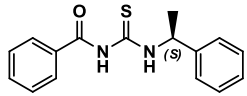
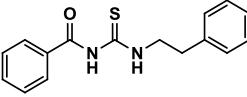
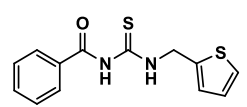
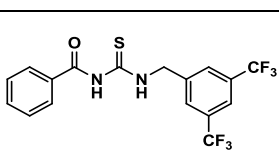
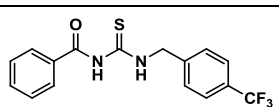
(continues)

Table 5.4. Summary of the high-throughput screening of the thiourea derivatives for the HDAC8 activators/inhibitors (continued)

Entry	ID	Structure	% Inhibition or Fold activation
16	TM-2-4		NA/NI
17	BNG-2-119		NA/NI
18	TM-2-7		NA/NI
19	TM-2-8		NA/NI
20	TM-2-16		NA/NI
21	TM-2-32		NA/NI
22	TM-II-48		NA/NI
23	TM-2-57		NA/NI
24	TM-2-60		NA/NI

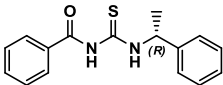
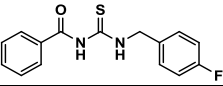
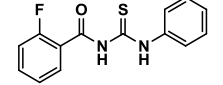
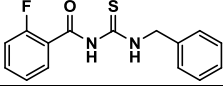
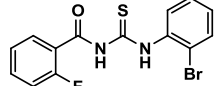
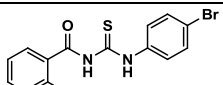
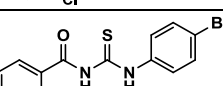
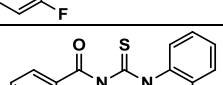
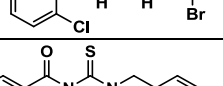
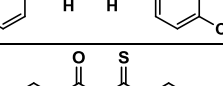
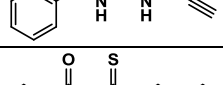
(continues)

Table 5.4. Summary of the high-throughput screening of the thiourea derivatives for the HDAC8 activators/inhibitors (continued)

Entry	ID	Structure	% Inhibition or Fold activation
25	TM-2-51		12 fold Activation
26	TM-2-87		2 fold Activation
27	TM-2-88		8.4 fold Activation
28	TM-2-90		3.3 fold Activation
29	TM-2-97		5.6 fold Activation
30	TM-2-101		1.1 fold Activation
31	TM-2-104		4.5 fold Activation
32	TM-2-105		2 fold Activation
33	TM-2-107		3 fold Activation
34	TM-2-125		1.1 fold Activation
35	TM-2-126		1.2 fold Activation

(continues)

Table 5.4. Summary of the high-throughput screening of the thiourea derivatives for the HDAC8 activators/inhibitors (continued)

Entry	ID	Structure	% Inhibition or Fold activation
36	TM-2-130		1.5 fold Activation
37	TM-2-131		3 fold Activation
38	TM-2-138		3.5 fold Activation
39	TM-2-139		1.0 fold Activation
40	TV-1-90		2.5 fold Activation
41	TV-1-91		NA/NI
42	TV-1-92		1.2 fold Activation
43	TV-1-93		1.6 fold Activation
44	TV-1-106		NA/NI
45	TV-1-113		NA/NI
46	TV-1-114		NA/NI

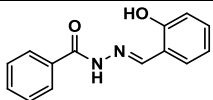
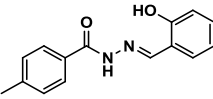
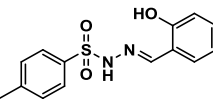
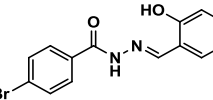
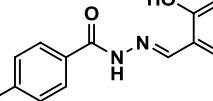
NI = No Inhibition, NA = No Activation, % = represents the % inhibition of HDAC8 enzyme activity at a concentration of 10 μ M inhibitor. "Fold activation" is defined as the initial rate of the HDA8 catalyzed reaction in the presence and the absence of the compound.

5.3.1.4. Screening of Hydrazone Derivatives Potency against the HDAC8 Enzyme

Activity

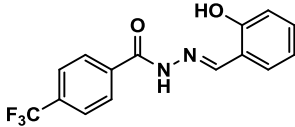
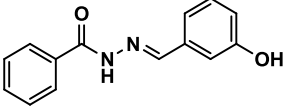
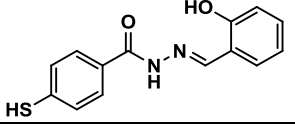
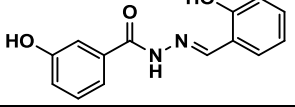
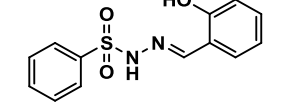
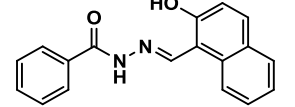
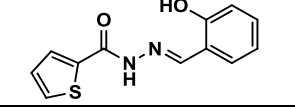
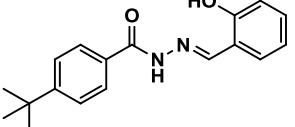
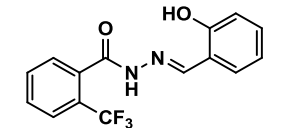
A series of hydrazone derivatives were synthesized and their effectiveness was tested on the HDAC8 catalyzed reaction at 10 μ M. Table 5.5 contains the summary of the high-throughput screening of the above compounds. Evidently, none of the compounds under study showed any inhibition or activation except for TM-1-182, TM-1-187, TM-1-234, TM-1-246, and TM-1-260, which inhibited the HDAC8 enzyme activity by 23 %, 9.3 %, 9 %, 12 %, and 7 %, respectively.

Table 5.5. Summary of the high-throughput screening of hydrazone derivative for the HDAC8 inhibitors/activators

Entry	ID	Structure	% Inhibition or fold activation
1	TM-1-121		NA/NI
2	TM-1-144		NA/NI
3	TM-1-170		NA/NI
4	TM-1-182		23 %
5	TM-1-187		9.3 %

(continues)

Table 5.5. Summary of the high-throughput screening of hydrazone derivative for the HDAC8 inhibitors/activators (continued)

Entry	ID	Structure	% Inhibition or fold activation
6	TM-1-234		9 %
7	TM-1-243		NA/NI
8	TM-1-246		12 %
9	TM-1-248		NA/NI
10	TM-1-254		NA/NI
11	TM-1-259		NA/NI
12	TM-1-260		7 %
13	TM-1-268		NA/NI
14	TM-1-272		NA/NI

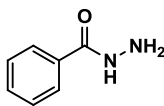

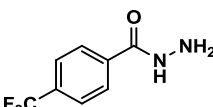
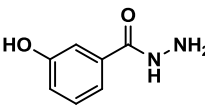
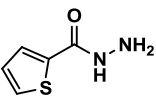
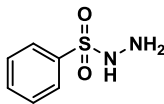
NI = No Inhibition, NA = No Activation.

% = represents the % inhibition of HDAC8 enzyme activity at 10 μ M of the inhibitor.

5.3.1.5. Screening of the Hydrazides Derivatives for a Potential Inhibitor/Activator for the HDAC8 Catalyzed Reaction

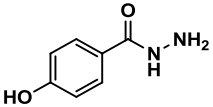
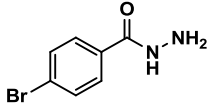
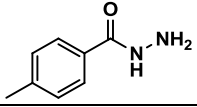
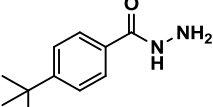
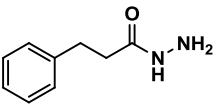
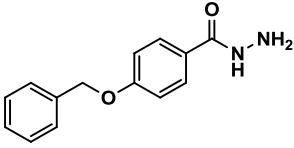
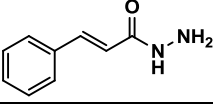
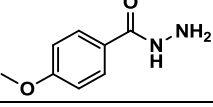
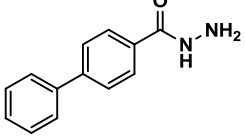
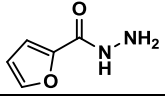
A series of the hydrazides derivatives were synthesized and their effectiveness were tested on the HDAC8 catalyzed reaction at 10 μ M. Table 5.6 contains the summary of the high-throughput screening of the above compounds. The most potent inhibitor among this class was TM-1-265 which inhibited the HDAC8 activity by 38 % at 10 μ M. The remaining compounds showed very minimal or no inhibition to the enzyme.

Table 5.6. Summary of the high-throughput screening result of hydrazide derivatives for the HDAC8 inhibitor/activator

Entry	ID	Structure	% Inhibition or fold activation
1	TM-1-108		14 %
2	TM-1-228		NA/NI
3	TM-1-231		9 %
4	TM-1-245		18 %
5	TM-1-253		9 %
6	TM-1-255		NA/NI

(continues)

Table 5.6. Summary of the high-throughput screening result of hydrazide derivatives for the HDAC8 inhibitor/activator (continued)

Entry	ID	Structure	% Inhibition or Fold activation
7	TM-1-256		23 %
8	TM-1-257		28 %
9	TM-1-258		14 %
10	TM-1-265		38 %
11	TM-2-6		12 %
12	TM-2-14		14 %
13	TM-2-19		NA/NI
14	TM-2-21		26 %
15	TM-2-31		25 %
16	TM-II-46		NA/NI

NI = No Inhibition

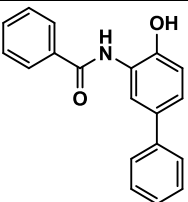
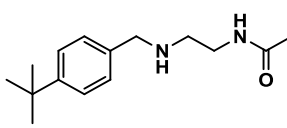
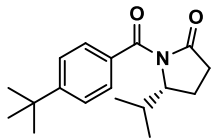
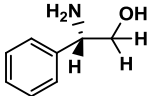
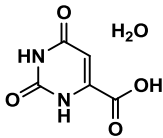
% = represents the % inhibition of HDAC8 enzyme activity at a concentration of 10 μ M inhibitor.

5.3.1.6. Screening of the Miscellaneous Compounds for Potential HDAC8

Inhibitor/Activator

In pursuit of discovering a novel class of HDAC8 inhibitor/activator, several miscellaneous compounds containing a different zinc-binding moiety were synthesized. Their effectiveness on the HDAC8 catalyzed reaction was tested in the presence of the 10 μ M of the compound. The summary of the high-throughput screening of the miscellaneous compounds using the trypsin-coupled assay is presented in Table 5.7. Unfortunately, none of the above compounds served as an effector (inhibitor/activator) of HDAC8.

Table 5.7. Summary of the high-throughput screening of the miscellaneous compounds for the HDAC8 inhibitors/activators

Entry	ID	Structure	% Inhibition or fold activation
1	YT-2-212		NA/NI
2	MK-249		NA/NI
3	M-264		NA/NI
4	VYU-2-63-1		NA/NI
5	VYU-2-63-3		NA/NI

(continues)

Table 5.7. Summary of the high-throughput screening of the miscellaneous compounds for the HDAC8 inhibitors/activators (continued)

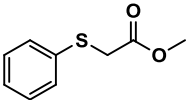
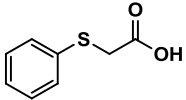
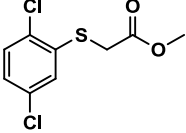
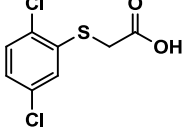
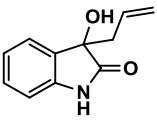
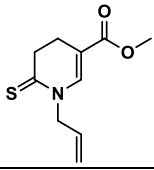
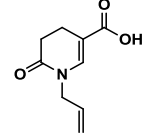
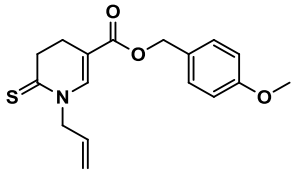
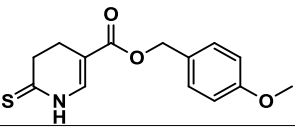
Entry	ID	Structure	% Inhibition or fold activation
6	VYU-2-86		NA/NI
7	VYU-2-87		NA/NI
8	VYU-2-88		NA/NI
9	VYU-2-89		NA/NI
10	BNG-2-23	 (R) Enantiomer	NA/NI
11	MT-119		NA/NI
12	MT-122		7.3 %
13	MT-124		19.5 %
14	MT-128		7.3 %

Table 5.7. Summary of the high-throughput screening of the miscellaneous compounds for the HDAC8 inhibitors/activators (continued)

Entry	ID	Structure	% Inhibition or Fold activation
15	MT-129		12.3 %
16	VYU-2-62-4		NA/NI
17	VYU-2-171		NA/NI
18	VYU-2-173		NA/NI
19	VYU-2-248		NA/NI
20	VYU-2-250		NA/NI
21	VYU-2-252		NA/NI
22	VYU-2-204-2		NA/NI
23	TV-1-55		NA/NI
24	BNG-3-60		NA/NI
25	BNG-4-87-1		NA/NI
26	TV-1-67		NA/NI

NI = No Inhibition

% = represents the % inhibition of HDAC8 enzyme activity at a concentration of 10 μ M inhibitor.

5.3.1.7. Inhibitory Potency of Fluorescent Analogs of SAHA and other Generic

Inhibitors

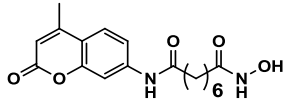
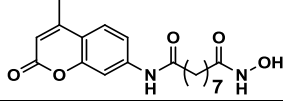
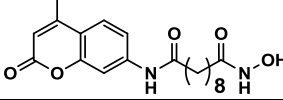
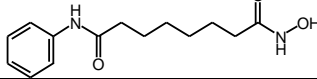
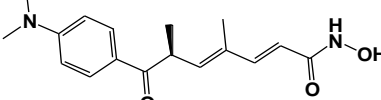
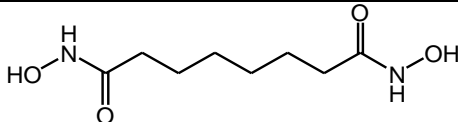
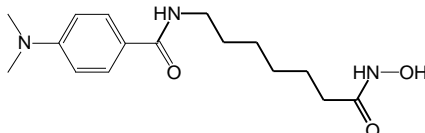
Fluorescent analogs of a ligand are preferred small molecules to study the ligand-protein interaction, which is especially useful where the intrinsic protein fluorescence is weak or absent. Additionally, the fluorescent ligand serves as a probe to investigate the structural-functional and the mechanistic features of the protein-ligand interaction [160]. In view of the above fact fluorescent analogs of a well known HDAC8 inhibitor (SAHA), such as TM-2-3 (coumarin-SAHA), BNG-3-93 and BNG-3-90 were synthesized. The chemical structure of the above inhibitors is shown in Table 5.8. All three inhibitors contain the Coumarin moiety serving as the cap group. Evidently, they have the identical chemical structure except for the differences in the length of the linker region. In order to check the inhibitory features of these compounds against HDAC8, the percent inhibition of the enzyme catalyzed reactions were measured in the presence of the 10 μ M of the compound. The percent inhibition in the HDAC8 activity due to TM-2-3, BNG-3-93, and BNG-3-90, respectively, were 94 %, 98 % and 23 %. Evidently, TM-2-3 and BNG-3-93, which, respectively, contains six and seven consecutive methylene groups in the linker region, has similar inhibition potency. There was a marked reduction in the percent inhibition of HDAC8 by BNG-3-90, which contains eight consecutive methylene groups in the linker region, implying that the length of the linker region of the inhibitor is a key determining factor for its binding to the enzyme. This could be presumably because of the limited space available in the hydrophobic tunnel of the enzyme where the linker binds.

SAHA (Suberoylanilide Hydroxamic acid), SBHA (Suberohydroxic acid), TSA (Trichostatin A), and M-344 (4-dimethylamino-N-(6-hydroxycarbamoyethyl) benzamide-

N-hydroxy-7-(4-dimethylaminobenzoyl) aminoheptanamide) are the well known HDAC8 inhibitors which belong to the structural class of Hydroxamate. TSA was the first inhibitor of this class and was discovered by Yoshida *et al.* [127]. The crystal structures of HDAC8 with TSA, SAHA and M-344 have been solved which clearly shows that that even with structurally similar ligand, the ligand-induced conformation changes in the protein are different [57]. The above inhibitors have been reported to show different *in vitro* as well as *in vivo* potency [57].

In order to compare inhibition potency of TM-2-3 (c-SAHA) with SAHA as well as the other hydroxamate inhibitors comprised of the similar length of the linker namely, TSA, SBHA and M-344, the inhibition constant (K_i) were determined as described in the Methods section. The initial rates of the HDAC8 catalyzed reaction were measured as a function of the inhibitor concentration. The solid lines shown in Figure 5.20 represent the best fit of the experimental data using the competitive K_i equation providing the K_i values of $0.11 \pm 0.02 \mu\text{M}$, $0.29 \pm 0.04 \mu\text{M}$, $0.12 \pm 0.02 \mu\text{M}$, $0.71 \pm 0.03 \mu\text{M}$, and $0.18 \pm 0.03 \mu\text{M}$, respectively, for TM-2-3, SAHA, TSA, SBHA, and M-344. Clearly, TM-2-3 is the most potent among these inhibitors, presumably because of the presence of the bulky cap which could interact more effectively with the surface of HDAC8 near the active site. SBHA being devoid of a cap group has the least inhibition potency among the above inhibitors.

Table 5.8. Inhibition potency of fluorescent analogs of SAHA and other hydroxamates

Entry	ID	Structure	% Inhibition or K_i
1	TM-2-3 (coumarin-SAHA)		94% $K_i = 0.1 \mu\text{M}$
2	BNG-3-93		98%
3	BNG-3-90		23%
4	SAHA		0.4 μM
5	TSA		0.12 μM
6	SBHA		0.7 μM
7	M-344		0.18 μM

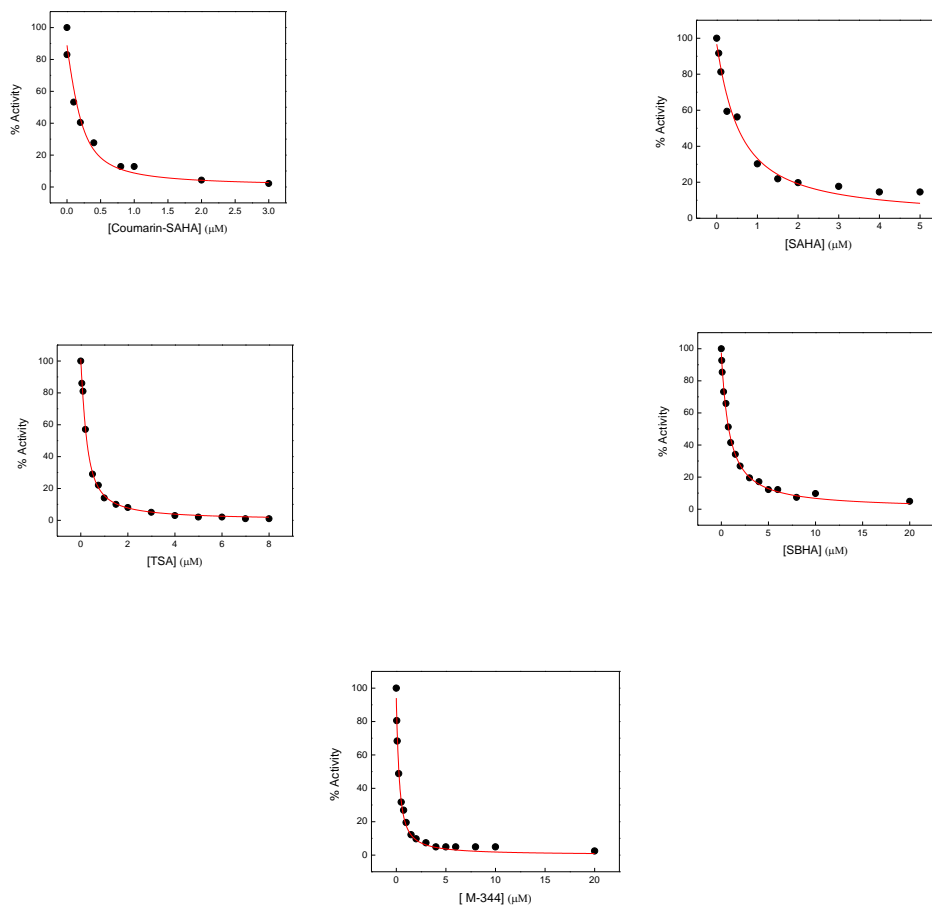
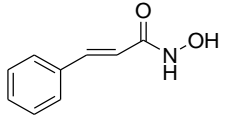
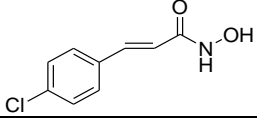
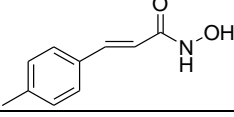
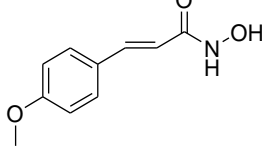
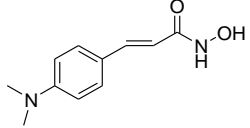
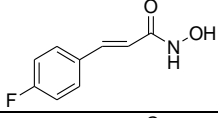
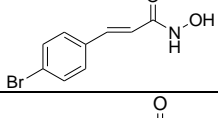
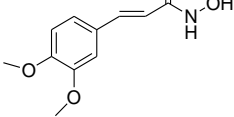
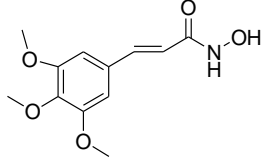
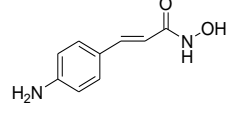


Figure 5.20. Steady state kinetics for the inhibition of HDAC8 enzyme activity by SAHA, TM-2-3 (c-SAHA), TSA, SBHA and M-334. They are, respectively, shown in panels A, B, C, D, and E. The initial rates of the HDAC8 catalyzed reaction were plotted as a function of the inhibitor concentration. The solid lines are the best fit of the data using the competitive K_i equation yielding the K_i values of $0.11 \pm 0.02 \mu\text{M}$, $0.29 \pm 0.04 \mu\text{M}$, $0.12 \pm 0.02 \mu\text{M}$, $0.71 \pm 0.03 \mu\text{M}$, and $0.18 \pm 0.03 \mu\text{M}$, respectively, for TM-2-3 (c-SAHA), SAHA, TSA, SBHA, and M-344.

5.3.1.8. Screening of the Hydroxamate Derivatives of Cinnamic Acid for a Potential Inhibitor/Activator of the HDAC8 Catalyzed Reaction

A canonical hydroxamate HDAC8 inhibitor contains a metal-binding group (hydroxamate), a linker and a cap. The linker and the cap group interact with the rim and the surface of the active site pocket, respectively [126]. However, several linkerless aryl hydroxamic acids have been reported as HDAC8 selective inhibitors [71]. It has been argued that in the aryl hydroxamic inhibitor, the aryl group binds to a sub-pocket, located in the vicinity of the active site, and is exclusively present in HDAC8 isozyme [57]. The crystallographic studies of HDAC8 with an aryl linker containing inhibitor, CRA-A, suggest that the aryl group is well accommodated in a hydrophobic sub-pocket [57]. In the light of the above information, several hydroxamate derivatives of cinnamic acid were synthesized where the backbone of cinnamic acid can serve as a very short linker. Their inhibitory potency was tested on the HDAC8 catalyzed reaction using the trypsin-coupled assay. The inhibition constant (K_i) of the inhibitor was determined by measuring the initial rate of the enzyme catalyzed reaction as a function of the inhibitor concentration. The data were analyzed using the competitive K_i equation yielding the K_i values as contained in the legends of Figures 5.21 and 5.22. The summary of the inhibition data of the hydroxamate derivative of cinnamic acid is presented in Table 5.9. The result clearly suggests that whenever the aryl group of the cinnamic acid is attached to polar moiety/atom namely, chlorine, fluorine, dimethylamino, etc., the value of K_i is higher, implying that the aryl group of the inhibitor presumably binds to a hydrophobic sub-pocket in the vicinity of the active site similar to linkerless inhibitor reported previously [71].

Table 5.9. Summary of the high-throughput screening result of the hydroxamate derivative of the cinnamic acid for the HDAC8 inhibitors/activator

Entry	Compound ID	Compound Structure	K _i (μM)
1	MH – 9/34B		0.1
2	MH – 9/35B		0.65
3	MH – 9/36B		0.45
4	MH – 9/37B		0.45
5	MH – 9/38B		0.318
6	MH – 9/39B		0.462
7	MH – 9/40B		0.850
8	MH – 9/41B		0.350
9	MH – 9/42B		0.437
10	MH – 9/44B		0.160

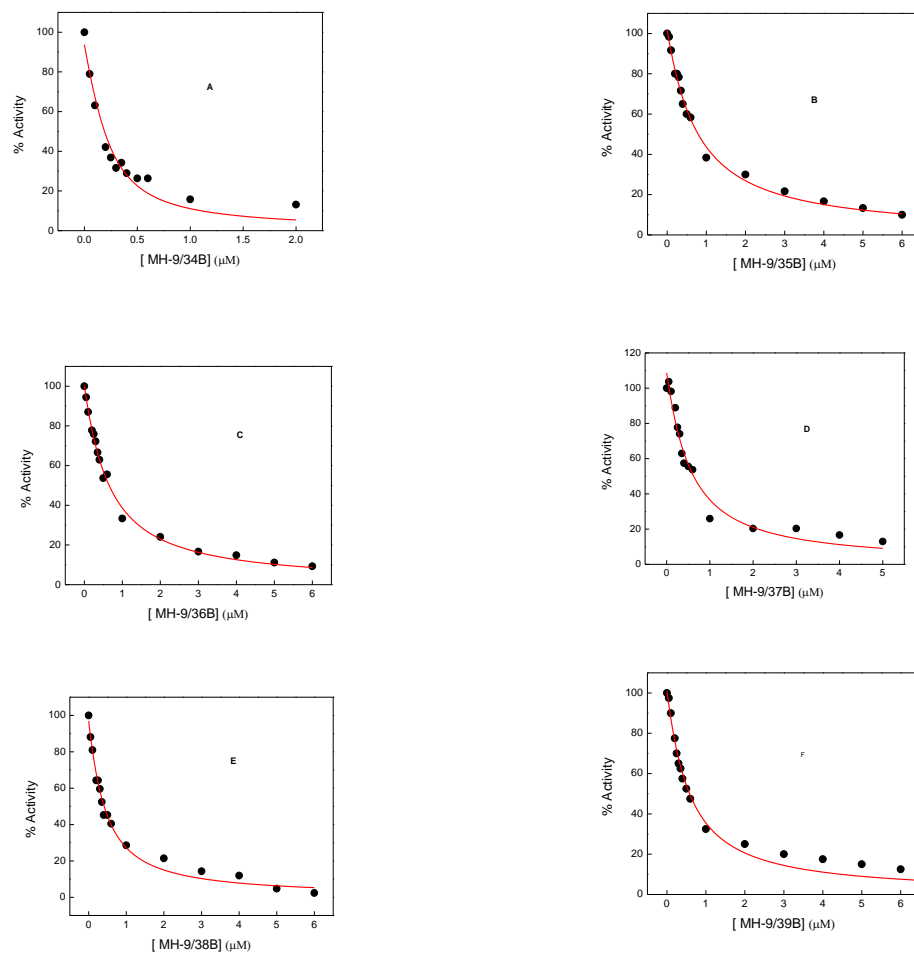


Figure 5.21. Steady state kinetics for the inhibition of HDAC8 enzyme activity by MH-9/34B, MH-9/35B, MH-9/36B, MH-9/37B, MH-9/38B, and MH-9/39B. They are, respectively, shown in panels A, B, C, D, E, and F. The initial rates of the HDAC8 catalyzed reaction were plotted as a function of the inhibitor concentration. The solid lines are the best fit of the data using the competitive K_i equation yielding the K_i values of $0.66 \pm 0.04 \mu\text{M}$, $0.42 \pm 0.02 \mu\text{M}$, $0.52 \pm 0.02 \mu\text{M}$, $0.50 \pm 0.03 \mu\text{M}$, $0.31 \pm 0.02 \mu\text{M}$, and $0.46 \pm 0.04 \mu\text{M}$, respectively, for MH-9/34B, MH-9/35B, MH-9/36B, MH-9/37B, MH-9/38B, and MH-9/39B.

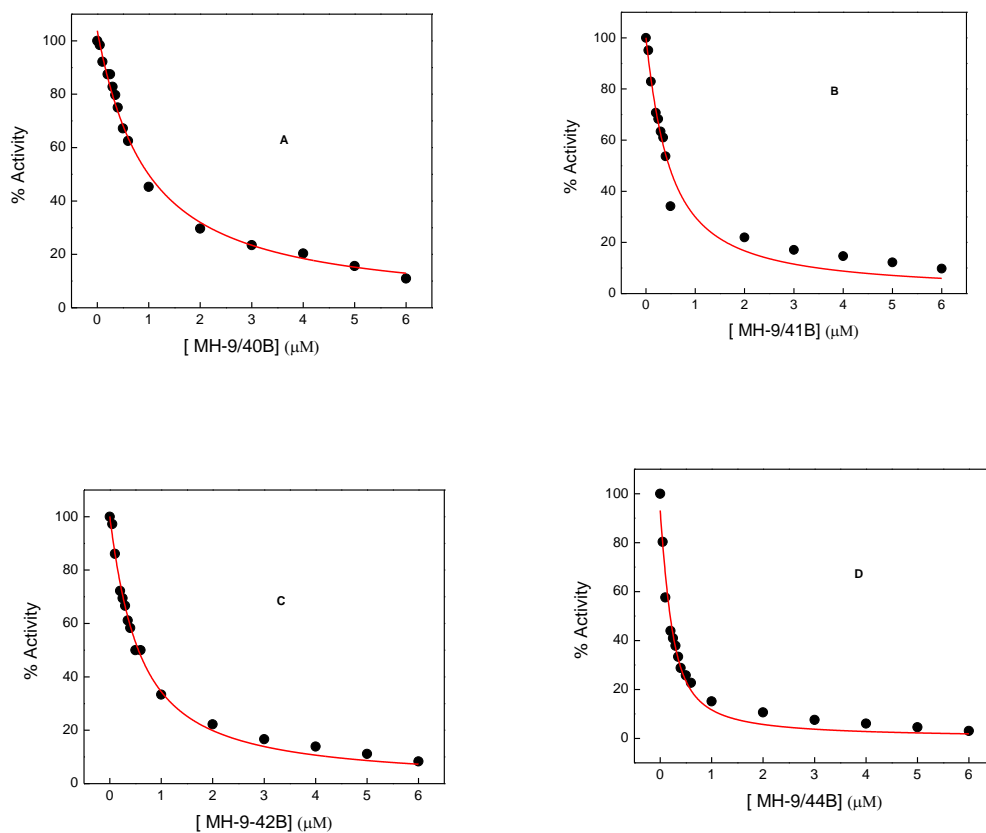
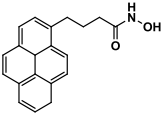
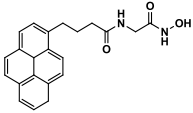
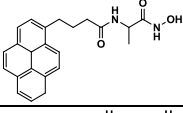
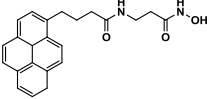
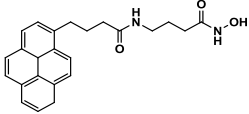
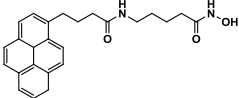


Figure 5.22. Steady state kinetics for the inhibition of HDAC8 enzyme activity by MH-9/40B, MH-9/41B, MH-9/42B, and MH-9/44B. They are, respectively, shown in panels A, B, C, and D. The initial rates of the HDAC8 catalyzed reaction were plotted as a function of the inhibitor concentration. The solid lines are the best fit of the data using the competitive K_i equation, yielding the K_i values of $0.86 \pm 0.08 \mu\text{M}$, $0.34 \pm 0.05 \mu\text{M}$, $0.43 \pm 0.02 \mu\text{M}$, and $0.16 \pm 0.02 \mu\text{M}$, respectively, for 9/40B, MH-9/41B, MH-9/42B, and MH-9/44B.

5.3.1.9. Evaluating the Potency of Hydroxamate Inhibitor Containing Pyrene Group as the Cap

A series of hydroxamate inhibitor containing the pyrene group as a cap (Table 5.10) were synthesized. The K_i value of the inhibitor was determined by measuring the initial rate of the HDAC8 catalyzed reaction as a function of an increasing concentration of the inhibitor. The data were analyzed using the competitive K_i equation. The solid lines shown in Figure 5.23 are the best fit of the data yielding the respective K_i values listed in Table 5.10.

Table 5.10. Inhibitory potency of hydroxamate-based inhibitors containing a pyrene moiety as a cap

Entry	Compound ID	Structure	K_i (μM)
1	MH-12/11		0.22
2	MH-12/5		1.75
3	MH-12/4		0.11
4	MH-12/6		1.88
5	MH-12/7		0.58
6	MH-12/9		0.48

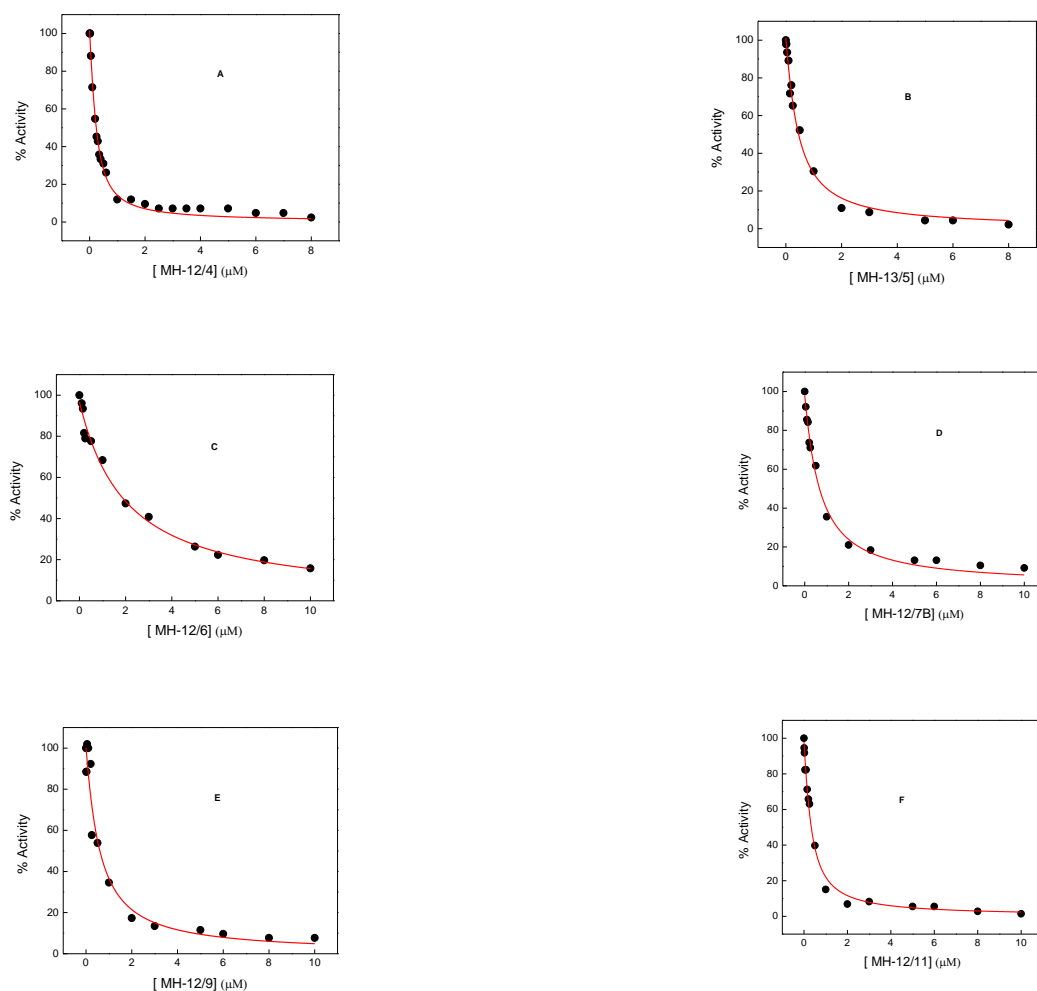
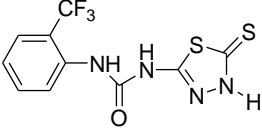
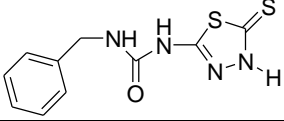
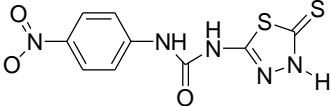
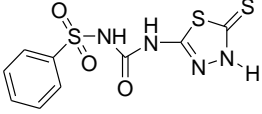
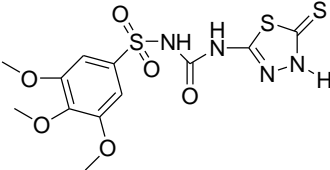


Figure 5.23. Steady state kinetics for the inhibition of HDAC8 enzyme activity by MH-12/4, MH-12/5, MH-12/6, MH-12/7, MH-12/9, and MH-12/11. They are, respectively, shown in panels A, B, C, D, E and F. The initial rates of the HDAC8 catalyzed reaction were plotted as a function of the inhibitor concentration. The solid lines are the best fit of the data using the competitive K_i equation yielding the K_i values of $0.11 \pm 0.01 \mu\text{M}$, $1.75 \pm 0.13 \mu\text{M}$, $1.88 \pm 0.16 \mu\text{M}$, $0.58 \pm 0.05 \mu\text{M}$, $0.48 \pm 0.10 \mu\text{M}$, and $0.22 \pm 0.02 \mu\text{M}$, respectively, MH-12/4, MH-12/5, MH-12/6, MH-12/7, MH-12/9, and MH-12/11.

5.3.1.10. Screening of the Urea Derivatives of 2-amino-5-mercapto, 1, 3, 4, -thiodiazole for a Potential Inhibitor/Activator of the HDAC8 Catalyzed Reaction

In pursuit of discovering the novel class of the HDAC inhibitor/activator, a series of urea derivatives of 2-amino-5-mercapto, 1, 3, 4-thiodiazole was synthesized. Their inhibition potency was evaluated by measuring HDAC8 activity in the presence of 10 μ M of the inhibitor. The result of the screening is summarized in Table 5.11. Unfortunately, none of the compounds served as an activator/inhibitor of the enzyme.

Table 5.11. Summary of the inhibition data of the urea derivatives of 2-amino-5-mercapto, 1, 3, 4, - thiodiazole

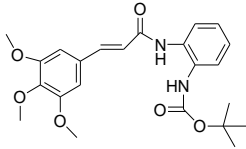
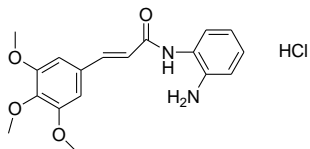
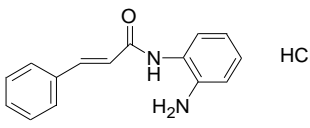
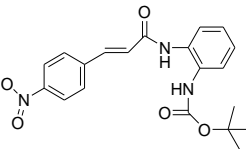
Entry	Compound ID	Compound Structure	% Inhibition
1	MH 7/27		NI
2	MH 7/25		NI
3	MH 7/26		NI
4	MH 7/28		NI
5	MH - 8/2		NI

NI = No Inhibition

5.3.1.11. Screening of the Cinnamic acid Derivatives of o-phenylenediamine for a Potential Inhibitor/activator of the HDAC8 Catalyzed Reaction

A series of cinnamic acid derivatives of o-phenylenediamine were synthesized in pursuit of designing a novel class of the HDAC8 inhibitors. Their inhibition potency was evaluated by measuring HDAC8 activity in the presence of 10 μM of the inhibitor. The summary of the result is presented in Table 5.12. None of the above compounds showed an appreciable inhibition/activation in HDAC8 activity, except MH-7/31, MH-8/15, and MH-9/18B, which inhibited the rate of the HDAC8 catalyzed reaction by 30 %, 40 %, and 40 %, respectively.

Table 5.12. Summary of the high-throughput screening result of the cinnamic acid derivatives of o-phenylenediamine for an HDAC8 inhibitor/activator

Entry	ID	Structure	% inhibition or K_i (μM)
1	MH 7/21		NI
2	MH 7/21 B		NI
3	MH 7/22B		NI
4	MH 7/24		10 %

(continues)

Table 5.12. Summary of the high-throughput screening result of the cinnamic acid derivatives of o-phenylenediamine for an HDAC8 inhibitor/activator (continued)

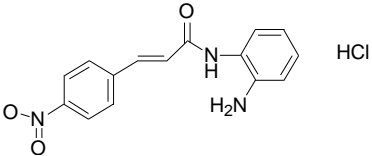
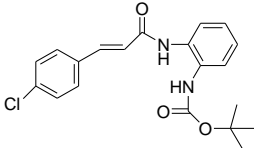
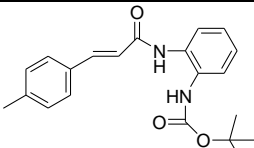
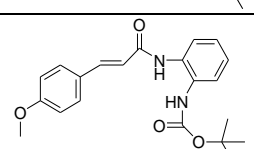
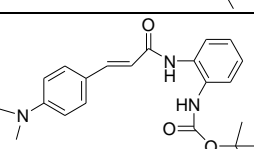
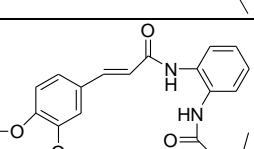
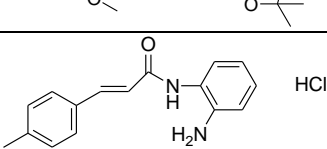
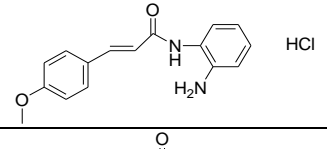
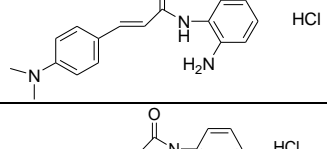
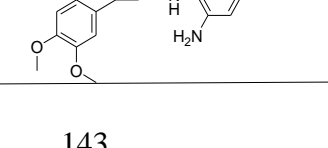
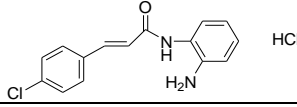
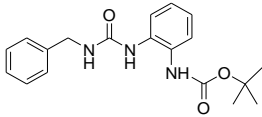
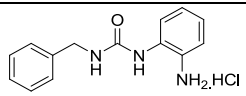
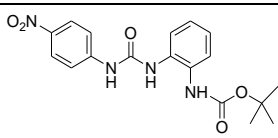
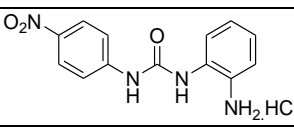
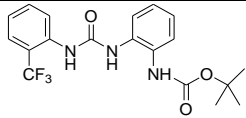
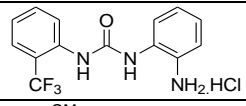
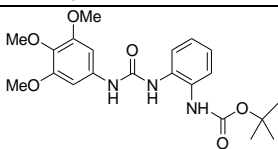
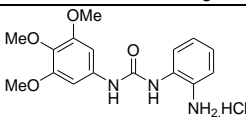
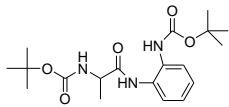
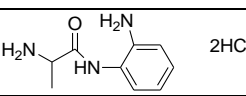
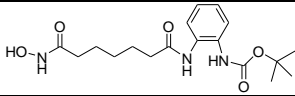
Entry	ID	Structure	% Inhibition
5	MH 7/24B		NI
6	MH 7/34		NI
7	MH 7/30		NI
8	MH 7/31		30 %
9	MH 7/32		NI
10	MH 7/33		NI
11	MH 7/30B		NI
12	MH 7/31B		NI
13	MH 7/32B		10 %
14	MH 7/33B		NI

Table 5.12. Summary of the high-throughput screening result of the cinnamic acid derivatives of *o*-phenylenediamine for an HDAC8 inhibitor/activator (continued)

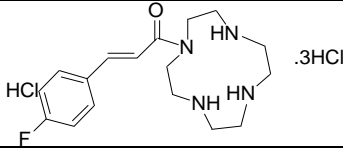
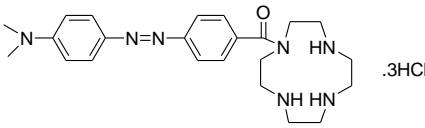
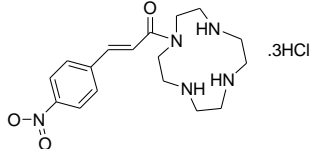
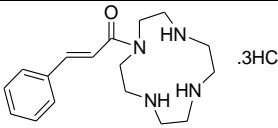
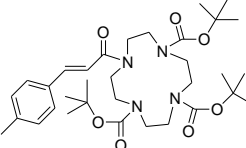
Entry	ID	Structure	% Inhibition
15	MH 7/34B		NI
16	MH - 8/15		40 %
17	MH - 8/15B		10 %
18	MH - 8/16		NI
19	MH - 8/16B		NI
20	MH - 8/17		NI
21	MH - 8/17B		10 %
22	MH - 8/19		NI
23	MH - 8/19B		40 %
24	MH 9/14		NI
25	MH 9/14B		NI
26	MH 9/16C		NI

NI = No Inhibition

5.3.1.12. Screening of the Cyclen-based Compounds for a Potential Inhibitor/Activator of the HDAC8 Catalyzed Reaction

A series of cyclen-based compounds were synthesized in pursuit of discovering a novel class of the HDAC8 inhibitors. Their inhibition potency was evaluated by measuring HDAC8 activity in the presence of 10 μM of the inhibitor. The summary of the result is presented in Table 5.13. None of the above compounds caused any appreciable inhibition/activation in HDAC8 activity, except MH-8/21 and MH-8/23 which inhibited the rate of the HDAC8 catalyzed reaction by 20 %.

Table 5.13. Summary of the high-throughput screening result of the *cyclen*-based compounds for an HDAC8 inhibitor/activator

Entry	ID	Structure	% inhibition or K_i (μM)
1	MH 7/12		NI
2	MH 6/95 B		NI
3	MH 7/14 B		NI
4	MH 7/ 13 B		NI
5	MH 7/35		NI

(continues)

Table 5.13. Summary of the high-throughput screening result of the *cyclen*-based compounds for an HDAC8 inhibitor/activator (continued)

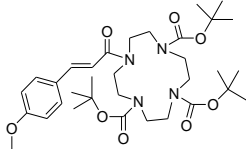
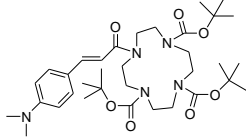
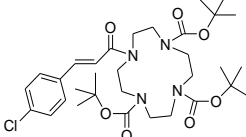
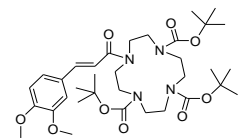
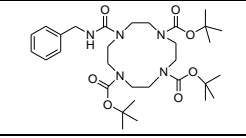
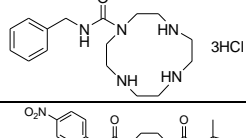
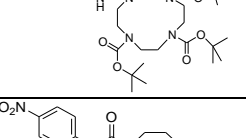
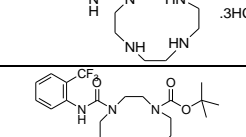
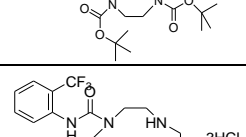
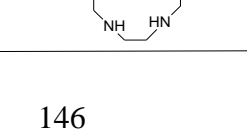
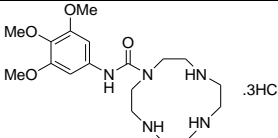
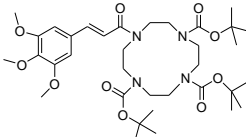
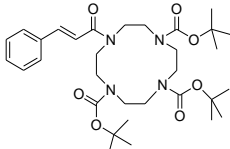
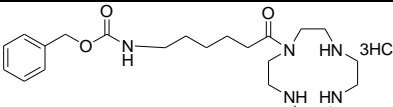
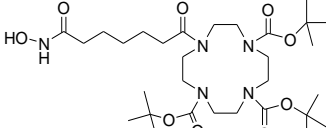
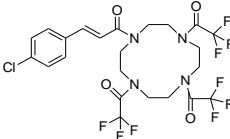
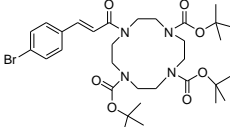
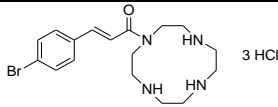
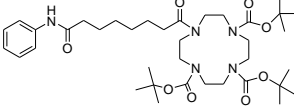
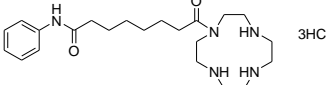
Entry	ID	Structure	% Inhibition
6	MH 7/36		NI
7	MH 7/37		NI
8	MH 7/38		NI
9	MH 7/39		10 %
10	MH – 8/21		20 %
11	MH – 8/21B		10 %
12	MH – 8/22		10 %
13	MH – 8/22 B		10 %
14	MH – 8/23		20 %
15	MH – 8/23B		NI

Table 5.13. Summary of the high-throughput screening result of the *cyclen*-based compounds for an HDAC8 inhibitor/activator (continued)

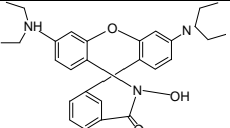
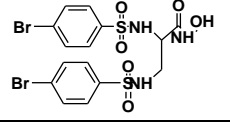
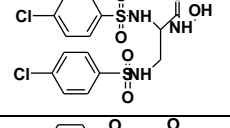
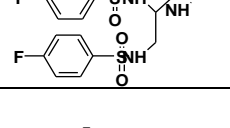
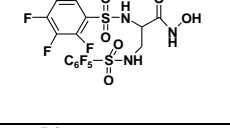
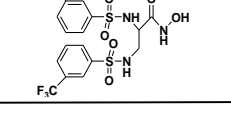
Entry	ID	Structure	% Inhibition
16	MH – 8/24		NI
17	MH 7/9		NI
18	MH 7/13		NI
19	MH 9/15B		NI
20	MH 9/15C		NI
21	MH 9/20B		NI
22	MH 9/21		NI
23	MH 9/21B		NI
24	MH 9/ 5		NI
25	MH 9/5B		NI

NI = No Inhibition

5.3.1.13. High Throughput Screening of Miscellaneous Inhibitors Obtained from Mallik's lab against HDAC8

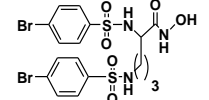
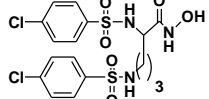
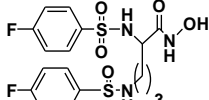
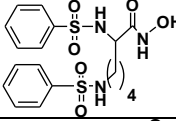
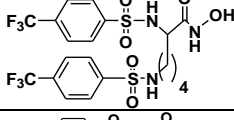
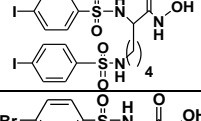
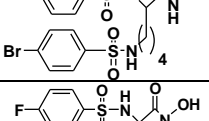
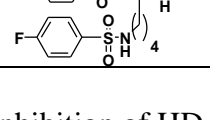
In pursuit of designing a novel class of HDAC8 inhibitor/activator, miscellaneous compounds containing different zinc-binding moiety were synthesized in the laboratory of Prof. Sanku Mallik. Their effectiveness on the HDAC8 catalyzed reaction was tested in the presence of the 10 μM of the compound. The result of the high-throughput screening of the miscellaneous compounds is summarized in Table 5.14. Several inhibitors were identified which have the inhibition potency in the micromolar range.

Table 5.14. Summary of the high-throughput screening of the miscellaneous compounds for the HDAC8 inhibitor/activator

Entry	ID	Structure	% inhibition or K_i (μM)
1	MS-I-97		30 %
2	M1		40 %
3	M3		NI
4	RS-V-84		40 %
5	RS V 61		1.7
6	RS-V-90		30 %

(continues)

Table 5.14. Summary of the high-throughput screening of the miscellaneous compounds for the HDAC8 inhibitor/activator (continued)

Entry	ID	Structure	% inhibition or K_i (μM)
7	RS-VI-17		30 %
8	RS-VI-01		25 %
9	RS-VI-19		30 %
10	RS-VI-54		30 %
12	RS-VI-13		25 %
13	RS-VI-21		20 %
14	RS-VI-22		25 %
15	RS-VI-24		30 %

NI = No Inhibition, % = represents the % inhibition of HDAC8 enzyme activity at a concentration of 10 μM inhibitor.

5.3.2. Isozyme Selectivity of the HDAC8 Effectors

The different isozyms of HDACs have been reported to be intimately linked with several human diseases. For example, class I HDACs (HDAC1, 2 and 3) are involved in variety of cancer [95-98]. In the gastric cancer, expression level of HDAC2 is high [97]. HDAC8 has been linked to the acute myeloid leukemia (AML), where an isozyme selective

inhibitor has a potential to be used for the treatment of the disease condition [104]. Additionally, HDAC8 selective activator could be used for the treatment of COPD [113] and Cornelia de Lange syndrome [36], by enhancing the enzyme activity. Because of the high therapeutic potential of isozyme selective HDAC8 activator/inhibitor, there has been a growing interest among researchers for designing a novel isozyme selective inhibitor/activator of HDACs. However, the task has been challenging due to the lack of the crystallographic studies for several isozymes except HDAC2, 4, 7, and 8. The problem is further exacerbated due to the high degree of sequence homology among different isozymes. Despite the above limitations, several isozyme selective inhibitors have been discovered [161].

In pursuit of discovering novel isozyme selective inhibitor/activator of HDAC8, it was imperative to check the isozyme selectivity the compounds identified as the novel class of the HDAC8 inhibitor (thiopyridine derivative containing sulfhydryl group) and activator (N-acetylthioureas). The most potent effectors among the class were chosen to evaluate their effectiveness on the different isozymes of human HDACs. The thiopyridine derivatives, namely VYU-2-24, VYU-2-221, VYU-2-270, VYU-3-54, and VYU-3-56, were tested for their effectiveness at 10 μ M on the initial velocity of the reaction catalyzed by the recombinant form of human HDAC isozymes, namely, HDAC1, HDAC2, HDAC3, HDAC6, HDAC8, and HDAC10. None of the above compounds inhibited any of the HDAC isozymes except HDAC8. As an exception VYU-3-54 did inhibit HDAC3 activity by 42 % at 10 μ M. In order to investigate the isozyme selectivity of HDAC8 activation by N-acetylthiourea derivatives, the effectiveness of the compounds were tested at 100 μ M on the recombinant form of human HDAC1, HDAC2, HDAC3, HDAC4, HDAC6, HDAC8,

HDAC10, and HDAC11 in the trypsin-coupled assay. The results are summarized in Table 5.16. Evidently, none of the HDAC isozymes except HDAC8 were activated by N-acetythiourea derivatives at 100 μ M concentration. However, one of the N-acetythiourea derivatives, TM-2-130 inhibited HDAC6 by 45 % in the above experimental condition.

Table 5.15. Activation/inhibition of HDAC isozymes at 100 μ M of compound

Entry	ID	HDAC 1	HDAC 2	HDAC 3	HDAC 4	HDAC 6	HDAC 10	HDAC 11
1	TM-2-51	8% Inh*	8% Inh	6% Inh	NA/NI	30% Inh	15% inh	14% Inh
2	TM-2-88	NA/NI [#]	6% Inh	5% Inh	NA/NI	5% Inh	10% Inh	10% Inh
3	TM-2-138	5% Inh	NA/NI	NA/NI	NA/NI	NA/NI	NA/NI	NA/NI
4	TM-2-97	5% Inh	NA/NI	NA/NI	NA/NI	NA/NI	NA/NI	NA/NI
5	TM-2-105	NA/NI	NA/NI	NA/NI	NA/NI	NA/NI	NA/NI	6% Inh
6	TM-2-90	5% Inh	NA/NI	NA/NI	NA/NI	NA/NI	NA/NI	NA/NI
7	TM-2-101	NA/NI	10% Inh	NA/NI	NA/NI	NA/NI	5% Inh	10% Inh
8	TM-2-104	NA/NI	5% Inh	NA/NI	NA/NI	NA/NI	10% Inh	10% Inh
9	TM-2-130	4% Act	6% Inh	6% Inh	NA/NI	45% Inh	5% Inh	8% Inh
10	TM-2-131	5% Inh	NA/NI	NA/NI	NA/NI	NA/NI	NA/NI	6 % Inh
11	TM-2-126	NA/NI	7% Inh	5% Inh	NA/NI	NA/NI	NA/NI	NA/NI
12	TM-2-125	NA/NI	NA/NI	NA/NI	NA/NI	10% Inh	10% Inh	10% Inh
13	TM-2-107	NA/NI	9% Inh	5% Inh	NA/NI	10% Inh	47% Inh	12% Inh
14	TM-2-139	NA/NI	NA/NI	NA/NI	NA/NI	NA/NI	5% Inh	14% Inh

Note: NA and NI, respectively, represent “no activation” and “no inhibition”.

5.3.3. Modulation of Steady State Enzyme Kinetic Parameters of HDAC8 by

Activators

A small molecule serving as an activator of the enzyme primarily enhances its catalytic efficiency, which is mediated by reducing the K_m value of the substrate and/or by enhancing the catalytic turn-over (k_{cat}) of the enzyme [162]. In order to elucidate the mechanism of the HDAC activation by N-acetylthiourea derivatives, K_m and k_{cat} value of HDAC8 with Fluro-de-LysTM substrate were determined in the presence of saturating concentration of the activator. Figure 5.24 shows the Michaelis-Menten plot for the HDAC8 catalyzed reaction in the presence of 50 μM TM-2-51. The solid line is the best fit of the experimental data with the K_m and V_{max} value as $199 \pm 24 \mu\text{M}$ and $3.72 \pm 0.13 \text{ RFU/s}$. The k_{cat} value was calculated to be 0.036 s^{-1} . The kinetic parameters of the HDAC8 catalyzed reaction were also measured in the presence of the other N-acetylthioureas and the results are listed in Table 5.16.

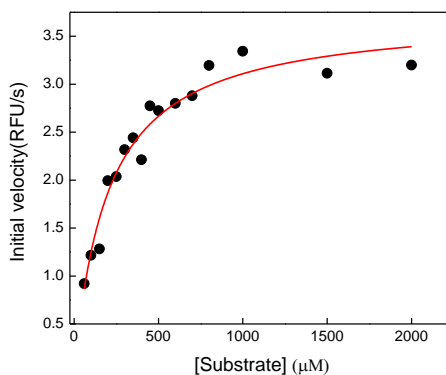


Figure 5.24. Initial velocities of the HDAC8 catalyzed reaction as a function of substrate concentration in the presence of 50 μM TM-2-51. The solid line is the best fit of the data using the Michaelis-Menten equation with K_m and V_{max} values as $199 \pm 24 \mu\text{M}$ and $3.72 \pm 0.13 \text{ RFU/sec}$. The value of k_{cat} of HDAC8 with the Fluoro-de-LysTM substrate was calculated as 0.036 s^{-1} .

Table 5.16. Steady state enzyme kinetic parameters of the HDAC8 catalyzed reaction in the absence and presence of the activator at 50 μM

Condition	$K_m(\mu\text{M})$	$k_{\text{cat}}(\text{s}^{-1})$	k_{cat}/K_m ($\text{M}^{-1}\text{s}^{-1}$)
Control (no activator)	543	0.007	12
TM-2-51	199	0.036	175
TM-2-104	250	0.032	128
TM-2-107	422	0.024	56
TM-2-131	313	0.034	108
TM-2-90	335	0.017	50
TM-2-138	210	0.028	133

The data presented in Table 5.16 show that N-acetylthiourea decreases the value of K_m and increases the k_{cat} value of HDAC8 measured with the Fluoro-de-LysTM substrate leading to enhancement in the steady state rate of the HDAC8 catalyzed reaction.

Considering the TM-2-51 as the most potent activator, it was imperative to further pursue the equilibrium binding studies with HDAC8. In that pursuit, the apparent activation constant of TM-2-51 was determined by measuring the initial velocity of the HDAC8 catalyzed reaction as a function of the activator concentration in the trypsin-coupled assay. The initial velocity of the HDAC8 catalyzed reaction was sigmoidally dependent on the activator concentration. The solid line in the Figure 5.24 shows the best fit of the experimental data for the binding of TM-2-51 to HDAC8 with the apparent activation constant and the Hill coefficient of $6.6 \pm 0.1 \mu\text{M}$ and 1.3, respectively. The value of Hill coefficient as 1.3, suggested that there were at least two binding sites of TM-2-51 within HDAC8. More importantly, the binding of the first molecule of TM-2-51 has an influence on the binding affinity of the second one, implying the positive cooperative feature [163].

A competitive inhibitor of HDAC8 such as SAHA serves as a substrate analog. However, its binding affinity is much higher as compared to the enzyme substrate. It is

tempting to presume that the binding of inhibitor (substrate analog) to HDAC8 would be affected in the presence of TM-2-5, analogous to what has been observed for the binding of Fluoro-de-LysTM substrate. In fact, the presence of the activator and the inhibitor are expected to influence the binding of each other to their respective site on the enzyme.

In order to assess the above features, the apparent activation constant and the Hill coefficient for the binding of TM-2-51 to HDAC8 were determined as a function of an increasing concentration of SAHA, and the results are listed in Table 5.17. Evidently, the value of the apparent activation constant of TM-2-51 gradually became higher with an increase in the concentration of SAHA. This could be presumably due to the fact that SAHA and TM-2-51 compete with each other for the binding to the same region of the enzyme site. Moreover, the binding affinity of SAHA is one order of magnitude higher than that of TM-2-5. Under the above situation the equilibrium dissociation constant of the TM-2-51 (measured as the apparent activation constant) is likely to increase in the presence of SAHA. The value of the Hill coefficient was reduced from 1.3 to nearly 1, implying to the fact that the presence of SAHA reduces/diminishes cooperative features associated with the binding of TM-2-51 to HDAC8.

In order to investigate the influence of TM-2-51 on the binding of a representative inhibitor to HDAC8, inhibition constant (K_i) of SAHA was determined as a function of an increasing concentration of TM-2-51, and the results are summarized in Table 5.18. Apparently, the K_i of SAHA was affected due to the presence of TM-2-51, albeit to the lesser degree. This is presumably due to the binding affinity of SAHA which is less likely to be displaced by a weaker ligand, TM-2-51.

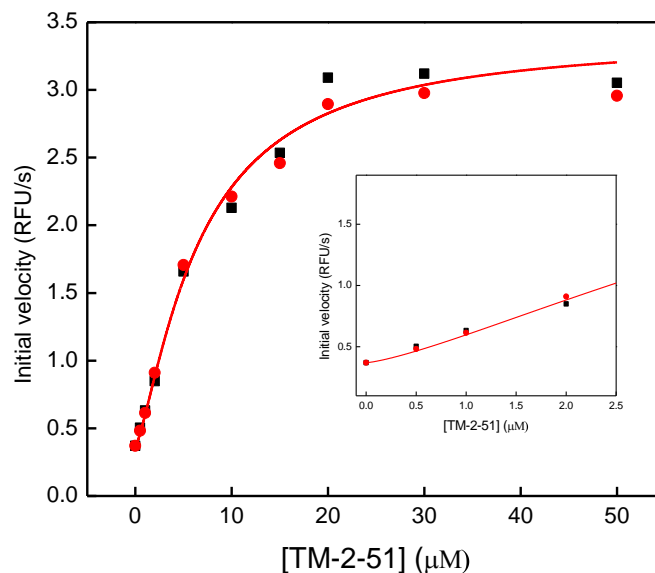


Figure 5.25. The cooperative binding of TM-2-51 to HDAC8. The initial velocities of the HDAC8 catalyzed reactions were measured as a function of TM-2-51 concentration. The experiment was performed in duplicate (red and black data points). The data were analyzed using the Hill Equation with the apparent activation constant (K_a) and the Hill coefficient as $6.6 \pm 0.1 \mu\text{M}$ and 1.3, respectively. The inset shows sigmoidal nature of the fitted curve in the lower concentration regime of the activator.

Table 5.17. The apparent activation constant and the Hill-coefficient for the binding of TM-2-51 to HDAC8 determined at various concentration of SAHA

SAHA(μM)	Apparent activation constant (K_a)(μM)	Hill coefficient
0	6.66 ± 0.84	1.32 ± 0.13
0.1	8.19 ± 1.36	0.98 ± 0.12
0.25	22.83 ± 10.30	0.80 ± 0.13
5	26.27 ± 10.15	0.97 ± 0.11
10	65.56 ± 15.54	0.92 ± 0.02

Table 5.18. The inhibition constant (K_i) of the HDAC8-SAHA complex measured at various concentrations of TM-2-51

TM-2-51(μ M)	K_i (μ M)
0	493 \pm 56
1	538 \pm 47
5	542 \pm 37
25	612 \pm 33
100	639 \pm 66

5.3.4. Coumarin-SAHA as a Probe to Determine the Binding Affinity of HDAC8

Inhibitors

A fluorescent ligand of an enzyme provides an important tool to investigate the structural-functional and mechanistic features of the ligand-protein interaction [160]. Moreover, it is used to develop a fluorescence-based competitive displacement assay to determine the binding affinity of the non-fluorescent ligands [149]. Additionally, it is a vital tool to study the transient kinetics of ligand-protein interaction as described in Section 5.4.

In pursuit of investigating the structural-functional and the mechanistic features of the protein-ligand interaction of HDAC8, a fluorescent analog of the representative HDAC8 inhibitor SAHA, coumarin-SAHA (c-SAHA), was synthesized by replacing the anilino moiety by 7-amino-4-methyl coumarin. Figure 5.26 shows the steady state fluorescence excitation and emission spectra of c-SAHA in the absence and the presence of HDAC8. As evident from the spectra, the steady state fluorescence of c-SAHA was quenched upon binding to HDAC8, which was utilized to determine the binding affinity of c-SAHA to HDAC8. Figure 5.27 shows the binding isotherm for the interaction of the HDAC8-c-SAHA obtained via the titration of a fixed concentration of c-SAHA as a function of an increasing concentration of HDAC8. The decrease in the fluorescence

intensity at 400 nm was plotted as a function of an increasing concentration of HDAC8. The solid line is the best fit of the experimental data using the quadratic Equation 4.4 (Methods section) with the K_d value of $160 \text{ nM} \pm 20 \text{ nm}$ for the HDAC8-c-SAHA complex.

In order to investigate the mechanism of the fluorescence quenching of c-SAHA upon binding to HDAC8, time-resolved fluorescence spectroscopic measurements were done. Figure 5.28 shows the fluorescence decay curves of the free and the enzyme bound form of c-SAHA, which conform to a single exponential rate equation as described in the Methods section. The data were analyzed using Equation 4.5 yielding the fluorescence life-time as 1.87 ns and 1.76 ns, respectively, for the free and the enzyme-bound form of c-SAHA. Evidently, the life-time of c-SAHA did not change upon binding to HDAC8, suggesting the static nature of the fluorescence quenching [164].

As described in the introduction section (Section 1.6), it has been widely debated that the *in vitro* HDAC8 activity assay which utilizes a fluorogenic peptide substrate produces an erroneous result. In that regard, attempts have been made to design a substrate-independent assay to investigate the direct binding of an effector to the enzyme. Coumarin-SAHA serves an ideal fluorescent inhibitor to develop a substrate-independent HDAC assay to determine the binding affinity of a non-fluorescent HDAC8 inhibitor. In order to determine the equilibrium dissociation constant (K_d) of a representative non-fluorescent inhibitors of HDAC8 namely, SAHA, TSA, M344 and SBHA, using c-SAHA as probe, the spectrofluorometric studies were performed as described in the Methods section. Figure 5.29 shows the change in the fluorescence signal of c-SAHA for the titration of the mixture, containing $0.5 \text{ } \mu\text{M}$ c-SAHA and $2 \text{ } \mu\text{M}$ competing ligand (TSA/SAHA/M344/SBHA), with increasing concentration of HDAC8. The data were analyzed using the DynaFit software

package providing the best fit of the experimental data with the K_d values of $0.34 \pm 0.12 \mu\text{M}$, $0.58 \pm 0.14 \mu\text{M}$, $0.32 \pm 0.09 \mu\text{M}$, and $0.75 \pm 0.36 \mu\text{M}$, respectively, for TSA, SAHA, M334, and SBHA. In order to ensure the validity of the experimental protocol, developed to estimate the binding affinity of the non-fluorescent ligand, the K_d values of the four test inhibitors were compared with their respective K_i values. The results are summarized in the Table 5.19. The K_d and the K_i values of the respective inhibitor were comparable which attests the authenticity of the analytical protocol.

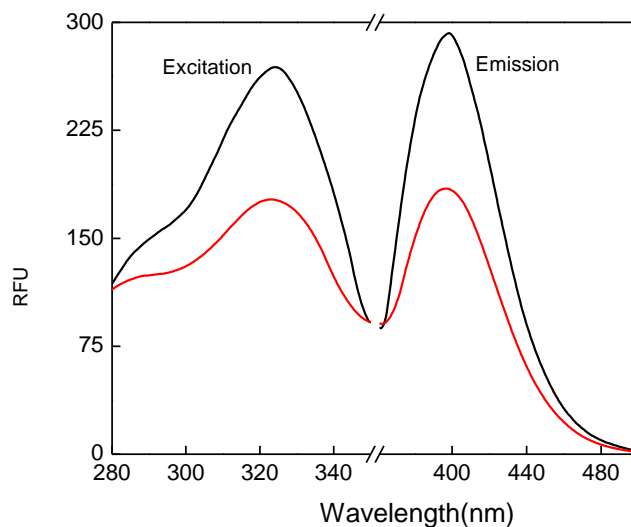


Figure 5.26. Excitation and fluorescence emission ($\lambda_{\text{ex}} = 325 \text{ nm}$) spectra of c-SAHA. The black and red lines represent the spectrum of the free and the enzyme-bound form of $0.5 \mu\text{M}$ c-SAHA, respectively.

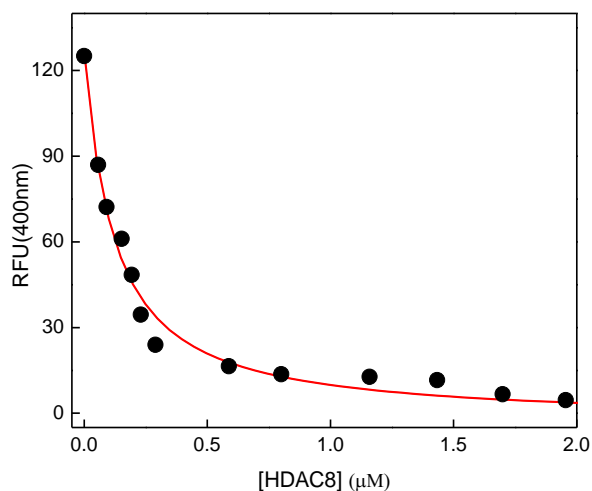


Figure 5.27. Binding isotherm for the interaction c-SAHA with HDAC8. The decrease in the steady state fluorescence intensity of 100 nM c-SAHA at 400 nm as a function of an increasing concentration of HDAC8 (total) is shown. The solid smooth line is the best fit of the experimental data using the quadratic equation for the K_d value of $0.16 \pm 0.02 \mu\text{M}$.

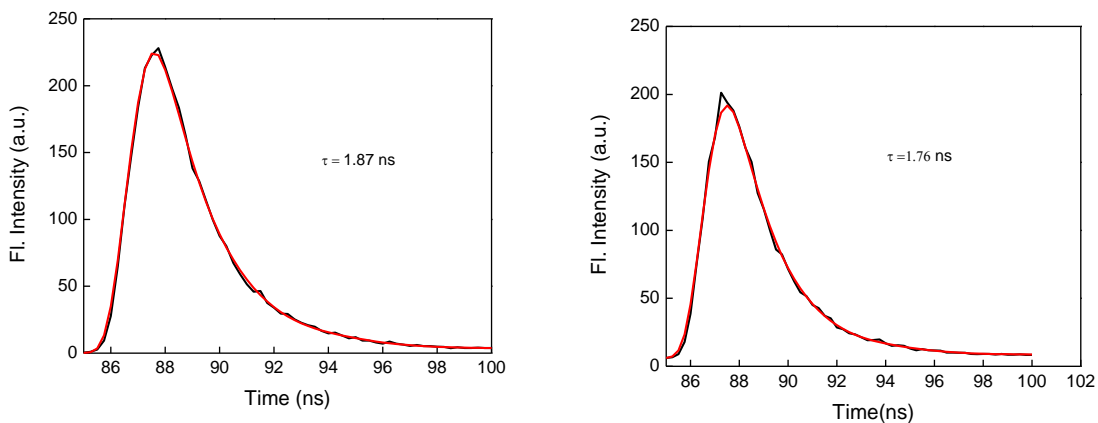


Figure 5.28. The time-resolved fluorescence decay ($\lambda_{\text{ex}} = 340 \text{ nm}$, $\lambda_{\text{em}} = 400 \text{ nm}$) curves for the free (left panel) and the enzyme-bound form (right panel) of c-SAHA. The red lines are the best fit of the experimental data according to the single exponential rate equation yielding the fluorescence life time of 1.87 and 1.76 ns, respectively, for the free and the HDAC8-bound form of c-SAHA.

Table 5.19. Comparison between K_i and K_d values of HDAC8 inhibitors

HDAC8 inhibitor	K_i (μM)	K_d (μM) determined by Fluorescence Displacement method
TSA	0.12 ± 0.02	0.34 ± 0.12
SAHA	$0.49 \pm 0.05 \mu\text{M}$	0.58 ± 0.14
M344	0.18 ± 0.02	0.32 ± 0.09
SBHA	0.71 ± 0.03	0.75 ± 0.36

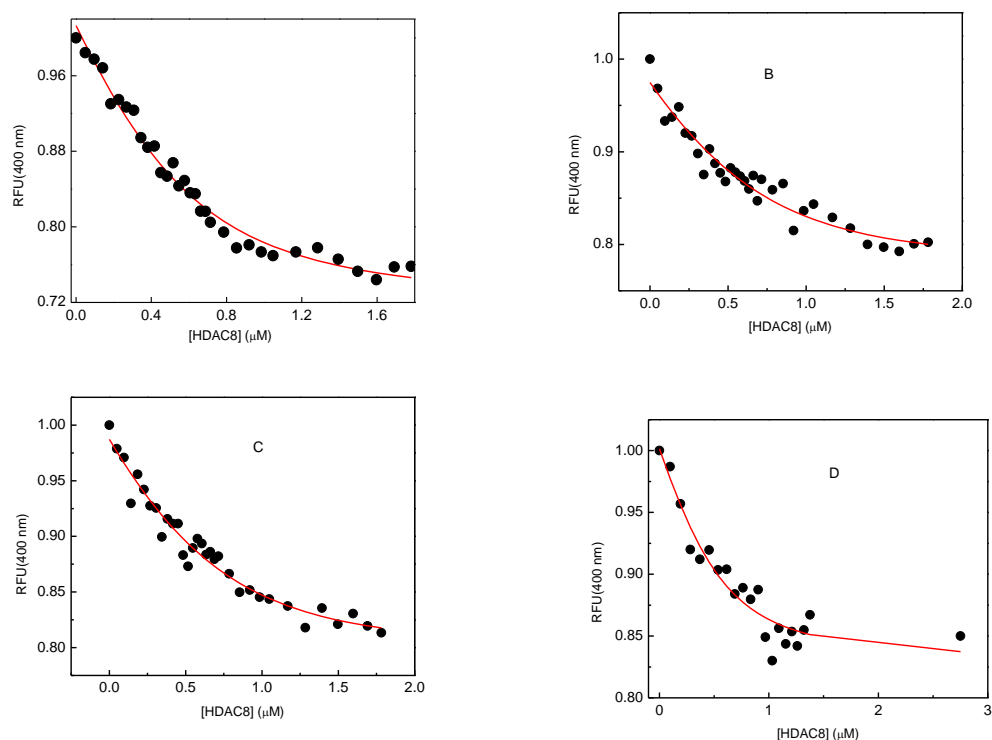


Figure 5.29. Determination of binding affinity of the representative HDAC8 inhibitors using the c-SAHA as a fluorescent probe. The change in the fluorescence intensity of c-SAHA due to the competitive binding of the non-fluorescent inhibitors, namely SAHA, TSA, M344 and SBHA to HDAC8 are shown in Panels A, B, C, and D, respectively. The decrease in the relative fluorescence intensity at 400 nm ($\lambda_{\text{ex}} = 325$ nm) of c-SAHA in the presence of the non-fluorescent inhibitor as a function of total concentration of HDAC8 is shown. The concentration of c-SAHA and the non-fluorescent inhibitor were maintained as $0.5 \mu\text{M}$ and $2 \mu\text{M}$, respectively. The data were analyzed using the DynaFit software. The solid lines are the best fit of the experimental data yielding the K_d values of $0.34 \pm 0.12 \mu\text{M}$, $0.58 \pm 0.14 \mu\text{M}$, $0.32 \pm 0.09 \mu\text{M}$, and $0.75 \pm 0.36 \mu\text{M}$, respectively, for TSA, SAHA, M33, and SBHA.

5.3.5. Binding Isotherms of HDAC-8 Effectors Interaction

The change in intrinsic fluorescence of a protein upon binding of a ligand is widely utilized to study the ligand-protein interaction [165]. As described in section 5.2.5, the intrinsic fluorescence of HDAC8 is quenched upon binding to an inhibitor, namely TSA, SAHA and VYU-2-24, which serves as the signal to monitor enzyme-inhibitor interaction. The binding isotherm of the HDAC8-inhibitor complexes were determined by monitoring the change in protein fluorescence at 340 nm ($\lambda_{ex} = 295$ nm) as a function the ligand concentration as described in the Methods section. Figure 5.30 shows the titration of a fixed concentration of HDAC8 (1.5 μ M) with an increasing concentration of the inhibitor. As the concentration of HDAC8 was comparable to that of the ligand during the course of titration, the binding isotherm was analyzed by a complete solution of the quadratic Equation 4.4 (Methods section). The solid lines are the best fit of the data yielding the equilibrium dissociation constant (K_d) of the HDAC8-TSA, HDAC8-SAHA and HDAC8-VYU-2-24 complexes being equal to 0.39 ± 0.08 μ M, 1.2 ± 0.2 μ M, and 17.09 ± 2.72 μ M for TSA, SAHA, and VYU-2-24, respectively. These values were comparable to the respective inhibition constant (K_i) values described in Section 5.3.1.

To determine the binding isotherm for the interaction of the HDAC8 activator (TM-2-51), a fixed concentration of HDAC8 was titrated with an increasing concentration of the ligand. The change in HDAC8 fluorescence signal (340 nm) was plotted as a function of the ligand concentration (Figure 5.31). The solid line is the best fit of the experimental data using the quadratic Equation 4.4, yielding the K_d value of 0.28 ± 0.04 μ M. It is important to emphasize here that the K_d value obtained here was one order of magnitude different from the apparent activation constant (6.6 μ M) determined via the steady state enzyme kinetic

assay. So, it was imperative to perform a spectrofluorometric titration of HDAC8 beyond 2 μM concentration of TM-2-5 in order to investigate the presence of the other weak binding sites. However, it was realized that the titration could not be performed because of the significant absorption of light in the UV region by TM-2-51, leading to an inner filter effect.

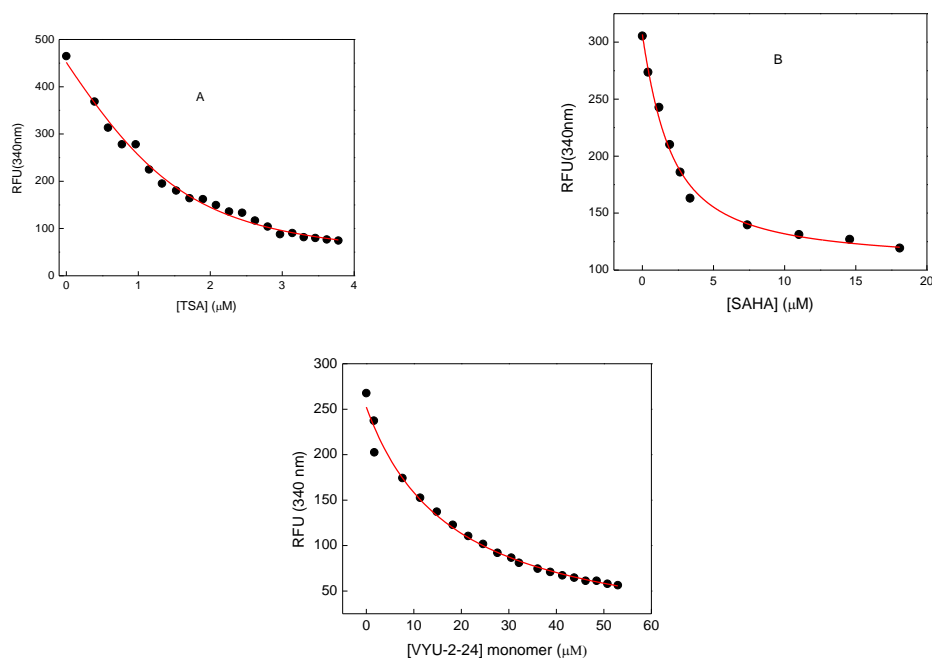


Figure 5.30. Binding isotherms for the interaction of TSA, SAHA, and VYU-2-24 with HDAC8. The panels show the decrease in tryptophan fluorescence intensity at 340 nm ($\lambda_{\text{ex}} = 295 \text{ nm}$) for the titration of 1.5 μM HDAC8 with an increasing concentration of the respective ligand. The solid lines are the best fit of the experimental data for the K_d values of $0.39 \pm 0.08 \mu\text{M}$, $1.2 \pm 0.2 \mu\text{M}$, and $17.09 \pm 2.72 \mu\text{M}$, respectively, for TSA, SAHA, and VYU-2-24.

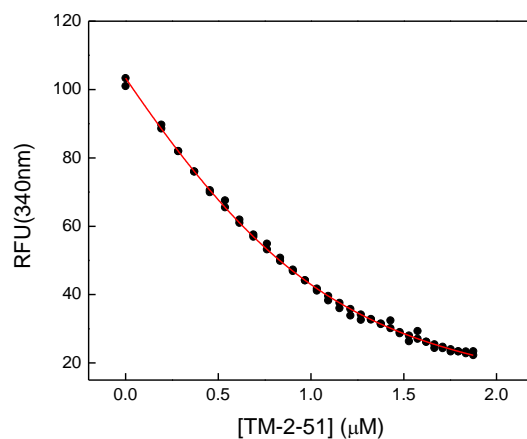


Figure 5.31. Binding isotherm for the interaction of TM-2-51 with HDAC8. The figure shows the decrease in tryptophan fluorescence intensity at 340 nm ($\lambda_{ex} = 295$ nm) for the titration of 1 μ M HDAC8 with an increasing concentration of TM-2-51. The solid line is the best fit of the experimental data yielding the K_d values of 0.28 ± 0.04 μ M.

5.4. Transient Kinetic Studies of Association and Dissociation of HDAC8 Inhibitors

The downstream cellular response of a ligand-protein interaction *in vivo* is often dictated by its thermodynamic and kinetic features [166]. It is widely known that the *in vivo* potency of an effector (inhibitor/activator) of an enzyme is positively correlated with its binding affinity, a thermodynamic parameter of a biomolecular interaction. This is primarily because an equilibrium binding affinity is proportional to the bound form of ligand to receptor/enzyme at equilibrium condition, and it is the bound form of a ligand to its cognate receptor which causes a downstream physiological effect.

Aside from the thermodynamic features, the outcome of a receptor-ligand interaction *in vivo* is often controlled via the progress of the binding reaction, which is dependent on the rate constants of the binding as well as the dissociation of the ligand from the receptor's site. The association/dissociation kinetic (transient kinetics) reportedly play a pivotal role in the regulation of several physiological events in a living cell. Jefferson Foote and Cesar Milstein found that the affinity maturation of an antibody during secondary/tertiary response is kinetically controlled, and it is dependent on the k_{on} rate constant of the bimolecular interaction [167]. Mark M. Davis and other investigators observed that the responsiveness of a T-cell is dependent on the dissociation off-rate (k_{off}) of the MHC-antigen from T-cell receptor (TCR) [168-169]. Breslow and colleagues argue that the associated side-effect of an HDAC inhibitor could be linked with the duration (time) for which it is bound to the enzyme, i.e., the dissociation off-rate of the inhibitor from the enzyme's site [114].

During the course of a rational drug design, it has been widely encountered that even the structurally similar ligands with a comparable binding affinity for the receptor

show a very different k_{on} and k_{off} rates, and that often even differ by 2-3 orders of magnitude [170]. Furthermore, a small modification in the chemical structure of a ligand is rarely manifested into any alteration in its equilibrium binding affinity for the target receptor. However, the transient kinetic parameters (k_{on} and k_{off} rate) of their interaction with the receptor would be remarkably different.

Although the transient kinetic parameters of a drug-receptor interaction serve as a predictive of *in vivo* potency of the drug, no attempts have been made to study the kinetics of association/dissociation an HDAC inhibitor to the enzyme. In that regard, a study was undertaken to elucidate the transient kinetic mechanism of binding as well as dissociation of the selected inhibitors, such as TSA, SAHA and VYU-2-24.

5.4.1. Transient Kinetics of Association of TSA, SAHA and VYU-2-24

In order to investigate the kinetic mechanism of the binding of TSA, SAHA and VYU-2-24 to HDAC8, the transient kinetic experiments were performed as described in the Methods section. It is important to note that TSA and SAHA are hydroxamate-based, structurally similar ligands, as opposed to VYU-2-24 which contains a thiol moiety as a metal binding group. The primary goal of the transient kinetic experiment was to discern the similarity and/or differences in the kinetic mechanism of the binding of the above two distinct classes of HDAC8 inhibitors. Notably, TSA and SAHA show a comparable *in vitro* potency even though they remarkably differ in their *in vivo* efficacy [141]. It is likely that the *in vivo* efficacy of the above inhibitors is dictated via the kinetics of receptor-ligand interaction, rather than its thermodynamics, which could be discerned via investigating their association kinetics as follows.

The binding of TSA, SAHA as well as VYU-2-24 to HDAC8 leads to quenching of the intrinsic protein fluorescence which was utilized to pursue the transient study using stopped-flow system as described in Methods section. The panel A of the Figures 5.32, 5.33, and 5.34 shows the representative stopped flow kinetic traces for the association of TSA, SAHA, and, VYU-2-24, respectively. All the experiments were performed under a pseudo first order condition. The change in the fluorescence signal of HDAC8 due to the binding of the inhibitor was obtained upon exciting the mixture at 280 nm and using the cut-off filter of 330 nm. From the representative association kinetics profile of the above inhibitors the following facts are quite evident. (1) The quenching of the intrinsic fluorescence of HDAC8 upon the binding of the inhibitors follows a bi-exponential profile which contains two distinct phases with equal amplitudes. (2) The fast phase is attributed to the initial binding/encounter of the inhibitor to the enzyme site, whereas the slow phase is due to isomerization of the initial encounter complex

The transient change in the fluorescence signal was analyzed using the double exponential rate Equation 4.7 (Methods section). The solid smooth lines shown in figures 5.32, 5.33 and 5.34 are the best fit of the experimental data, yielding the values of the relaxation rate constants (observed rate constants) for the fast ($1/\tau_{\text{fast}}$) and the slow ($1/\tau_{\text{slow}}$) phase. The values of the relaxation rate constants are contained in the figure legend.

In order to further delineate the kinetic mechanism of the protein-ligand interaction it was imperative to investigate the dependency of the relaxation rate constant on the ligand concentration. The panel B of the figures 5.32, 5.33 and 5.34 shows the concentration dependence of both the relaxation rate constants. Evidently, the magnitude of the fast relaxation rate constant ($1/\tau_{\text{fast}}$) is linearly dependent on the ligand concentration whereas

the slower one ($1/\tau_{\text{slow}}$) essentially remains constant. In view of the above information the following model was proposed for the binding of the inhibitor (I)- TSA, SAHA, and VYU-2-24- to HDAC8 (Scheme 5.1).



$$k_{\text{obs1}} = k_{+1} [I] + k_{-1} \qquad k_{\text{obs2}} = k_{+2} + k_{-2}$$

Scheme 5.1. Two step binding mechanism of HDAC8 inhibitors

In the above scheme k_{obs1} and k_{obs2} , respectively, represent the fast and slow relaxation rate constants. The individual rate constants representative of each step are shown as k_{+1} , k_{-1} , k_{+2} , and k_{-2} . It is important to note that binding of all the three ligand (TSA, SAHA, and VYU-2-24) to HDAC8 follow a similar kinetic mechanism which contains two kinetically resolvable steps. The linear regression analysis of the data for the fast relaxation rate constant with the gradient and intercept, respectively, provides the values of k_{+1} and k_{-1} . The slow relaxation rate constant, which represents the isomerization step, is independent of the ligand concentration, and it is comprised of the sum of k_{+2} and k_{-2} . The values of these rate constants obtained for the respective ligand are contained in the figure legends. Notably, a similar two step binding mechanism has been proposed by Trentham and coworker for the binding of 2-Chloro-(ϵ - amino -Lys₇₅)-[6-[4-(N, N-diethylamino) phenyl] - 1, 3, 5-triazin-4-yl] calmodulin with the smooth muscle myosin light chain [171].

In order to validate the authenticity of the model proposed for the binding of TSA, SAHA and VYU-2-24, it was imperative to obtain the equilibrium dissociation constant

from the transient kinetic method, and to compare with the value obtained from equilibrium binding experiment. In other words, it was important to determine the equilibrium dissociation constant taking the values of all the rate constants involved in the binding mechanism, i.e., k_{+1} , k_{-1} , k_{+2} , and k_{-2} . Notably, the individual values of k_{+2} and k_{-2} could not be determined from the association kinetics experiments mentioned here. However, the value of the above two rate constants can be obtained from the dissociation off-rate measurements of the inhibitor as described in the next section.

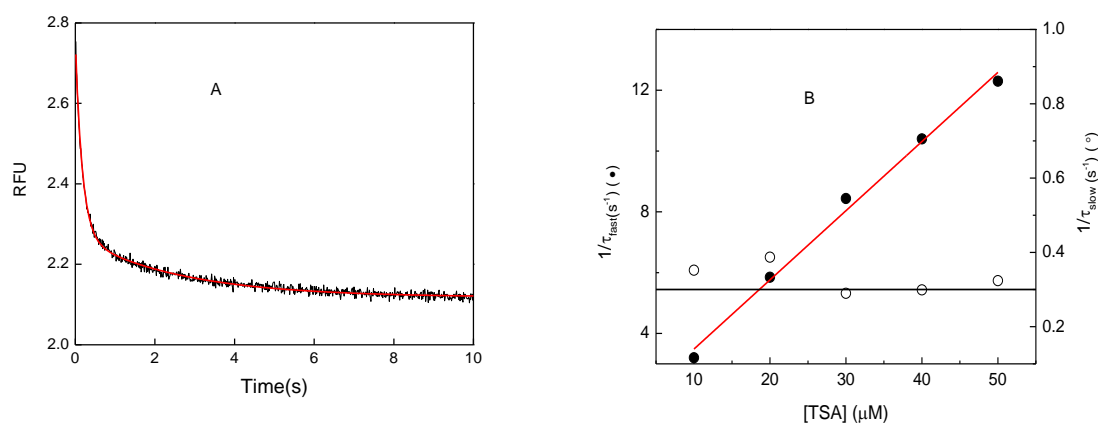


Figure 5.32. Transient kinetics of the interaction of TSA with HDAC8. Panel A shows the stopped flow kinetic trace for the decrease in tryptophan fluorescence of HDAC8 upon binding to TSA at 25 $^{\circ}\text{C}$. The mixing concentrations of the enzyme and TSA were 1 μM and 10 μM , respectively. The solid smooth line is the best fit of the data according to the double exponential rate equation with relaxation rate constants for the fast and the slow phase as $5.58 \pm 0.09 \text{ s}^{-1}$ and $0.21 \pm 0.01 \text{ s}^{-1}$, respectively. Panel B shows the concentration dependence of both the relaxation rate constants. A linear regression line to the data (●) determines the gradient (k_{+1}) and the intercept (k_{-1}), respectively, as $2.2 \times 10^5 \text{ M}^{-1} \text{ s}^{-1}$ and 1.2 s^{-1} . The horizontal line shows the best fit of the data (○) providing the magnitude of the $k_{\text{obs}2}$ ($= k_{+2} + k_{-2}$) as 0.37 s^{-1} .

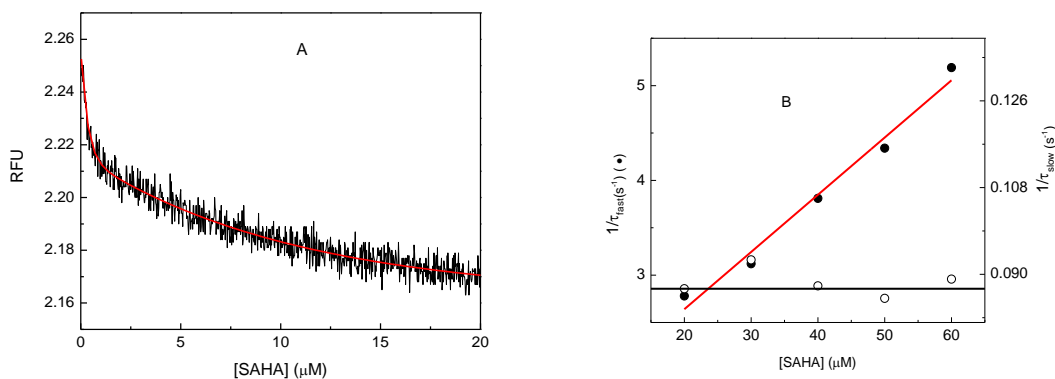


Figure 5.33. Transient kinetics of the interaction of SAHA with HDAC8. Panel A shows the stopped flow kinetic trace for the decrease in tryptophan fluorescence of HDAC8 upon binding to SAHA at 25 °C. The mixing concentrations of the enzyme and SAHA were 1 μM and 20 μM, respectively. The solid smooth line is the best fit of the data according to the double exponential rate equation with relaxation rate constant for the fast and the slow phase as $2.78 \pm 0.31 \text{ s}^{-1}$ and $0.087 \pm 0.043 \text{ s}^{-1}$, respectively. Panel B shows the concentration dependence of both the relaxation rate constants. A linear regression line to the data (●) determines the gradient (k_{+1}) and the intercept (k_{-1}), respectively, as $6 \times 10^4 \text{ M}^{-1} \text{ s}^{-1}$ and 1.4 s^{-1} . A best fit of the data (○) showing the horizontal line determines the magnitude of the k_{obs2} ($= k_{+2} + k_{-2}$) as 0.089 s^{-1} .

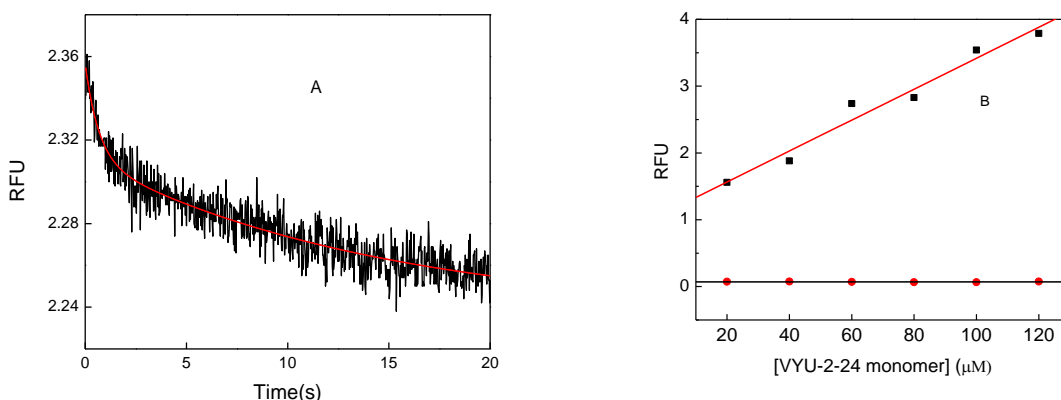
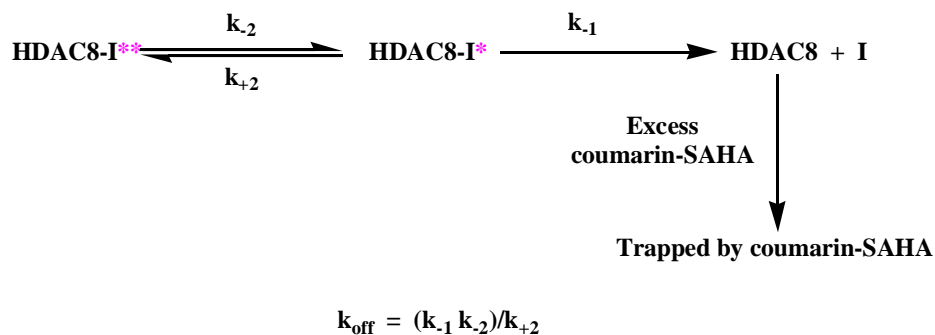


Figure 5.34. Transient kinetics of the interaction of VYU-2-24 with HDAC8. Panel A shows the stopped flow kinetic trace for the decrease in tryptophan fluorescence of HDAC8 upon binding to VYU-2-24 at 25 °C. The mixing concentrations of the enzyme and VYU-2-24 were 1 μM and 10 μM , respectively. The solid smooth line is the best fit of the data according to the double exponential rate equation with relaxation rate constant for the fast and the slow phase as $1.56 \pm 0.32 \text{ s}^{-1}$ and $0.072 \pm 0.013 \text{ s}^{-1}$, respectively. Panel B shows the concentration dependence of both the relaxation rate constants. A linear regression line to the data (black square) determines the gradient (k_{+1}) and the intercept (k_{-1}), respectively, as $2.3 \times 10^4 \text{ M}^{-1} \text{ s}^{-1}$ and 1.1 s^{-1} . A best fit of the data (0) showing the horizontal line determines the magnitude of the $k_{\text{obs}2}$ ($= k_{+2} + k_{-2}$) as 0.07 s^{-1} .

5.4.2. Dissociation Off-rate Measurements of HDAC8 Inhibitors

In view of thoroughly delineating the kinetic mechanism of the interaction of the TSA, SAHA, and VYU-2-24 to HDAC8, it was essential to determine their dissociation off-rate from the enzyme site. Moreover, the dissociation off-rate of an inhibitor could serve as predictive of its *in vivo* efficacy where the HDAC mediated cellular pathways are kinetically regulated. In that pursuit, the dissociation off rate of selected HDAC8 inhibitors, namely, TSA, SAHA, VYU-2-24, SBHA, and M344 was determined. The dissociation off-rate of the above inhibitors, which are essentially non-fluorescent in nature, was determined utilizing c-SAHA as a fluorescent probe. The c-SAHA serves as a competitive

ligand which triggers the dissociation of the non-fluorescent inhibitor when utilized in an excessively high concentration. In the light of a two-step binding model (Scheme 5.1) proposed for the binding of TSA, SAHA and VYU-2-24, their dissociation from the enzyme site triggered via an excessive concentration of c-SAHA can be represented by the following scheme:



Scheme 5.2. Dissociation kinetics of HDAC8 inhibitors from the enzyme's site

In the above scheme the dissociation off-rate (k_{off}) of a non-fluorescent HDAC8 inhibitor is comprised of three individual rate constants, namely k_{-1} , k_{-2} and k_{+2} . Figure 5.35 shows the stopped flow kinetic traces for the dissociation of bound inhibitor, namely TSA, SAHA, VYU-2-24, SBHA, and M344 from the enzyme site. The experimental conditions are contained in the figure legend. Evidently, the dissociation of all the above inhibitors showed a single exponential profile. The solid lines in figure 5.34 are the best fit of the experimental data using the single exponential rate Equation 4.6 (Methods section) with the dissociation-off rate of 0.11 s^{-1} , 0.41 s^{-1} , 0.18 s^{-1} , 1.01 s^{-1} , and 1.05 s^{-1} , respectively, for TSA, SAHA, VYU-2-24, SBHA, and M344. Evidently, the dissociation off-rate of SAHA is about 4 fold higher than TSA. The therapeutic implication of the above finding is described in discussion section.

Taking into account the value of the dissociation off-rates of TSA, SAHA and VYU-2-24, in combination with the quantitative measurement of the rate constants obtained from their association kinetics, it was possible to discern all the four rate constants, i.e., k_{+1} , k_{-1} , k_{+2} , and k_{-2} , involved in the HDAC8-inhibitor interaction (Table 5.20). The equilibrium dissociation constant for the binding of the inhibitor was determined from the above four rate constants (Table 5.20). Evidently, the equilibrium dissociation constant of the inhibitor obtained via the transient kinetic method is in close agreement with the values determined from equilibrium experiment (spectrofluorometric titration), validating the authenticity of the two-step binding mechanism proposed for interaction of TSA, SAHA, and VYU-2-24 with HDAC8.

Table 5.20. Comparison of K_d calculated from transient kinetic method with spectrofluorometric titration

Ligand	k_{+1} ($M^{-1}s^{-1}$)	k_{-1} (s^{-1})	k_{+2} (s^{-1})	k_{-2} (s^{-1})	K_d (kinetic method) μM	K_d (spectrofluorometric titration method) μM
TSA	2.3×10^5	1.2	0.34	0.03	0.49	0.39 ± 0.08
SAHA	6.0×10^4	1.4	0.069	0.02	6.8	1.2 ± 0.2
VYU-2-24	2.3×10^4	1.1	0.06	0.01	7.6	17.09 ± 2.72

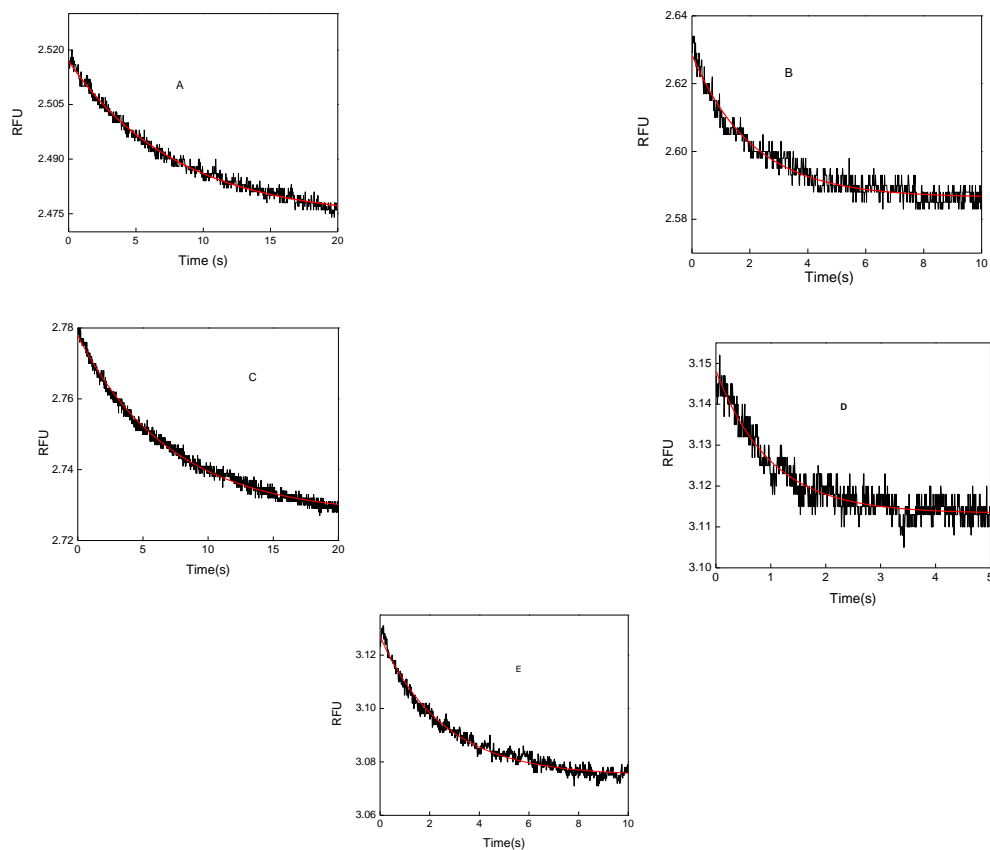
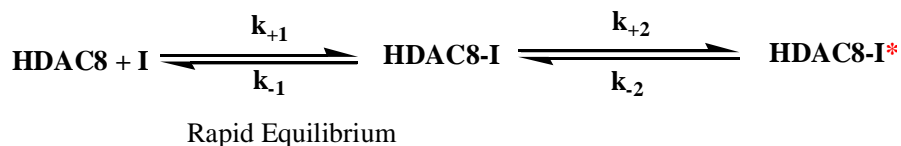


Figure 5.35. The representative stopped-flow traces for the dissociation of the enzyme-bound HDAC8 inhibitor. The respective traces for TSA, SAHA, VYU-2-24, SBHA, and M344, respectively, shown in panels A-E from the enzyme's site. The dissociation of the enzyme-bound ligand was triggered by the mixing of the HDAC8-ligand complex with the high concentration of c-SAHA. The premixing concentrations of the individual species in the stopped flow syringes were as follows $[\text{HDAC8}] = 1\ \mu\text{M} + [\text{ligand}] = 20\ \mu\text{M}$ (syringe 1) versus $[\text{c-SAHA}] = 100\ \mu\text{M}$ (syringe 2). The solid smooth lines are the best fit of the experimental data according to the single exponential rate equation, yielding the dissociation off rate constants of $0.11 \pm 0.02\ \text{s}^{-1}$, $0.41\ \text{s}^{-1} \pm 0.04\ \text{s}^{-1}$, $0.18 \pm 0.01\ \text{s}^{-1}$, $0.71 \pm 0.03\ \text{s}^{-1}$, and $0.18 \pm 0.02\ \text{s}^{-1}$, respectively, for TSA, SAHA, VYU-2-24, SBHA, and M344.

5.4.3. Association Kinetics of c-SAHA to HDAC8

Coumarin-SAHA (c-SAHA) was synthesized as a fluorescent analog of SAHA to study the binding (equilibrium as well as the transient kinetic) of non-fluorescent inhibitors of HDAC8. However, it was of a great interest to compare the transient kinetics of the interaction c-SAHA to HDAC8 to that of SAHA. Moreover, both the above inhibitors are structurally same except for their cap groups. It is important to note at this point that both c-SAHA and HDAC8 significantly absorbs the UV-visible light (280-300 nm range) because of which their binding studies could not be performed via the monitoring the intrinsic protein fluorescence.

The association kinetics of c-SAHA was studied by monitoring the time-dependent change in the fluorescence signal of c-SAHA upon binding to HDAC8 in the stopped-flow system. The reaction mixture was excited at 325 nm, and the fluorescence signal was obtained using a cut-off filter of 340 nm. Figure 5.36 (Panel A) shows the representative stopped-slow kinetic trace for the binding of c-SAHA with HDAC8. It is important to note that the observed change in the fluorescence signal of c-SAHA upon binding to HDAC8 was monophasic. The data were analyzed using the single exponential rate Equation 4.6 (Methods section) to obtain the relaxation rate constant. To further investigate the kinetic mechanism of the HDAC8-c-SAHA interaction, the value of the relaxation rate constant (observed rate constant) was determined as a function of c-SAHA concentration (Figure 5.36, Panel B). Evidently, the relaxation rate constant is hyperbolically dependent on the ligand concentration, which implies the following two-step binding mechanism for the interaction of c-SAHA to HDAC8 (Scheme 5.3).



$$k_{\text{obs}} = \frac{k_{+2} [\text{c-SAHA}]}{K_c + [\text{c-SAHA}]} + k_{-2} \quad K_c = k_{-1}/k_{+1}$$

Scheme 5.3. Two step binding mechanism for the association c-SAHA to HDAC8

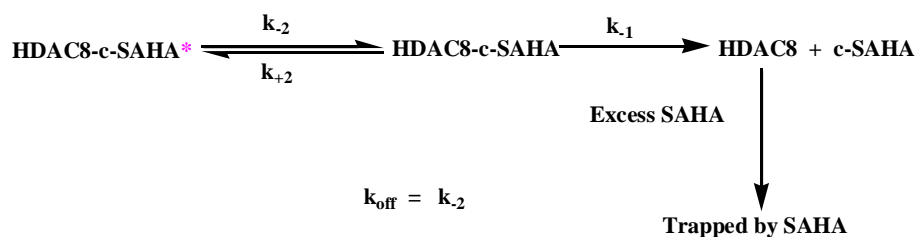
In the above model the first step represents the rapid equilibration of c-SAHA with HDAC8, forming a transient intermediate which undergoes a slow isomerization/relaxation to produce the final ligand-protein complex [172]. Furthermore, the overall reaction rate for attaining the equilibrium, which is represented by observed rate constant (k_{obs}) / relaxation rate constant ($1/\tau$), is dependent on the fraction of c-SAHA existing as transient intermediate generated upon the rapid equilibration with protein.

The experimental data obtained for relaxation rate constant dependence for binding of c-SAHA to HDAC8 was analyzed using the equation shown in Scheme 5.3. The solid line in the Figure 5.36, Panel B represents the best fit of the experimental data for the hyperbolic dependence of the relaxation rate constant (with an offset). The dissociation off-rate of c-SAHA, measured by an independent experiment (described in Section 5.4.4), was taken as an offset. The analysis of the data provided the relaxation rate constant at the saturating concentration of coumarin-SAHA ($1/\tau_{\text{max}}$), at the zero concentration of c-SAHA ($1/\tau_{\text{min}} = k_{\text{off}}$), and the concentration of c-SAHA to achieve half of the maximal saturation (K_c) as $23.7 \pm 2.7 \mu\text{M}$, $0.77 \pm 0.03 \text{ s}^{-1}$ and $6.07 \pm 3.1 \mu\text{M}$, respectively. It is important to note that the value of relaxation rate constant obtained at saturating concentration of c-SAHA represents the sum of k_{+2} and k_{-2} . Taking into account the values of K_c , k_{+2} and k_{-2} , the

equilibrium dissociation constant (K_d) was determined for the binding of c-SAHA to HDAC8 as $0.20\mu\text{M}$. The above K_d value obtained via the transient kinetic method was in a very close agreement with the one determined by equilibrium method (Section 5.3.4), validating the authenticity of the two-step binding model proposed for the interaction of c-SAHA to HDAC8.

5.4.4. Dissociation Off-rate of c-SAHA

The dissociation-off rate of c-SAHA was determined by monitoring the time dependent increase in the c-SAHA fluorescence due to its displacement from the HDAC-c-SAHA complex, triggered by SAHA (a non-fluorescent inhibitor) in the stopped flow experiment as described in the following scheme.



Scheme 5.4. Dissociation kinetics of c-SAHA from the enzyme's site

Figure 5.37 shows the representative stopped flow kinetic trace for the dissociation of c-SAHA. The experimental conditions of the measurement are contained in the figure legend. Evidently, the dissociation of c-SAHA followed a single exponential profile. The data were analyzed using the single exponential rate Equation 4.6 with the dissociation off-rate of c-SAHA as $0.77\pm 0.03\text{ s}^{-1}$. A comparison of the dissociation off-rate constants of SAHA (0.41 s^{-1}) and c-SAHA (0.77 s^{-1}) clearly shows that the latter ligand (c-SAHA) dissociates faster from the enzyme's site even though its equilibrium binding affinity is nearly one order of magnitude higher than that of the former (SAHA).

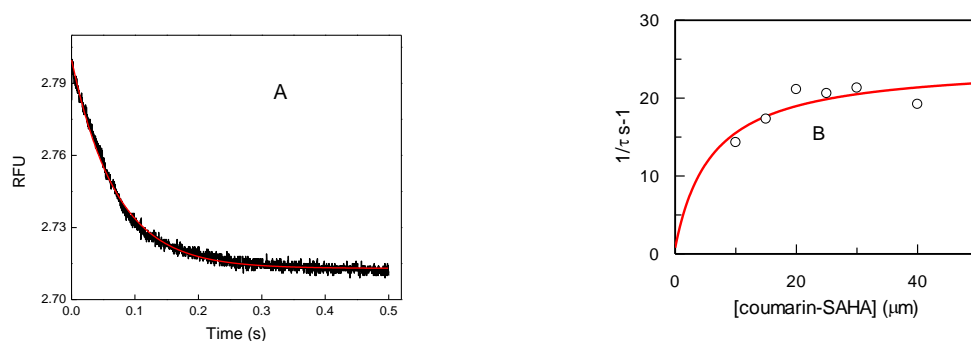


Figure 5.36. Transient kinetics of the interaction of c-SAHA with HDAC8. Panel A shows the stopped flow kinetic trace for the decrease in coumarin-SAHA fluorescence upon binding to HDAC8 at 25 °C. The mixing concentrations of the enzyme and coumarin-SAHA were 1 μM and 10 μM , respectively. The solid smooth line is the best fit of the data according to the single exponential rate equation with relaxation rate constant as $14.30 \pm 0.05 \text{ s}^{-1}$. Panel B shows coumarin-SAHA concentration dependence of the relaxation rate constants. The data at zero concentration of coumarin-SAHA was taken from dissociation off rate measurement as shown in Figure 35. The data were analyzed using the hyperbolic equation. The best fit of the experimental data yielded the following values of the relaxation rate constants: at the saturating concentration of coumarin-SAHA ($1/\tau_{\text{max}}$), at the zero concentration of coumarin-SAHA ($1/\tau_{\text{min}} = k_{\text{off}}$), and the concentration of coumarin-SAHA to achieve half of the maximal saturation (K_c) as $23.7 \pm 2.7 \text{ } \mu\text{M}$, $0.77 \pm 0.03 \text{ s}^{-1}$, and $6.07 \pm 3.1 \text{ } \mu\text{M}$, respectively.

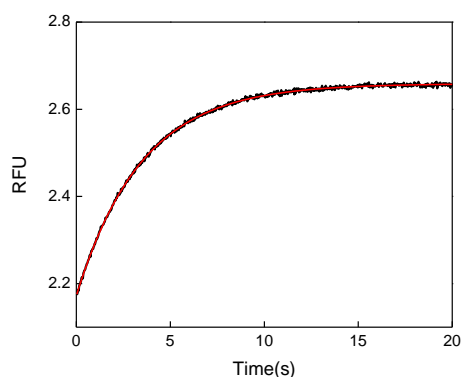


Figure 5.37. The representative stopped-flow trace for the dissociation of the bound coumarin-SAHA from HDAC8. The dissociation of the enzyme bound ligand was triggered by the mixing the HDAC8-c-SAHA complex with the high concentration of SAHA. The premixing concentrations of the individual species in the stopped flow syringes were as follows $[\text{HDAC8}] = 1 \mu\text{M} + [\text{c-SAHA}] = 10 \mu\text{M}$ (syringe 1) versus $[\text{SAHA}] = 200 \mu\text{M}$ (syringe 2). The solid line is the best fit of the experimental data according to the single exponential rate equation for the dissociation off-rate constant of $0.77 \pm 0.03 \text{ s}^{-1}$.

5.5. Thermodynamics of the Inhibitor-HDAC8 Interaction

The *in vitro* potency of a ligand/drug is positively correlated with its binding affinity (K_a) with the receptor. However, the efficacy of a drug cannot be predicted based on the binding affinity [166]. Even structurally similar ligands with a same/similar binding affinity have been shown to have a different mode of binding, which is likely to influence their *in vivo* efficacy [173]. The difference in the binding mode is primarily due to the differences in enthalpy (ΔH) and entropy (ΔS) changes associated with binding, even in the case where the change in free energy of binding (ΔG) remains the same. Furthermore, a change in the heat capacity (ΔC_p) associated with the ligand-protein interaction is widely utilized as predictive of the nature of forces involved in the macromolecular interaction—polar vs. hydrophobic forces [174].

Isothermal titration calorimetry (ITC) is a very convenient, reliable, and widely utilized method to determine the thermodynamic parameters, namely, ΔG , ΔH , ΔS , and ΔC_p for the binding of a ligand to receptor [175]. It is important to note that the above thermodynamic parameters can also be obtained from spectroscopic techniques, which primarily suffer from following limitations. A spectroscopic signal is often dependent on the attachment of an external reporter group (fluorophore) which has a propensity to perturb the native conformation of the macromolecule. Furthermore, in a spectroscopic method, ΔH and ΔS are derived from the temperature dependence of the equilibrium association constant (K_a). The equilibrium binding affinity (K_a) is a function of ΔG , and it essentially remains the same at different temperature due to an inherent enthalpy-entropy compensation associated with a biomolecular interaction [184]. Hence, it is very difficult to

reliably measure ΔH (Van't Hoff's enthalpy) and ΔS by performing an equilibrium binding study as a function of temperature.

Isothermal titration calorimetry has been widely utilized in lead optimization and decision making process [176]. Erensto Freire and colleagues have reviewed the enthalpic optimization of inhibitors for HMG-coA reductase and HIV proteases in order to improve their *in vivo* efficacy [173]. It has been argued that enthalpic optimization of drug serves as a useful tool to enhance the efficacy of a drug. However, it is difficult to perform an enthalpic optimization of a drug candidate primarily because of the enthalpy-entropy compensation involved in a macromolecular interaction [184]. On the other hand, an entropic optimization of a lead compound is relatively easy to accomplish, but it often produces a drug which shows a poor aqueous solubility and/or binds to a non-specific target. Connelly *et al.* performed a thermodynamic study for the binding of FK506 and rapamycin to the target (FK506), which provides valuable information for the rational drug design [178]. John Ladbury has extensively reviewed the utility of ITC studies in the structure-based drug design [179]. Furthermore, thermodynamic parameters derived from ITC studies could also be utilized as a predictive of the downstream cellular response of a macromolecular interaction. For instance, Mark M. Devis and co-workers reported that the T-cell activation is dependent on the flexibility of interaction between T-cell receptor (TCR) and MHC-antigen, which could be represented by ΔC_p of the macro-molecular interaction [180].

In view of the significance of an ITC study in lead optimization as well structure-based drug designing, a research project was undertaken to decipher the thermodynamics of the binding of the selected HDAC8 inhibitors, namely, TSA, SAHA and VYU-2-24 to the

enzyme. The first two inhibitors are structurally similar, and they belong to the same class (hydroxamate) as opposed to VYU-2-24. As described in the discussion section, the calorimetric studies performed with the above inhibitors provided valuable information which could be utilized to optimize an HDAC8 inhibitor in order to enhance its *in vivo* efficacy.

5.5.1. Isothermal Titration Calorimetric (ITC) Studies for the Binding of HDAC8 Inhibitors

ITC experiments were performed to investigate the thermodynamics of the binding of the HDAC8 inhibitors, namely, TSA, SAHA, and VYU-2-24 as described in the Methods section. The c value is considered an important parameter in designing an ITC which is defined as the product of the enzyme-ligand association constant (K_a) and the total concentration of the enzyme ($[E]_t$) i.e., $c = K_a \cdot ([E]_t)$. In order to satisfy the c value in the range of 10-100 to obtain a reliable binding isotherm, it was essential to use at least 10 μM HDAC8 in the ITC experiments, taking into account the K_d values of the ligand determined via the spectrofluorometric studies as 0.5-4 μM (Table 5.20).

Figures 5.38, 5.39 and 5.40 show the titration of 10 μM HDAC8 with 45 injections (4 μl each) of 200 μM of TSA, SAHA and VYU-2-24 (dimer) respectively, in 50 mM Tris buffer pH 7.5 containing 100 mM NaCl, 3 mM MgCl_2 , 10 % glycerol and 1 mM TCEP at 25 $^\circ\text{C}$. The top panel of the above figures shows the raw calorimetric data, representing the amount of heat produced (negative exothermic peaks) following each injection of the inhibitor. The area under each peak represents the amount of heat produced upon the binding of the inhibitor to HDAC8. Evidently, as the titration progresses, the area under the peak progressively becomes smaller due to an increased occupancy of the enzyme by the

inhibitor. The bottom panel of the figures shows the plot of the amount of heat generated per injection as a function of the molar ratio of the ligand. The smooth line in Figure 5.38 represents the best fit of the experimental data according to the equations described by Wiseman *et al.* [150], which yield the stoichiometry (n) of the HDAC8-TSA complex (moles of bound TSA) per mole of HDAC8) of 0.82 ± 0.12 , the association constant (K_a) of $1.67 \times 10^6 \pm 2.5 \times 10^5 \text{ M}^{-1}$, and the standard enthalpy change (ΔH^0) of $-8.9 \pm 0.28 \text{ kcal/mol}$. The best fit of the experimental data for the binding of SAHA to HDAC8 (Figure 5.39) provided the values as follows : stoichiometry (n) of the HDAC8-SAHA complex (moles of bound SAHA) per mole of HDAC8) of 0.71 ± 0.13 , the association constant (K_a) of $8.1 \times 10^5 \pm 3.3 \times 10^5 \text{ M}^{-1}$, and the standard enthalpy change (ΔH^0) of $-10.95 \pm 0.15 \text{ kcal/mol}$. ITC data analysis of the binding of the VYU-2-24 to HDAC8 (Figure 5.39) provided the stoichiometry (n) of the HDAC8-VYU-2-24 complex (moles of bound VYU-2-24) per mole of HDAC8) of 0.86 ± 0.13 , the association constant (K_a) of $1.35 \times 10^6 \pm 8.4 \times 10^4 \text{ M}^{-1}$, and the standard enthalpy change (ΔH^0) of $-3.93 \pm 0.07 \text{ kcal/mol}$. The summary of the thermodynamic parameters for the binding of three inhibitors is shown in Table 5.21.

The casual perusal of data presented in Table 5.21 highlights the following significant points about the thermodynamics for interaction of an HDAC8 inhibitor to enzyme at 25°C . (1) A single molecule of inhibitor binds to each HDAC8 enzyme site i.e., the stoichiometry of binding is one. (2) The binding affinity of TSA is higher than that of SAHA and VYU-2-24, which is similar to what was observed as *in vitro* inhibitory potency described in Section 5.3. (3) The binding of all three ligands is enthalpically driven, and the entropic penalty is the minimum for the binding of TSA. (4) Assuming the standard state,

the free energy change (ΔG^0) for the binding of TSA, SAHA, and VYU-2-24 are ($\Delta G^0 = -RT \ln K_a$) -8.6, -8.4, and -8.5 kcal/mole, respectively.

Table 5.21. Summary of the thermodynamic parameters for the binding of TSA, SAHA, and VYU-2-24 at 25 °C

Inhibitor	ΔG^0 (kcal/mol)	ΔH^0 (kcal/mol)	$T\Delta S^0$ (kcal/mol)	$K_a(M^{-1})$	Stoichiometry
SAHA	-8.4	-10.9	-2.5	8.1×10^5	0.71
TSA	-8.6	-8.9	-0.3	1.67×10^6	0.82
VYU-2-24	-8.4	-3.9	+4.4	1.56×10^6	0.86

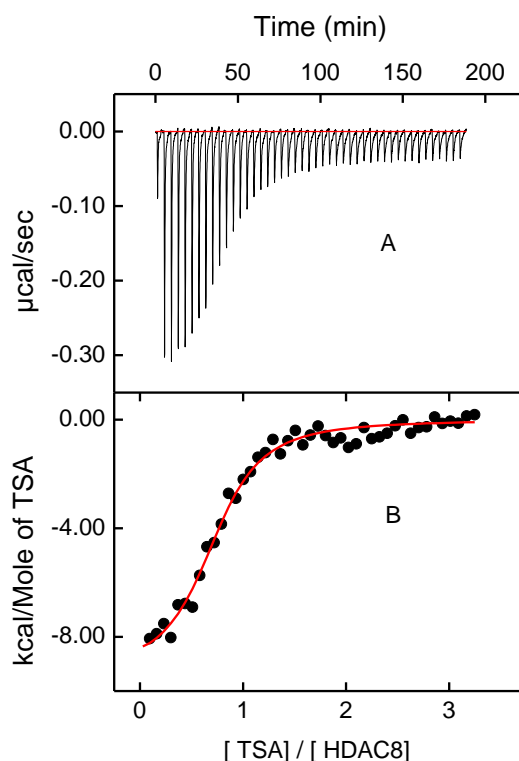


Figure 5.38. Representative ITC profile for the binding of TSA to HDAC8. The titration of HDAC8 by TSA was performed in 50 mM Tris, pH 7.5 containing 100 mM NaCl, 3 mM $MgCl_2$, 10 % glycerol and 1 mM TCEP at 25 °C. Panel A shows the raw data generated by the titration of 1.45 ml of 10 μM HDAC8 by forty-five injections (4 μl each) of 200 μM TSA. The area under each peak was integrated and plotted against the molar ratio of TSA to HDAC8 in Panel B. The solid smooth line represents the best fit of the experimental data for the stoichiometry (n) of the HDAC8-TSA complex (moles of bound TSA) per mole of HDAC8) as 0.82 ± 0.12 , the association constant (K_a) of $1.67 \times 10^6 \pm 2.5 \times 10^5 M^{-1}$, and the standard enthalpy change (ΔH^0) of -8.9 ± 0.28 kcal/mol.

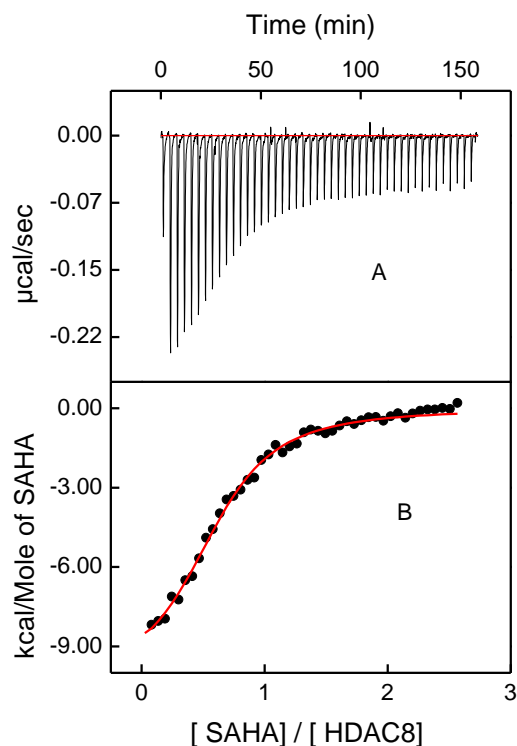


Figure 5.39. Representative ITC profile for the binding of SAHA to HDAC8. The titration of HDAC8 by SAHA was performed in 50 mM Tris pH 7.5 containing 100 mM NaCl, 3 mM MgCl_2 , 10 % glycerol and 1 mM TCEP at 25 $^{\circ}\text{C}$. Panel A shows the raw data generated by the titration of 1.45 ml of 10 μM HDAC8 by forty-five injections (4 μl each) of 200 μM SAHA. The area under each peak was integrated and plotted against the molar ratio of SAHA to HDAC8 in Panel B. The solid smooth line represents the best fit of the experimental data for the stoichiometry (n) of the HDAC8-SAHA complex (moles of bound SAHA) per mole of HDAC8) as 0.71 ± 0.13 , the association constant (K_a) of $8.1 \times 10^5 \pm 3.3 \times 10^5 \text{ M}^{-1}$, and the standard enthalpy change (ΔH^0) of $-10.95 \pm 0.15 \text{ kcal/mol}$.

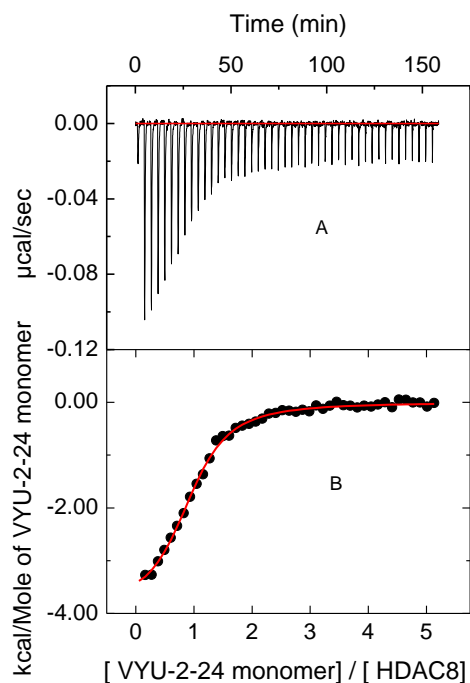


Figure 5.40. Representative ITC profile for the binding of VYU-2-24 to HDAC8. The titration of human HDAC8 by VYU-2-24 was performed in 50 mM Tris, pH 7.5 containing 100 mM NaCl, 3 mM MgCl₂, 10 % glycerol and 1 mM TCEP at 25 °C. Panel A shows the raw data generated by titration of 1.45 ml of 10 µM HDAC8 by forty-five injections (4 µl each) of 200 µM VYU-2-24. The area under each peak was integrated and plotted against the molar ratio of VYU-2-24 to HDAC8 in Panel B. The solid smooth line represents the best fit of the experimental data for the stoichiometry (*n*) of the HDAC8-VYU-2-24 complex (moles of bound VYU-2-24) per mole of HDAC8) as 0.86 ± 0.13 , the association constant (K_a) of $1.35 \times 10^6 \pm 8.4 \times 10^4 \text{ M}^{-1}$, and the standard enthalpy change (ΔH^0) of $-3.93 \pm 0.28 \text{ kcal/mol}$.

5.5.2. Stoichiometry of Proton Consumption or Release upon Binding of an inhibitor to HDAC8

A standard enthalpy change (ΔH^0) derived from the binding isotherm in an ITC experiments is not solely contributed by the physical forces governing the protein-ligand interactions [175]. They quite often include the contribution from the ionization enthalpy of the buffer species, which is primarily because of the protonation or deprotonation process coupled with the protein-ligand interaction. Hence, in order to determine the intrinsic

enthalpy (ΔH^0_{int}) of the HDAC8-inhibitor complex, the enthalpic contribution associated with the protonation-deprotonation processes was subtracted from the ΔH^0_{obs} . Furthermore, in order to determine the stoichiometry of the proton absorbed or released during the course of the protein-ligand interaction, ITC experiments were performed in the different buffers of the known ionization enthalpy, while maintaining the pH, ionic strength and temperature the same. The buffers used in the experiments were HEPES, Bicine, Triethanolamine, and Tris. The ionization enthalpy (ΔH^0_{ion}) of Hepes, Bicine, Triethanolamine, and Tris buffer were taken as 5.02, 6.46, 8.03, and 11.34 kcal/mol, respectively.

The data in Table 5.23, 5.24 and 5.25 summarize the thermodynamic parameters for the binding of TSA, SAHA and VYU-2-24, respectively, where the ITC experiments were performed in different buffers of the same ionic strength and pH at 25 °C. Evidently, ΔH^0 for the binding of TSA and SAHA to HDAC8 is dependent on the ionization enthalpy of the buffer, as opposed to VYU-2-24.

The difference in the protonation/deprotonation associated with the binding of the above inhibitors to HDAC8 is presumably due to difference in their zinc binding group and/or difference in conformational modulation of protein structure upon ligand binding. Furthermore, a thorough analysis of the data shown in Table 5.23 and 5.24 reveals that ΔH^0_{obs} for TSA and SAHA increases as a function of H^0_{ion} (Figures 5.40 and 5.41), suggesting that the binding of TSA and SAHA to HDAC8 releases protons to the buffer media. In order to estimate the number of proton released per mole of the HDAC8-inhibitor at pH 7.5, the data of figures 5.41, 5.42 and 5.43 were analyzed according to the following linear relationship:

$$\Delta H^0_{\text{obs}} = \Delta H^0_{\text{int}} + p\Delta H^0_{\text{ion}} \quad \text{Eq. 5.1}$$

In the above equation ΔH^0_{int} represents the intrinsic enthalpy of ligand binding, and p is the number of proton released to the buffer media to stabilize the ligand-protein complex at pH 7.5. The linear regression of the experimental data of Figure 5.41 yields the values for ΔH^0_{int} and p as -0.89 kcal/mol and -0.74 proton released / (mole of HDAC8-TSA) complex, respectively. The best fit of the experimental data of Figure 5.42, respectively, yields the values for ΔH^0_{int} and p as -2.3 kcal/mol and -0.75 proton released / (mole of HDAC8-SAHA) complex. The linear regression analysis of the experimental data for VYU-2-24 yields the value for ΔH^0_{int} and p of -8.57 kcal/mol and +0.05 proton absorbed / (mole of HDAC8-VYU-2-24) complex, respectively (Figure 5.43).

It is important to note that the intrinsic enthalpy (ΔH^0_{ion}) of VYU-2-24 is 2-3fold higher than TSA/ SAHA, suggesting that a highly specific binding of VYU-2-24 to HDAC8. Furthermore, the binding of both TSA as well SAHA releases the same number of protons to the buffer media and their intrinsic enthalpy binding differ by 2.5 fold. A higher binding enthalpy of SAHA as compared to TSA clearly suggests that the former ligand binds more specifically to HDAC8. A therapeutic implication of the above results is described in in Discussions section.

Table 5.22. Intrinsic enthalpy for the binding of inhibitors to HDAC8

Inhibitor	Intrinsic Enthalpy (kcal/mol)	No. of proton exchanged
SAHA	-2.54	-0.70
TSA	-1.02	-0.77
VYU-2-24	-3.92	+0.05

Table 5.23. Effect of buffers on the binding of TSA to HDAC8 at 25 °C

Buffer	<i>n</i>	$K_a \times 10^5 (M^{-1})$	ΔH^0_{obs} (kcal/mol)
Hepes	0.76±0.02	93±2	-3.8±0.12
Bicine	0.83±0.03	76±0.1.7	-6.34±0.32
Triethanolamine	0.75±0.09	10±1.4	-7.68±0.28
Tris	0.82±0.12	16.7±2.5	-8.9±0.28

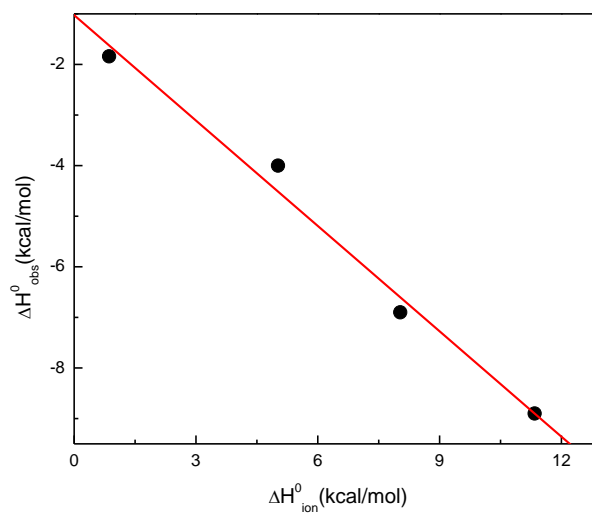


Figure 5.41. Dependence of the ΔH^0_{obs} for the binding of TSA to HDAC8 on the ΔH^0_{ion} of different buffers. The ionization enthalpy (ΔH^0_{ion}) of Hepes, Bicine, Triethanolamine and Tris buffers was taken as 5.02, 6.46, 8.03 and 11.34 kcal/mol, respectively. The solid line is the linear regression analysis of the data yielding the slope (*p*, number of proton released per mole of HDAC8) and intercept (intrinsic enthalpy for binding of TSA to HDAC8, ΔH^0_{int}) of -0.77 and -1.02 kcal/mol, respectively.

Table 5.24. Effect of buffers on the binding of SAHA to HDAC8 25 °C

Buffer	<i>n</i>	$K_a \times 10^5 (M^{-1})$	ΔH^0_{obs} (kcal/mol)
Hepes	0.81±0.02	43.3±5.5	-6.25±0.13
Bicine	0.75±0.03	31.7±4.3	-7.10±0.24
Triethanolamine	0.75±0.01	28.2±2.77	-8.33±0.35
Tris	0.71±0.13	8.1±3.3	-10.95±0.15

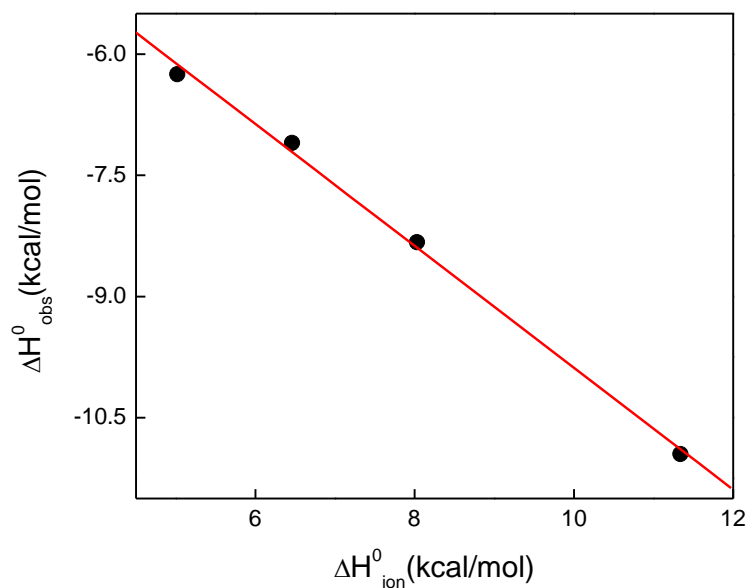


Figure 5.42. Dependence of the ΔH^0_{obs} for the binding of SAHA to HDAC8 is dependent on the ΔH^0_{ion} of different buffers. The ionization enthalpy (ΔH^0_{ion}) of Hepes, Bicine, Triethanolamine and Tris buffers was taken as 5.02, 6.46, 8.03 and 11.34 kcal/mol, respectively. The solid line represents the linear regression analysis of the data yielding the slope (*p*, number of proton released per mole of HDAC8) and the intercept (intrinsic enthalpy for binding of SAHA to HDAC8, ΔH^0_{int}) of -0.7 and -2.54 kcal/mol, respectively.

Table 5.25. Effect of buffers on the binding of VYU-2-24 to HDAC8 25 °C

Buffer	<i>n</i>	$K_a \times 10^5 (M^{-1})$	ΔH^0_{obs} (kcal/mol)
Hepes	0.76±0.02	40±3.6	-3.98±0.29
Bicine	0.9±0.01	23.4±1.93	-3.89±0.25
Triethanolamine	0.85±0.01	35.2±1.3	-3.58±0.13
Tris	0.71±0.13	8.1±3.3	-3.93±0.07

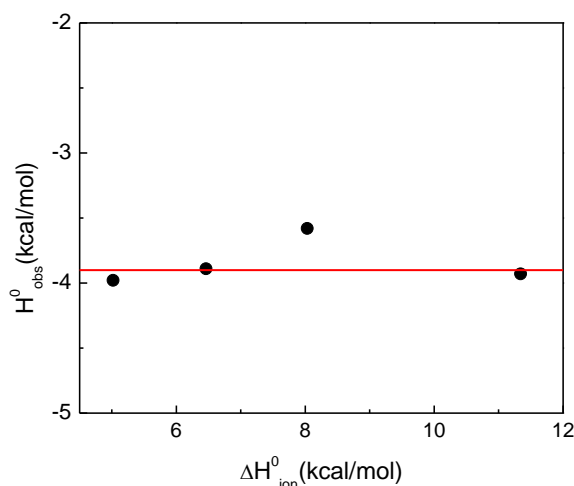


Figure 5.43. Dependence of the ΔH^0_{obs} for the binding of VYU-2-24 to HDAC8 is dependent on the ΔH^0_{ion} of different buffers. The ionization enthalpy (ΔH^0_{ion}) of Hepes, Bicine, Triethanolamine and Tris buffers was taken as 5.02, 6.46, 8.03 and 11.34 kcal/mol respectively. The solid line represents the linear regression analysis of the data yielding the slope (*p*, number of proton absorbed per mole of HDAC8) and intercept (intrinsic enthalpy for binding of SAHA to HDAC8, ΔH^0_{int}) of +0.05 and -3.93 kcal/mol, respectively.

5.5.3. Temperature Dependence of the ITC studies

The thermodynamic parameters derived from ITC studies for a macromolecular interaction are often correlated with structural data. For instance, the change in heat capacity (ΔC_p) associated with binding is correlated with the burial of the polar and non-polar surface upon the formation of ligand-protein complex [181, 182]. The positive and negative ΔC_p values are often correlated, respectively, with the polar and hydrophobic interactions. The ΔC_p , which originates from the burial of a hydrophobic surface of protein,

is often estimated based on the change in heat capacity of an organic molecule when it is transferred to aqueous solution [183]. The change in heat capacity (ΔC_p) is the temperature derivative of enthalpy (ΔH) measured at constant pressure. In order to determine the ΔC_p for the binding of a ligand to protein, the enthalpy of binding (ΔH) is determined at different temperature. The ΔH is plotted as a function of temperature and the slope of the plot provides the value of ΔC_p .

In order to determine the ΔC_p for the binding of HDAC8 inhibitors, namely, TSA, SAHA, and VYU-2-24 to the enzyme, their binding enthalpies were determined at different temperature. The temperature dependent ITC experiment were performed in the standard Tris buffer at pH 7.5 (50 mM Tris, pH 7.5 containing 100 mM NaCl, 3 mM MgCl₂, 10 % glycerol and 1 mM TCEP). The thermodynamic parameters derived from the temperature-dependent titration experiments are listed in Table 5.26, 5.27 and 5.28, respectively, for TSA, SAHA, and VYU-2-24. Evidently, the data in the above tables revealed that ΔG^0 remains practically invariant with the change in temperature. Both the ΔH^0 and ΔS^0 decreases with an increase in the temperature. Figures 5.44, 5.45 and 5.46 show the plots of ΔG^0 and ΔH^0 as a function of $T\Delta S^0$, respectively, for TSA, SAHA, and VYU-2-24. Note that in all three cases ΔH^0 increased linearly as a function of $T\Delta S^0$, suggesting a strong enthalpy-entropy compensation for the binding of the ligand to HDAC8.

In a simplistic term, the molecular origin of the enthalpy-entropy compensation involved a macromolecular interaction is explained as follows. With an increase in the temperature, the water molecules bound to the non-polar/hydrophobic surfaces, often called “icebergs”, become more disordered which reduces the gain from the entropy. Furthermore, it provides an opportunity to make the non-covalent interactions which

enhance the favorability of the enthalpic gain in macromolecular interaction. Thus, a loss in entropy is balanced by gain in enthalpy leading to the enthalpy-entropy compensation. Notably, enthalpy-entropy compensation is a general feature of a weak macromolecular interaction involving water [184].

The data of Tables 5.26, 5.27, and 5.28 were further analyzed by plotting ΔH^0 as a function of temperature as shown in Figures 5.47, 5.48, and 5.49. The linear dependence of ΔH^0 on temperature for TSA provided a slope of $-0.25 \pm 0.03 \text{ kcal mol}^{-1} \text{ K}^{-1}$ and an intercept (at 0 K) of $65.66 \pm 12.9 \text{ kcal/mol}$. The linear ΔH^0 on temperature for SAHA provided a slope of $-0.23 \pm 0.02 \text{ kcal mol}^{-1} \text{ K}^{-1}$ and an intercept (at 0 K) of $58.9 \pm 8 \text{ kcal/mol}$. Likewise, the linear dependence of ΔH^0 on temperature for VYU-2-24 provided the slope of $-0.19 \pm 0.05 \text{ kcal mol}^{-1} \text{ K}^{-1}$ and an intercept (at 0 K) of $51.8 \pm 17.1 \text{ kcal/mol}$. The slope of these plots served as a measure of the heat capacity changes (ΔC_p^0) associated with binding of an inhibitor to HDAC8. As elaborated in the discussion section, a strong negative value of ΔC_p^0 suggested that the binding of all the inhibitors under study was primarily contributed by the hydrophobic forces. Furthermore, ΔC_p for the binding of TSA is greater than that of SAHA, suggesting the fact that the binding of the former ligand (TSA) is entropically more favored than the latter. Notably, the active site pocket of HDAC8 contains a hydrophobic tunnel, and it is not surprising to see that binding of the canonical inhibitors (TSA and SAHA) as well as VYU-2-24 is dominated by hydrophobic forces.

Table 5.26. Temperature dependence of ITC parameters for the binding of TSA to HDAC8

Temperature(^o K)	<i>n</i>	ΔG^0 (kcal/mol)	ΔH^0 (kcal/mol)	$T\Delta S^0$ (kcal/mol)
278	0.78±0.04	-9.05	-3.8±0.17	5.2
283	0.81±0.06	-9.3	-6.57±0.28	2.82
288	0.69±0.03	-8.7	-7.46±0.21	1.23
293	0.72±0.01	-8.6	-8.69±0.16	-0.08
298	0.82±0.02	-8.6	-8.9±0.28	-0.26

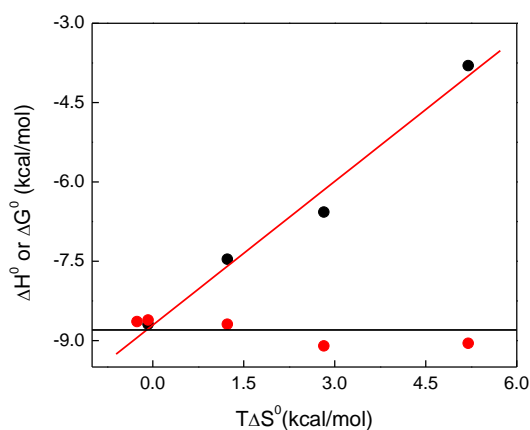


Figure 5.44. Enthalpy-entropy compensation plot for the binding of TSA to HDAC8. The experiments were performed in 50 mM Tris, pH 7.5, containing 100 mM NaCl, 3 mM MgCl₂, 10 % glycerol and 1 mM TCEP. The dependence of ΔG^0 and ΔH^0 on $T\Delta S^0$ is shown by red and black circles, respectively. The linear regression analysis for the data of ΔH^0 versus $T\Delta S^0$ yields the magnitudes of the slope and the intercept as 0.90 ± 0.08 and -8.70 ± 0.26 kcal/mol, respectively.

Table 5.27. Temperature dependence of thermodynamic parameters for the binding of SAHA to HDAC8

Temperature(^o K)	<i>n</i>	ΔG^0 (kcal/mol)	ΔH^0 (kcal/mol)	$T\Delta S^0$ (kcal/mol)
278	0.73±0.01	-8.6	-6.64±0.15	1.99
283	0.68±0.13	-8.5	-6.77±0.24	1.77
288	0.71±0.01	-8.6	-8.57±0.28	0.01
293	0.73±0.03	-8.4	-8.69±0.16	-1.46
298	0.71±0.13	-8.4	-10.95±0.15	-2.53

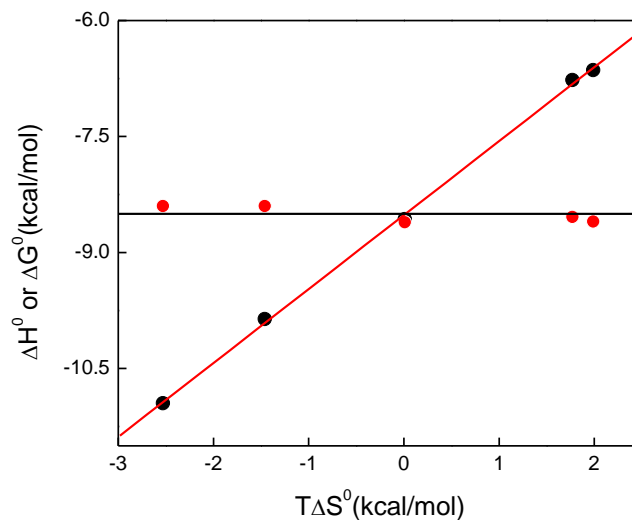


Figure 5.45. Enthalpy-entropy compensation plot for the binding of SAHA to HDAC8. The experiments were performed in 50 mM Tris pH 7.5, containing 100 mM NaCl, 3 mM MgCl₂, 10 % glycerol and 1 mM TCEP. The dependence of ΔG^0 and ΔH^0 on $T\Delta S^0$ is shown by red and black circles, respectively. The linear regression analysis for the data of ΔH^0 versus $T\Delta S^0$ yields the magnitudes of the slope and the intercept as 0.95 ± 0.01 and -8.51 ± 0.02 kcal/mol, respectively.

Table 5.28. Temperature dependence of thermodynamic parameters for the binding of VYU-2-24 to HDAC8

Temperature(⁰ K)	<i>n</i>	ΔG^0 (kcal/mol)	ΔH^0 (kcal/mol)	$T\Delta S^0$ (kcal/mol)
283	0.91±0.2	-8.32	-2.36±0.19	5.96
288	0.83±0.02	-8.49	-2.67±0.21	5.66
293	0.71±0.11	-8.7	-3.00±0.08	5.36
298	0.76±0.13	-8.54	-3.93±0.07	4.4

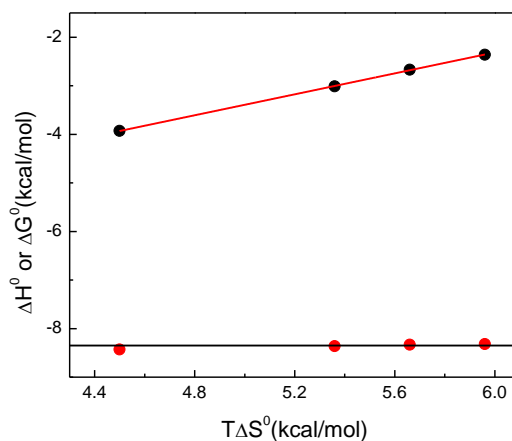


Figure 5.46. Enthalpy-entropy compensation plot for the binding of VYU-2-24 to HDAC8. The experiments were performed in 50 mM Tris, pH 7.5, containing 100 mM NaCl, 3 mM MgCl₂, 10 % glycerol and 1 mM TCEP. The dependence of ΔG^0 and ΔH^0 on $T\Delta S^0$ is shown by red and black circles, respectively. The linear regression analysis for the data of ΔH^0 versus $T\Delta S^0$ yields the magnitude of the slope and the intercept as 0.99 ± 0.01 and 8.32 ± 0.05 kcal/mol, respectively.

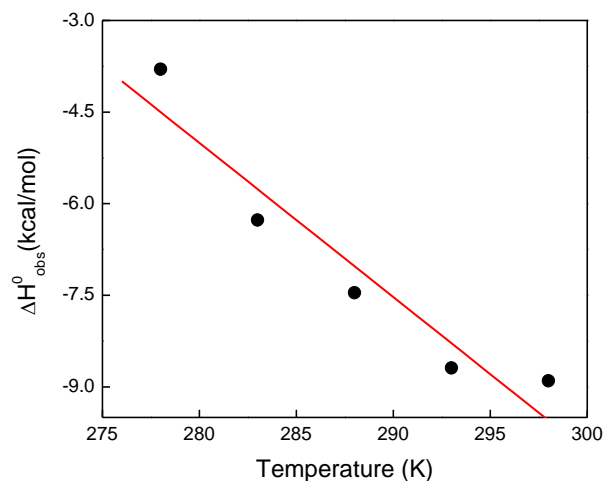


Figure 5.47. Effect of temperature on the enthalpy of binding (ΔH°) of TSA to HDAC8. The solid line is the best fit of the experimental data for a ΔC_p° (slope) of -0.21 ± 0.04 kcal mol⁻¹ K⁻¹ and an intercept (at 0 K) of 65.66 ± 12.9 kcal/mol.

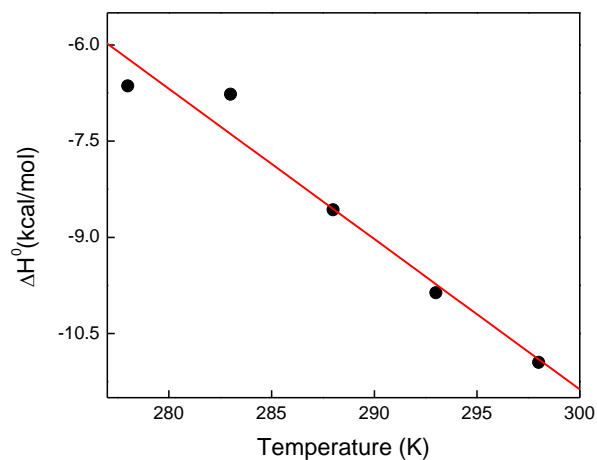


Figure 5.48. Effect of temperature on the enthalpy of binding (ΔH°) of SAHA to HDAC8. The solid red line is the best fit of the experimental data for a ΔC_p° (slope) of -0.23 ± 0.02 kcal mol⁻¹ K⁻¹ and an intercept (at 0 K) of 58.9 ± 8 kcal/mol.

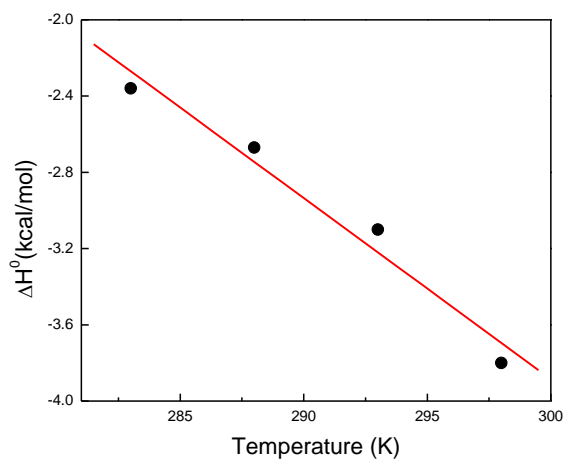


Figure 5.49. Effect of temperature on the enthalpy of binding (ΔH^0) of VYU-2-24 to HDAC8. The solid red line is the best fit of the experimental data yielding a ΔC_p^0 (slope) of $-0.09 \pm 0.01 \text{ kcal mol}^{-1} \text{ K}^{-1}$ and an intercept (at 0 K) of $24.6 \pm 3.6 \text{ kcal/mol}$.

5.5.4. Isothermal Titration Calorimetric Studies for the Binding of HDAC8 Activator

As described in Section 5.3.2, TM-2-51 serves as an isozyme- selective activator of HDAC8. The HDAC8 activation was observed in the trypsin-coupled enzyme assay which utilizes a fluorogenic substrate (Fluoro-de-LysTM). It has been widely debated that the currently known activators of Sirtuin1 (class III HDAC) bind to enzyme only in the presence a fluorogenic peptide substrate [185]. The binding in the above case is reportedly mediated via a bulky fluorogenic moiety of the substrate.

In order to confirm that the TM-2-51 truly serves as an activator of HDAC8, it was imperative to test whether it binds to the enzyme in the absence any fluorogenic substrate (Fluoro-de-LysTM). Additionally, it was of great interest to investigate a mutual influence of an HDAC8 inhibitor and an activator on the thermodynamic profile of each other. In view of investigating the above facts the following ITC experiments were performed.

Figure 5.50 (left panel) shows the titration of 10 μ M HDAC8 with 45 injections (4 μ l each) of 500 μ M of TM-2-51 in 50 mM Tris buffer pH 7.5, containing 100 mM NaCl , 3 mM MgCl₂, 10 % glycerol and 1 mM TCEP at 25 °C. The top panel of the figure shows the raw calorimetric data, denoting the amount of heat produced (negative exothermic peaks) following each injection of the activator. The area under each peak represents the amount of heat produced upon binding of an activator to HDAC8. It is important to note that as the titration progresses the area under the peak becomes smaller initially, which rises again in middle of the titration prior to attaining saturation at the end. The above feature of the ITC profile implies the presence of more than one interacting binding site of the activator within HDAC8. The bottom panel of the Figure 5.50 shows the plot of the amount of heat generated per injection as a function of the molar ratio of TM-2-51. The

data were analyzed using the sequential binding site mode, and the solid line is the best fit of the experimental data yielding the following thermodynamic parameters: $K_1 = 1.1 \times 10^6 \pm 3.0 \times 10^4 \text{ M}^{-1}$, $\Delta H^0_1 = -14.1 \pm 0.18 \text{ kcal/mol}$, $K_2 = 8.33 \times 10^4 \pm 2.3 \times 10^3 \text{ M}^{-1}$, $\Delta H^0_2 = -7.04 \pm 0.89 \text{ kcal/mol}$, $K_3 = 1.69 \times 10^5 \pm 3.8 \times 10^3 \text{ M}^{-1}$, $\Delta H^0_3 = -49.5 \pm 0.8 \text{ kcal/mol}$. Notably, TM-2-51 contains more than one binding sites on HDAC8, and the binding of the first molecule of TM-2-51 enhances the binding affinity of second ligand (positive cooperativity). The above cooperative feature in the binding was also observed in the measurement of the apparent activation constant of TM-2-51 (Section 5.3.3). Furthermore, since TM-2-51 binds to HDAC8 even in absence of any other ligand (the substrate independent binding), it appears to serve as a true activator of the enzyme.

In order to discern the effect of SAHA on the thermodynamics of the binding of TM-2-51, an ITC experiment was performed in the presence of a saturating concentration of SAHA as described in the Methods section. Figure 5.50 (right panel) shows the titration of 10 μM of the HDAC8-SAHA complex with 45 injections (4 μl) of 500 μM of TM-2-51 in 50 mM Tris buffer pH 7.5 containing 100 mM NaCl, 3 mM MgCl_2 , 10 % glycerol and 1 mM TCEP at 25 $^\circ\text{C}$. The casual perusal of the raw data implied the presence of more than one binding sites of TM-2-51 within HDAC8. The bottom panel of the Figure 5.50 (right panel) shows the plot of the amount of heat generated per injection as a function of the molar ratio of TM-2-51. The data were analyzed using the three sequential site binding model, and the solid line is the best fit of the experimental data yielding the following thermodynamic parameters: $K_1 = 9.9 \times 10^5 \pm 6.3 \times 10^4 \text{ M}^{-1}$, $\Delta H^0_1 = -6.7 \pm 0.2 \text{ kcal/mol}$, $K_2 = 1.46 \times 10^5 \pm 2.0 \times 10^4 \text{ M}^{-1}$, $\Delta H^0_2 = -3.1 \pm 0.39 \text{ kcal/mol}$, $K_3 = 3.73 \times 10^5 \pm 1.9 \times 10^4 \text{ M}^{-1}$, $\Delta H^0_3 = -9.47 \pm 0.31 \text{ kcal/mol}$. Evidently, the thermodynamic parameters of the binding of TM-2-51

were modulated by the presence of SAHA, suggesting that an enzyme-bound SAHA influences the binding of TM-2-51 to HDAC8. The above feature corroborates with fact that, the apparent activation constant and Hill coefficient for the binding of TM-2-51 to HDAC8 is affected in the presence of SAHA (Table 5.17).

To investigate whether the presence of TM-2-51 had any influence on the thermodynamics of binding of SAHA to HDAC8, an ITC experiment was performed under the following conditions. Figure 5.51 shows the titration of 10 μM of the HDAC8-TM-2-51 complex with 45 injections (4 μl each) of 200 μM of SAHA in 50 mM Tris buffer pH 7.5, containing 100 mM NaCl, 3 mM MgCl_2 , 10 % glycerol and 1 mM TCEP at 25 $^\circ\text{C}$. The data were analyzed for a single site binding model yielding the stoichiometry (n) of the HDAC8-SAHA complex (moles of bound SAHA) per mole of HDAC8) of 0.82 ± 0.02 , the association constant (K_a) of $1.37 \times 10^6 \pm 1.39 \times 10^5 \text{ M}^{-1}$, and the standard enthalpy change (ΔH^0) of $-8.08 \pm 0.27 \text{ kcal/mol}$.

Notably, the binding affinity of SAHA for HDAC8 essentially remained unaffected in the presence of TM-2-51 to the enzyme site. A similar conclusion was obtained from the measurement of the inhibition constant of SAHA in a function of increasing concentration of TM-2-51 (Table 5.18). However, the standard enthalpy of binding (ΔH) of SAHA to HDAC8 was reduced approximately by 3 kcal/mol, implying that the binding of TM-2-51 to HDAC8 modulates the microscopic environment of the active site pocket of the enzyme. Notably, the TM-2-51 mediated modulation in the geometry of HDAC8 catalytic machinery could easily enhance the catalytic efficiency of the enzyme (Table 5.16).

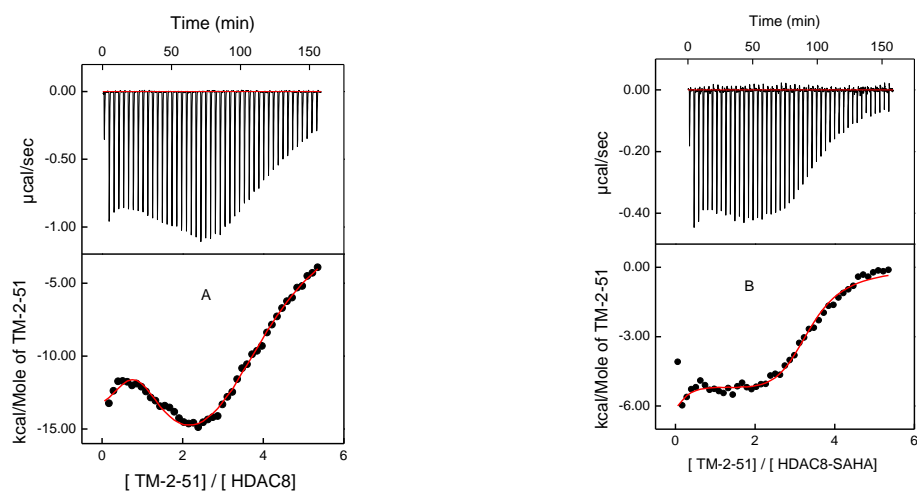


Figure 5.50. Titration of the free and SAHA-bound form of HDAC8 by TM-2-51. The experiments were performed in 50 mM Tris pH 7.5, containing 100 mM NaCl, 3 mM MgCl₂, 10 % glycerol and 1 mM TCEP at 25 °C. The top panels show the raw data generated by titration of 1.45 ml of 10 µM HDAC8 by forty-five injections (4 µl each) of the 500 µM TM-2-51. The area under each peak was integrated and plotted against the molar ratio of TM-51 to HDAC8 in bottom B. The solid line represents the best fit of the experimental data for sequential binding site model with $K_1 = 1.1 \times 10^6 \pm 3.0 \times 10^4 \text{ M}^{-1}$, $\Delta H^0_1 = -14.1 \pm 0.18 \text{ kcal/mol}$, $K_2 = 8.33 \times 10^4 \pm 2.3 \times 10^3 \text{ M}^{-1}$, $\Delta H^0_2 = -7.04 \pm 0.89 \text{ kcal/mol}$, $K_3 = 1.69 \times 10^5 \pm 3.8 \times 10^3 \text{ M}^{-1}$, $\Delta H^0_3 = -49.5 \pm 0.8 \text{ kcal/mol}$ for the SAHA-free form of HDAC8. The thermodynamic parameters for the SAHA-bound form of the enzyme were as follows: $K_1 = 9.9 \times 10^5 \pm 6.3 \times 10^4 \text{ M}^{-1}$, $\Delta H^0_1 = -6.7 \pm 0.2 \text{ kcal/mol}$, $K_2 = 1.46 \times 10^5 \pm 2.0 \times 10^4 \text{ M}^{-1}$, $\Delta H^0_2 = -3.1 \pm 0.39 \text{ kcal/mol}$, $K_3 = 3.73 \times 10^5 \pm 1.9 \times 10^4 \text{ M}^{-1}$, $\Delta H^0_3 = -9.47 \pm 0.31 \text{ kcal/mol}$.

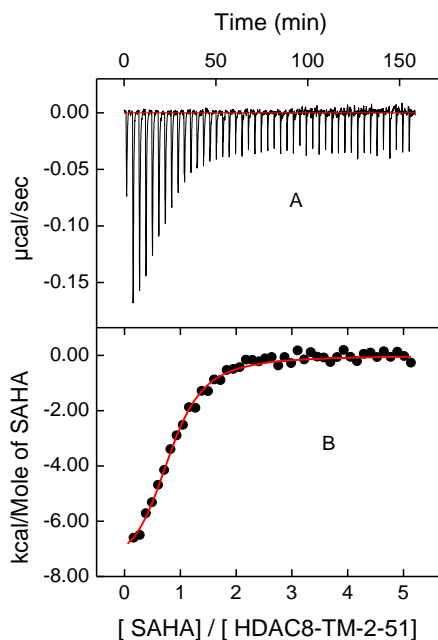


Figure 5.51. Titration of the TM-2-51-bound form of HDAC8 by SAHA. The experiment was performed in 50 mM Tris pH 7.5 containing 100 mM NaCl, 3 mM MgCl_2 , 10 % glycerol and 1 mM TCEP at 25 $^{\circ}\text{C}$. Panel A shows the raw data generated by titration of 1.45 ml of 10 μM of the HDAC8-TM-2-51 by forty-five injections (4 μl each) of 200 μM SAHA. The area under each peak was integrated and plotted against the molar ratio of SAHA to HDAC8 in Panel B. The solid smooth line represents the best fit of the experimental data for the stoichiometry (n) of the HDAC8-SAHA complex (moles of bound SAHA) per mole of HDAC8) of 0.82 ± 0.02 , the association constant (K_a) of $1.37 \times 10^6 \pm 1.39 \times 10^5 \text{ M}^{-1}$, and the standard enthalpy change (ΔH^0) of $-8.08 \pm 0.27 \text{ kcal/mol}$.

5.5.5. Temperature Dependence of Transient Kinetic Studies

The magnitude of the rate constant of a reaction is predominantly dictated via the nature/specificity of the molecular interactions aside from the orientation of reacting species [186]. The measurement of the temperature dependence of the rate constant involved in a macromolecular interaction provides an avenue to discern even a subtle difference in the energetics of the binding and /or dissociation of structurally similar ligands which often show a marked difference in their *in vivo* efficacy. Notably, the downstream cellular response of a ligand/effector, which modulates a kinetically regulated process in a living cell, is primarily dependent on the mechanism as well as the energetics of the ligand-receptor interaction [187]. In order to investigate the energetics of the transient kinetics of interaction of TSA and SAHA to HDAC8, the stopped-flow experiments were performed at different temperature. The outcomes of the above study clearly suggest that thermodynamic parameters, such as free energy (ΔG), enthalpy (ΔH) and entropy (ΔS), involved in the transient kinetics of interaction of TSA and SAHA with HDAC8, differ significantly. Notably, a significant difference in the energetics involved in the kinetics of an inhibitor binding to HDAC8 could have a profound impact on its *in vivo* potency.

5.5.5.1. Temperature Dependence of Association Kinetics of HDAC8-TSA/SAHA Interaction

The transient kinetics experiments for the interaction of TSA and SAHA with HDAC8 was performed at different temperature via a stopped-flow system as described in Methods section. Figure 5.52 shows the temperature dependence of the observed rate constant for the association of TSA and SAHA (left and right panel, respectively).

Evidently, for both the ligands, $k_{\text{obs}1}$ ($1/\tau_{\text{fast}}$) was found to increase exponentially as a function of temperature, whereas $k_{\text{obs}2}$ ($1/\tau_{\text{slow}}$) essentially remained constant. The above finding strongly suggests the fact that the bimolecular step (Scheme 5.2) for the binding of TSA and SAHA contains a significant contribution from a favorable enthalpy as opposed to the isomerization step which is essentially entropically favored. The activation energy of the bimolecular step of the ligand-protein interaction was calculated using the Arrhenius Equation 4.8 described in the Methods section. The activation energy (E_a) for the biomolecular step (fast phase) of the association of TSA and SAHA were 12 kcal/mol and 15 kcal/mol, respectively. Notably, the activation energy for the association of SAHA to HDAC8 is 3 kcal/mol greater than that of TSA, because of which the bimolecular step is slower in the former case.

In order to investigate the affect on temperature on the individual rate constants of the biomolecular step, i.e., k_{+1} and k_{-1} , their values were deduced from observed rate constant (k_{obs}) determined as a function of temperature. Figure 5.53 and 5.54 show the Arrhenius plot for the temperature dependence of k_{+1} and k_{-1} , respectively. The solid lines in the above figures represent the linear regression fit of the experimental data, yielding the energy of activation (E_a). Furthermore, the values of E_a were used to calculate the enthalpy of activation (ΔH^\ddagger) for the biomolecular step at 25 °C. Table 5.29 shows the magnitude of the activation parameters for the biomolecular step of the binding of TSA and SAHA.

The data presented in Table 5.29 show that the activation energy (E_a) for the forward and the reverse reactions of the bimolecular step of the ligand-protein interaction is higher for SAHA as compared to TSA, which explains the fact that the binding of SAHA to HDAC8 is inherently slower. Furthermore, the binding of SAHA is enthalpically favored by 3

kcal/mol over TSA, which is close agreement with results obtained from ITC studies (Table 5.22). It is important to note at this point that the isomerization step of the binding of both TSA as well as SAHA has no enthalpic contribution (entropically driven process). A slow isomerization of protein-ligand complex is primarily mediated via a hydrophobic force which is liable to enhance the entropy of the system [188].

Table 5.29. Activation parameters for the bimolecular step of the binding of TSA and SAHA to HDAC8

Activation parameter	TSA (kcal/mol)	SAHA (kcal/mol)
$E_a(k_{+1})$	9.3	11.4
$E_a(k_{-1})$	13.5	18.5
$\Delta H^\ddagger(k_{+1})$	8.6	10.8
$\Delta H^\ddagger(k_{-1})$	14.0	19.1
ΔH (Bimolecular)	-5.4	-8.3

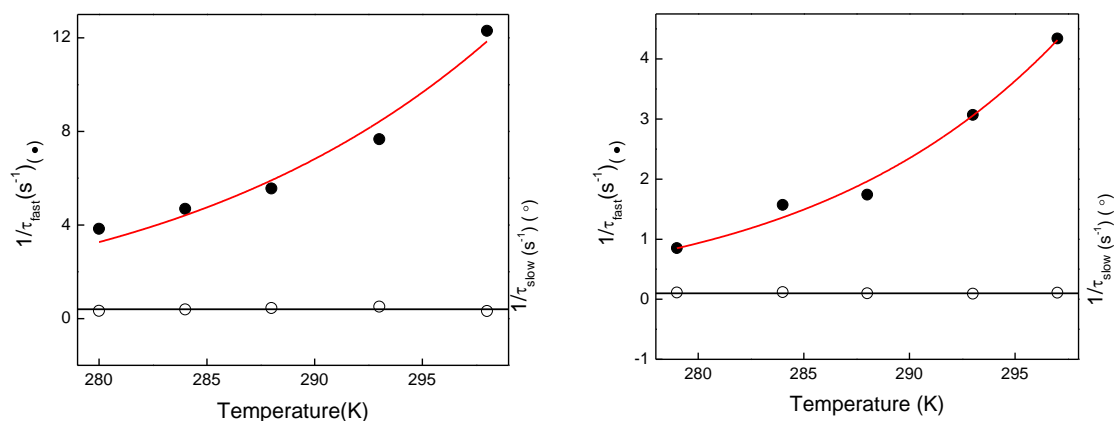


Figure 5.52. Temperature dependence of the relaxation rate constants for the bimolecular and the isomerization step of the HDAC8 interaction with TSA and SAHA. They are shown in left and right panels, respectively. The Arrhenius activation energy for the bimolecular step for TSA and SAHA were calculated from the best fit of experimental data using the Arrhenius equation as 12 and 15 kcal/mol, respectively. The isomerization step has zero activation energy.

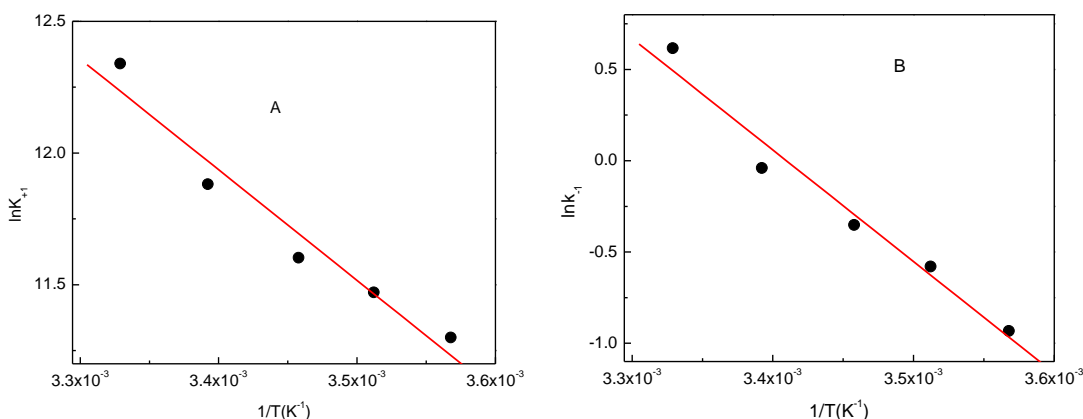


Figure 5.53. Arrhenius plots for the forward (k_{+1}) and reverse (k_{-1}) rate constants for association step for the interaction of TSA to HDAC8. They are shown in panel (A) and panel (B), respectively. The solid smooth lines are linear regression fit of the experimental data for the energy of activation of 9.3 kcal/mol and 13.5 kcal/mol respectively for forward and reverse reactions. The enthalpy of activation (ΔH^\ddagger) calculated at 25 $^\circ\text{C}$ were 8.6 kcal/mole and 14.0 kcal/mole.

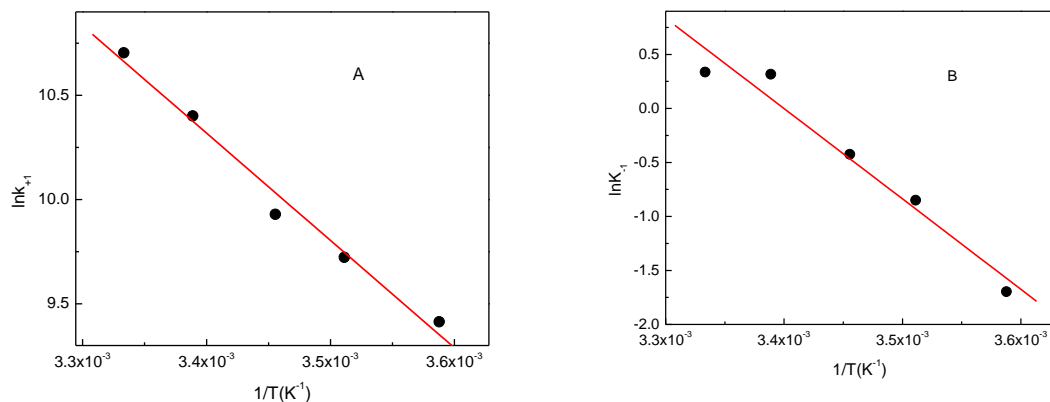


Figure 5.54. Arrhenius plots for the forward (k_{+1}) and reverse (k_{-1}) rate constants for association step for the interaction of SAHA to HDAC8. They are shown in panel (A) and panel (B) respectively. The solid smooth lines are linear regression fit of the experimental data for the energy of activation of 11.4 kcal/mol and 18.5 kcal/mol respectively for forward and reverse reactions. The enthalpy of activation (ΔH^\ddagger) calculated at 25 $^\circ\text{C}$ were 10.8 kcal/mole and 19.1 kcal/mol.

5.5.5.2. Temperature Dependence of k_{off} of TSA and SAHA from the Enzyme's Site

The dissociation off-rate of a ligand from the enzyme's site provides the information about the length of time a ligand is bound to the receptor [166]. However, it does not provide the information about the energetics of the dissociation kinetics. In pursuit of investigating the above facts, the dissociation off-rate of TSA and SAHA were determined by performing the stopped-flow experiments at different temperatures. Figure 5.55 shows the Arrhenius plots for the dissociation off-rate of TSA and SAHA. The solid lines are the best fit of the experimental data according to the Arrhenius Equation with the activation free energy (E_a) of 6.4 kcal/mol and 15 kcal/mol, respectively, for the dissociation of TSA and SAHA from the enzyme's site.

It is important to note that the activation energy (E_a) for the dissociation of SAHA is about 2-fold higher than that of TSA. However, the dissociation-off rate of SAHA is about 3-4 fold higher than TSA at 25 °C. Evidently, entropy plays a greater role in the dissociation of TSA from the enzyme site than that of SAHA. Taking the values of dissociation off-rates of TSA and SAHA at different temperature, in combination with their temperature dependence association kinetics, it became possible to obtain the activation parameters of both the bimolecular as well as the isomerization step. The detail energetics of the transient kinetics of the interaction of TSA and SAHA with HDAC8 is discussed in the discussion section.

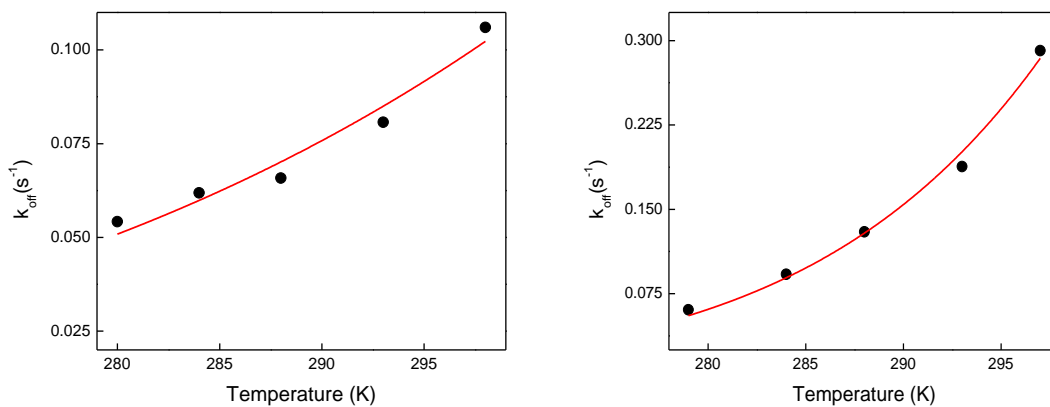


Figure 5.55. Arrhenius plots for the observed dissociation off-rate of TSA and SAHA measured using c-SAHA. They are shown in left and right panel, respectively. The solid lines are the best fit of the experimental data using the Arrhenius equation with the activation energy as 5.6 kcal/mole and 12.8 kcal/mole for TSA and SAHA, respectively.

5.6. Conformational Stability of Recombinant Human HDAC8

Optical spectroscopic methods, such as fluorescence spectroscopy and circular dichroism spectroscopy are widely utilized to study the conformation stability of protein [189]. The intrinsic fluorescence of a protein is primarily due to the presence of aromatic amino acids, such as Phe, Tyr, and Trp. Aside from studying the ligand-protein interaction described above; the intrinsic fluorescence of a protein is often a method of choice to study its conformational stability against the denaturants, such as guanidinium hydrochloride and urea. Furthermore, a conformational thermal/stability of a protein, which is often altered upon a ligand binding, is conveniently studied utilizing Circular Dichroism (CD) spectroscopy [190].

In order to investigate the effect of the binding of selected HDAC8 inhibitors, namely, SAHA and VYU-2-24 on the conformational as well as the thermal stability of the enzyme, various optical spectroscopic methods were utilized as described in the Methods section. The experimental data suggest that the conformational/thermal stability of HDAC8 is enhanced upon binding to its ligand.

5.6.1. Guanidinium Chloride (GdmCl) Induced Unfolding of HDAC8

The conformational stability of HDAC8 was measured by monitoring the change in protein fluorescence due to the GdmCl induced unfolding. Figure 5.56 shows the change in fluorescence emission spectra of the folded and the unfolded form of HDAC8. The intrinsic fluorescence of the protein was quenched and the emission maximum was red shifted upon unfolding, which could be attributed to the change in the microenvironment of the tyrosine and the tryptophan residues of the protein. To enhance the reliability of the measurement, it was imperative to choose a wavelength where the difference in the relative fluorescence

intensities of the folded and the unfolded states was the maximum. The signal to noise ratio was enhanced by taking the ratio of the fluorescence intensities at 354 nm and 340 nm as the normalized fluorescence signal. As described in the Methods section, the protein was incubated with GdmCl (0-7 M) at room temperature to attain the equilibrium before taking the fluorescence spectra.

Figure 5.57 shows the GdmCl induced unfolding transition of the free and the SAHA-bound form of HDAC8 in left and right panel, respectively. The normalized fluorescence signal of HDAC8 was plotted as a function of GdmCl concentration. The solid lines are the best fit of the experimental data using the equation for the two state unfolding mechanism (Equation 4.11, Methods section) with the ΔG^0_{N-U} for unfolding at zero concentration of GdmCl as 6.1 ± 0.8 kcal/mol and 9.8 ± 1.4 kcal/mol, respectively, for free and SAHA-bound form of HDAC8. Evidently, the binding of SAHA to HDAC8 enhanced the conformational stability of the protein by 3.7 kcal/mol. In other words, HDAC8 becomes more stable against chemical denaturation upon binding to SAHA, which could be attributed to the ligand-induced conformational adaptability/modulation in the HDAC8 structure. Notably, the crystal structures of apo and SAHA bound forms of HDAC8 have shown a significant difference in the protein structure [57, 64].

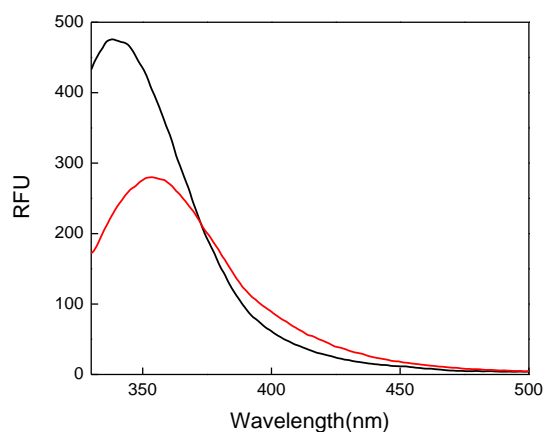


Figure 5.56. The steady state emission spectra of 2 μM of the native (black trace) and the GdmCl-denatured (red trace) form of HDAC8. The spectra were taken in 10 mM Tris-Cl, pH 7.5, 100 mM NaCl, 3 mM MgCl_2 , 10 % glycerol, 1 mM TCEP) upon excitation at 295 nm.

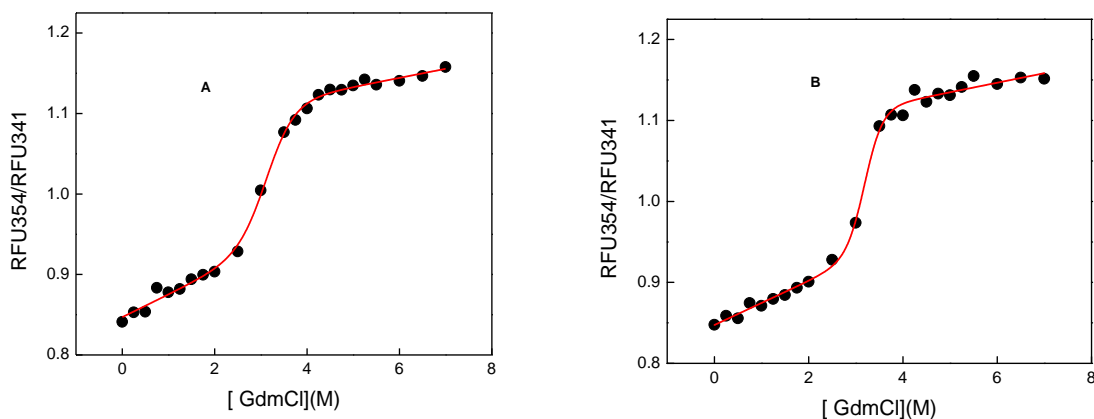


Figure 5.57. Guanidinium chloride induced unfolding of the free (Panel A) and SAHA-bound form (Panel B) of HDAC8 as monitored by the change in the ratio of the fluorescence emission intensities at 354 nm and 341 nm ($\lambda_{\text{ex}} = 295$ nm). The solid lines are the best fit of the data using the Santoro-Bolen equation [52] for the two-state unfolding mechanism with the $\Delta G^0_{\text{N-U}}$ for unfolding at zero concentration of GdmCl as 6.1 ± 0.8 kcal/mol and 9.8 ± 1.4 kcal/mol, respectively, for the free (2 μM HDAC8) and the SAHA-bound form (2 μM HDAC8 + 12 μM SAHA) of the enzyme.

5.6.2. Thermal Denaturation of HDAC8

As described in Section 5.6.1, binding of SAHA to HDAC8 enhances the conformational stability of the protein against chemical denaturation. It is likely that the thermal stability of HDAC8 is also modulated upon binding to SAHA. The above feature was investigated by studying the thermal unfolding of HDAC8 monitored via the change in the CD signal as a function of temperature.

Figure 5.58 shows a heat-induced unfolding transition of the free and the SAHA-bound form of HDAC8 (left and right panel, respectively). The ellipticity (mdeg) at 222 nm was plotted as a function of temperature. The solid line is the best fit of the experimental data using the equation for the two-state thermal unfolding mechanism (Equation 4.12) with T_m and the Van't Hoff enthalpy for protein unfolding as 309 K and 69.5 ± 2.8 kcal/mol, respectively, for the free form of HDAC8. The corresponding values for the SAHA-bound form of HDAC8 were 315 K and 72.5 ± 3.5 kcal/mol. Notably, T_m (melting temperature) is defined as the temperature at which the concentration of the folded and the unfolded protein are equal. The Van't Hoff enthalpy is the amount of heat required to unfold the protein at the standard state, which is derived from the temperature dependence of the equilibrium constant. Clearly, binding of SAHA to HDAC8 increases both the melting temperature (by 6 °C) and as well as the Van't Hoff enthalpy (by 3 kcal/mol) of the protein. The change in above parameters is primarily due to the pairing/coupling of protein unfolding equilibrium with the ligand-binding equilibrium [191].

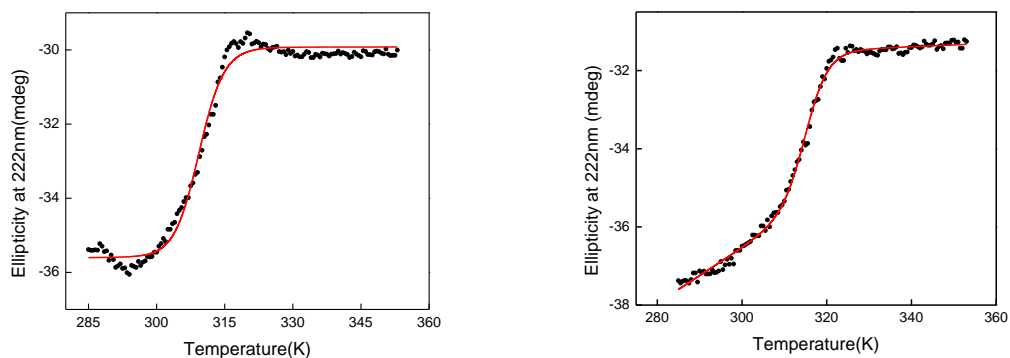


Figure 5.58. Temperature dependence of the ellipticity at 222 nm of 8 μM of the free and the SAHA-bound form of HDAC8. They are shown in the left and right panel, respectively. The experiments were performed in Jasco spectropolarimeter with 1 mm path length quartz cuvette in 5 mM Tris-Cl pH 8.0 containing 0.5 % glycerol, 5 mM TCEP and 15 mM KCl. The temperature scan rate was 1 $^{\circ}\text{C}/\text{min}$. The solid lines are the best fit of the experimental data using the equation for the two step thermal unfolding mechanism with the T_m and Van't Hoff enthalpy for protein unfolding as 309 K and 69.5 ± 2.8 kcal/mol, respectively for the free form of HDAC8. The corresponding values for the SAHA-bound form of HDAC8 were 315 K and 72.5 ± 3.5 kcal/mol.

5.6.3. Ligand-induced Modulation in the Secondary Structure of HDAC8

Binding of a ligand to protein is often associated with modulation in secondary structure of a protein [190]. In order to investigate the above feature for the binding of SAHA to HDAC8, the Circular Dichroism (CD) spectroscopic measurements were performed as described in the Methods section. In a typical Circular Dichroism spectrum of a protein, the signal in the far-UV region is majorly contributed by peptide bonds, which serve as the backbone of the secondary structure of the protein. Especially, the α -helix has a strong and the characteristic CD signal in the far-UV region.

Figure 5.59 shows the changes in the secondary structure of HDAC8 induced upon the binding to SAHA. As evident from the CD spectra, the binding of SAHA modulates the secondary structure of HDAC8.

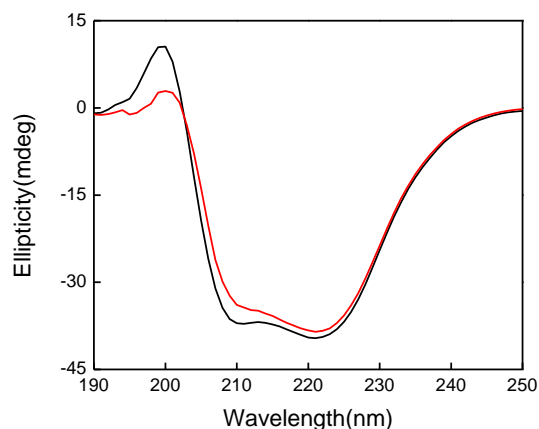


Figure 5.59. The Ligand induced alteration in the secondary structure of HDAC8. CD spectra of 8 μ M of the free (black trace) and the SAHA-bound (red trace) forms of HDAC8 are shown here. The concentration of SAHA used in this experiment was 20 μ M. The spectra were taken in a 1 mm path length quartz cuvette in 5 mM Tris-Cl pH 8.0 containing 0.5 % glycerol, 5 mM TCEP and 15 mM KCl.

5.6.4. Time-resolved Fluorescence Spectroscopic Measurement for Ligand-induced Conformational Changes in HDAC8

The time-resolved fluorescence spectroscopy is the method of choice to study the ligand induced conformation changes in the protein [164]. Notably, the above measurement is free from any inner filter effect often encountered in the steady state fluorescence spectroscopic measurements. In order to investigate the ligand-induced conformational changes HDAC8 upon the binding of VYU-2-24, the tryptophan life-time of HDAC8 was determined. Figure 5.60 shows the tryptophan fluorescence decay curves of the free and the ligand (VYU-2-24)-bound form of HDAC8 (the left and right panel, respectively). The red lines are the best fit of the experimental data using the double exponential rate equation with $\tau_{\text{short}} = 0.91 \pm 0.08$ ns and $\tau_{\text{long}} = 3.48 \pm 0.08$ ns with the respective associated amplitude of 59 and 41 for the free form of HDAC8. The corresponding values for the VYU-2-24-bound form of HDAC8 were: $\tau_{\text{short}} = 0.51 \pm 0.13$ ns and $\tau_{\text{long}} = 2.96 \pm 0.06$ ns with the respective associated amplitude of 53 and 47 %. Evidently, the values of both the longer and shorter life time of HDAC8's tryptophan were reduced upon binding of VYU-2-24 which could be attributed to the change in its microenvironment because of conformational modulation in the protein structure. However, it is difficult to deduce the change in the microenvironment of individual tryptophan in the above case because of the inherent complexity of the fluorescence decay curve originated from five tryptophans of HDAC8. Irrespectively, it does suggest that the fluorescence quenching of HDAC8 mediated due to the binding of VYU-2-24 is dynamic in nature [164].

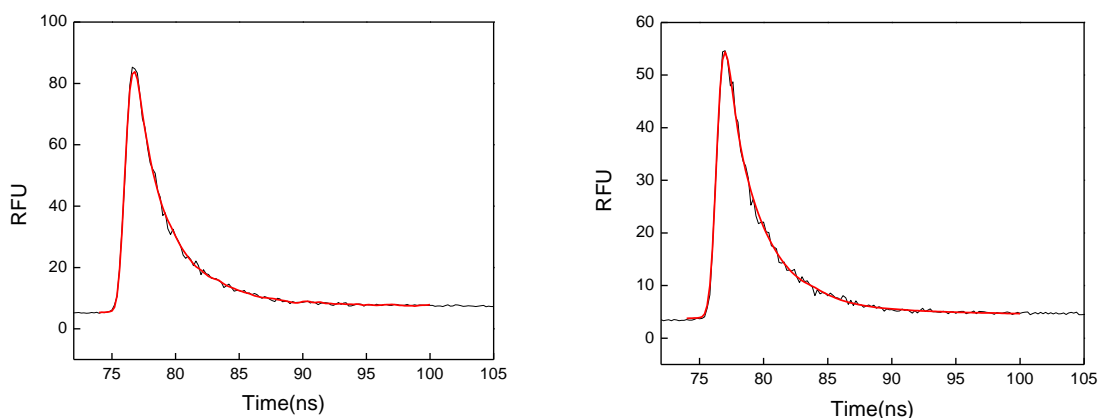


Figure 5.60. Effect of the binding of VYU-2-24 on the tryptophan fluorescence life time of HDAC8. The time resolved fluorescence measurement were done using QuantaMaster™ (Photon Technology International). The left and right panel, respectively, show the fluorescence decay curve of tryptophan for the free (4 μ M enzyme) and the VYU-2-24-bound (4 μ M enzyme + 204 μ M VYU-2-24) form of HDAC8. The data were analyzed using Felix32™ software available from PTI (Photon Technology International). The red lines are the best fit of the experimental data using the double exponential rate equation with $\tau_{\text{short}} = 0.91 \pm 0.08$ ns and $\tau_{\text{long}} = 3.48 \pm 0.08$ ns with the associated amplitude of 59 and 41 % for the free form of HDAC8. The corresponding values for the VYU-2-24-bound form of HDAC8 were: $\tau_{\text{short}} = 0.51 \pm 0.13$ ns and $\tau_{\text{long}} = 2.96 \pm 0.06$ ns with the associated amplitude of 53 and 47 %.

CHAPTER 6. DISCUSSION

The recombinant form of human HDAC8 was cloned, expressed and purified from *E. coli*. A trypsin-coupled *in vitro* HDAC8 enzyme assay was optimized in a continuous format utilizing Fluoro-de-Lys™ as a substrate. In pursuit of discovering novel effectors of HDAC8, various small molecules were synthesized, and their *in vitro* efficacy was tested utilizing the above trypsin-coupled assay in a high-throughput format. Thiopyridine and N-acetylthiourea derivatives were identified as novel, isozyme-selective inhibitors and activators of HDAC8, respectively.

In view of the fact that utilization of a fluorogenic substrate in an HDAC assay is liable to produce an erroneous/unreliable result, a substrate-independent HDAC8 assay was developed utilizing a fluorescent analog of a pan-HDAC inhibitor, coumarin-SAHA, to determine the binding affinity of a non-fluorescent HDAC inhibitor. Furthermore, c-SAHA served as an important tool to investigate the transient kinetics of interaction of HDAC8 inhibitors to the enzyme.

It has been widely reported in the literature that the *in vivo* efficacy of a ligand/drug is dependent on transient kinetics and thermodynamics of the receptor-ligand interaction, aside from and its bioavailability, pharmacokinetics, and half-life. Towards this end, the transient kinetics of interaction of selected HDAC8 inhibitors to the enzyme was thoroughly investigated. A comparison of the transient kinetic parameters of the HDAC8-inhibitor interactions revealed that even structurally similar ligands contain very different mechanisms of binding and dissociation.

The structurally similar ligands/drugs with a similar binding affinity reportedly show a remarkable difference in the nature and specificity of interaction with their

targets/receptors, resulting into a marked difference in their *in vivo* efficacy. Isothermal titration calorimetric studies were performed to investigate the thermodynamics of binding of structurally similar inhibitors to HDAC8. The experimental data revealed that the enthalpic efficiency of an HDAC inhibitor could serve a predictor of its *in vivo* efficacy. Hence, the enthalpy of binding of an HDAC8 inhibitor could be utilized for the lead optimization process to select the best inhibitor in the class.

The binding of ligand to receptor often influences its conformational stability of the latter which often affect its interaction with other binding partners in a physiological milieu. In view of the above facts, the conformation and thermal stability of HDAC8 were thoroughly investigated both in the absence and the presence of different class types of inhibitors. The experimental data revealed that the conformation stability of HDAC8 is markedly influenced upon a ligand-binding.

6.1. Thiopyridine Derivatives as Isozyme-selective Inhibitor of HDAC8

An isozyme selective HDAC inhibitor is likely to cause a lower side effect as compared to a pan-inhibitor. This is because an isozyme-selective exclusively targets a specific HDAC isozyme responsible for a particular disease condition, and it does not interfere with functioning of other isozymes vital for normal physiological processes.

Aside from the therapeutic benefits, an isozyme selective inhibitor serves as an important tool to study the involvement of a specific HDAC isozyme in various cellular processes. It is important to note that si-RNA mediated gene knock-down of a specific HDAC isozyme could also be utilized for the above purpose which suffers from the following limitation. The si-RNA method eliminates/reduces the expression of HDAC in a cell as opposed to an inhibitor of the enzyme which modulates its activity/conformation.

The inhibitor-bound form of HDAC can still interact with other macromolecule, albeit differently, and it would produce a different cellular response as compared to si-RNA mediated knocking down of the enzyme.

An HDAC8 selective inhibitor has a great potential for the treatment of neuroblastoma, which accounts for about 8 % of the pediatric cancer in USA. HDAC8 is reportedly overexpressed in neuroblastoma cells. Notably, an HDAC8-selective inhibitor induces differentiation in neuroblastoma cells, as opposed to a pan-HDAC inhibitor which fails to produce any anticancer effect [192]. Furthermore, an HDAC8 selective inhibitor has a great potential to alleviate the diseased conditions associated with T-cell derived tumors [192].

Various attempts have been made to synthesize a class and/or isozyme specific inhibitors of human HDACs. The linkerless hydroxamate-based inhibitors have been found to be selective for HDAC8 [71]. It has been argued that the selectivity in the above case is primarily achieved due to the binding of the inhibitor to a sub-pocket located in the vicinity of the active site, which is similar to what has been observed in the HDAC8-CRA-A complex [57]. The binding of CRA-A, which contains an aromatic linker moiety, displaces the F152 away from M274 leading to formation of the sub-pocket (Fig 6.1).

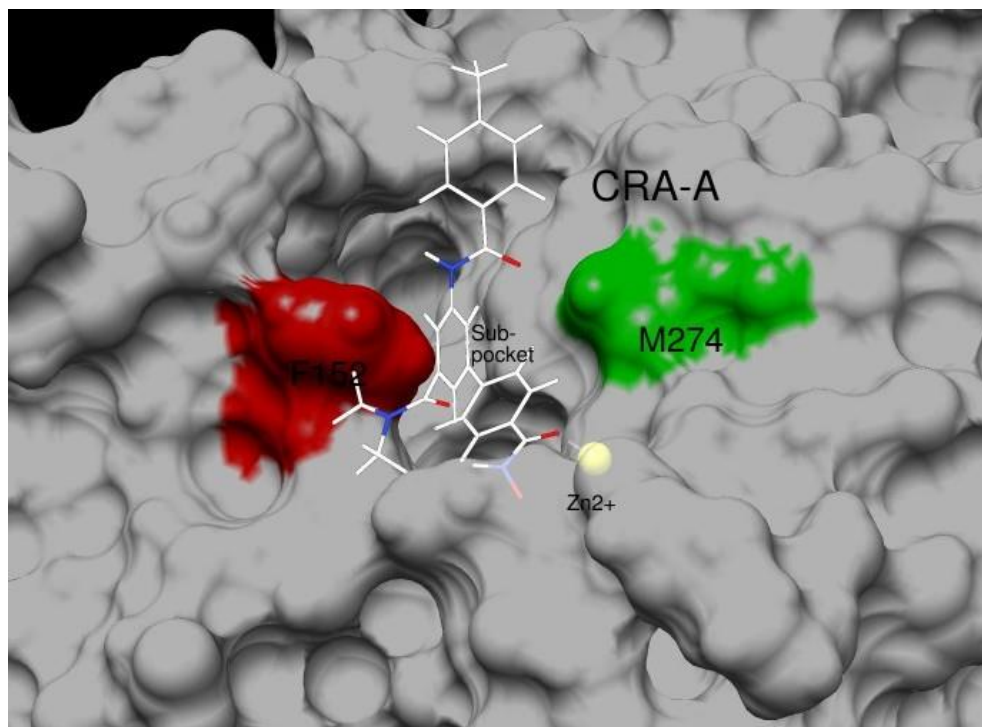


Figure 6.1. The interaction of CRA-A with HDAC8. The aromatic linker moiety of CRA-A binds to the sub-pocket formed due to the displacement of the HDAC8 residue F152 (red) away from M274 (green).

S. Balasubramaniam and co-workers designed PCI-34051 as an HDAC8-selective inhibitor [193]. The above compound contains a bulky linker moiety which has been proposed to bind to the sub-pocket and mediate an isozyme selective inhibition of HDAC8. Additionally, the isozyme-selective inhibitors for class I HDAC have been developed via the exploitation of the acetate release channel [129].

In the initial high-throughput screening of the library of the small molecules, thiopyridine derivatives were found to inhibit HDAC8 activity with an inhibitory potency in the micro-molar range. In order to discover a novel isozyme selective HDAC inhibitor, it was important to test the *in vitro* potency of the thiopyridine derivatives against various

isozymes of human HDACs. Surprisingly, the above inhibitors served as isozyme selective inhibitors of HDAC8. Now, the question arises as to why the thiopyridine derivatives selectively inhibit HDAC8 as opposed to other HDAC isozymes.

Based on the known HDAC8 selective inhibitors in the study undertaken, it is logical to propose a mechanism of isozyme-selective inhibition of HDAC8 via the thiopyridine derivatives, namely, VYU2-24, VYU-2-221, VYU-2-270, and VYU-3-54, as follows. The thiopyridine moiety in the above inhibitors serves as a zinc-binding group. More importantly, due to bulkiness of the thiopyridine ring it could easily access the acetate-release channel of HDAC8 which is likely to provide the marked isozyme selectivity observed. Furthermore, the linker group attached to the thiopyridine moiety could be accommodated in the hydrophobic tunnel or the sub-pocket depending upon its chemical nature. For example, the aromatic linker moiety of VYU-2-24 and VYU-2-70 could be accommodated in the sub-pocket, whereas the aliphatic linker moiety of VYU-2-221 and VYU-3-54 is likely to bind to the hydrophobic tunnel of HDAC8. The above argument is further strengthened by the fact that the polarity/bulkiness of the group attached to the aromatic linker moiety (BNG-2-167, VYU-2-166, MT-111, MT-114, MT-106, MT-109, and MT-116) remarkably influences the inhibitory potency of the inhibitor tested against HDAC8 (Table 5.2).

Based on the structure-activity relationship of the thiopyridine derivatives, namely, VYU-2-219, VYU-2-221, VYU-2-264, VYU-2-266, BNG-3-36, and VYU-3-54 (Table 5.2), which contain an aliphatic linker moiety attached to the thiopyridine ring, it appears that the length/polarity of the linker affects the inhibitory potency.

A thorough understanding of the precise mechanism of the isozyme selective inhibition of HDAC8 via thiopyridine derivatives has to await the crystallographic studies. Irrespectively, the thiopyridine derivatives have a great promise for the treatment of various human diseases linked with HDAC8. Notably, this is the first discovery of a non-hydroxamate based isozyme selective inhibitor of human HDAC8.

6.2. N-acetylthiourea Serves as an Isozyme-selective Activator of Human HDAC8

N-acetylthiourea derivatives were discovered for the first time as the isozyme selective activators of human HDAC8. Notably, an HDAC8 selective activator has the potential to alleviate the disease conditions, such as COPD and CLdS, aside from various forms of cancers where the expression of the wild type p53 gene is suppressed by HDAC8. Interestingly, N-acetylthiourea derivatives reportedly serve as inhibitors of Sirt1, a member of class III HDAC [159].

In order to discern the mechanism of the isozyme-specific activation of HDAC8 mediated via an N-acetylthiourea derivative, the structural-functional and mechanistic studies of HDAC8 catalyzed reaction were performed in the presence of the most potent activator, TM-2-51. It was observed that TM-2-51 decreases the K_m value of the Fluoro-de-LysTM substrate by two fold and enhances the catalytic turn-over rate (k_{cat}) of HDAC8 for the above substrate by about five fold (Table 5.16).

It has been widely debated that the activation of human Sirt 1(class III HDAC) by resveratrol and other known activators is primarily mediated via an interaction between the bulky fluorogenic moiety of the substrate and the activator [89]. In other words, the activation observed in the above case is not a true enzyme-activation. In order to investigate whether the HDAC8 activation by TM-2-51 is real, and which is not mediated

merely via its interaction with the fluorogenic moiety of the Fluoro-de-LysTM substrate, a detail ligand-binding study was performed.

The direct binding of TM-2-51 to HDAC8 was investigated utilizing isothermal titration calorimetry (Result section 5.5.4). Evidently, TM-2-51 binds to HDAC8 even in the absence of any ligand, implying the fact TM-2-51 could serve as a true activator of the enzyme. Furthermore, TM-2-51 binds to more than one site present on HDAC8 (Figure 5.50). In order to gain insight about the mechanism of HDAC8 activation by TM-2-51, steady state enzyme kinetic experiments were performed as followed. The initial velocity of the HDAC8 catalyzed reaction measured as a function of TM-2-51 was found to be sigmoidally dependent on the activator concentration with an apparent activation constant of 6.6 μ M and Hill coefficient of 1.3, suggesting that more than one molecule of TM-2-51 binds to HDAC8 in a positive co-operative manner (Figure 5.25). The above finding corroborate with the result obtained from ITC showing more than one binding sites for TM-2-51 on HDAC8 (Figure 5.50).

In pursuit of investigating the influence of the binding of a substrate or a substrate-analog (inhibitor) on the binding features of TM-2-51 to HDAC8, the binding studies were performed via steady state enzyme kinetics as well as isothermal titration calorimetry. The apparent activation constant (K_a) and the Hill coefficient for the binding of TM-2-51 to HDAC8 was found to be affected in the presence of SAHA (Table 5.17), which corroborates with result obtained from the ITC study for the binding of TM-2-51 to the SAHA-bound form of HDAC8 (Figure 5.50). Clearly, SAHA (a substrate analog), which does not contain any bulky fluorogenic moiety, as opposed to a fluorogenic peptide substrate, modulates the binding of TM-2-51.

As a corollary of the above fact, the binding feature of SAHA to HDAC8 was found to be modulated in the presence of TM-2-51. Even though the affinity constant/inhibition constant of SAHA remained almost the same in the presence of TM-2-51 in the allosteric site, the binding enthalpy (ΔH) of SAHA to HDAC8 was reduced by 3 kcal/mol. The above finding strongly suggests that the geometry of the active site pocket is modulated due to binding of TM-2-51, which could easily account for the enhanced catalytic efficiency of the HDAC8 in the presence of the activator (Table 5.16).

It is important to note that TM-2-51 serves as an isozyme-selective activator of HDAC8, and therefore, the mechanism of isozyme-selective activation needs to be rationalized based on the mode of its interaction to the enzyme-substrate complex. A thorough elucidation of the precise mechanism of HDAC8 activation by TM-2-51 has to wait for X-ray crystallographic studies. However, an attempt was made to gain the mechanistic insight into the HDAC8 activation by TM-2-51 utilizing molecular docking.

The molecular docking of TM-2-51 was performed utilizing AutoDock Vina [194] by taking the co-ordinates of HDAC8-substrate complex (pdb 2V5W). A blind docking of TM-2-51 to the HDAC8-substrate complex showed the presence of at least two distinct binding sites for the ligand (data not shown), which corroborates with the results obtained from steady state enzyme kinetic as well as the ITC studies of the ligand-binding. As shown in Figure 6.2, most of the activator molecules were found to be clustered near the active site pocket of HDAC8. A closer examination of the interactions involved in the binding of the activator to the HDAC8-substrate complex (Figure 6.3) shows that Y306 of HDAC8 (replaced by F306 to capture the substrate binding) makes a π - π stacking interaction with one of the aromatic rings of TM-2-51 as well as the coumarin moiety of

the fluorogenic peptide substrate. Notably, Y306 is a vital residue involved in substrate binding as well as the stabilization of the oxyanion tetrahedral intermediate generated during HDAC8 catalysis. In view of the above facts, it is not surprising to see that K_m and k_{cat} of HDAC8 catalyzed reaction measured on a fluorogenic peptide substrate is modulated in the presence of TM-2-51. Additionally, it is very likely that TM-2-51 would make a π - π stacking with Y306 (albeit weakly) even in the absence of the coumarin moiety, and hence it would serve as a real activator of the HDAC8. Irrespective of the above findings and/or arguments, it is important to confirm via utilizing a natural substrate that the activation of HDAC8 mediated via TM-2-51 is real.

The molecular docking studies described in the previous paragraph provide an insight about the isozyme-selective activation of HDAC8 mediated via TM-2-51. It is important to note here that HDAC8's residues F152 and M274 interact with the second aromatic ring of the activator (TM-2-51). The relative orientation of the above two residues is responsible for the formation of a sub-pocket in HDAC8, which has been observed in case of the HDAC8-CRA-A complex [57]. It can be argued that the second aromatic ring of TM-2-51 is accommodated in the sub-pocket which is exclusively present in HDAC8, leading to an isozyme selective activation. The above argument is further strengthened by the fact that the bulkiness, aromaticity, and polarity of the second ring of the activator molecule have a strong correlation with the structure-activity relationship of HDAC8 activation mediated via N-acetylthiourea derivatives (Table 5.4).

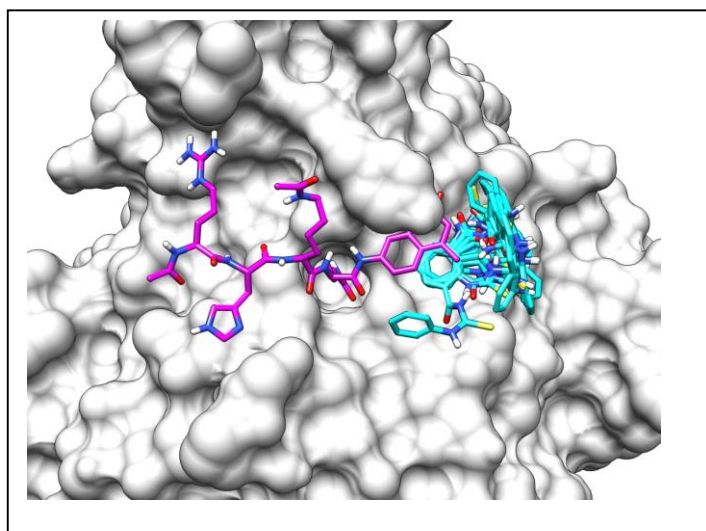


Figure 6.2. Molecular docking of TM-2-51 to HDAC8. The majority of the docked molecules of TM-2-51 are clustered near the active site of HDAC8. The backbone of the fluorogenic peptide substrate and TM-2-51 are shown by purple and cyan, respectively.

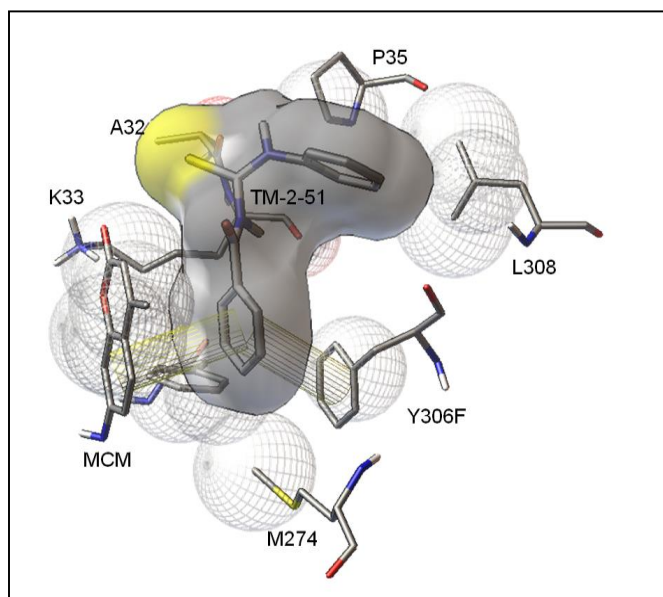


Figure 6.3. Closer view of the HDAC8-substrate-TM-2-51 complex. One of the aromatic rings of TM-2-51 makes a π - π interaction with the Y306F and the coumarin moiety of the substrate.

6.3. Coumarin-SAHA as a Fluorescent Probe to Determine the Binding Affinity and Dissociation Off-rate of HDAC8 Inhibitors

It is widely known that the rate of HDAC catalyzed reaction measured on a fluorogenic peptide substrate does not truly represent the deacetylation reaction *in vivo* or with a natural substrate. Furthermore, the authenticity of the effector and its potency determined via an *in vitro* HDAC enzyme assay is often questioned, primarily because of the chemical nature of substrate used in the assay. In that pursuit, attempts have been made by various research groups to develop a substrate-independent assay to determine the binding affinity of an HDAC inhibitor (Introduction Section 1.6).

Coumarin-SAHA served as a novel fluorescent probe to develop a substrate-independent assay to determine the binding affinity of an HDAC8 inhibitor. The above assay is essentially a fluorescent displacement assay, which offers the following advantages over the currently utilized substrate-independent assay to determine the binding affinity of an HDAC8 inhibitor. (1) The synthesis of c-SAHA is very easy and inexpensive; (2) Since c-SAHA is a fluorescent analog of a pan-HDAC inhibitor, the analytical method could be conveniently used for determining the binding affinity of an inhibitor to almost every HDAC isozyme; (3) c-SAHA can be selectively excited at 325 nm ($\lambda_{\max} = 325$ nm) without an interference caused due to protein or other non-fluorescent ligand, which significantly reduces the inner filter effect and enhances the reliability of the experimental results; (4) Aside from the binding affinity of an HDAC inhibitor, c-SAHA serves as a novel fluorescent probe to determine the dissociation off-rate (k_{off}) of a non-fluorescent HDAC inhibitor utilizing a stopped-flow system (Figure 5.35); (5) As opposed to the previously developed substrate-independent assay which is based on FRET, fluorescence anisotropy,

fluorescence life-time measurements requiring an expensive equipment and skilled personnel [90-92], the analytical protocol/assay developed using c-SAHA is quite simple, inexpensive which could be performed on a simple spectrofluorometer.

6.4. Transient Kinetics of Interaction of Inhibitor to HDAC8

6.4.1. Association/Dissociation Kinetics of TSA, SAHA, and VYU-2-24

In pursuit of delineating the mechanistic features of the interaction of the HDAC8 inhibitors, namely TSA, SAHA, and VYU-2-24, to the enzyme, their association and the dissociation kinetics were thoroughly investigated utilizing a stopped-flow system. Although the association of all the above inhibitors to HDAC8 follows a two-step binding mechanism (Scheme 5.2), the followings are the salient differences. (1) The relaxation rate constant for the bimolecular step of the TSA-binding about 2-fold higher than that of SAHA and VYU-2-24, which could be explained from the fact that orientation factor plays a significant role in the binding of TSA to HDAC8. The dimethyl aniline moiety of TSA makes a π - π interaction with Y100 (Figure 6.4), which is likely to enhance the second order rate constant for the association of TSA to HDAC8. (2) The isomerization of the transient enzyme-inhibitor complex is faster in case of binding of TSA as compared to SAHA and VYU-2-24, which could be easily explained from the fact that F152 makes a hydrophobic interaction with dimethyl aniline moiety of TSA. Notably, in the case binding of SAHA to HDAC8, the F152 interacts with the aliphatic linker moiety of the inhibitor [57]. (3) Since both the bimolecular as well as the isomerization step involved in the binding of TSA is faster than that of SAHA/VYU-2-24, the overall association kinetics for the former ligand to HDAC8 is faster than the others.

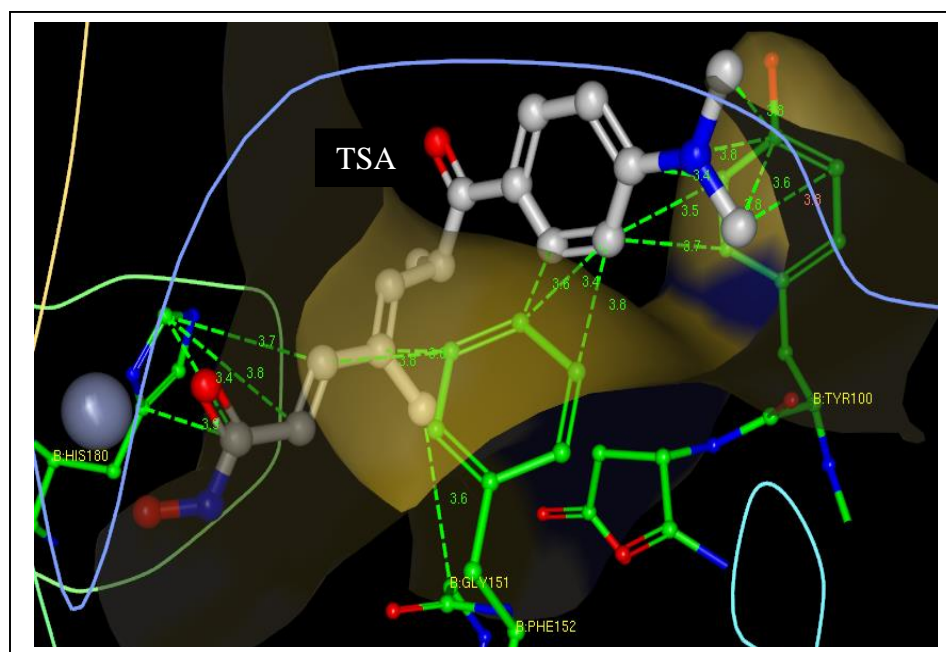


Figure 6.4. Interaction between dimethyl aniline moiety of TSA and Y100 in HDAC8-TSA complex. The π - π stacking is shown with dashed green lines.

In order to gain insight about the mechanism of dissociation of TSA, SAHA, and VYU-2-24 from the HDAC8's site, their dissociation-off rates were measured utilizing c-SAHA as a displacing ligand via the stopped-flow system (Figure 5.35). Notably, k_{off} of SAHA is about 4-fold higher than that of TSA. Additionally, dissociation off-rate of VYU-2-24 is 2-fold higher than that of SAHA. The slow dissociation of TSA from the HDAC8's site could be explained from the fact that the π - π stacking and a strong hydrophobic interaction between dimethyl aniline moiety of the inhibitor and Y100 (Figure 6.4) impair its dissociation from the enzyme's site. Furthermore, due to a higher rigidity and the bulkiness of the linker group of TSA as compared to SAHA, the dissociation off-rate of the former ligand is liable to be slow.

The underlying difference in the transient kinetics of binding and dissociation of an HDAC8 inhibitor could have a strong therapeutic implication. It is important to note that the extent of the intrinsic fluorescence quenching of HDAC8 is also markedly higher in case of the TSA-binding to HDAC8 as compared to SAHA one, suggesting that the ligand-induced conformational changes in HDAC8 are remarkably different for the binding of TSA and SAHA. Not surprisingly, the orientation of L1 loop is remarkably different in the case of the binding of TSA vs. SAHA [57]. The above differences in the extent and the kinetics of the ligand-induced conformational change could have a profound effect on the efficacy of an inhibitor, especially where the HDAC8-mediated cellular processes are kinetically controlled. It is important to note here that the efficacy of an HDAC8 inhibitor cannot be solely predicted on the basis of the transient kinetic parameters of its interaction with the enzyme. Nonetheless, based on the comparative transient kinetics of interaction of TSA and SAHA it is tempting to propose that a higher efficacy of an HDAC inhibitor in clinical setting could be achieved via optimization of the transient kinetics parameters of interaction with the enzyme. The slow association kinetics and the fast dissociation kinetics of SAHA from HDAC8's site could be one of the prime reasons for SAHA being a better drug candidate over the others for the treatment of various forms of human cancer. However, it is important to mention here that the transient kinetic parameters for the interaction of an HDAC inhibitor would be dependent on the type of the HDAC isozyme, and it would be premature to judge/predict the *in vivo* efficacy of an HDAC inhibitor solely based on the experimental finding described here.

6.4.2. Comparison of the Transient Kinetics of Binding and Dissociation of SAHA and c-SAHA

Although SAHA and c-SAHA are structurally same except for the difference in their cap group, the observed mechanism of the binding of the above ligands to HDAC8 is remarkably different. Notably, the two step binding mechanism involved in the binding of SAHA vs. c-SAHA differs in the following ways. (1) Unlike SAHA, the transient enzyme-inhibitor complex formed during the association of c-SAHA to HDAC8 is in rapid equilibrium with free form of ligand and enzyme, and the observed rate constant is dependent on the concentration of the above species (Scheme 5.3). (2) The association kinetics of SAHA to HDAC8 contains a two distinct kinetically resolvable steps i.e., bimolecular and isomerization step, as opposed to the c-SAHA binding where the bimolecular step is very fast and irresolvable. (3) Irrespective of the kinetics of the bimolecular step, the transient enzyme-inhibitor complex of both the ligands undergoes a slow isomerization leading to the formation of the final protein-ligand complex. Notably, the isomerization step for the c-SAHA binding is about three orders of magnitude higher than that of SAHA, leading to the faster association kinetics for the former ligand. The above observed difference in rate of the isomerization could be attributed to the presence of a bulky cap moiety in case of c-SAHA as compared to SAHA.

The dissociation off-rate (k_{off}) of c-SAHA from the HDAC8's site was found be significantly different from that of SAHA (Figure 5.37). Although c-SAHA contains a bulkier cap moiety as compared to SAHA, its dissociation off-rate is about two fold higher than that of SAHA. This is presumably due to the inherent differences in the energetics involved in the dissociation of the above two ligands, which could be investigated via the

comparative temperature-dependent transient kinetic studies for interaction of c-SAHA and SAHA to HDAC8. Taken together, a remarkable difference in the transient kinetics of binding as well dissociation of SAHA and c-SAHA from the HDAC's site strongly suggests that even the structurally similar ligands could have a very different mechanism of binding and dissociation, which is likely to have a significant impact on *in vivo* efficacy of the ligand.

6.4.3. Temperature-dependent Transient Kinetic Study for the Interaction of TSA and SAHA

The temperature-dependent transient kinetic studies (Section 5.5.5) performed to discern the energetics of the interaction of TSA and SAHA with HDAC8 highlight the following significant differences.

1. The bimolecular step involved in the association kinetics of TSA and SAHA contains a favorable enthalpic as well as entropic contribution, as opposed to the isomerization step which is solely driven by favorable entropy (Figure 5.52).
2. The overall free energy (ΔG^0) for the binding of TSA (-8.5 kcal/mol) is about 1.5 kcal/mol higher than that of SAHA (-7.0 kcal/mol). Notably, ΔG^0 for the bimolecular step is 5 to 9 fold higher as compared to isomerization step (Table 6.1), implying the fact that initial ligation/encounter of the above ligands with the enzyme leads to a large change in the free energy.
3. The change in entropy (ΔS^0) associated with the bimolecular step of the binding of TSA and SAHA is starkly different. There is an entropic penalty of about 2 kcal/mol for the binding of SAHA, as opposed to the TSA-binding which is entropically favored by 1.8 kcal/mol. Such a remarkable difference in the

entropic changes associated with bimolecular step could presumably be due to a strong hydrophobic interaction between the cap moiety of TSA and Y100 as well as a greater bulkiness/rigidity of the linker moiety of TSA.

4. Although the isomerization step for the binding of TSA and SAHA is solely driven by a favorable entropy, the entropic contribution in the former case is about 2-fold higher than that of the latter. The above feature could again be rationalized based the strong hydrophobic interaction in concomitant with the removal of water molecule from the enzyme/ligand surface during the isomerization of the transient HDAC8-TSA complex.

The values of the temperature-dependent transient kinetic parameters for the interaction of TSA and SAHA are listed in Table 6.1.

The dissociation off-rate of TSA and SAHA from the HDAC's site measured at different temperature elucidate differences in the energetics involved in their dissociation. The Arrhenius activation energy for the dissociation of SAHA (12.5 kcal/mol) is over two-fold higher than that for TSA (5.6 kcal/mol) (Figure 5.55). A greater value of the activation energy (E_a) for the dissociation of SAHA could be conceived from the fact that SAHA makes more specific interactions (H-bonding) with HDAC8 (Figure 6.5) as compared to TSA, and that it would require more energy to break the specific interaction during the dissociation of SAHA from the enzyme's site. Even though the E_a value for the dissociation for TSA is smaller than that of SAHA, it is important to note that dissociation of SAHA is about 4-fold higher than that of TSA at 25 °C. The above feature could be explained from the fact that the faster isomerization step involved in HDAC8-TSA interaction impairs the dissociation of the ligand from the enzyme's site.

The energetics involved in the transient kinetics of association as well dissociation of TSA and SAHA from enzyme's site is summarized in the form of the free-energy diagrams (Figure 6.6 and 6.7). A remarkable difference in the energetics as well as the mechanism of the binding/dissociation of TSA and SAHA could account for a marked difference in their efficacy in the clinical settings. Human HDAC8 contains several non-histone targets, and it is very likely that several of the HDAC8-regulated cellular processes are kinetically controlled.

It is important to note at this point that the experimental results described here should be used with a caution to predict the efficacy of an HDAC inhibitor. TSA and SAHA are pan-HDAC inhibitor, and their energetics of the transient kinetics of interaction with other HDAC isozymes could be different. Nonetheless, the temperature-dependent transient studies described above provide valuable information about the interaction of an inhibitor to HDAC8, which could be useful in the optimization of a lead compound.

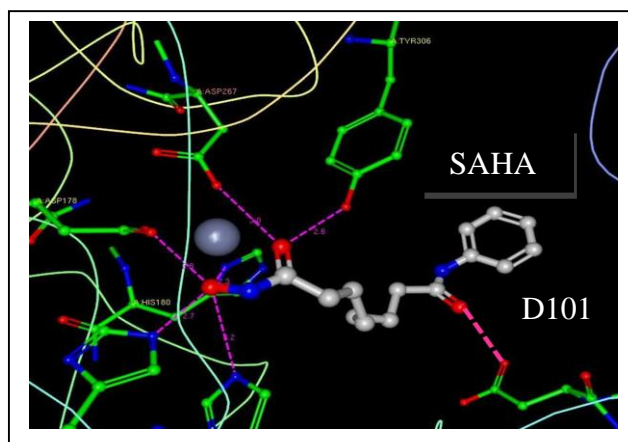


Figure 6.5. The hydrogen-bonding interaction between HDAC8 and SAHA. The hydrogen bonding is shown with dashed lines.

Table 6.1. Transient kinetic parameters for the interaction of TSA and SAHA with HDAC8

Parameter (Energy in kcal/mol)	TSA	SAHA
ΔG^0 (overall)	-8.57	-7.0
$\Delta G^0(k_{-1}/k_{+1})$	-7.2	-6.3
ΔG_{k+1}^\ddagger	10.1	10.9
ΔH_{k+1}^\ddagger	8.6	10.8
ΔG_{k-1}^\ddagger	17.3	17.23
ΔH_{k-1}^\ddagger	14.0	19.1
$\Delta H^0(k_{-1}/k_{+1})$	-5.4	-8.3
$\Delta G^0(k_{-2}/k_{+2})$	-1.4	-0.72
ΔG_{k+1}^\ddagger	18.10	19.03
ΔG_{k-2}^\ddagger	19.5	19.7

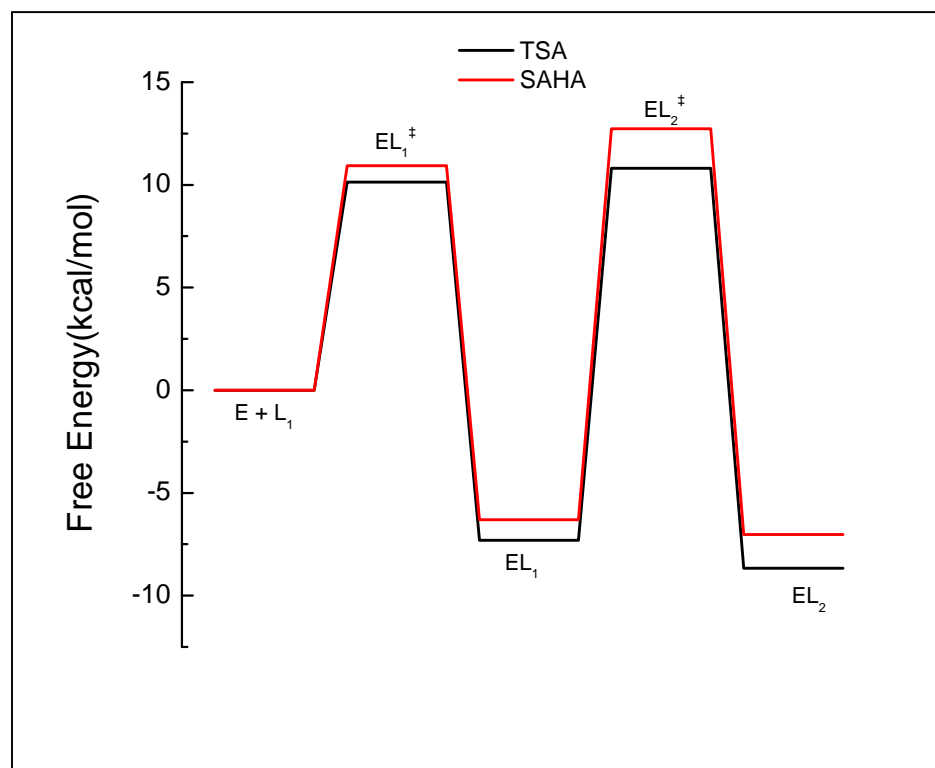


Figure 6.6. Free energy profile for the binding of TSA and SAHA. The free energies of the enzyme and the ligand were taken as being equal to zero.

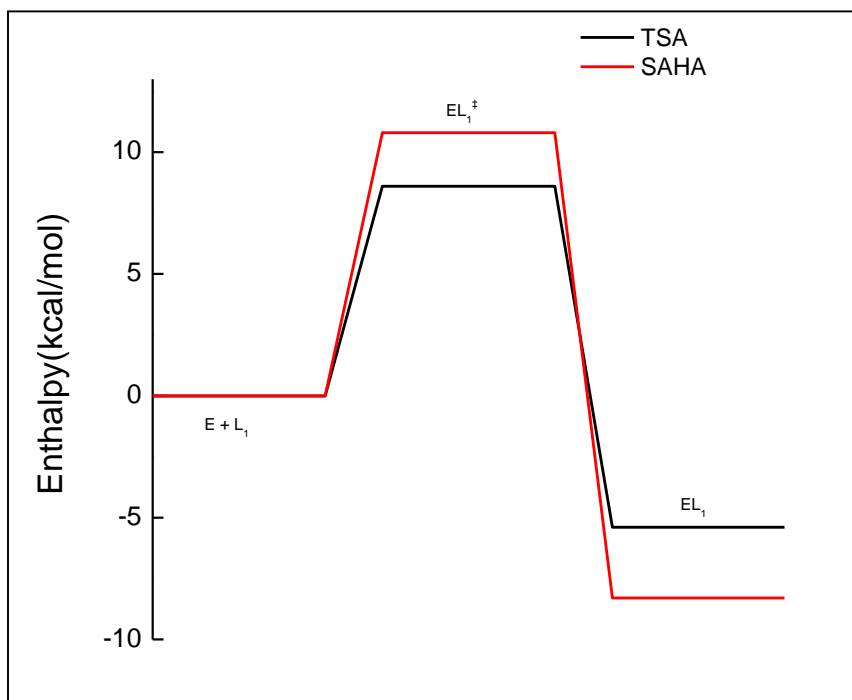


Figure 6.7. Enthalpic profile for the bimolecular complexes of HDAC8 with TSA and SAHA. The enthalpies of the enzyme and the inhibitor were taken as being equal to zero.

6.5. ITC Studies for the Binding of HDAC8 Inhibitors to Enzyme

The isothermal titration calorimetric studies performed for the binding of selected inhibitors, namely TSA, SAHA, and VYU-2-24, to HDAC8 revealed several significant facts about the thermodynamics as well as the nature and specificity of the ligand-protein interaction in the above cases which can be summarized as follows. (1) The enthalpy change (ΔH^0_{obs}) associated with binding of SAHA (-10.95 kcal/mol) to HDAC8 determined in a standard Tris buffer at 25 °C is greater than that of TSA (-8.9 kcal/mol) as well as VYU-2-24 (-7.9 kcal/mol). (2) The intrinsic enthalpy (ΔH_{int}) for the binding of VYU-2-24 (-8.57 kcal/mol) is the highest among all the three ligands under study (Table 5.22). Furthermore, ΔH_{int} for the binding of SAHA (-2.3 kcal/mol) is about 2-fold higher than that of TSA (-0.84 kcal/mol). (3) The change in heat capacity (ΔC_p) for the binding of TSA (0.25 kcal/mol/K) to HDAC8 is higher than that of SAHA (0.23 kcal/mol/K) and VYU-2-24 (0.19 kcal/mol/K). (4) There is strong enthalpy-entropy compensation for the binding of all the above inhibitors to HDAC8.

The thermodynamic data described above for the binding of TSA, SAHA, and VYU-2-24 can be interpreted in the light of crystallographic studies as well as the nature of ligand-protein interaction as follows.

1. The higher value of ΔH^0 for the binding of SAHA to HDAC8 as compared to TSA could be attributed to the fact that the former ligand makes more specific interactions (hydrogen bonding) with the protein (Figure 6.5). Evidently, D101 makes a favorable hydrogen bond with the carbonyl oxygen of the amide group (connector), located between the cap and the aliphatic linker moiety of SAHA.

The above hydrogen bond does not exist in the case of the HDAC8-TSA because of

the π - π interaction between dimethylamino aniline (cap) moiety of TSA and Y100, which displaces the connector (a ketone moiety) away from the D101. Additionally, ketone moiety present in TSA is a poor hydrogen bond acceptor as compared to the amide group of SAHA. Notably, presence of an additional hydrogen bond could easily account for the observed difference in the binding enthalpy (ΔH^0) of TSA and SAHA by 2-3 kcal/mol.

2. Although SAHA makes more specific interactions with HDAC8 as compared to TSA, its binding affinity is about an order of magnitude lower than the latter (TSA). Evidently, the gain in free energy (ΔG^0) due to favorable ΔH^0 is overcome by an entropic penalty. The entropic (ΔS^0) penalty associated with the binding of SAHA to HDAC8 could arise from the following facts. The formation of a specific hydrogen bond between SAHA and D101 residue located on the active site pocket-forming loop (L2) of HDAC8 significantly reduces the flexibility of the above loop resulting into an entropic penalty. Additionally, the formation of the above hydrogen bond forces the aromatic cap moiety of SAHA to be exposed towards the bulk solvent, which further adds to the entropic penalty. Aside from the above specific interaction, the orientation of the L1 loop (pocket-forming loop) in the HDAC8-SAHA complex is significantly different as compared to the HDAC8-TSA complex [57]. The L1 loop is oriented more towards the active site pocket in the HDAC8-SAHA complex, which would reduce its mobility/flexibility leading to an entropic penalty.
3. A 2-3 fold difference in the intrinsic enthalpy of binding of VYU-2-24 as opposed to TSA and SAHA is primarily due to the difference in the zinc-

binding group of the above inhibitors. The pK_a of the thiopyridine moiety of VYU-2-24 is about -1.38 [195], and hence it exists as fully deprotonated form at pH 7.5 prior to binding to the catalytic zinc ion of HDAC8. As opposed to thiopyridine moiety of VYU-2-24, pK_a of the hydroxamate moiety of TSA/SAHA is significantly higher (8.9), which decreases upon binding to the catalytic zinc ion, releasing a proton to the buffer media. The ITC experiments performed with VYU-2-24, TSA, and SAHA utilizing buffers of different ionization enthalpy (Section 5.5.2) clearly shows the binding of the former ligand (VYU-2-24) releases no proton to the buffer media, as opposed to the binding of a hydroxamate-based inhibitor (TSA and SAHA), where NEARLY one proton is released. Notably, deprotonation of the hydroxamate moiety has been reported in the case of binding of a hydroxamate-based inhibitor to other metalloenzyme such as Matrix Metalloproteases (MMPs) [196]. Contrary to above finding, using a computational method, Ying K and coworkers have reported that the hydroxamate moiety of an HDAC inhibitor remains fully protonated upon binding to the enzyme [197]. The observed discrepancy could be precisely resolved by performing the pH dependent ITC experiments for the binding of the hydroxamate-based inhibitor to HDAC8.

4. The ΔC_p for the binding of both TSA and SAHA is negative, which could be attributed to the fact the aliphatic linker moiety of the above inhibitors is well accommodated in the hydrophobic tunnel of HDAC8, primarily via a hydrophobic interaction. The negative value of ΔC_p is essentially originates from burial of non-polar surfaces due to the formation of ligand-protein

complex [181-182]. Furthermore, in view of the fact that the binding of SAHA makes an additional hydrogen bond with HDAC8 as compared to TSA, it is not surprising to see that the ΔC_p for the binding of the former ligand (-0.23 kcal/mol/K) is higher than that of the latter (-0.21 kcal/mol/K).

5. Irrespective of the chemical nature of the inhibitor used in the ITC studies for investigating the thermodynamics of the inhibitor-HDAC8 interaction, the enthalpy-entropy compensation was observed for the binding of all three inhibitors under study (Result Section 5.5.3). Notably, the enthalpy-entropy compensation is a common feature observed in macromolecular interaction involving water [184].

It is important to note that the thermodynamic parameters for the interaction of TSA and SAHA with HDAC8 obtained from transient kinetic studies are in close agreement with the values obtained from ITC studies. The overall change in enthalpy (ΔH^0) for the binding of SAHA is ~ 2 kcal/mol greater than that of TSA (Table 6.1). Furthermore, entropic changes (ΔS^0) involved in binding of TSA to HDAC8 is higher as compared to the SAHA-binding, which results into a higher binding free energy (ΔG^0) or K_a in the former case.

The difference in the mode of binding i.e., enthalpically vs. entropically favored binding of a drug/lead compound has a therapeutic implication. Even though a lead compound is not solely optimized based on the thermodynamic parameters of its binding to the target, it has been widely known that the enthalpically optimized drug usually shows a higher efficacy in the clinical setting, primarily because of a higher specificity of the drug-target interaction [173]. For instance, Ernesto Friere and colleagues have reported that

among HIV protease inhibitors and the statins (HMG-coA inhibitors); the best in class contains the highest enthalpy of binding to their targets [173]. Thus, in addition to the biophysical parameters, such as bioavailability, pharmacokinetics, log P value, and the other Lipinski's parameters, an enthalpic change (ΔH^0) involved in drug-target interaction play crucial role in determining *in vivo* efficacy of a drug [198]. Unfortunately, it is difficult to enhance the enthalpic efficiency of a lead compound because of the enthalpy-entropy compensation [199].

A comparison of the ITC studies for the binding of TSA and SAHA to HDAC8 provides a clue for the observed higher *in vivo* efficacy of the latter ligand. Although *in vitro* potency of SAHA is lower than that of TSA, its binding to the target is more specific (higher ΔH^0 of binding), which would significantly reduces the toxicity/side effect associated with the non-specific binding of the drug to other targets. This could be one of the possible reasons for SAHA being a better HDAC inhibitor over the others in a clinical setting, and hence it was approved by the FDA for the treatment of T-cell lymphoma. Taken together, optimization of the lead compound solely based on the criteria of enhancing the binding affinity (K_a)/binding free energy (ΔG^0) is often inadequate and misleading. ITC derived thermodynamic parameters for the HDAC8-inhibitor interaction could be utilized for the lead optimization process in order to enhance the *in vivo* efficacy of a drug.

6.6. Conformational Stability of HDAC8

An investigation of the conformational stability of HDAC8 upon ligand-binding (Section 5.6) revealed the following facts. (1) The binding of an inhibitor (SAHA) to HDAC8 enhances the thermal stability of the protein. The melting temperature and the

Van't Hoff enthalpy of HDAC8 unfolding were increased by 5 °C and 3 kcal/mol, respectively, upon binding to SAHA (Figure 5.58). (2) The ΔG_{N-U}^0 for the unfolding of HDAC8 mediated via GdmCl was increased by ~4.0 kcal/mol upon binding to SAHA (Figure 5.57). (3) The secondary structure of HDAC8 is modulated upon binding to an inhibitor (SAHA)

An enhancement in the thermal stability of protein upon ligand-binding has been widely reported in literature. For example, thermal stability of straptavidin/avidin is increased upon binding to biotin [200]. Utilizing the hydrogen/deuterium (H/D) exchanged method it has been found that binding of a ligand to the receptor reduces the conformation flexibility of protein's residues located in the vicinity of the ligand-binding site, which is due to the specific non-covalent (hydrogen bonding and Van der Waals interaction) interactions between ligand and protein [201]. As a result of the above features of the ligand-protein interaction, the thermal stability of protein is enhanced upon binding to a ligand. In view of the above facts it is not surprising to see that thermal stability of HDAC8 is enhanced upon binding to SAHA.

A modulation in the conformation/flexibility of residues near the ligand-binding site introduced upon a ligand-binding is transmitted towards the other region of the protein [202]. The above feature is especially crucial for the allosteric/non-allosteric binding of an effector molecule to an enzyme/target leading to a modulation in the enzyme activity as well as its interaction/association with other macromolecule in the physiological milieu [203]. For instance, binding of TFMK (trifluoromethylketone) inhibitor to HDAC4 leads to the dissociation of HDAC4 from the N-CoR-HDAC3-HDAC4 complex [67]. It is very likely that an architecture of chromatin-remodeling as well as the various macromolecular

complexes, which contains various HDAC isozymes, would be modulated in the presence of an HDAC effector. Gerard Drewes and co-workers have suggested that the selectivity/potency of an HDAC inhibitor should be evaluated utilizing HDAC complexes rather than purified recombinant form of the protein [204]. Notably, HDAC8 seems to interact with only a limited number of proteins *in vivo*. Nonetheless, the HDAC8 selective effectors, such as TM2-51 and VYU-2-24, have a potential to modulate the cellular pathways associated with HDAC8 in various pathological conditions.

REFERENCES

1. Ramakrishnan, V. Histone Structure and the Organization of the Nucleosome. *Annual Review of Biophysics and Biomolecular Structure* **26**, 83–112 (1997).
2. Jenuwein, T. & Allis, C. D. Translating the Histone Code. *Science* **293**, 1074–1080 (2001).
3. Clapier, C. R. & Cairns, B. R. The Biology of Chromatin Remodeling Complexes. *Annual Review of Biochemistry* **78**, 273–304 (2009)
4. Gardner, K. E., Allis, C. D. & Strahl, B. D. Operating on chromatin, a colorful language where context matters. *J. Mol. Biol.* **409**, 36–46 (2011).
5. Berger, S. L. Histone modifications in transcriptional regulation. *Curr. Opin. Genet. Dev.* **12**, 142–148 (2002).
6. Oliver, S. S. & Denu, J. M. Dynamic Interplay between Histone H3 Modifications and Protein Interpreters: Emerging Evidence for a ‘Histone Language’. *ChemBioChem* **12**, 299–307 (2011).
7. Gregoret, I., Lee, Y.-M. & Goodson, H. V. Molecular Evolution of the Histone Deacetylase Family: Functional Implications of Phylogenetic Analysis. *Journal of Molecular Biology* **338**, 17–31 (2004).
8. Leipe, D. D. & Landsman, D. Histone deacetylases, acetoin utilization proteins and acetylpolyamine amidohydrolases are members of an ancient protein superfamily. *Nucleic Acids Res.* **25**, 3693–3697 (1997).
9. Choudhary, C. *et al.* Lysine Acetylation Targets Protein Complexes and Co-Regulates Major Cellular Functions. *Science* **325**, 834–840 (2009).
10. De RUIJTER, A. J. M., Van GENNIP, A. H., Caron, H. N., Kemp, S. & Van KUILENBURG, A. B. P. Histone deacetylases (HDACs): characterization of the classical HDAC family. *Biochemical Journal* **370**, 737 (2003).

11. North, B. J. & Verdin, E. Sirtuins: Sir2-related NAD-dependent protein deacetylases. *Genome Biology* **5**, 224 (2004).
12. Reichert, N., Choukrallah, M.-A. & Matthias, P. Multiple roles of class I HDACs in proliferation, differentiation, and development. *Cell. Mol. Life Sci.* **69**, 2173–2187 (2012).
13. Gao, L., Cueto, M. A., Asselbergs, F. & Atadja, P. Cloning and functional characterization of HDAC11, a novel member of the human histone deacetylase family. *J. Biol. Chem.* **277**, 25748–25755 (2002).
14. Gray, S. G. & Ekström, T. J. The human histone deacetylase family. *Exp. Cell Res.* **262**, 75–83 (2001).
15. Yang, X.-J. & Seto, E. Collaborative spirit of histone deacetylases in regulating chromatin structure and gene expression. *Curr. Opin. Genet. Dev.* **13**, 143–153 (2003).
16. Hayakawa, T. & Nakayama, J.-I. Physiological roles of class I HDAC complex and histone demethylase. *J. Biomed. Biotechnol.* **2011**, 129383 (2011).
17. Montgomery, R. L. *et al.* Histone deacetylases 1 and 2 redundantly regulate cardiac morphogenesis, growth, and contractility. *Genes Dev.* **21**, 1790–1802 (2007).
18. Galasinski, S. C., Resing, K. A., Goodrich, J. A. & Ahn, N. G. Phosphatase inhibition leads to histone deacetylases 1 and 2 phosphorylation and disruption of corepressor interactions. *J. Biol. Chem.* **277**, 19618–19626 (2002).
19. Wilting, R. H. *et al.* Overlapping functions of Hdac1 and Hdac2 in cell cycle regulation and haematopoiesis. *EMBO J.* **29**, 2586–2597 (2010).
20. Zupkovitz, G. *et al.* The cyclin-dependent kinase inhibitor p21 is a crucial target for histone deacetylase 1 as a regulator of cellular proliferation. *Mol. Cell. Biol.* **30**, 1171–1181 (2010).
21. Ye, F. *et al.* HDAC1 and HDAC2 regulate oligodendrocyte differentiation by disrupting the beta-catenin-TCF interaction. *Nat. Neurosci.* **12**, 829–838 (2009).
22. Chen, Y. *et al.* HDAC-mediated deacetylation of NF- κ B is critical for Schwann cell myelination. *Nat. Neurosci.* **14**, 437–441 (2011).

23. Miller, K. M. *et al.* Human HDAC1 and HDAC2 function in the DNA-damage response to promote DNA nonhomologous end-joining. *Nat. Struct. Mol. Biol.* **17**, 1144–1151 (2010).
24. Yang, W.-M., Tsai, S.-C., Wen, Y.-D., Fejer, G. & Seto, E. Functional domains of histone deacetylase-3. *J. Biol. Chem.* **277**, 9447–9454 (2002).
25. Zhang, X. *et al.* Histone deacetylase 3 (HDAC3) activity is regulated by interaction with protein serine/threonine phosphatase 4. *Genes Dev.* **19**, 827–839 (2005).
26. Watson, P. J., Fairall, L., Santos, G. M. & Schwabe, J. W. R. Structure of HDAC3 bound to co-repressor and inositol tetrakisphosphate. *Nature* **481**, 335–340 (2012).
27. Montgomery, R. L. *et al.* Maintenance of cardiac energy metabolism by histone deacetylase 3 in mice. *J. Clin. Invest.* **118**, 3588–3597 (2008).
28. Hu, E. *et al.* Cloning and characterization of a novel human class I histone deacetylase that functions as a transcription repressor. *J. Biol. Chem.* **275**, 15254–15264 (2000).
29. Buggy, J. J. *et al.* Cloning and characterization of a novel human histone deacetylase, HDAC8. *Biochem. J.* **350 Pt 1**, 199–205 (2000).
30. Van den Wyngaert, I. *et al.* Cloning and characterization of human histone deacetylase 8. *FEBS Letters* **478**, 77–83 (2000).
31. Waltregny, D. *et al.* Histone deacetylase HDAC8 associates with smooth muscle alpha-actin and is essential for smooth muscle cell contractility. *FASEB J.* **19**, 966–968 (2005).
32. Yang, X.-J. & Seto, E. The Rpd3/Hda1 family of lysine deacetylases: from bacteria and yeast to mice and men. *Nat. Rev. Mol. Cell Biol.* **9**, 206–218 (2008).
33. Lee, H., Rezai-Zadeh, N. & Seto, E. Negative regulation of histone deacetylase 8 activity by cyclic AMP-dependent protein kinase A. *Mol. Cell. Biol.* **24**, 765–773 (2004).
34. Haberland, M., Mokalled, M. H., Montgomery, R. L. & Olson, E. N. Epigenetic control of skull morphogenesis by histone deacetylase 8. *Genes Dev.* **23**, 1625–1630 (2009).

35. Oehme, I. *et al.* Histone deacetylase 8 in neuroblastoma tumorigenesis. *Clin. Cancer Res.* **15**, 91–99 (2009).
36. Dearnorff, M. A. *et al.* HDAC8 mutations in Cornelia de Lange syndrome affect the cohesin acetylation cycle. *Nature* **489**, 313–317 (2012).
37. Ito, K. *et al.* Decreased histone deacetylase activity in chronic obstructive pulmonary disease. *N. Engl. J. Med.* **352**, 1967–1976 (2005).
38. Gao, J., Siddoway, B., Huang, Q. & Xia, H. Inactivation of CREB mediated gene transcription by HDAC8 bound protein phosphatase. *Biochem. Biophys. Res. Commun.* **379**, 1–5 (2009).
39. Durst, K. L., Lutterbach, B., Kummalue, T., Friedman, A. D. & Hiebert, S. W. The inv(16) fusion protein associates with corepressors via a smooth muscle myosin heavy-chain domain. *Mol. Cell. Biol.* **23**, 607–619 (2003).
40. Bertos, N. R., Wang, A. H. & Yang, X. J. Class II histone deacetylases: structure, function, and regulation. *Biochem. Cell Biol.* **79**, 243–252 (2001).
41. Martin, M., Kettmann, R. & Dequiedt, F. Class IIa histone deacetylases: regulating the regulators. *Oncogene* **26**, 5450–5467.
42. McKinsey, T. A., Zhang, C. L. & Olson, E. N. Control of muscle development by dueling HATs and HDACs. *Curr. Opin. Genet. Dev.* **11**, 497–504 (2001).
43. Vega, R. B. *et al.* Histone deacetylase 4 controls chondrocyte hypertrophy during skeletogenesis. *Cell* **119**, 555–566 (2004).
44. Chang, S. *et al.* Histone deacetylases 5 and 9 govern responsiveness of the heart to a subset of stress signals and play redundant roles in heart development. *Mol. Cell. Biol.* **24**, 8467–8476 (2004).
45. Dequiedt, F. *et al.* HDAC7, a thymus-specific class II histone deacetylase, regulates Nur77 transcription and TCR-mediated apoptosis. *Immunity* **18**, 687–698 (2003).

46. Lahm, A. *et al.* Unraveling the hidden catalytic activity of vertebrate class IIa histone deacetylases. *PNAS* **104**, 17335–17340 (2007).
47. Fischle, W. *et al.* Enzymatic activity associated with class II HDACs is dependent on a multiprotein complex containing HDAC3 and SMRT/N-CoR. *Mol. Cell* **9**, 45–57 (2002).
48. Zhou, X., Marks, P. A., Rifkind, R. A. & Richon, V. M. Cloning and characterization of a histone deacetylase, HDAC9. *Proc. Natl. Acad. Sci. U.S.A.* **98**, 10572–10577 (2001).
49. Hubbert, C. *et al.* HDAC6 is a microtubule-associated deacetylase. *Nature* **417**, 455–458 (2002).
50. Haggarty, S. J., Koeller, K. M., Wong, J. C., Grozinger, C. M. & Schreiber, S. L. Domain-selective small-molecule inhibitor of histone deacetylase 6 (HDAC6)-mediated tubulin deacetylation. *Proc. Natl. Acad. Sci. U.S.A.* **100**, 4389–4394 (2003).
51. Li, Y., Shin, D. & Kwon, S. H. Histone deacetylase 6 plays a role as a distinct regulator of diverse cellular processes. *FEBS J.* **280**, 775–793 (2013).
52. Hook, S. S., Orian, A., Cowley, S. M. & Eisenman, R. N. Histone deacetylase 6 binds polyubiquitin through its zinc finger (PAZ domain) and copurifies with deubiquitinating enzymes. *Proc. Natl. Acad. Sci. U.S.A.* **99**, 13425–13430 (2002).
53. Fischer, D. D. *et al.* Isolation and characterization of a novel class II histone deacetylase, HDAC10. *J. Biol. Chem.* **277**, 6656–6666 (2002).
54. Gao, L., Cueto, M. A., Asselbergs, F. & Atadja, P. Cloning and Functional Characterization of HDAC11, a Novel Member of the Human Histone Deacetylase Family. *J. Biol. Chem.* **277**, 25748–25755 (2002).

55. Lombardi, P. M., Cole, K. E., Dowling, D. P. & Christianson, D. W. Structure, mechanism, and inhibition of histone deacetylases and related metalloenzymes. *Curr. Opin. Struct. Biol.* **21**, 735–743 (2011).
56. Finnin, M. S. *et al.* Structures of a histone deacetylase homologue bound to the TSA and SAHA inhibitors. *Nature* **401**, 188–193 (1999).
57. Somoza, J. R. *et al.* Structural snapshots of human HDAC8 provide insights into the class I histone deacetylases. *Structure* **12**, 1325–1334 (2004).
58. Vannini, A. *et al.* Crystal structure of a eukaryotic zinc-dependent histone deacetylase, human HDAC8, complexed with a hydroxamic acid inhibitor. *Proc. Natl. Acad. Sci. U.S.A.* **101**, 15064–15069 (2004).
59. Vannini, A. *et al.* Substrate binding to histone deacetylases as shown by the crystal structure of the HDAC8–substrate complex. *EMBO reports* **8**, 879–884 (2007).
60. Gantt, S. L., Joseph, C. G. & Fierke, C. A. Activation and Inhibition of Histone Deacetylase 8 by Monovalent Cations. *J. Biol. Chem.* **285**, 6036–6043 (2010).
61. Haider, S., Joseph, C. G., Neidle, S., Fierke, C. A. & Fuchter, M. J. On the function of the internal cavity of histone deacetylase protein 8: R37 is a crucial residue for catalysis. *Bioorg. Med. Chem. Lett.* **21**, 2129–2132 (2011).
62. Cole, K. E., Dowling, D. P., Boone, M. A., Phillips, A. J. & Christianson, D. W. Structural basis of the antiproliferative activity of largazole, a depsipeptide inhibitor of the histone deacetylases. *J. Am. Chem. Soc.* **133**, 12474–12477 (2011).
63. Dowling, D. P., Gattis, S. G., Fierke, C. A. & Christianson, D. W. Structures of metal-substituted human histone deacetylase 8 provide mechanistic inferences on biological function. *Biochemistry* **49**, 5048–5056 (2010).
64. Dowling, D. P., Gantt, S. L., Gattis, S. G., Fierke, C. A. & Christianson, D. W. Structural studies of human histone deacetylase 8 and its site-specific variants complexed with substrate and inhibitors. *Biochemistry* **47**, 13554–13563 (2008).

65. Bressi, J. C. *et al.* Exploration of the HDAC2 foot pocket: Synthesis and SAR of substituted N-(2-aminophenyl)benzamides. *Bioorg. Med. Chem. Lett.* **20**, 3142–3145 (2010).
66. Watson, P. J., Fairall, L., Santos, G. M. & Schwabe, J. W. R. Structure of HDAC3 bound to co-repressor and inositol tetraphosphate. *Nature* **481**, 335–340 (2012).
67. Bottomley, M. J. *et al.* Structural and Functional Analysis of the Human HDAC4 Catalytic Domain Reveals a Regulatory Structural Zinc-binding Domain. *Journal of Biological Chemistry* **283**, 26694–26704 (2008).
68. Schuetz, A. *et al.* Human HDAC7 Harbors a Class IIa Histone Deacetylase-specific Zinc Binding Motif and Cryptic Deacetylase Activity. *J. Biol. Chem.* **283**, 11355–11363 (2008).
69. Kouzarides, T. Acetylation: a regulatory modification to rival phosphorylation? *EMBO J* **19**, 1176–1179 (2000).
70. Wolfson, N. A., Ann Pitcairn, C. & Fierke, C. A. HDAC8 substrates: Histones and beyond. *Biopolymers* **99**, 112–126 (2013).
71. Krennhrubec, K., Marshall, B. L., Hedglin, M., Verdin, E. & Ulrich, S. M. Design and evaluation of ‘Linkerless’ hydroxamic acids as selective HDAC8 inhibitors. *Bioorg. Med. Chem. Lett.* **17**, 2874–2878 (2007).
72. Bolden, J. E., Peart, M. J. & Johnstone, R. W. Anticancer activities of histone deacetylase inhibitors. *Nat Rev Drug Discov* **5**, 769–784 (2006).
73. Yan, W. *et al.* Histone deacetylase inhibitors suppress mutant p53 transcription via histone deacetylase 8. *Oncogene* **32**, 599–609 (2013).
74. Wilson, B. J., Tremblay, A. M., Deblois, G., Sylvain-Drolet, G. & Giguère, V. An Acetylation Switch Modulates the Transcriptional Activity of Estrogen-Related Receptor α . *Molecular Endocrinology* **24**, 1349–1358 (2010).

75. Lee, H., Sengupta, N., Villagra, A., Rezai-Zadeh, N. & Seto, E. Histone Deacetylase 8 Safeguards the Human Ever-Shorter Telomeres 1B (hEST1B) Protein from Ubiquitin-Mediated Degradation. *Mol. Cell. Biol.* **26**, 5259–5269 (2006).
76. Wegener, D., Hildmann, C. & Schwienhorst, A. Recent progress in the development of assays suited for histone deacetylase inhibitor screening. *Mol. Genet. Metab.* **80**, 138–147 (2003).
77. Nare, B. *et al.* Development of a Scintillation Proximity Assay for Histone Deacetylase Using a Biotinylated Peptide Derived from Histone-H4. *Analytical Biochemistry* **267**, 390–396 (1999).
78. Hoffmann, K., Jung, M., Brosch, G. & Loidl, P. A non-isotopic assay for histone deacetylase activity. *Nucl. Acids Res.* **27**, 2057–2058 (1999)
79. Wegener, D., Wirsching, F., Riester, D. & Schwienhorst, A. A Fluorogenic Histone Deacetylase Assay Well Suited for High-Throughput Activity Screening. *Chemistry & Biology* **10**, 61–68 (2003).
80. Schultz, B. E. *et al.* Kinetics and comparative reactivity of human class I and class IIb histone deacetylases. *Biochemistry* **43**, 11083–11091 (2004).
81. Hildmann, C. *et al.* A new amidohydrolase from *Bordetella* or *Alcaligenes* strain FB188 with similarities to histone deacetylases. *J. Bacteriol.* **186**, 2328–2339 (2004).
82. Fatkins, D. G. & Zheng, W. A spectrophotometric assay for histone deacetylase 8. *Anal. Biochem.* **372**, 82–88 (2008).
83. Halley, F. *et al.* A bioluminogenic HDAC activity assay: validation and screening. *J Biomol Screen* **16**, 1227–1235 (2011).
84. Baba, R., Hori, Y., Mizukami, S. & Kikuchi, K. Development of a fluorogenic probe with a transesterification switch for detection of histone deacetylase activity. *J. Am. Chem. Soc.* **134**, 14310–14313 (2012).

85. Riester, D., Wegener, D., Hildmann, C. & Schwienhorst, A. Members of the histone deacetylase superfamily differ in substrate specificity towards small synthetic substrates. *Biochemical and Biophysical Research Communications* **324**, 1116–1123 (2004).
86. Riester, D., Hildmann, C., Grünewald, S., Beckers, T. & Schwienhorst, A. Factors affecting the substrate specificity of histone deacetylases. *Biochem. Biophys. Res. Commun.* **357**, 439–445 (2007).
87. Gurard-Levin, Z. A. & Mrksich, M. The activity of HDAC8 depends on local and distal sequences of its peptide substrates. *Biochemistry* **47**, 6242–6250 (2008).
88. Gurard-Levin, Z. A., Kim, J. & Mrksich, M. Combining Mass Spectrometry and Peptide Arrays to Profile the Specificities of Histone Deacetylases. *ChemBioChem* **10**, 2159–2161 (2009).
89. Borra, M. T., Smith, B. C. & Denu, J. M. Mechanism of human SIRT1 activation by resveratrol. *J. Biol. Chem.* **280**, 17187–17195 (2005).
90. Riester, D., Hildmann, C., Schwienhorst, A. & Meyer-Almes, F.-J. Histone deacetylase inhibitor assay based on fluorescence resonance energy transfer. *Anal. Biochem.* **362**, 136–141 (2007).
91. Mazitschek, R., Patel, V., Wirth, D. F. & Clardy, J. Development of a fluorescence polarization based assay for histone deacetylase ligand discovery. *Bioorg. Med. Chem. Lett.* **18**, 2809–2812 (2008).
92. Riester, D. *et al.* Non-isotopic dual parameter competition assay suitable for high-throughput screening of histone deacetylases. *Bioorg. Med. Chem. Lett.* **19**, 3651–3656 (2009).
93. Marks, B. D., Fakhoury, S. A., Frazee, W. J., Eliason, H. C. & Riddle, S. M. A Substrate-Independent TR-FRET Histone Deacetylase Inhibitor Assay. *J Biomol Screen* **16**, 1247–1253 (2011).

94. Gantt, S. L., Gattis, S. G. & Fierke, C. A. Catalytic activity and inhibition of human histone deacetylase 8 is dependent on the identity of the active site metal ion. *Biochemistry* **45**, 6170–6178 (2006).
95. Ropero, S. & Esteller, M. The role of histone deacetylases (HDACs) in human cancer. *Molecular Oncology* **1**, 19–25 (2007).
96. Choi, J.-H. *et al.* Expression Profile of Histone Deacetylase 1 in Gastric Cancer Tissues. *Cancer Science* **92**, 1300–1304 (2001).
97. Song, J. *et al.* Increased expression of histone deacetylase 2 is found in human gastric cancer. *APMIS* **113**, 264–268 (2005).
98. Wilson, A. J. *et al.* Histone deacetylase 3 (HDAC3) and other class I HDACs regulate colon cell maturation and p21 expression and are deregulated in human colon cancer. *J. Biol. Chem.* **281**, 13548–13558 (2006).
99. Witt, O., Deubzer, H. E., Lodrini, M., Milde, T. & Oehme, I. Targeting histone deacetylases in neuroblastoma. *Curr. Pharm. Des.* **15**, 436–447 (2009).
100. Fraga, M. F. *et al.* Loss of acetylation at Lys16 and trimethylation at Lys20 of histone H4 is a common hallmark of human cancer. *Nat Genet* **37**, 391–400 (2005).
101. Blagosklonny, M. V. *et al.* Histone deacetylase inhibitors all induce p21 but differentially cause tubulin acetylation, mitotic arrest, and cytotoxicity. *Mol. Cancer Ther.* **1**, 937–941 (2002).
102. Kim, H.-J. & Bae, S.-C. Histone deacetylase inhibitors: molecular mechanisms of action and clinical trials as anti-cancer drugs. *Am J Transl Res* **3**, 166–179 (2011).
103. Yan, W. *et al.* Histone deacetylase inhibitors suppress mutant p53 transcription via histone deacetylase 8. *Oncogene* **32**, 599–609 (2013).
104. Lin, R. J. *et al.* Role of the histone deacetylase complex in acute promyelocytic leukaemia. *Nature* **391**, 811–814 (1998).

105. Dokmanovic, M., Clarke, C. & Marks, P. A. Histone Deacetylase Inhibitors: Overview and Perspectives. *Mol Cancer Res* **5**, 981–989 (2007).
106. Gräff, J. & Tsai, L.-H. The Potential of HDAC Inhibitors as Cognitive Enhancers. *Annual Review of Pharmacology and Toxicology* **53**, 311–330 (2013).
107. Chuang, D.-M., Leng, Y., Marinova, Z., Kim, H.-J. & Chiu, C.-T. Multiple roles of HDAC inhibition in neurodegenerative conditions. *Trends in Neurosciences* **32**, 591–601 (2009).
108. Guan, J.-S. *et al.* HDAC2 negatively regulates memory formation and synaptic plasticity. *Nature* **459**, 55–60 (2009).
109. Chuang, D.-M., Leng, Y., Marinova, Z., Kim, H.-J. & Chiu, C.-T. Multiple roles of HDAC inhibition in neurodegenerative conditions. *Trends in Neurosciences* **32**, 591–601 (2009).
110. McKinsey, T. A. Therapeutic potential for HDAC inhibitors in the heart. *Annu. Rev. Pharmacol. Toxicol.* **52**, 303–319 (2012)
111. Cao, D. J. *et al.* Histone deacetylase (HDAC) inhibitors attenuate cardiac hypertrophy by suppressing autophagy. *PNAS* **108**, 4123–4128 (2011).
112. Halili, M. A., Andrews, M. R., Sweet, M. J. & Fairlie, D. P. Histone deacetylase inhibitors in inflammatory disease. *Curr Top Med Chem* **9**, 309–319 (2009).
113. Histone Deacetylase Activity and COPD. *New England Journal of Medicine* **353**, 528–529 (2005).
114. Marks, P. A. & Breslow, R. Dimethyl sulfoxide to vorinostat: development of this histone deacetylase inhibitor as an anticancer drug. *Nat Biotech* **25**, 84–90 (2007).
115. Johnstone, R. W. & Licht, J. D. Histone deacetylase inhibitors in cancer therapy: Is transcription the primary target? *Cancer Cell* **4**, 13–18 (2003).

116. Histone deacetylases inhibitors as anti-angiogenic agents altering vascular endothelial growth factor signaling. , *Published online: 17 January 2002; | doi:10.1038/sj.onc.1205108* **21**, (2002).
117. Magner, W. J. *et al.* Activation of MHC class I, II, and CD40 gene expression by histone deacetylase inhibitors. *J. Immunol.* **165**, 7017–7024 (2000).
118. Van Lint, C., Emiliani, S. & Verdin, E. The expression of a small fraction of cellular genes is changed in response to histone hyperacetylation. *Gene Expr.* **5**, 245–253 (1996).
119. Anti-tumour activity *in vitro* and *in vivo* of selective differentiating agents containing hydroxamate. *Br J Cancer* **80**, 1252–1258 (1999).
120. Chang, J. *et al.* Differential response of cancer cells to HDAC inhibitors trichostatin A and depsipeptide. *Br J Cancer* **106**, 116–125 (2012).
121. Garber, K. HDAC inhibitors overcome first hurdle. *Nat. Biotechnol.* **25**, 17–19 (2007).
122. Zhang, B. *et al.* Effective Targeting of Quiescent Chronic Myelogenous Leukemia Stem Cells by Histone Deacetylase Inhibitors in Combination with Imatinib Mesylate. *Cancer Cell* **17**, 427–442 (2010).
123. Gupta, P., Reid, R. C., Iyer, A., Sweet, M. J. & Fairlie, D. P. Towards isozyme-selective HDAC inhibitors for interrogating disease. *Curr Top Med Chem* **12**, 1479–1499 (2012).
124. Subramanian, S., Bates, S. E., Wright, J. J., Espinoza-Delgado, I. & Piekarcz, R. L. Clinical Toxicities of Histone Deacetylase Inhibitors. *Pharmaceuticals* **3**, 2751–2767 (2010).
125. Mavromoustakos, T. *et al.* Strategies in the rational drug design. *Curr. Med. Chem.* **18**, 2517–2530 (2011).

126. Bertrand, P. Inside HDAC with HDAC inhibitors. *Eur J Med Chem* **45**, 2095–2116 (2010).
127. Yoshida, M., Kijima, M., Akita, M. & Beppu, T. Potent and specific inhibition of mammalian histone deacetylase both *in vivo* and *in vitro* by trichostatin A. *J. Biol. Chem.* **265**, 17174–17179 (1990).
128. Ueda, H. *et al.* FR901228, a novel antitumor bicyclic depsipeptide produced by *Chromobacterium violaceum* No. 968. I. Taxonomy, fermentation, isolation, physico-chemical and biological properties, and antitumor activity. *J. Antibiot.* **47**, 301–310 (1994).
129. Whitehead, L. *et al.* Human HDAC isoform selectivity achieved via exploitation of the acetate release channel with structurally unique small molecule inhibitors. *Bioorg. Med. Chem.* **19**, 4626–4634 (2011).
130. Marmion, C. J., Griffith, D. & Nolan, K. B. Hydroxamic Acids – An Intriguing Family of Enzyme Inhibitors and Biomedical Ligands. *European Journal of Inorganic Chemistry* **2004**, 3003–3016 (2004).
131. Seiser, T., Kamena, F. & Cramer, N. Synthesis and biological activity of largazole and derivatives. *Angew. Chem. Int. Ed. Engl.* **47**, 6483–6485 (2008).
132. Jose, B. *et al.* Novel histone deacetylase inhibitors: cyclic tetrapeptide with trifluoromethyl and pentafluoroethyl ketones. *Bioorg. Med. Chem. Lett.* **14**, 5343–5346 (2004).
133. Suzuki, N. *et al.* Design, synthesis, and biological activity of boronic acid-based histone deacetylase inhibitors. *J. Med. Chem.* **52**, 2909–2922 (2009).
134. Kapustin, G. V. *et al.* Phosphorus-Based SAHA Analogues as Histone Deacetylase Inhibitors. *Org. Lett.* **5**, 3053–3056 (2003).

135. Charrier, C., Bertrand, P., Gesson, J.-P. & Roche, J. Synthesis of rigid trichostatin A analogs as HDAC inhibitors. *Bioorg. Med. Chem. Lett.* **16**, 5339–5344 (2006).
136. Charrier, C., Roche, J., Gesson, J.-P. & Bertrand, P. Antiproliferative activities of a library of hybrids between indanones and HDAC inhibitor SAHA and MS-275 analogues. *Bioorganic & Medicinal Chemistry Letters* **17**, 6142–6146 (2007).
137. Montero, A., Beierle, J. M., Olsen, C. A. & Ghadiri, M. R. Design, Synthesis, Biological Evaluation, and Structural Characterization of Potent Histone Deacetylase Inhibitors Based on Cyclic α/β -Tetrapeptide Architectures. *J. Am. Chem. Soc.* **131**, 3033–3041 (2009).
138. Wang, D.-F., Helquist, P., Wiech, N. L. & Wiest, O. Toward selective histone deacetylase inhibitor design: homology modeling, docking studies, and molecular dynamics simulations of human class I histone deacetylases. *J. Med. Chem.* **48**, 6936–6947 (2005).
139. Siliphaivanh, P. *et al.* Design of novel histone deacetylase inhibitors. *Bioorganic & Medicinal Chemistry Letters* **17**, 4619–4624 (2007).
140. Whitehead, L. *et al.* Human HDAC isoform selectivity achieved via exploitation of the acetate release channel with structurally unique small molecule inhibitors. *Bioorg. Med. Chem.* **19**, 4626–4634 (2011).
141. Wagner, J. M., Hackanson, B., Lübbert, M. & Jung, M. Histone deacetylase (HDAC) inhibitors in recent clinical trials for cancer therapy. *Clinical Epigenetics* **1**, 117–136 (2010).
142. Novotny-Diermayr, V. *et al.* SB939, a novel potent and orally active histone deacetylase inhibitor with high tumor exposure and efficacy in mouse models of colorectal cancer. *Mol. Cancer Ther.* **9**, 642–652 (2010).
143. Beckers, T. *et al.* Distinct pharmacological properties of second generation HDAC inhibitors with the benzamide or hydroxamate head group. *International Journal of Cancer* **121**, 1138–1148 (2007).

144. Bonfils, C. *et al.* Evaluation of the Pharmacodynamic Effects of MGCD0103 from Preclinical Models to Human Using a Novel HDAC Enzyme Assay. *Clin Cancer Res* **14**, 3441–3449 (2008).
145. Bandyopadhyay, D., Mishra, A. & Medrano, E. E. Overexpression of Histone Deacetylase 1 Confers Resistance to Sodium Butyrate–Mediated Apoptosis in Melanoma Cells through a p53-Mediated Pathway. *Cancer Res* **64**, 7706–7710 (2004).
146. Ropero, S. *et al.* A truncating mutation of HDAC2 in human cancers confers resistance to histone deacetylase inhibition. *Nat. Genet.* **38**, 566–569 (2006).
147. Cabrita, L. D., Dai, W. & Bottomley, S. P. A family of E. coli expression vectors for laboratory scale and high throughput soluble protein production. *BMC Biotechnol.* **6**, 12 (2006).
148. Bradford, M. M. A rapid and sensitive method for the quantitation of microgram quantities of protein utilizing the principle of protein-dye binding. *Analytical Biochemistry* **72**, 248–254 (1976).
149. Kuzmič, P., Moss, M. L., Kofron, J. L. & Rich, D. H. Fluorescence displacement method for the determination of receptor-ligand binding constants. *Analytical Biochemistry* **205**, 65–69 (1992).
150. Wiseman, T., Williston, S., Brandts, J. F. & Lin, L. N. Rapid measurement of binding constants and heats of binding using a new titration calorimeter. *Anal. Biochem.* **179**, 131–137 (1989).
151. Morin, P. E. & Freire, E. Direct calorimetric analysis of the enzymic activity of yeast cytochrome c oxidase. *Biochemistry* **30**, 8494–8500 (1991).
152. Santoro, M. M. & Bolen, D. W. A test of the linear extrapolation of unfolding free energy changes over an extended denaturant concentration range. *Biochemistry* **31**, 4901–4907 (1992).

153. Whitmore, L. & Wallace, B. A. DICHROWEB, an online server for protein secondary structure analyses from circular dichroism spectroscopic data. *Nucl. Acids Res.* **32**, W668–W673 (2004).
154. Beckett, D. in *Methods in Enzymology* (Michael L. Johnson, J. M. H. and G. K. A.) **Volume 488**, 1–16 (Academic Press, 2011).
155. Ondetti, M. A., Rubin, B. & Cushman, D. W. Design of specific inhibitors of angiotensin-converting enzyme: new class of orally active antihypertensive agents. *Science* **196**, 441–444 (1977).
156. Suzuki, T. *et al.* Thiol-based SAHA analogues as potent histone deacetylase inhibitors. *Bioorg. Med. Chem. Lett.* **14**, 3313–3317 (2004).
157. Chen, J. S., Faller, D. V. & Spanjaard, R. A. Short-chain fatty acid inhibitors of histone deacetylases: promising anticancer therapeutics? *Curr Cancer Drug Targets* **3**, 219–236 (2003).
158. Bermúdez-Lugo, J. A. *et al.* Exploration of the valproic acid binding site on histone deacetylase 8 using docking and molecular dynamic simulations. *J Mol Model* **18**, 2301–2310 (2012).
159. Lain, S. *et al.* Discovery, *In Vivo* Activity, and Mechanism of Action of a Small-Molecule p53 Activator. *Cancer Cell* **13**, 454–463 (2008).
160. Daly, C. J. & McGrath, J. C. Fluorescent ligands, antibodies, and proteins for the study of receptors. *Pharmacol. Ther.* **100**, 101–118 (2003).
161. Itoh, Y., Suzuki, T. & Miyata, N. Isoform-selective histone deacetylase inhibitors. *Curr. Pharm. Des.* **14**, 529–544 (2008).
162. Fersht, A. *Structure and Mechanism in Protein Science: A Guide to Enzyme Catalysis and Protein Folding.* (W. H. Freeman, 1998).

163. Segel, I. H. *Enzyme Kinetics: Behavior and Analysis of Rapid Equilibrium and Steady-State Enzyme Systems*. (Wiley-Interscience, 1993).
164. Lakowicz, J. R. *Principles of Fluorescence Spectroscopy*. (Springer, 2006).
165. Beckett, D. in *Methods in Enzymology* (Michael L. Johnson, J. M. H. and G. K. A.) **Volume 488**, 1–16 (Academic Press, 2011).
166. Williams, A. F. Out of equilibrium. *Nature* **352**, 473–474 (1991).
167. Foote, J. & Milstein, C. Kinetic maturation of an immune response. *Nature* **352**, 530–532 (1991).
168. Matsui, K., Boniface, J. J., Steffner, P., Reay, P. A. & Davis, M. M. Kinetics of T-cell receptor binding to peptide/I-Ek complexes: correlation of the dissociation rate with T-cell responsiveness. *Proc. Natl. Acad. Sci. U.S.A.* **91**, 12862–12866 (1994).
169. Govern, C. C., Paczosa, M. K., Chakraborty, A. K. & Huseby, E. S. Fast on-rates allow short dwell time ligands to activate T cells. *Proc. Natl. Acad. Sci. U.S.A.* **107**, 8724–8729 (2010).
170. Markgren, P.-O. *et al.* Relationships between Structure and Interaction Kinetics for HIV-1 Protease Inhibitors. *J. Med. Chem.* **45**, 5430–5439 (2002).
171. Török, K. & Trentham, D. R. Mechanism of 2-chloro-(epsilon-amino-Lys75)-[6-[4-(N,N-diethylamino)phenyl]-1,3,5-triazin-4-yl]calmodulin interactions with smooth muscle myosin light chain kinase and derived peptides. *Biochemistry* **33**, 12807–12820 (1994).
172. Bernasconi, C. F. *Relaxation Kinetics*. (Academic Press Inc, 1976).
173. Ladbury, J. E., Klebe, G. & Freire, E. Adding calorimetric data to decision making in lead discovery: a hot tip. *Nat Rev Drug Discov* **9**, 23–27 (2010).
174. Murphy, K. P. & Freire, E. in *Advances in Protein Chemistry* (C.B. Anfinsen, F. M. R.) **Volume 43**, 313–361 (Academic Press, 1992).

175. Velázquez-Campoy, A., Ohtaka, H., Nezami, A., Muzammil, S. & Freire, E. Isothermal titration calorimetry. *Curr Protoc Cell Biol* **Chapter 17**, Unit 17.8 (2004).
176. Freire, E. Do enthalpy and entropy distinguish first in class from best in class? *Drug Discovery Today* **13**, 869–874 (2008)
177. Lafont, V. *et al.* Compensating Enthalpic and Entropic Changes Hinder Binding Affinity Optimization. *Chemical Biology & Drug Design* **69**, 413–422 (2007).
178. Connelly, P. R. & Thomson, J. A. Heat capacity changes and hydrophobic interactions in the binding of FK506 and rapamycin to the FK506 binding protein. *PNAS* **89**, 4781–4785 (1992).
179. Ladbury, J. E. Isothermal titration calorimetry: application to structure-based drug design. *Thermochimica Acta* **380**, 209–215 (2001).
180. Krogsgaard, M. *et al.* Evidence that structural rearrangements and/or flexibility during TCR binding can contribute to T cell activation. *Mol. Cell* **12**, 1367–1378 (2003).
181. Prabhu, N. V. & Sharp, K. A. Heat capacity in proteins. *Annu Rev Phys Chem* **56**, 521–548 (2005).
182. Loladze, V. V., Ermolenko, D. N. & Makhatadze, G. I. Heat capacity changes upon burial of polar and nonpolar groups in proteins. *Protein Science : A Publication of the Protein Society* **10**, 1343 (2001).
183. Edsall, J. T. Apparent Molal Heat Capacities of Amino Acids and Other Organic Compounds. *J. Am. Chem. Soc.* **57**, 1506–1507 (1935).
184. Dunitz, J. D. Win some, lose some: enthalpy-entropy compensation in weak intermolecular interactions. *Chem. Biol.* **2**, 709–712 (1995).

185. Dittenhafer-Reed, K. E., Feldman, J. L. & Denu, J. M. Catalysis and Mechanistic Insights into Sirtuin Activation. *ChemBioChem* **12**, 281–289 (2011).
186. Gutfreund, H. *Enzymes: Physical Principles*. (John Wiley & Sons Ltd, 1975).
187. Gutfreund, H. *Kinetics for the Life Sciences: Receptors, Transmitters and Catalysts*. (Cambridge University Press, 1995).
188. Richards, F. M. Structure of Proteins. *Annual Review of Biochemistry* **32**, 269–300 (1963).
189. *Protein Structure: A Practical Approach*. (Oxford University Press, USA, 1997).
190. Johnson, W. C. Secondary Structure of Proteins Through Circular Dichroism Spectroscopy. *Annual Review of Biophysics and Biophysical Chemistry* **17**, 145–166 (1988).
191. Schellman, J. A. The Thermodynamic Stability of Proteins. *Annual Review of Biophysics and Biophysical Chemistry* **16**, 115–137 (1987).
192. Balasubramanian, S., Verner, E. & Buggy, J. J. Isoform-specific histone deacetylase inhibitors: The next step? *Cancer Letters* **280**, 211–221 (2009).
193. Balasubramanian, S. *et al.* A novel histone deacetylase 8 (HDAC8)-specific inhibitor PCI-34051 induces apoptosis in T-cell lymphomas. *Leukemia* **22**, 1026–1034 (2008).
194. Trott, O. & Olson, A. J. AutoDock Vina: Improving the speed and accuracy of docking with a new scoring function, efficient optimization, and multithreading. *Journal of Computational Chemistry* **31**, 455–461 (2010).
195. Jones, R. A. & Katritzky, A. R. 262. Potentially tautomeric pyridines. Part II. 2-, 3-, and 4-Acetamido- and -benzamido-pyridine. *J. Chem. Soc.* 1317–1323 (1959).

196. Parker, M. H. *et al.* Analysis of the binding of hydroxamic acid and carboxylic acid inhibitors to the stromelysin-1 (matrix metalloproteinase-3) catalytic domain by isothermal titration calorimetry. *Biochemistry* **38**, 13592–13601 (1999).
197. Wu, R., Lu, Z., Cao, Z. & Zhang, Y. Zinc chelation with hydroxamate in histone deacetylases modulated by water access to the linker binding channel. *J. Am. Chem. Soc.* **133**, 6110–6113 (2011).
198. Freire, E. Do enthalpy and entropy distinguish first in class from best in class? *Drug Discov. Today* **13**, 869–874 (2008).
199. Gilli, P., Ferretti, V., Gilli, G. & Borea, P. A. Enthalpy-entropy compensation in drug-receptor binding. *J. Phys. Chem.* **98**, 1515–1518 (1994).
200. González, M. *et al.* Interaction of biotin with streptavidin. Thermostability and conformational changes upon binding. *J. Biol. Chem.* **272**, 11288–11294 (1997).
201. Celej, M. S., Montich, G. G. & Fidelio, G. D. Protein stability induced by ligand binding correlates with changes in protein flexibility. *Protein Science* **12**, 1496–1506 (2003).
202. Freire, E. The propagation of binding interactions to remote sites in proteins: Analysis of the binding of the monoclonal antibody D1.3 to lysozyme. *PNAS* **96**, 10118–10122 (1999).
203. Tsai, C.-J., Ma, B. & Nussinov, R. Folding and binding cascades: Shifts in energy landscapes. *PNAS* **96**, 9970–9972 (1999).
204. Bantscheff, M. *et al.* Chemoproteomics profiling of HDAC inhibitors reveals selective targeting of HDAC complexes. *Nat Biotech* **29**, 255–265 (2011).